1-1-2007

Diesel engine performance comparisons of high temperature and low temperature combustion with conventional and biodiesel fuels

Mwila Clarence Mulenga
University of Windsor

Follow this and additional works at: https://scholar.uwindsor.ca/etd

---

DIESEL ENGINE PERFORMANCE COMPARISONS OF
HIGH TEMPERATURE AND LOW TEMPERATURE COMBUSTION WITH
CONVENTIONAL AND BIODIESEL FUELS

by

Mwila Clarence Mulenga

A Dissertation
Submitted to the Faculty of Graduate Studies
through the Department of Mechanical, Automotive and Materials Engineering
in Partial Fulfillment of the Requirements for
the Degree of Doctor of Philosophy at the
University of Windsor

Windsor, Ontario, Canada

2007

Canada

ABSTRACT

The main objective of the work underlying the dissertation was in-cylinder simultaneous reduction of nitrogen oxides (NO_x) and particulate matter (PM) in diesel-/biodiesel-fuelled engines. Empirical investigations were performed for comparisons between (1) engine cycle performance of conventional diesel high and low temperature combustion processes (HTC and LTC), and (2) the use of neat commercial biodiesel and conventional diesel in the HTC and LTC modes. A four-cylinder common-rail direct-injection (DI) diesel engine and a single-cylinder DI engine with mechanical injection configuration were employed. The tests were conducted under independently controlled single- and multi-event injections, exhaust gas recirculation (EGR), boost and backpressure to achieve the LTC mode. Furthermore, engine cycle, chemical kinetics and multi-dimensional simulations were performed primarily as tools facilitating the explanation of empirical results.

Deduced from extensive empirical analyses, the exhaust emissions and fuel efficiency of the diesel engines employed characterised strong resilience to biodiesel fuels when the engines were operated in conventional HTC cycles. The results offered a promising perspective of the neat biodiesel fuels. As the engine cycles approached the LTC, dissimilar engine performance between the use of conventional diesel and biodiesel fuels was observed. In the late single-shot strategy with heavy EGR rates (EGR-incurred LTC), which could be utilised to improve the fuel efficiency of diesel/biodiesel LTC cycles at low loads, the biodiesel was found to sustain a broader range of loads than the diesel

fuel. This was mainly attributable to the biodiesel's higher Cetane number (CN) and combustion-accessible fuel oxygen.

At high load LTC, the diesel fuel early-multiple injections with EGR facilitated mixture homogeneity that is more difficult to generate with a single pulse injection. Conversely, the biodiesel early-injection strategy presented numerous challenges apropos of the homogeneous fuel/air mixture formation, especially at medium-to-high load conditions. This was attributed to the low volatility and high viscosity and CN of the investigated biodiesel fuel.

The empirical analyses, especially involving the EGR-incurred LTC, presented a platform for model-based control with an improved ignition delay correlation. The new correlation, which considered the CN and oxygen concentrations in the fuel and intake air, captured the ignition delay trends with good agreement.

Keywords: Biodiesel, common-rail diesel engines, diesel fuel, EGR, HCCI, HTC, ignition delay, LTC, simultaneous reduction of NO_x and soot, 0-D modelling, CHEMKIN, KIVA.

To my parents,

Mr. George Bwalya Mulenga and Mrs. Mary-Winfred Mwila Shinga Mulenga.

To my wife and son,

Charity Kalo Mulenga and George Bwalya-Mapalo Mulenga.

ACKNOWLEDGEMENTS

Clarence Mwila Mulenga
Windsor, Ontario
Canada
November 2007.

TABLE OF CONTENTS

LIST OF TABLES

LIST OF FIGURES

CHAPTER IV

CHAPTER V

CHAPTER VI

CHAPTER VII

CHAPTER VIII

CHAPTER IX

CHAPTER X

CHAPTER XI

APPENDIX E

NOMENCLATURE

ABDC	After Bottom Dead Centre	[°CA]
AKI	Anti-Knock Index	[-]
ASTM	American Society for Testing and Materials	
ATDC	After Top Dead Centre	[°CA]
a	Crank radius	[mm, cm]
BBDC	Before Bottom Dead Centre	[°CA]
BDF	Biodiesel Fuel	
BMEP	Brake Mean Effective Pressure	[bar]
BSFC	Brake Specific Fuel Consumption	[g/kW-hr]
B100	Neat (100%) biodiesel fuel determined from ASTM or EN standards	
CAD	Crank Angle Degrees	[°CA]
CAI	California Analytical Instruments	
CARB	California Air Resource Board	
CCI	Calculated Cetane Index	[-]
CEN	*Comité Européen de Normalisation* (European Committee for Standardisation)	
CI	Compression Ignition	
CN	Cetane Number (CCI may be used for some fuels)	[-]
CoV$_B$	Coefficient of variance in parameter B	[%]
DI	Direct Injection	
DIN	*Deutsches Institut für Normung e.V.* (German Institute for Standardisation)	
DOC	Diesel Oxidation Catalyst	

DPF	Diesel Particulate Filter	
E_a	Activation energy	[J/kg.mol]
EFCT	End of Fuel Condensation Time	[°CA]
E_{Frac}	LHV ratio of the in-cylinder fuel to CO	[-]
EGR	Exhaust Gas Recirculation	
EI	Emissions Index	[g/kg of fuel]
EN	European Norms	
EOC	End of Combustion	[°CA]
EPA	US Environmental Protection Agency	
EVO	Exhaust Valve Open	[°CA]
FBP	Final Boiling Point	[°C, K]
FSN	Filter Smoke Number	
FT	Fischer-Tropsch	
GTL	Gas-to-Liquid	
HCCI	Homogeneous Charge Compression Ignition	
HC_{Frc}	Energy fraction of exhaust UHC to in-cylinder fuel	[%]
H-FID	Heated-Flame Ionisation Detector	
HRR CA50	Crank Angle of 50% Heat-Released	[°CA]
HSDI	High-Speed Direct Injection	
HTC	High Temperature Combustion	
IBP	Initial Boiling Point	[°C, K]
ICE	Internal Combustion Engine	
IMEP	Indicated Mean Effective Pressure	[bar]

ISFC	Indicated Specific Fuel Consumption	[g/kW-hr]
ISO	International Organisation for Standardisation	
IVC	Intake Valve Close	[°CA]
k$_f$, k$_r$	Forward and reverse reaction rate coefficients	[m^6/kmol^2-s]
LNT	Lean NOx Trap	
LHV	Lower Heating Value	[MJ/kg, J/g]
LTC	Low Temperature Combustion	
l	Connecting rod length	[mm]
MAF	Mass Air Flow	
MON	Motor Octane Number	[-]
Mw	Molecular weight	[kg/kmol]
max	Maximum	
min	Minimum	
m$_f$	Fuelling rate	[g/s, mg/cycle]
N	Engine speed	[rpm]
NBB	National Biodiesel Board	
NDIR	Non-Dispersive Infra-Red	
NIST	National Institute of Standards and Technology	
NRCan	Natural Resources Canada	
P	Average cylinder pressure (during τ_{ID})	[bar]
P$_{Intake}$	Intake Pressure	[bar]
PM	Particulate Matter	
ppm	Parts per million	

R_u	Universal gas constant	[J/kmol-K]
rpm	Engine revolutions per minute	
Q_{in}	Heat addition to the thermodynamic system	[J]
Q_{out}	Heat rejection from a thermodynamic system	[J]
RON	Research Octane Number	[-]
r_{egr}	EGR ratio	[%]
SAES	Synthetic Atmosphere Engine Simulations	
SCR	Selective Catalytic Reduction	
SI	Spark Ignition	
SOC	Start of Combustion	[°CA]
SOI	Start of Injection	[°CA]
T	Mean cylinder temperature (during τ_{ID})	[°C, K]
TDC	Top Dead Centre	[°CA]
THC	Total Hydrocarbons	[ppm]
T_{intake}	Intake temperature	[°C, K]
TWC	Three-Way Catalytic converter	
UHC	Un-burnt Hydrocarbons	[ppm]
V_c	Combustion chamber volume	[m³, litres]
V_d	Engine displacement volume	[m³, litres]
W_{in}	Work done on the gas	[J]
W_{ind}	Indicated work	[J]
$W_{net,out}$	Net work output from a heat engine	[J]
W_{out}	Work done by the gas	[J]

<u>Greek Symbols</u>

α	Cut-off or load ratio	[-]
χ	Critical pressure, temperature or normal boiling point	[-]
χ_0	First empirical constant for calculation of χ	[-]
χ_1	Second empirical constant for calculation of χ	[-]
χ_2	Third empirical constant for calculation of χ	[-]
ε	Compression ratio	[-]
ϕ	Equivalence ratio	[-]
η_{Brake}	Brake thermal efficiency	[%]
η_{Diesel}	Theoretical thermal efficiency for Diesel cycle	[%]
η_{Dual}	Theoretical thermal efficiency for Dual cycle	[%]
η_{Ind}	Indicated thermal efficiency	[%]
η_{Otto}	Theoretical thermal efficiency for Otto cycle	[%]
η_{Vol}	Volumetric efficiency	[%]
λ	Excess air/fuel ratio	[-]
λ_{Cyl}	In-cylinder/effective excess air/fuel ratio (λ_{Eff} or λ_E)	[-]
θ	Engine crank angle	[°CA]
ρ_a	Air density	[kg/m^3, g/m^3]
τ_{ID}	Ignition delay	[ms, °CA]
τ_{NO}	Chemical characteristic time for NO formation	[s]
ξ	Boost ratio	[-]

PREFACE

Bonitatem et Disciplinam et Scientiam Doce Me

This dissertation was conducted in the Clean Diesel Engine Research Laboratory at the University of Windsor in Windsor, Ontario province of Canada. The laboratory is directed by Dr. Ming Zheng, the Canada Research Chair in Clean Diesel Engine Technologies and Dr. Graham T. Reader, the Dean of the Faculty of Engineering.

Activities in the laboratory, which has active collaboration with leading diesel research and manufacturing industries, are focused on green technology by providing a comprehensive research and development programme for modern diesel engines. The laboratory is equipped with state-of-the-art testing facilities that includes DC motoring and eddy current dynamometers, modern common-rail diesel engines, intelligent control systems, engine system conditioning units and fully automated data acquisition and analysis systems. The main target is to achieve simultaneous ultra-low emissions of NO_x and soot from diesel engines through in-cylinder and after-treatment control strategies. Among the in-cylinder control schemes being investigated are the clean diesel combustion approach, alternate green fuels such as biodiesel and ultra-low-sulphur diesel fuels, *inter alia*. The active flow embedded diesel particulate filters, diesel oxidation catalysts and lean-NO_x traps constitute the advanced after-treatment schemes being investigated.

LIST OF PUBLICATIONS

Refereed Publications

1. Ming Zheng, **Mwila C. Mulenga**, Meiping Wang, Graham T. Reader and Jimi Tjong, "An Improvement on Low Temperature Combustion in Neat Biodiesel Engine Cycles", SAE Offer No. 08SFL-0341 (Under Review, Submitted to the 2008 SAE Powertrain and Fluid Systems Conference).

2. Ming Zheng, **Mwila C. Mulenga**, Xiaoye Han, Yuyu Tan, Martin S. Kobler, Suek-Jin Ko, Meiping Wang and Jimi Tjong, "Low Temperature Combustion of Neat Biodiesel Fuel on a Common-rail Diesel Engine", SAE Offer No. 08PFL-391 (Accepted for publication at the 2008 SAE World Congress).

3. Ming Zheng, Yuyu Tan, **Mwila Clarence Mulenga** and Meiping Wang, "Thermal Efficiency Analyses of Diesel Low Temperature Combustion Cycles", *SAE Transactions Journal of Fuels and Lubricants,* SAE Paper No. 2007-01-4019, 2007.

4. Ming Zheng, **Mwila C. Mulenga**, Graham T. Reader, Meiping Wang, David S-K. Ting and Jimi Tjong, "Biodiesel Engine Performance and Emissions in Low Temperature Combustion", *Fuel Journal* (Article in press, May 2007).

5. Ming Zheng, **Mwila C. Mulenga**, Graham T. Reader, Yuyu Tan, Meiping Wang and Jimi Tjong, "Neat Biodiesel Fuel Engine Tests and Preliminary Modelling", SAE Paper 2007-01-0616, 2007.

6. Ming Zheng, Usman Asad, Raj Kumar, Graham T. Reader, **Mwila C. Mulenga**, Meiping Wang and Jimi S. Tjong, "An Investigation of EGR Treatment on the Emission and Operating Characteristics of Modern Diesel Engines", SAE Paper 2007-01-1083, 2007.

7. Ming Zheng, **Mwila C. Mulenga**, Graham T. Reader, Meiping Wang and David S-K. Ting, "Influence of Biodiesel Fuel on Diesel Engine Performance and Emissions in Low Temperature Combustion", SAE Paper 2006-01-3281, 2006.

8. Ming Zheng, Graham T. Reader, Dong Wang, Jun Zuo, Raj Kumar, **Mwila C. Mulenga**, Usman Asad, David S-K. Ting and Meiping Wang, "A Thermal Response Analysis on the Transient Performance of Active Diesel After-treatment", *SAE Transactions Journal of Fuels and Lubricants*, Paper 2005-01-3885, 2005.

9. **Mwila C. Mulenga**, Graham T. Reader, David S-K. Ting and Ming Zheng, "Potential for Reduced CO and NO_x Emissions from an HCCI Engine using H_2O_2 Addition", SAE Paper 2003-01-3204, 2003.

10. **Mwila C. Mulenga**, Ming Zheng, David S-K. Ting and Graham T. Reader, "Prospect of Reduced CO and NO_x in Diesel Dual Fuel Engines", ASME Internal Combustion Engine Division and Rail Transportation Division Fall Technical Conference, ASME Paper ICEF2003-768, 2003.

11. **Mwila C. Mulenga**, Graham T. Reader, David S-K. Ting and Ming Zheng, "Effect of Hydrogen Peroxide on Premixed Iso-octane/Air Combustion", ASME International Joint Power Generation Conference ASME Paper IJPGC2003-40108, 2003.

Other Publications

12. Three (3) Co-authored Non-disclosed Industrial Final Reports, 2006-2007.

13. Six (6) AUTO21™ Industrial-based and HQP Poster Presentations, 2003-2007.

14. Y. Tan, **M.C. Mulenga**, U. Asad, D.S-K. Ting, M. Wang, G.T. Reader, and M. Zheng, "Preliminary Analysis of Fuel Efficiency of Diesel HCCI Cycles", Combustion Institute/Canadian Section (CI/CS), 2007.

15. X. Han, U. Asad, R. Kumar, **M.C. Mulenga**, S. Banerjee, M. Wang, G.T. Reader and M. Zheng, "Empirical Studies of Diesel Low Temperature Combustion on a Modern Diesel Engine", Combustion Institute/Canadian Section (CI/CS), 2007.

16. Ming Zheng, Graham T. Reader, Raj Kumar, **Clarence Mulenga**, Usman Asad, Yuyu Tan and Meiping Wang, "Adaptive Control to Improve Low Temperature Diesel Engine Combustion", Advanced Combustion Technologies Session of the 12th Diesel Engine-Efficiency Emissions Research (DEER) Conference, 2006.

17. **M.C. Mulenga**, M. Zheng, G.T. Reader, D.S-K. Ting, Y. Tan, U Asad and M. Wang, "Investigating EGR on Low-temperature Combustion NO_x and PM in Diesel Engines", Combustion Institute/Canadian Section (CI/CS), 2006.

18. R. Kumar, M. Zheng, G. Reader, **C. Mulenga**, W. Bombardier, S. Ko and M. Wang, "A Study on the Energy and Emission Efficacy of Multi-Pulse Fuel Injection on Low-Temperature Combustion", Combustion Institute/Canadian Section (CI/CS), 2006.

CHAPTER I

INTRODUCTION

1.1 The Diesel Engine

Reciprocating, piston internal combustion engines, which are essentially either spark-ignited (SI) or compression-ignited (CI), have enjoyed wide application as a power source for both stationary and mobile equipment for over a century. In SI engines, such as gasoline-fuelled (petrol) engines, a fuel/air mixture is compressed and a spark introduced to initiate ignition and subsequent combustion. Combustion in SI engines is, therefore, dominated by overall near-stoichiometric premixed burning with a flame front propagating steadily throughout the mixture (Bosch 1996, Heywood 1988, Stone 1999). The fuels in gasoline engines are described by their propensity to resist auto-ignition such as Motor Octane Number (MON) or Research Octane Number (RON) with the average of the two referred to as the Anti-Knock Index (AKI) (Stone 1999). In CI engines, such as diesel-fuelled engines, in contrast, the liquid fuel is injected when the air is compressed to high temperatures and pressures. The fuel undergoes chemical and physical preparation leading to ignition and subsequent combustion. The fuels in diesel engines are defined by their easiness to auto-ignite such as Cetane Number (CN) and Calculated Cetane Index (CCI) (Bosch 1996, Stone 1999). Note that other types of engines, such as the Wankel engine, are not discussed in this dissertation.

Compared to the gasoline engine the diesel engine was considered to be noisy and dirty, among automotive consumers worldwide. In recent years, however, the diesel engine has benefited from tremendous improvements in all the areas where it was traditionally weak

such as noise, smoke and power output while its key advantage of being more efficient has been further improved. Modern turbo-charged diesel engines are quiet, clean and have excellent torque characteristics. Furthermore, because of its reduced fuel consumption compared to the gasoline engine, the diesel engine has gained interest from parties with environmental concerns due to its potential to comparatively reduce the emissions of carbon dioxide (CO_2), a greenhouse gas.

1.1.1 Combustion in Diesel Engines

The energy release history in diesel engines is affected by the speed, EGR rate, fuel schedule, boost and load, among others. Figure 1-1 and Figure 1-2 present typical normalised heat-release rates from a single-shot direct injection (DI) diesel engine, in the Clean Diesel Engine Research Laboratory at the University of Windsor, at low and high load conditions, respectively. It is apparent from the figures that the load effect is quite significant in this engine. The points A to D denote the start of injection (SOI), ignition timing (also called start of combustion SOC), start of diffusion burning and end of combustion (EOC), respectively. The diesel combustion process could be described as follows (Bosch 1996, Heywood 1988, Stone 1999):

A to B: Ignition delay period. When the liquid fuel is injected into the cylinder, it undergoes atomisation, vaporisation and mixing with the air. Some pre-ignition chemical reactions would also take place to bring the charge to combustible limits. This period is essentially referred to as physical and chemical preparation of the charge.

2

B to C: Premixed combustion phase. The fuel prepared during the ignition delay period ignites and burns rapidly. This period is sometimes called uncontrolled combustion. It is this burning phase that is believed to give the diesel engine its knocking sound because of the increased rate-of-pressure rise.
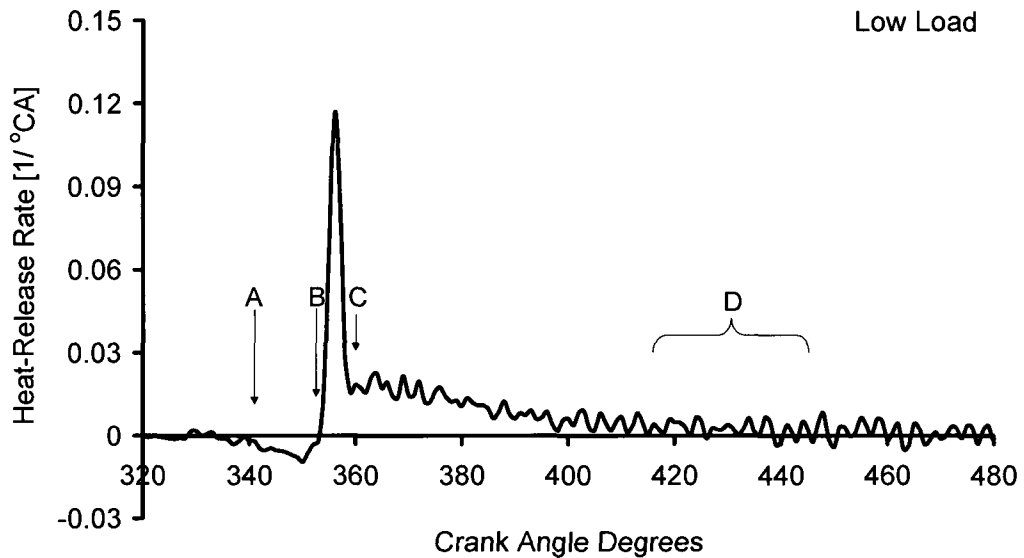
Figure 1-1: Typical heat-release rate from a classical diesel engine at low load.
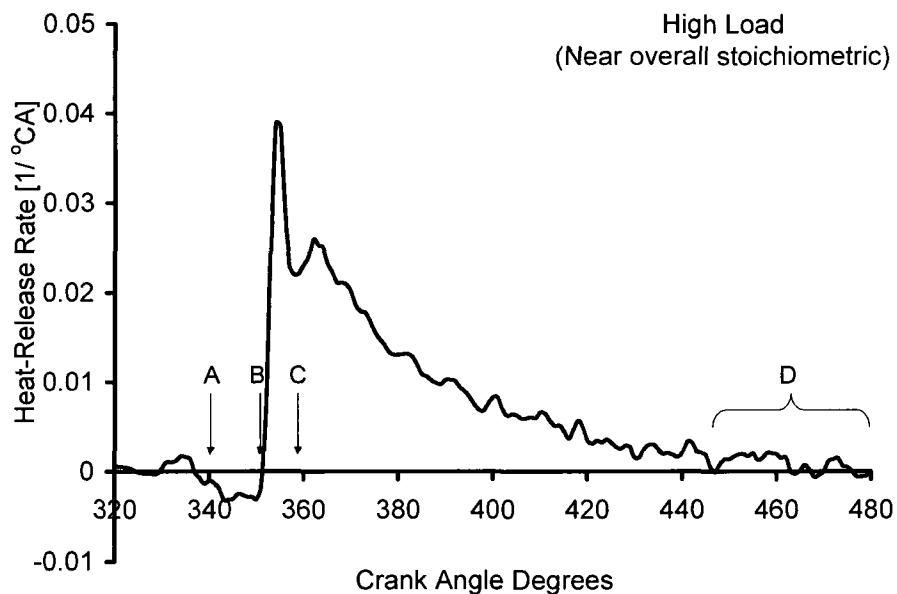
Figure 1-2: Typical heat-release rate from a classical diesel engine high load.

C to D: Diffusion-controlled phase. Combustion occurs at a rate determined by the preparation of the fresh air/fuel mixture i.e. mixing-controlled combustion.

D: Late combustion phase. This is similar to the mixing-controlled phase until all the fuel or oxygen is utilised.

At low loads the fraction of energy released during the premixed phase of combustion is relatively higher. Consequently, with enhanced premixed burning strategies such as high fuel injection pressure, boosting, retarded SOI and exhaust gas recirculation (EGR), it is possible to moderate the diffusion burning phase at such conditions. On the contrary, at high load conditions, where the diffusion burning is predominant, aggressive strategies such a combination of high injection pressure, boosting, EGR and multiple injections are commonly employed.

1.1.2 Exhaust Emissions

If a hydrocarbon-based fuel of composition $C_\alpha H_\beta O_\gamma$ is reacted with air, its complete combustion would yield carbon dioxide, water, oxygen (if lean mixture) and nitrogen as shown in Figure 1-3 (Heywood 1988, Stone 1999, Turns 2000). The variable λ is the excess air-to-fuel ratio defined as the ratio between the actual air-to-fuel ratio and the stoichiometric air-to-fuel ratio so that $\lambda > 1$ for lean mixtures, $\lambda < 1$ for rich mixtures and $\lambda = 1$ for stoichiometric mixtures. Alternatively, the reciprocal of λ known as equivalence fuel/air ratio, ϕ, may be employed. The products of complete combustion are essentially non-toxic however CO_2 is believed to contribute to global warming due to its greenhouse

effect. In practical applications, however, the combustion is always accompanied by toxic species resulting from incomplete combustion such as carbon monoxide (CO), un-burnt hydrocarbons (UHC) and particulate matter (PM) and oxides of nitrogen (NO_x), which are products of high temperature combustion of nitrogen and oxygen. The major combustion pollutant species and their effects on the local environment are discussed below.

$$\text{Reactants}: C_\alpha H_\beta O_\gamma + \lambda\left(\alpha + \frac{\beta}{4} - \frac{\gamma}{2}\right)\left\{O_2 + \frac{79.05}{20.95} N_2\right\}$$

$$\text{Products}: \alpha CO_2 + \frac{\beta}{2} H_2O + (1-\lambda)\left(\alpha + \frac{\beta}{4} - \frac{\gamma}{2}\right)O_2 + \lambda\left(\alpha + \frac{\beta}{4} - \frac{\gamma}{2}\right)\frac{79.05}{20.95} N_2$$

Carbon Dioxide   Water   Oxygen   Nitrogen

COMPLETE COMBUSTION

$$\text{Reactants}: C_\alpha H_\beta O_\gamma + \lambda\left(\alpha + \frac{\beta}{4} - \frac{\gamma}{2}\right)\left\{O_2 + \frac{79.05}{20.95} N_2\right\}$$

$$\text{Products}: n_1 CO_2 + n_2 H_2O + n_3 O_2 + n_4 N_2 + n_5 CO + n_6 UHC + n_7 NOx + n_8 PM + \ldots$$

Carbon Dioxide   Water   Oxygen   Nitrogen Carbon Monoxide   Un-burnt Hydrocarbons   Nitrogen Oxides   Soot/PM

Not Regulated   Regulated Pollutant Species

PRACTICAL COMBUSTION

Figure 1-3: Combustion of a lean hydrocarbon-based fuel with air (Turns 2000).

1.1.2 (a) Carbon Monoxide

Carbon monoxide is a colourless, odourless and tasteless gas. It is usually a product of incomplete combustion of carbon-containing compounds. Inhalation of air with a

volumetric concentration of 0.3% CO could result in serious health consequences (Bosch 1996).

In the hydrocarbon combustion mechanism, the formation of CO is believed to be one of the principal reaction steps. Equation 1-1 summarises the typical hydrocarbon breakdown process where R is the hydrocarbon radical (Heywood 1988). The CO is then oxidised to CO_2 as shown in Equation 1-2, which is a CO oxidation reaction of cardinal significance in hydrocarbon-air flames (Heywood 1988, Turns 2000).

$$RH \rightarrow R \rightarrow RO_2 \rightarrow RCHO \rightarrow RCO \rightarrow CO \qquad\qquad \text{Equation 1-1}$$

$$CO + OH \underset{k_r}{\overset{k_f}{\Leftrightarrow}} CO_2 + H \qquad\qquad \text{Equation 1-2}$$

In single-zone chemical kinetics simulations, the presence of OH intermediate radical species tends to facilitate the oxidation of CO leading to the complete combustion of lean fuel/air mixtures once ignition is attained (Mulenga *et al.* 2003a, 2003b, 2003c). Conversely, in practical applications, the combustion of lean fuel/air mixtures produces high CO and UHC emissions due, in the main, to incomplete conversion attributable to the lowered combustion temperatures. This has been particularly observed in homogeneous charge compression ignition (HCCI) mode of combustion which is discussed further in forthcoming sections.

1.1.2 (b) Un-burnt Hydrocarbons

Un-burnt hydrocarbons are present in a variety of forms that include paraffins, olefins and aromatic hydrocarbons (C_nH_m) while aldehydes ($C_nH_m.CHO$), ketones ($C_nH_m.CO$) and carboxylic acids ($C_nH_m.COOH$) are products of partially-burnt hydrocarbons (Bosch 1996). When exposed to sunlight and nitrous oxides, they react to form oxidants, which could be a source of irritation to mucous membranes while some hydrocarbons are considered to be carcinogenic.

1.1.2 (c) Oxides of Nitrogen

Oxides of nitrogen are basically nitric oxide (NO) and nitrogen dioxide (NO_2) although during combustion, NO is the dominant species produced but is later oxidised to NO_2 in the environment. Pure NO_2 is a poisonous reddish-brown gas with a penetrating odour and the concentrations in exhaust gases and polluted air could induce irritation in the mucous membranes in animals including humans (Bosch 1996, Stone 1999, Turns 2000). Furthermore, in the environment, NO_2 reacts in the presence of ultra-violet light with non-methane hydrocarbons to produce a photochemical smog.

When air is used as the oxidiser, the NO_x yield is affected primarily by the prevailing temperature, oxygen concentration and residence time during the reaction (Stone 1999, Turns 2000). Thermal NO_x formation, which is the general path of NO_x generation in internal combustion engines, could be described by the extended Zeldovich mechanism shown in Equation 1-3a to 1-3b (Stone 1999, Turns 2000).

$$O + N_2 \underset{k_r}{\overset{k_f}{\Leftrightarrow}} NO + N \qquad\qquad\qquad \text{Equation 1-3a}$$

$$N + O_2 \underset{k_r}{\overset{k_f}{\Leftrightarrow}} NO + O \qquad\qquad\qquad \text{Equation 1-3b}$$

$$N + OH \underset{k_r}{\overset{k_f}{\Leftrightarrow}} NO + H \qquad\qquad\qquad \text{Equation 1-3c}$$
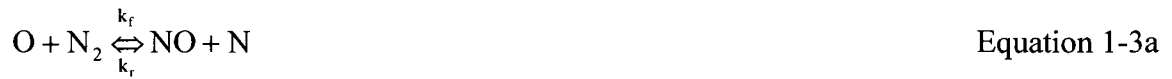
The rate coefficient for Equation 1-3a is believed to have a very large "activation temperature" ($E_A/R_u \sim 38370K$) and thus is extremely temperature-dependent. Using equilibrium assumptions, the characteristic NO formation time, τ_{NO}, may be estimated from Equation 1-4 (Heywood 1988) and the resulting variation with temperature at different pressures is shown in Figure 1-4. As a rule of thumb, the thermal NO_x formation threshold is taken as 1800K (Turns 2000).

$$\tau_{NO} = \frac{8 \times 10^{-16} \times T \times \exp\left(\dfrac{58.3 \times 10^3}{T}\right)}{\sqrt{p}} \qquad\qquad \text{Equation 1-4}$$

Noted, under the prevailing conditions in engine combustion applications, the NO formation process is kinetically controlled (Heywood 1988). Consequently, τ_{NO} is usually comparable to or longer than the times characteristic of changes in engine conditions. Nonetheless, for near-stoichiometric conditions at maximum pressures and burnt gas temperatures, as may be found in the local diesel flame, τ_{NO} is around the 1ms range and equilibrium NO concentrations may be attained.

8
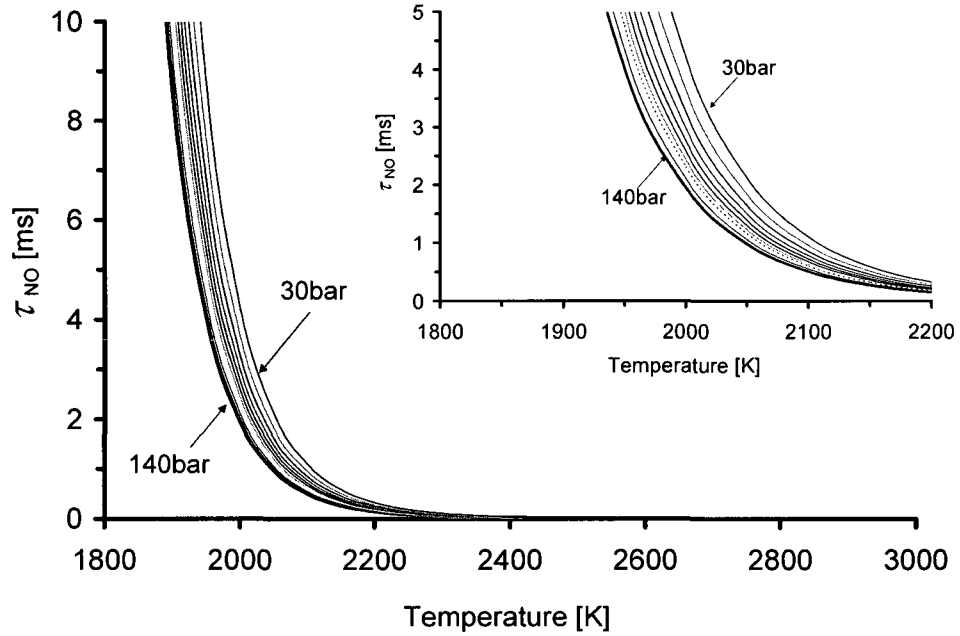
Figure 1-4: Variation of the τ_{NO} with temperature at different pressures.

Conversely, in the fuel-lean ($\lambda > 1.25$) and low temperature conditions the NO_x formation

is believed to occur through the N_2O-intermediate mechanism with the three steps shown

in Equations 1-5a to 1-5c (Turns 2000).

$$O + N_2 + M \underset{k_r}{\overset{k_f}{\Leftrightarrow}} N_2O + M \qquad\qquad \text{Equation 1-5a}$$

$$H + N_2O \underset{k_r}{\overset{k_f}{\Leftrightarrow}} NO + NH \qquad\qquad \text{Equation 1-5b}$$

$$O + N_2O \underset{k_r}{\overset{k_f}{\Leftrightarrow}} NO + NO \qquad\qquad \text{Equation 1-5c}$$

The Fenimore prompt NO mechanism is yet another pathway for NO_x formation. In this

mechanism, the hydrocarbon radicals react with molecular nitrogen to form amines and

cyano compounds which are then converted to intermediate species that ultimately form

NO as shown in Equations 1-6a and 1-6b (Turns 2000):

$$CH + N_2 \underset{k_r}{\overset{k_f}{\Leftrightarrow}} HCN + N \quad \text{(Primary and rate-limiting step)} \qquad \text{Equation 1-6a}$$

$$C + N_2 \underset{k_r}{\overset{k_f}{\Leftrightarrow}} CN + N \quad \text{(Cyno formation step)} \qquad \text{Equation 1-6b}$$
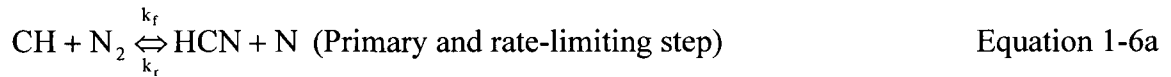
For air/fuel mixture strengths of $\lambda > 0.83$ the conversion of hydrogen cyanide (HCN) to

form NO is believed to follow the chain sequence shown in Equation 1-7 (Turns 2000):

$$HCN + O \underset{k_r}{\overset{k_f}{\Leftrightarrow}} NCO + H \qquad \text{Equation 1-7a}$$

$$NCO + H \underset{k_r}{\overset{k_f}{\Leftrightarrow}} NH + CO \qquad \text{Equation 1-7b}$$

$$NH + H \underset{k_r}{\overset{k_f}{\Leftrightarrow}} N + H_2 \qquad \text{Equation 1-7c}$$

$$N + OH \underset{k_r}{\overset{k_f}{\Leftrightarrow}} NO + H \qquad \text{Equation 1-7d}$$
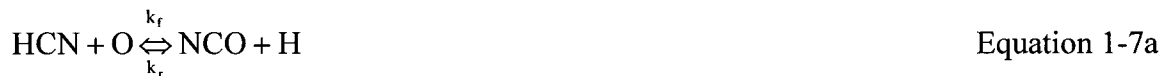
1.1.2 (d) Particulate Matter

Particulate matter are defined as all substances (aside from unbound water), which, under

normal circumstances are present in exhaust gases in a solid (ash, carbon) or liquid state

(Bosch 1996). Particulate matter, therefore, includes smoke, soot, soluble organic fraction

(SOF) and liquid droplets, among others, made up of several different chemical species.

Inhalation of PM could have serious health effects especially when the fine matter penetrates deep into the lung's *alveolar* region affecting pulmonary lung function (Vedal 1995). Particulate matter may also contribute to the development of chronic *bronchitis*, be a predisposing factor to acute bacterial and viral *bronchitis* (especially in sensitive individuals), aggravate *bronchial asthma, pulmonary emphysema* and existing *cardiovascular* disease, have effects on *mucociliary* clearance and other host defence mechanisms and could also promote morphological alteration of lung tissue, which could lead to cancer (Vedal 1995). From the environmental perspective, PM could cause visibility degradation and its soiling effects could have a "nuisance impact".

The primary PM produced in non-premixed internal combustion engines is soot (Heywood 1988 and Turns 2000). Soot forms on the rich side of the diffusion flames through fuel pyrolysis. Therefore, formation of soot is an intrinsic property of diffusion flames. At high temperatures and with availability of oxygen, the soot will be oxidised. The resulting soot emitted, therefore, depends on the competition between soot formation and soot oxidation rates (Akihama *et al.* 2001, Kitamura *et al.* 2003, Miyamoto *et al.* 1990, Turns 2000). For instance, under the low load condition of Figure 1-1, the engine-out soot had a filter smoke number (FSN) of less than 0.01, which is approximately 0.1mg/m^3 soot concentration, because the low amount of in-cylinder soot formed was oxidised with relative ease due to accessibility to the oxygen. In contrast, at the high load condition shown in Figure 1-2, the increased fuelling rate resulted in increased in-cylinder soot formation and decreased accessibility to oxygen thus a high soot level of more than 3FSN (115mg/m^3).

1.1.3 Exhaust Emissions Regulation

It is evident that the exhaust pollutant species discussed above are undesirable. In recent years, more stringent measures have been introduced to reduce emissions of pollutants from combustion processes especially those involving hydrocarbon fuels (EPA 2007). These regulated pollutants include CO, UHC, soot/PM and NO_x. The clean air regulations have led to resolute efforts in search for emission reduction strategies which should result in ultra-low emissions of the toxic species by the year 2010 and beyond. In diesel engine applications, the two main stringent numerical emission limit standards for North America are the Tier II BIN 5 and the EPA 2010 for light duty and on-highway heavy duty vehicles, respectively (Ecopoint Inc. 2007).

1.1.3 (a) Tier II BIN 5 Emission Standard

Under the Tier II regulation, the same emission standards apply to all vehicle weight categories. Essentially, cars, minivans, light-duty trucks and sports utility vehicles (SUVs) have the same emission limit regardless of the fuels they use (Ecopoint Inc 2007). Consequently, vehicles fuelled by gasoline, diesel or alternative fuels all must meet the same standards. Table 1-1 shows the vehicle categories used in the EPA Tier II standards. It is mandated that engines in commercial vehicles above a gross vehicle weight rating (GVWR) of 8500 lbs (3900kg), such as cargo vans or light trucks, should be certified to the heavy duty engine emission standards.

The standards are structured into 8 permanent certification levels of different stringency called certification bins where Bin 1 is the cleanest, Zero Emission Vehicle (ZEV). The

standards specifically restrict emissions of CO, NO$_x$, PM, formaldehyde (HCHO) and non-methane organic gases (NMOG) or non-methane hydrocarbons (NMHC). When tested on the Federal Test Procedure 75 (FTP 75), the full useful life standards are shown in Table 1-2. Note that the fleet average NO$_x$ standard is 0.07g/mi (0.044g/km), which corresponds to Tier II Bin 5. At the time of this dissertation, the North American Automakers were considering the introduction of light-duty diesel-fuelled passenger vehicles on the market hence the Tier II Bin 5 emissions standard was the initial target.

Table 1-1: Vehicle categories employed in EPA Tier II standards (Ecopoint Inc 2007).

Vehicle Category			Abbreviation	Requirements
Light-Duty Vehicle			LDV	max 8000 lb GVWR
Light-Duty Truck	Light light-duty truck		LDT	max 8500 lb GVWR
				max 6000 lb curb weight
				max 45ft^2 frontal area
		LLDT		max 6000 lb GVWR
		Light-duty truck 1	LDT1	max 3750 lb LVW[a]
		Light-duty truck 2	LDT2	min 3750 lb LVW[a]
	Heavy light-duty truck	HLDT		min 6000 lb GVWR
		Light-duty truck 3	LDT3	max 5750 lb ALVW[b]
		Light-duty truck 4	LDT4	min 5750 lb ALVW[b]
Medium-Duty Passenger Vehicle			MDPV	max 10000 lb GVWR[c]
– Gross vehicle weight rating				
(loaded vehicle weight) = curb weight + 300lb				
V (adjusted loaded vehicle weight) = average of GVWR and curb weight				
acturers may alternatively certify engines for diesel fuelled MDPVs through the heavy-duty diesel engine regulations				

14

Table 1-2: Tier II emission standards, FTP 75, g/mi (Ecopoint Inc 2007)

Permanent Bin Number	Full Useful Life				
	NMOG[a]	CO	NOx[b]	PM	HCHO
8	0.125 (0.156)	4.2	0.2	0.02	0.018
7	0.090	4.2	0.15	0.02	0.018
6	0.090	4.2	0.10	0.01	0.018
5	0.090	4.2	0.07	0.01	0.018
4	0.070	2.1	0.04	0.01	0.011
3	0.055	2.1	0.03	0.01	0.011
2	0.010	2.1	0.02	0.01	0.004
1	0.000	0.0	0.00	0.00	0.000

[a] For diesel fuelled engines, NMOG (non-methane organic gases) means NMHC (non-methane hydrocarbons)
[b] Average manufacturer fleet NO_x standard is 0.07g/mi for Tier II vehicles.

1.1.3 (b) EPA 2010 Heavy-duty Diesel Engine Emissions Standards

In the USA, heavy-duty vehicles are defined as vehicles of GVWR of above 8,500 lbs under the federal jurisdiction and above 14,000 lbs in California (model year 1995 and later) (Ecopoint 2007). Diesel engines used in heavy-duty vehicles are further divided into service classes by GVWR, as shown in Table 1-3 while Figure 1-5 shows the numerical NO_x and PM emission trends for heavy-duty diesel engines (EPA 2007). The heavy-duty diesel engine emissions for the model year 2007 to 2010 should comply with 0.14, 15.5, 0.20 and 0.01g/bhp-hr of NMHC, CO, NO_x and PM, respectively.

Table 1-3: EPA heavy-duty diesel engine vehicle category (Ecopoint 2007)

Diesel Engine Category	Abbreviation	min GVWR	max GVWR
Light heavy-duty (California, 1995+)	LHDDE	8500 (14000)	19500 (19500)
Medium heavy-duty	MHDDE	19500	33000
Heavy heavy-duty (including urban bus)	HHDE	>33000	
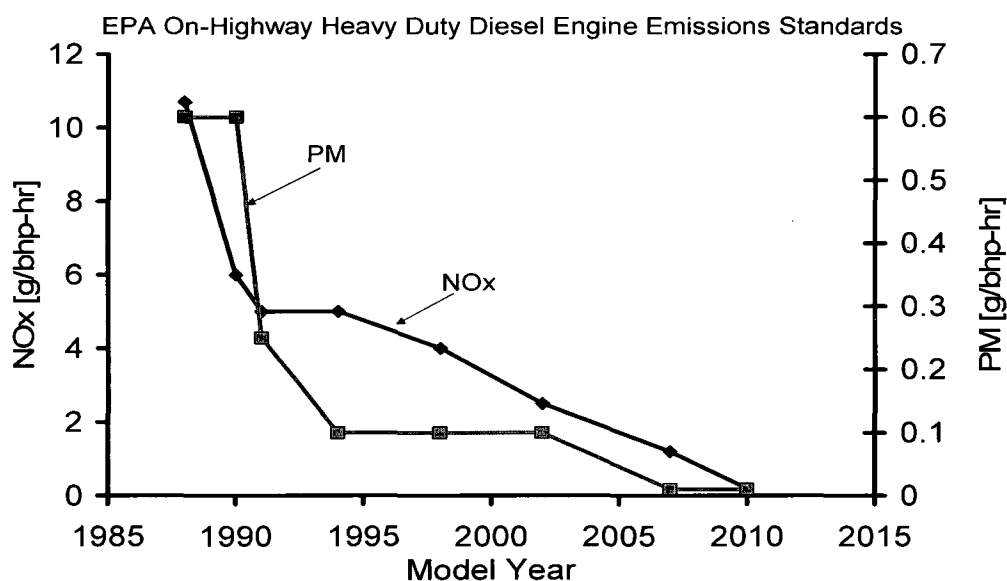
Figure 1-5: Heavy-duty diesel engine emissions standards (EPA 2007).

1.1.4 Emissions from Diesel Engines

A comparison of the diesel and SI exhaust characteristics is shown in Figure 1-6 (Zheng 2002). With respect to the SI engines, the in-cylinder formation of total hydrocarbons (THC), CO and NO_x is high. The THC and CO are formed from the crevice volume and wall quenching effects while the NO_x is formed from the high temperatures attributed to stoichiometric premixed flame propagation. The PM formation is near-zero because of the almost non-existent diffusion burning phase. The tail-pipe emissions are reduced by the effective operation of the Three-Way Catalytic Converter (TWC) owing to the high exhaust gas temperatures of SI engines and lean-to-rich cyclic operation. Conversely, because diesel engines are overall lean-burn systems with local near-stoichiometric high temperature combustion (HTC), the engine-out CO, THC and NO_x levels are much lower than those from SI engines. However, the diffusion-controlled combustion results in increased PM emissions especially at high load conditions. The efficient operation of the TWC is difficult to realise because of the wide load-dependent exhaust temperature range and surplus oxygen. Consequently, diesel after-treatment devices such as diesel oxidation catalysts (DOC), diesel particulate filters (DPF), lean NO_x traps (LNT) and selective reduction catalysts (SCR), among others, are being pursued, in combination with in-cylinder clean diesel combustion strategies, to reduce the tail-pipe emissions from diesel engines (Bosch 1996, EPA 2004, Stone 1999, Zheng *et al.* 2002, 2005).

NO$_x$ (ppm)   THC&CO (ppm)   PM [g/kW-hr]
                10000   0.1

      1000

  300   300   30   0.01
          10

  ▦ Diesel   Texh [°C]
                        ▦ ▧ 800   Exh. O$_2$
  ▧ SI without
    Converter   600
  ▧ SI with   20%
    Converter   350
                        100   5%   0.1%
                                       -0.1%
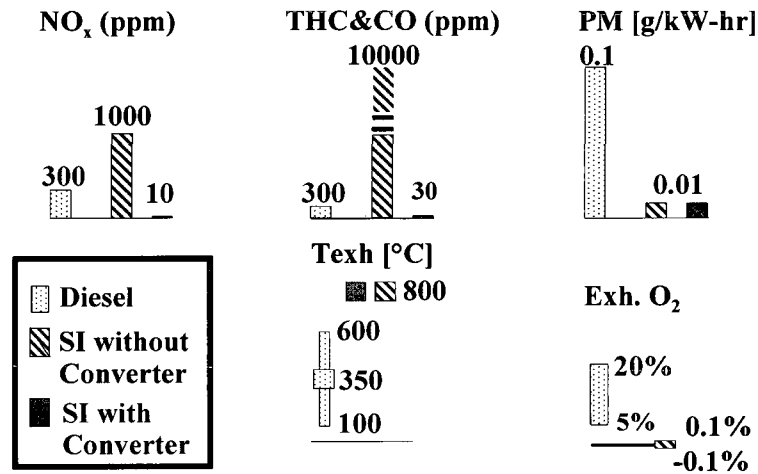
Figure 1-6: Comparison of CI and SI engine exhaust characteristics (Zheng 2002).

1.1.5 The Classical Diesel Dilemma

Even though conventional diesel engines are overall lean-burn systems, the classical

high-temperature heterogeneous nature of the combustion process presents numerous

challenges regarding NO$_x$ and PM emissions reduction. In the classical diesel engines, the

flames tend to initialise in and propagate to regions where the air/fuel ratios are near-

stoichiometric (Flynn *et al.* 1999, Hiroyasu *et al.* 1990, Stone 1999, Zhao *et al.* 1996,

Zheng *et al.* 2004, 2006b). In such combustion processes, therefore, the HTC

predominates resulting in an inherent NO$_x$/PM trade-off as shown in the empirical results

of Figure 1-7 from the Clean Diesel Engine Research Laboratory at the University of

Windsor (Zheng *et al.* 2006b).

18

Engine Type	Classical Diesel	Common-Rail	Common-Rail	Common-Rail
No. of Injections	1	1	2	6
BMEP [bar]	3.4	4.4	6.1	3.6
Fuel Pressure [bar]	NOP: 200	Rail: 1200	Rail: 1200	Rail: 1200
Intake Pressure [bar] (abs)	1	2.75	2.0	2.7
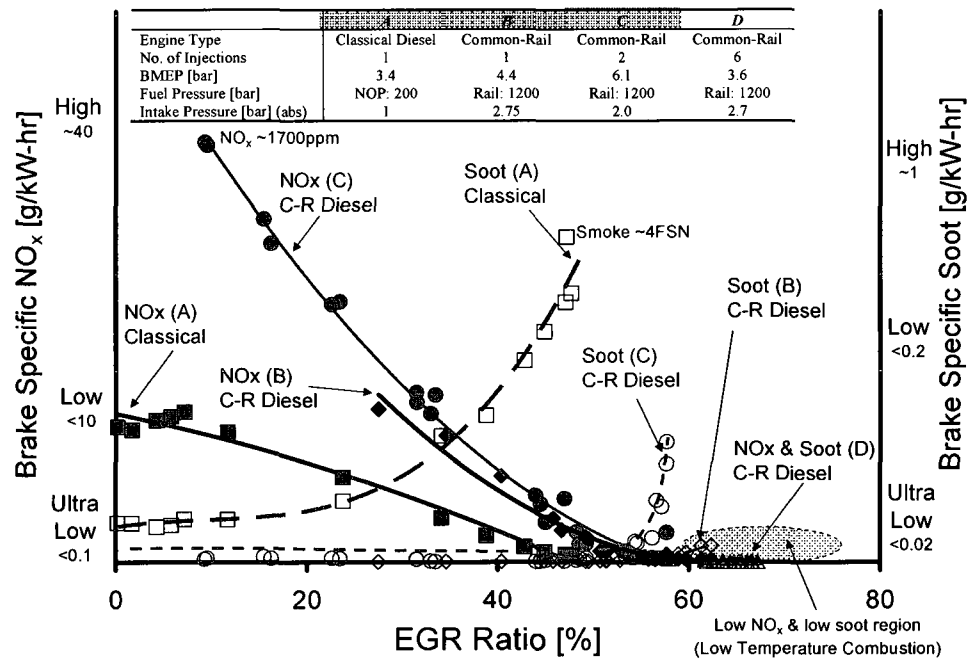
Figure 1-7: Diesel combustion NO_x and soot vs. EGR (Zheng *et al.* 2006b).

In the diesel HTC mode, the use of exhaust gas recirculation (EGR) and injection-timing retard has been effective in reducing in-cylinder NO_x formation. The use of EGR lowers the flame temperature as well as oxygen concentration of the working fluid thereby decreasing the in-cylinder NO_x formation through mainly the thermal, dilution and chemical effects (Zheng *et al.* 2004). However, further increases in EGR tend to increase the soot/PM formation, especially at high load conditions because of the predominant diffusion-controlled combustion where lack of oxygen would lead to soot formation on the rich side of the reaction zone (Flynn *et al.* 1999, Hiroyasu *et al.* 1990, Stone 1999, Turns 2000, Zhao *et al.* 1996, Zheng *et al.* 2004, 2006b).

Injection-timing retard during the compression stroke mainly decreases the ignition delay period resulting in a weaker mixture that burns during the premixed phase of combustion consequently comparatively decreasing the in-cylinder NO_x formation (Akihama *et al.*

2001, Flynn *et al.* 1999, Kitamura *et al.* 2003, Hiroyasu *et al.* 1990, Zhao *et al.* 1996, Zheng *et al.* 2004, 2006b). Further injection-timing retard, however, tends to increase soot formation due to incomplete combustion of fuel pyrolysis products attributed to the decreasing temperatures during the expansion stroke (Jacobs *et al.* 2005).

1.1.6 Solution to the Diesel Dilemma

1.1.6 (a) Low Temperature Combustion

Low temperature combustion (LTC) strategies applied to CI engines, such as HCCI-enabling technologies and smokeless diesel combustion, promise the in-cylinder simultaneous reduction of NO_x and PM (Akihama *et al.* 2001, Bessonette *et al.* 2007, Chen *et al.* 2000, Christensen *et al.* 1999, Helmantel & Denbratt 2004, 2006, Jacobs *et al.* 2005, Kitamura *et al.* 2003, Kodama *et al.* 2007, Kumar *et al.* 2007, Miles 2006, Mulenga *et al.* 2003, Najt 1983, Stanglmaier & Roberts 1999, Su *et al.* 2005, Thring 1989 and Zheng 2002, 2006a, 2006b, 2007b, 2007c, 2007e). One of the means of achieving the diesel LTC mode could be through injection scheduling (including timing) and/or use of high rates of EGR. The resulting increased ignition delay period provides more time for the mixture to reach near-homogeneity and the subsequent combustion could be similar to HCCI mode.

Figure 1-8 illustrates the low NO_x and low soot pathway on a λ-T plane discussed by Zheng *et al.* (2007e). Combustion of a diesel fuel in an excessively lean or rich homogeneous cylinder charge tends to release less heat than under stoichiometric conditions thus the LTC mode prevails. The representative cases for such LTC conditions

are the low-load lean HCCI ($\lambda>2$) and the fuel-rich reforming ($\lambda\approx0.7\sim0.5$) (Akimaha *et al.* 2001 and Zheng *et al.* 2004). In contrast, when the fuel/air ratio is near-stoichiometric the combustion process tends to render high flame temperatures that need to be lowered with heavy EGR in order to qualify for the LTC mode. The representative cases here are the high-load HCCI and the smokeless combustion on the lean or rich side of stoichiometry, respectively (Akimaha *et al.* 2001, Kodama *et al.* 2007 and Zheng *et al.* 2004).
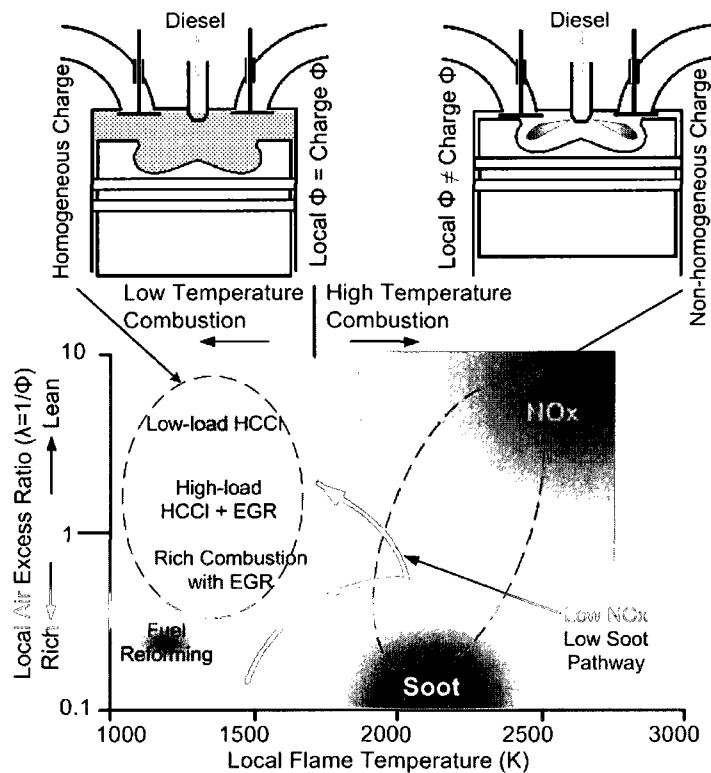
Figure 1-8: 1/ɸ-T plane showing the HTC and LTC pathway (Zheng *et al.* 2007e).

In SI engines the typical ignition delay (τ_{ID}) is in tens of milliseconds (ms), while for conventional diesel engines, it is in fractional to 1 ms range. The τ_{ID} period in LTC mode has been found to be in between the above two, around 5~7ms range (Zheng 2006a). Table 1-4 describes stages during the ignition delay period for conventional diesel HTC

and LTC modes. Note that $\tau_{ID} > 7ms$ would be the HCCI type of combustion. Figure 1-9 depicts the mixing time available from intake valve closing (IVC) to piston top dead centre (TDC) at different engine speeds. The IVC in diesel engines without variable valve actuation normally ranges from 220 to 235°CA thus presenting an engine speed of around 1500rpm as the boundary for the physical and chemical preparation before TDC. This, of course, assumes that the SOI is in the intake port.

Table 1-4: Description of diesel HTC and LTC processes (Zheng 2006a).

	Diesel HTC	Diesel LTC
Physical & Chemical Preparation duration.	0.5~1.5ms of mixing & τ_{ID}.	3~20 ms of fuel to air mixing and early reaction.
Subjected Conditions.	Compression and high temperature.	Low to high temperatures by compression.
Ignition Timing Control.	Directly controllable via injection timing control.	Indirectly moderated by λ, EGR, boost, and injection schedule.
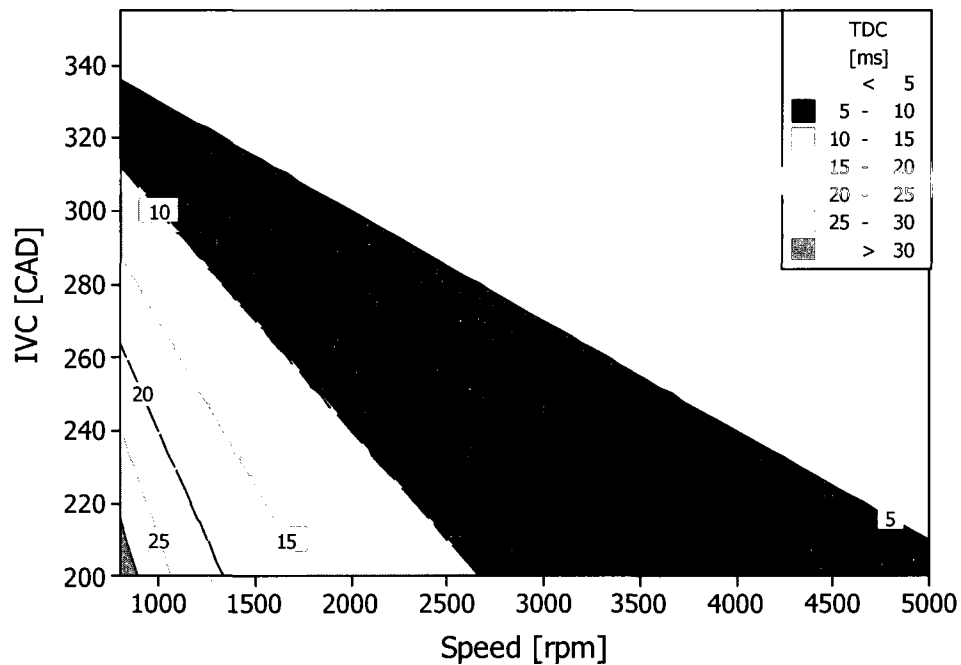
Figure 1-9: Available mixing time [ms] from IVC to TDC at different engine speeds.

1.1.6 (b) Alternative Fuels

The concern over depleting world reserves of fossil fuels, and more stringent emission regulations, have also led to the increased search for alternative fuels. In the USA, alternative fuels as defined by the Energy Policy Act of 1992 (EPAct) include, biodiesel, electricity, ethanol, hydrogen, methanol, natural gas, propane and P-series fuels (EPA 2007). The Government of Canada, through the Natural Resources Canada, lists biodiesel, electricity, ethanol, hydrogen, natural gas and propane as alternative fuels (NRCan 2007). In addition, gas-to-liquid (GTL) fuels, such as those based on the Fischer-Tropsch process, are also being considered as possible alternative fuels.

1.2 Motivation of the Dissertation

In recent years, the concern over depleting world reserves of fossil fuels, energy security and stringent emission regulations for harmful pollutants have led to resolute efforts in search for renewable alternative fuels and ultra-low emission combustion strategies. Biodiesel fuel, which is identified as a clean alternative for conventional diesel fuel, has become commercially available in a number of countries. Because it has characteristics approximately similar to fossil diesel fuel, neat (100%) biodiesel may be directly employed in some diesel engines without prior engine modifications. Whereas biodiesel HTC has met increased research in recent years, to the author's knowledge there is limited published information correlating the in-cylinder combustion characteristics with the engine performance and emissions in biodiesel LTC. The main objective of dissertation was to correlate the combustion process with the engine performance and in-cylinder simultaneous reduction of NO_x and soot in diesel-/biodiesel-fuelled engines.

1.3 Significance of the Dissertation

As discussed in Section 1.1.6, the LTC mode has the capability of simultaneously reducing the in-cylinder formation of NO_x and soot. In compression-ignition engines fuelled with conventional diesel fuels, the LTC mode demonstrates a promising solution to the classical diesel dilemma hence the research is ongoing to explore its potential to facilitate the diesel engine exhaust compliance with the stringent emissions regulations. The identification of innovative clean combustion strategies has also been extended to renewable alternative fuels. Biodiesel is increasingly being considered as part of the solution to the global warming problem. The prospect of biodiesel as a renewable diesel alternative has thus accelerated its use and research in recent years. The author has, therefore, successfully conducted a systematic documentation, through refereed (peer reviewed) publications, of the use of conventional diesel and neat biodiesel fuels in diesel engines in the high and low temperature combustion modes. The analysis in this dissertation has contributed to the understanding of conventional diesel and neat biodiesel combustion as the search for energy-efficient LTC strategies continues with the goal of simultaneously reducing NO_x and soot in diesel engines. The contributions of the dissertation include:

- Conventional diesel and neat biodiesel in-cylinder simultaneous reduction of NO_x and soot was correlated with the heat-release rates and ignition delay period. This presents a platform for the model-based control in diesel-/biodiesel-fuelled engine LTC mode.

- A novel approach to the fuel delivery scheduling commensurate with diesel/biodiesel LTC cycle efficiency proposing the end of fuel condensation time (EFCT).

- Improved the Watson (Stone 1999) ignition delay correlation to include the effects of fuel oxygen, CN and intake O_2 concentration. The new correlation was validated on experimental data.

- An innovative approach to quantify the diesel LTC cycle efficiency in relation to combustion phasing, duration and shaping and the fraction of exhaust UHC with respect to the in-cylinder fuel.

- Demonstration of the use of neat biodiesel fuels without prior engine modifications for emissions and power output. The study contributes to the database of fuel properties and would help biodiesel producers to investigate the engine performance and emissions of their B100 fuels/blends from various feedstocks.

1.4 Dissertation Outline

Figure 1-10 presents the outline of this dissertation. The fundamentals of internal combustion engines are introduced in Chapter II. Thereafter, the literature review, which includes diesel HTC and LTC, diesel fuel properties and alternative fuels such as biodiesel, is discussed in Chapter III. Chapter IV is the core of the dissertation and presents the methodology. The EGR analysis is reported in Chapter V where the excess air-to-fuel ratios for the fresh charge and in-cylinder conditions are analysed and their relationship developed. Chapters VI to IX present the modelling and empirical results. A general discussion, which includes fuel delivery scheduling for LTC and the short- and long-term prospects of biodiesel fuels, is presented in Chapter X. Finally, the conclusions are drawn and recommendations made in Chapter XI.
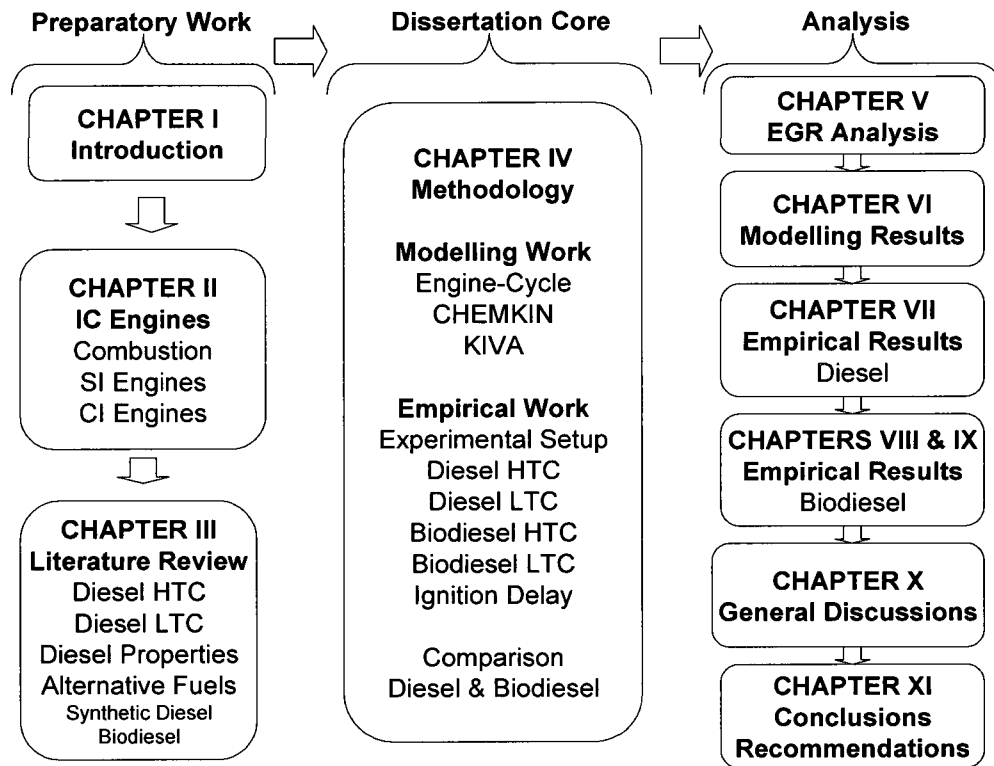
Figure 1-10: Schematic representation of the dissertation outline.

CHAPTER II

INTERNAL COMBUSTION ENGINES

In this Chapter the thermodynamic aspects of internal combustions, which include an introduction to heat engines and the ideal air standard cycles, are first discussed. This is followed by an introduction to the engine mechanical cycle, engine performance characteristics and evaluation of the energy released. Finally, the aspects of spark-ignited and compression-ignited engines are presented.

2.1 Introduction to Heat Engines

Discussing internal combustion engines would be incomplete if the first and second laws of thermodynamics were not introduced. The first law, which is essentially an expression of the conservation of energy principle, states that "energy can be neither created nor destroyed; it can only change forms" (Çengel & Boles 2002). The second law, which asserts that energy has both quality and quantity, states that processes occur in a specific direction of energy. It is therefore inferred that work can be converted to heat directly and completely however converting heat to work requires the use of an external device called a heat engine. Even though there are several types of heat engines, their operation can be characterised by Figure 2-1.

In practical applications, the implementation of the high temperature source results in increased thermodynamic cycle efficiency. Nonetheless, this results in increased NO_x formation especially if a combustor is employed. The low temperature sink, on the other hand, is associated with the complicacy of design and implementation for instance the

turbocharger. The most common gas power cycles discussed in internal combustion engines are the Otto, Diesel and Dual cycles, which are introduced below.
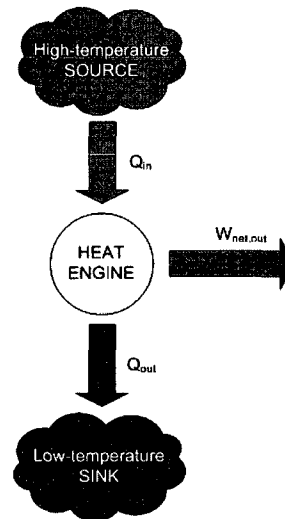
Figure 2-1: Characteristics of a heat engine (Çengel & Boles 2002).

2.1.1 Ideal Air Standard Otto Cycle

The Otto cycle, shown in Figure 2-2, is used as basis of comparison for spark ignition engines, small high-speed direct injection (HSDI) diesel engines without in-cylinder NO_x control and HCCI mode of combustion. The non-flow processes are:

1 to 2: Isentropic compression (Work done on the gas W_{in})

2 to 3: Constant volume heat addition (Q_{in})

3 to 4: Isentropic expansion (Work done by the gas W_{out})

4 to 1: Constant volume heat rejection (Q_{out})
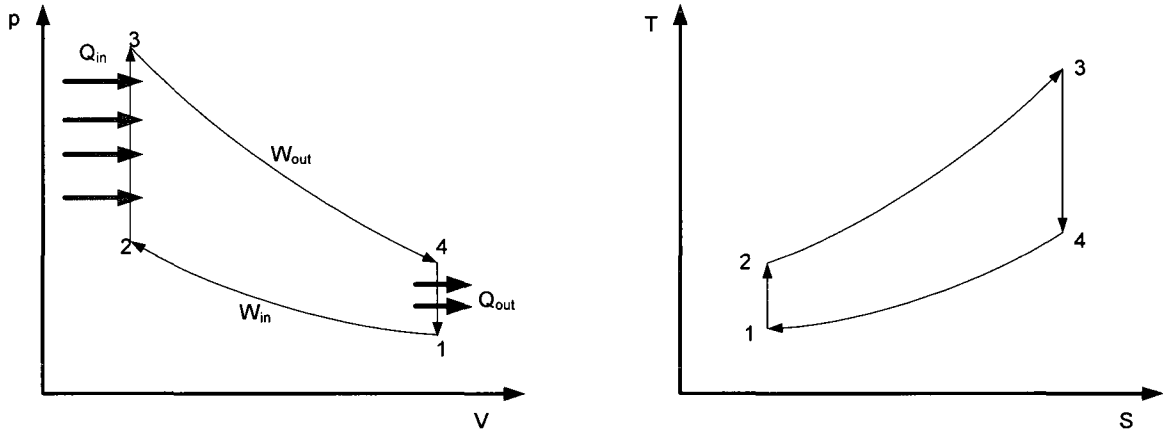
Figure 2-2: Ideal Air Standard Otto cycle (Çengel & Boles 2002).
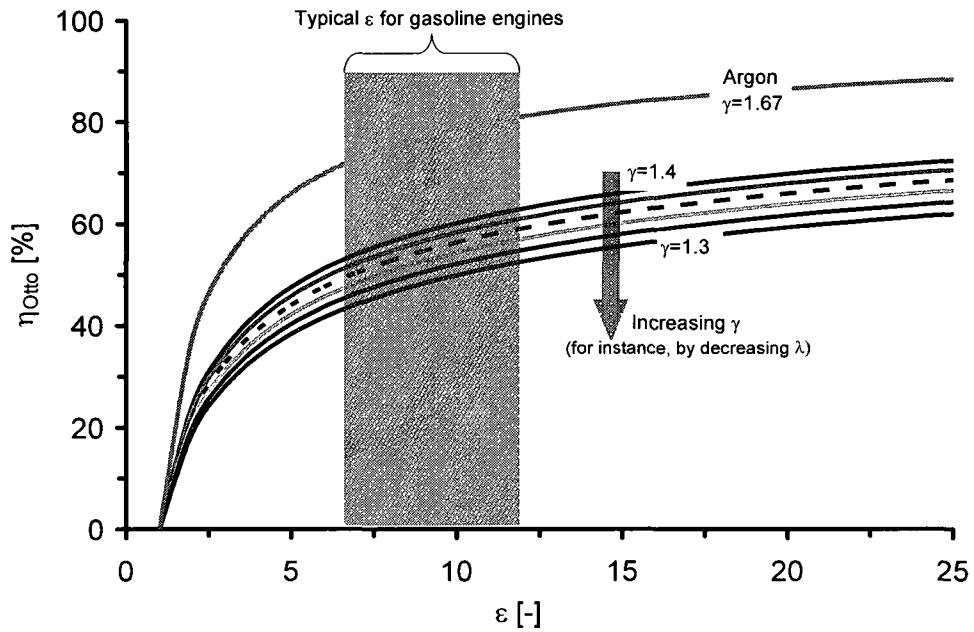
Figure 2-3: Variation of Otto cycle thermal efficiency with compression ratio.

The thermal efficiency of the Otto cycle depends on the compression ratio, ε, and the ratio of specific heats, γ as shown in Equation 2-1 (Stone 1999). Figure 2-3 shows the variation of η_{Otto} with ε and γ.

$$\eta_{Otto} = 1 - \frac{1}{\varepsilon^{\gamma-1}}$$

Equation 2-1

29

The constant volume heat addition of the ideal Otto cycle is similar to the simultaneous mixture auto-ignition in HCCI engines. Unfortunately, this type of combustion produces very high pressure-rise rates, $dP/d\theta$, which are translated into engine combustion noise. In production diesel engines, the maximum rate-of-pressure rise is limited to 10~15bar/°CA. The increase in EGR helps to lower the $(dP/d\theta)_{Max}$, especially when heavy to excessive EGR is applied. However, the engine usually suffers from unstable operation and incomplete combustion that is indicated by the elevated UHC and CO emissions. Nevertheless, the heavy use of EGR has been applied as the *de facto* primary practice to reduce the combustion noise for either the thoroughly mixed or the partially mixed homogeneous charge combustion processes under high loads.

2.1.2 Ideal Air Standard Diesel Cycle

The Diesel cycle, shown in Figure 2-4, may be representative of the combustion in large compression-ignition engines, such as marine engines, where the fuel injection is arranged in such a way that combustion occurs at approximately constant pressure to limit the peak pressure (Stone 1999). The non-flow processes are:

1 to 2: Isentropic compression

2 to 3: Constant pressure heat addition while the volume expands through a ratio V_3/V_2, the cut-off or load ratio, α.

3 to 4: Isentropic expansion

4 to 1: Constant volume heat rejection
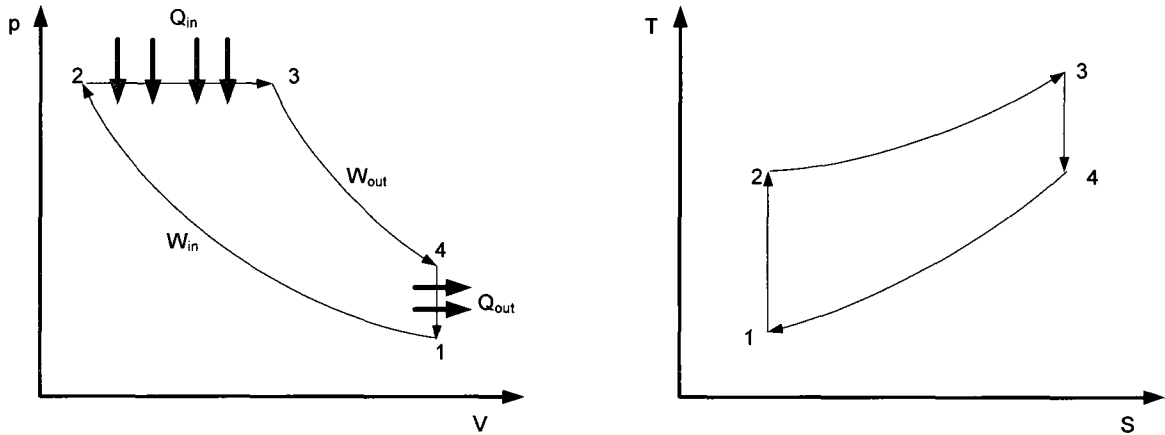
Figure 2-4: Ideal Air Standard Diesel cycle (Çengel & Boles 2002).

The thermal efficiency of the Diesel cycle depends on ε, γ and α as presented in Equation 2-2 (Stone 1999). Figure 2-5 shows the variation of η_{Diesel} with ε and α.

$$\eta_{Diesel} = 1 - \frac{1}{\varepsilon^{\gamma-1}} \left[\frac{\alpha^{\gamma} - 1}{\gamma(\alpha - 1)} \right]$$

Equation 2-2
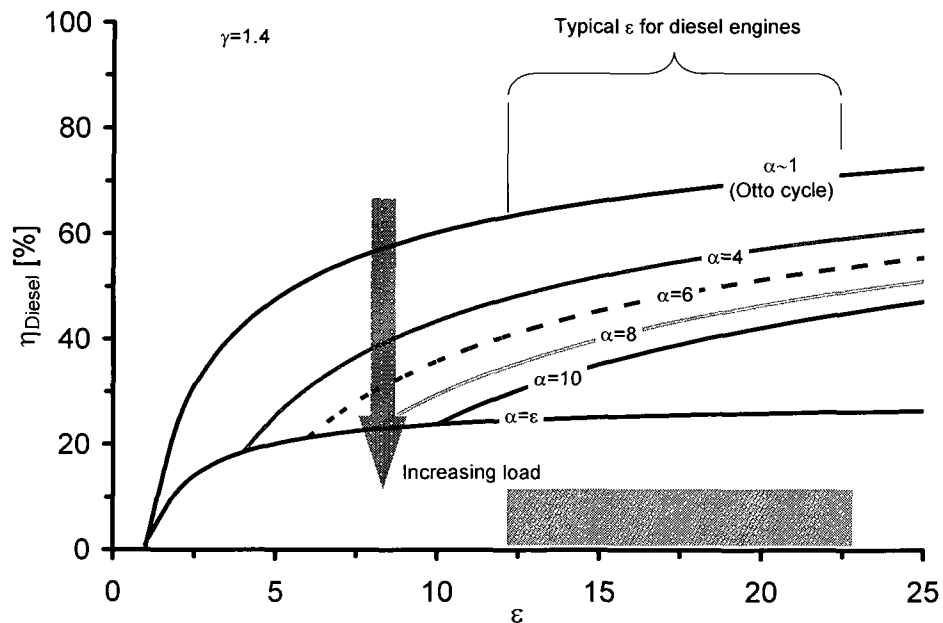
Figure 2-5: Variation of Diesel cycle thermal efficiency with ε and α (Stone 1999).

Under peak load with high boost conditions in diesel engines, the peak combustion pressures have to be moderated to avoid failure of the mechanical structure. This is achieved by injection strategies that produce near-constant pressure combustion i.e. $P_2 \approx P_3$ in Figure 2-4.

2.1.3 Ideal Air Standard Dual Cycle

In practical applications, combustion does not occur at constant volume or constant pressure. A combination of the Otto and Diesel cycles, known as the Dual, Limited Pressure or Mixed cycle is introduced as shown in Figure 2-6 (Çengel & Boles 2002, Stone 1999). The non-flow processes are:

1 to 2: Isentropic compression

2 to 3: Constant volume heat addition with pressure ratio $r_p = p_3/p_2$

3 to 4: Constant pressure heat addition through α.

4 to 5: Isentropic expansion

5 to 1: Constant volume heat rejection
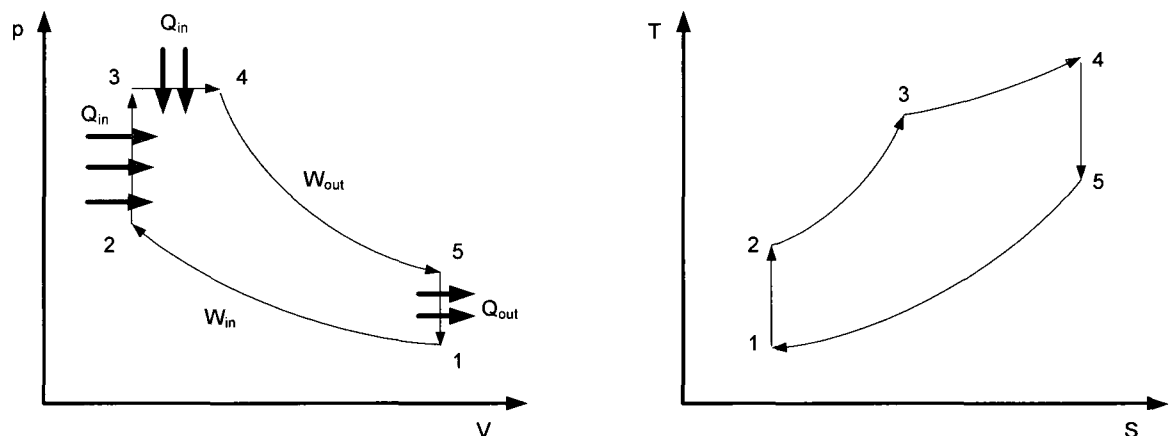
Figure 2-6: Ideal Air Standard Dual cycle (Çengel & Boles 2002).

The thermal efficiency of the Dual cycle depends on ε, γ, α and r_p (Stone 1999):

$$\eta_{Dual} = 1 - \frac{1}{\varepsilon^{\gamma-1}}\left[\frac{r_p\alpha^{\gamma} - 1}{\left(r_p - 1\right) + \gamma r_p\left(\alpha - 1\right)}\right] \qquad \text{Equation 2-3}$$

Under high load conditions in diesel engines, the constant volume heat addition of the Dual cycle (Step 2-3) could correspond to the premixed phase of combustion introduced in Figures 1-1 and 1-2. The constant pressure heat addition (Step 3-4), however, could correspond to the diffusion phase.

The ideal air standard cycles are primarily used as a basis for improvement of the internal combustion engines. Nonetheless, the internal combustion engines, which are work-producing devices, do not operate in a thermodynamic cycle. They operate, instead, in a mechanical cycle since the working fluid does not undergo a complete cycle as in thermodynamic cycles.

2.2 Engine Mechanical Cycle

Figure 2-7 presents the pressure vs. crank angle (p-θ) for a typical four-stroke internal combustion engine. Figure 2-8 shows the corresponding pressure vs. volume diagram. These plots were obtained from the Yanmar NFD170 single cylinder DI diesel engine in the Clean Diesel Engine Research Laboratory at the University of Windsor.

Conventionally, the p-θ diagram is measured directly from engine dynamometer tests. The cylinder pressures are usually acquired with the help of a pressure transducer and the engine crank angle position by an encoder. In practice the V-θ relationship shown in Equation 2-4 is used to convert the p-θ diagram to the p-V diagram i.e. from Figure 2-7 to Figure 2-8.

$$V = V_c \left[1 + \frac{1}{2}(\varepsilon - 1) \left(1 - \cos\theta + \frac{l}{a} - \sqrt{\left(\frac{l}{a}\right)^2 - \sin^2\theta} \right) \right] \qquad \text{Equation 2-4}$$

where V_c is the combustion chamber volume, ε is the compression ratio, l is the connecting rod length, a is the crank radius (i.e. ½ the piston stroke) and θ is the engine crank angle.
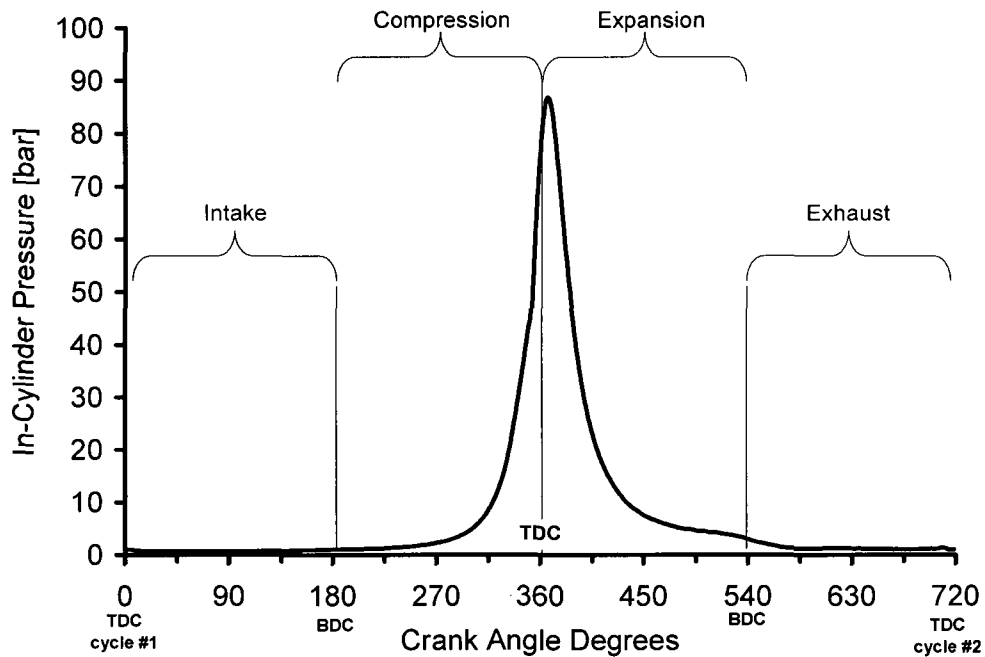
Figure 2-7: The four strokes of a conventional internal combustion engine.

34
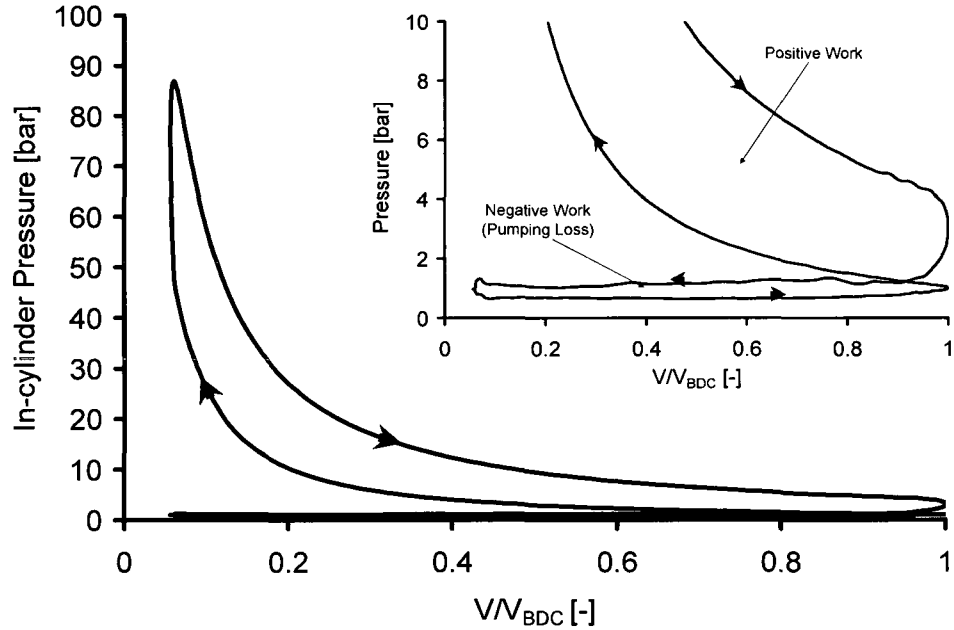
Figure 2-8: Cylinder pressure vs. volume for a naturally-aspirated 4-stroke CI engine.

The work done by the gases on the piston, indicated work W_{ind}, is represented by the area enclosed on the p-V curve. The indicated mean effective pressure, IMEP, is a measure of the indicated work output per unit swept volume.

$$W_{ind} = \oint PdV$$ Equation 2-5

$$IMEP = \frac{W_{ind}}{V_s}$$ Equation 2-6

The pressure and volume during the compression and expansion processes of gases are usually governed by the relation pV^n=constant where n is a constant (Çengel & Boles 2002). When a system undergoes a process that obeys this relation it is referred to as a polytropic process and n is the polytropic constant.

$$p_1 V_1^n = p_2 V_2^n = pV^n$$ Equation 2-7a

which becomes

35

$$\frac{p_1}{p_2} = \left(\frac{V_2}{V_1}\right)^n$$
Equation 2-7b

In terms of the natural log, Equation 2-7b becomes

$$\ln\left(\frac{p_1}{p_2}\right) = n\ln\left(\frac{V_2}{V_1}\right)$$
Equation 2-7c

Plotting the p-V diagram on a logarithmic basis yields some interesting results as seen in Figure 2-9 (Stone 1999):

- The pumping loop can be seen more clearly (an alternative to linear magnification in Figure 2-8).

- The compression process is a straight line hence the assumption of polytropic process is reasonable (*n* from IVC to SOI was 1.38 for this case).

- Departure from a straight line just before TDC indicates the SOC.
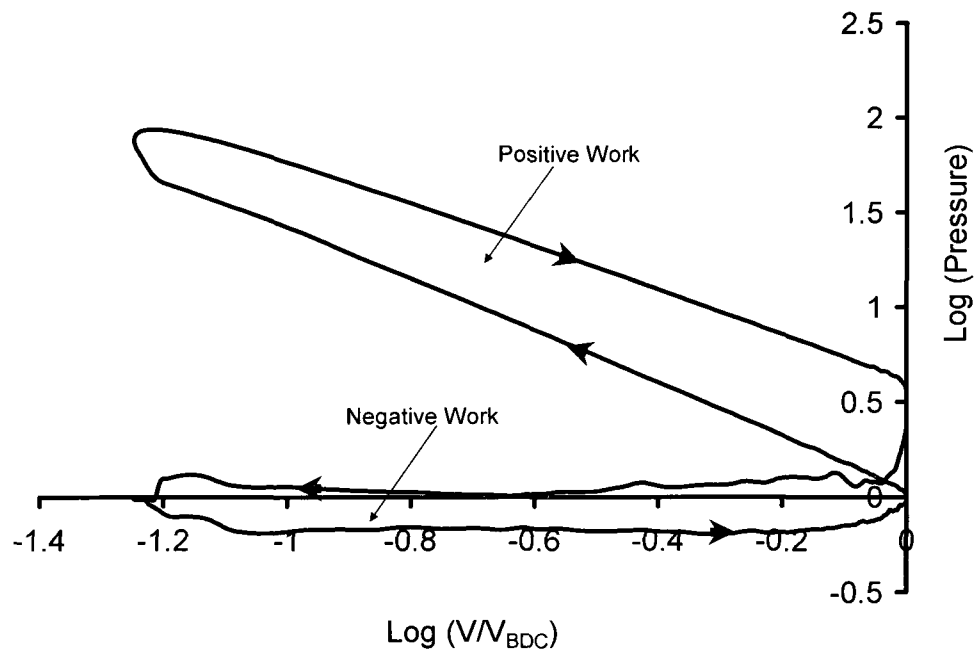
Figure 2-9: Logarithmic pressure vs. volume for a naturally-aspirated 4-stroke CI engine.

36

2.2.1 Engine Performance Characteristics

The engine fuel efficiency is commonly represented in the Brake Specific Fuel Consumption (BSFC), which is the net fuel consumption rate, $\dot{m}_f$ [g/s] divided by the effective power at the shaft (brake power) [kW].

$$BSFC = \frac{3600 \times \dot{m}_f}{\dot{W}} \text{ [g/kW-hr]} \qquad \text{Equation 2-8}$$

The brake thermal efficiency of the engine is the brake power divided by the rate of fuel energy supplied into the cylinders:

$$\eta_{Brake} = \frac{\dot{W}}{\dot{m}_f \times LHV} = \frac{360000}{LHV \times BSFC} \text{ [\%]} \qquad \text{Equation 2-9}$$

In diesel HTC without in-cylinder NO_x control mechanisms, the input fuel energy conversion may be estimated as 1/3 to the brake power, 1/3 to the auxiliaries and 1/3 to the exhaust (Zheng 2002). The engine load is normally evaluated from the Brake Mean Effective Pressure (BMEP) which represents the engine shaft Torque [Nm] on per engine displacement (V_d [m^3]) per cycle

$$BMEP = \frac{4\pi \times Torque}{100000 \times V_d} \text{ [bar]; for a 4-stroke engine} \qquad \text{Equation 2-10}$$

For diesel engines at a fixed engine speed, it is common practice to use the relative load level as:

$$Relative\ Load = \frac{BMEP}{BMEP_{Max}} = \frac{Torque}{Torque_{Max}} \qquad \text{Equation 2-11}$$

37

For a single-cylinder engine or a single cylinder of a multi-cylinder engine, however, the indicated performance is more commonly evaluated so as to exclude the power loss discrepancies of the auxiliary equipment (Zheng 2002, 2006a). The indicated power of the single cylinder could be derived from the net area enclosed by the p-V trace W_i [kJ] multiplied by the firing rate of the cylinder:

$$\dot{W}_i = \frac{N \times W_i}{120} = \frac{100 \times IMEP \times V_d \times N}{120} \ [kJ] \qquad \text{Equation 2-12}$$

for 4-stroke engines; N is the engine speed [rpm] and IMEP is in [bar].

Similarly, the indicated specific fuel consumption (ISFC) can be determined from

$$ISFC = \frac{3600 \times \dot{m}_f}{\dot{W}_i} = \frac{3600 \times m_f}{W_i} \ [g/kW\text{-}hr] \qquad \text{Equation 2-13}$$

and the indicated thermal efficiency from:

$$\eta_i = \frac{W_i}{LHV \times m_f} = \frac{\dot{W}_i}{LHV \times \dot{m}_f} = \frac{360000}{LHV \times ISFC} \ [\%] \qquad \text{Equation 2-14}$$

Assuming sufficient boost, inter-cooling and EGR cooling, the amount of fresh air taken to the cylinder can be estimated from the cylinder displacement V_d, the density of the fresh air ρ_a [g/m^3], the boost ratio ξ, the intake volumetric efficiency η_{Vol} and the EGR ratio r_{egr}:

$$m_a = \left(1 - r_{egr}\right) \times m_{int} = \left(1 - r_{egr}\right) \times \eta_{Vol} \times \xi \times \rho_a \times V_d \ [g] \qquad \text{Equation 2-15}$$

From the definition of excess air-to-fuel ratio λ (Stone 1999) and Equation 2-15,

$$m_f = \frac{m_a}{\lambda} \times \left(\frac{m_f}{m_a}\right)_s = \left(\frac{m_f}{m_a}\right)_s \times \frac{(1 - r_{egr}) \times \eta_{Vol} \times \xi \times \rho_a \times V_d}{\lambda} \quad [g]$$ Equation 2-16

Then the theoretical IMEP can be evaluated thus

$$IMEP = \frac{LHV}{100} \times \left(\frac{m_f}{m_a}\right)_s \times \frac{\eta_i \times (1 - r_{egr}) \times \eta_{Vol} \times \xi \times \rho_a}{\lambda} \quad [bar]$$ Equation 2-17

With a conventional diesel fuel of LHV 42.9kJ/g and a stoichiometric air-to-fuel ratio of 14.6:1 the expression for the expected IMEP is shown in Equation 2-18 (Zheng 2002, 2006a)

$$IMEP = 0.029 \frac{\eta_i \times (1 - r_{egr}) \times \eta_{Vol} \times \xi \times \rho_a}{\lambda} \quad [bar]$$ Equation 2-18

The variation of IMEP with λ is shown in Figure 2-10 and Figure 2-11 with EGR and boost sweeps, respectively. Noted, the in-cylinder λ decreases with increasing EGR as shown in Figure 2-12 and demonstrated in Chapter V. Furthermore, the IMEP is limited by the maximum pressure that the mechanical structure could safely sustain. To date advanced production engines can conveniently achieve up to 22~25bar IMEP in conventional diesel cycles. It is not uncommon to find modern heavy-duty diesel engines operating at a peak cylinder pressure of 180bar.

Assumptions
η_{Ind}: 52%
η_{Vol}: 85%
P_{intake}: 1bar (abs)
ξ: 1
ρ_a: 1.29kg/m3
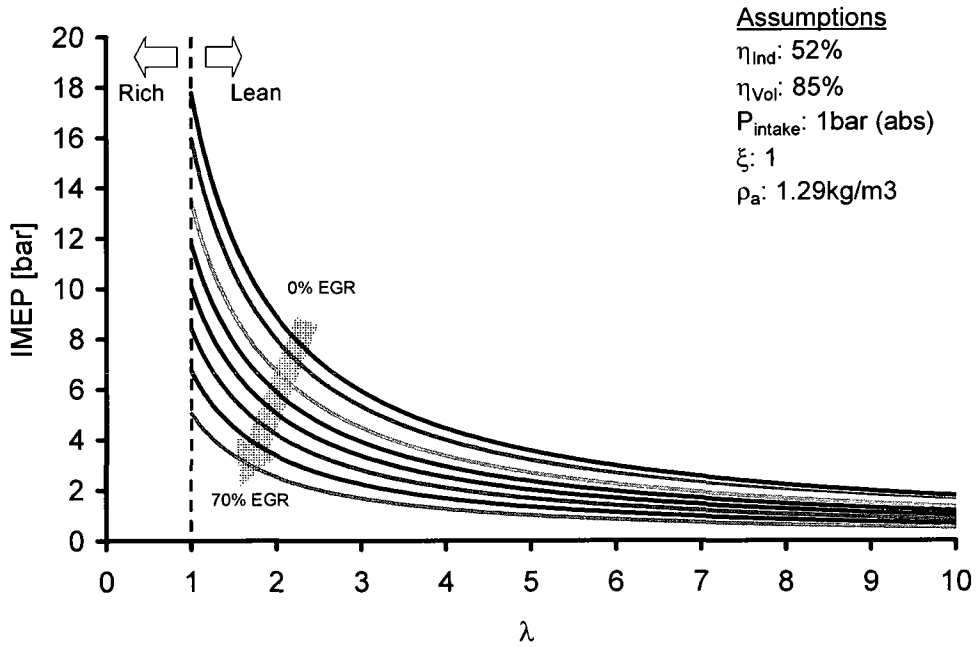
Figure 2-10: Effect of fuel/air mixture strength and EGR ratio on IMEP.
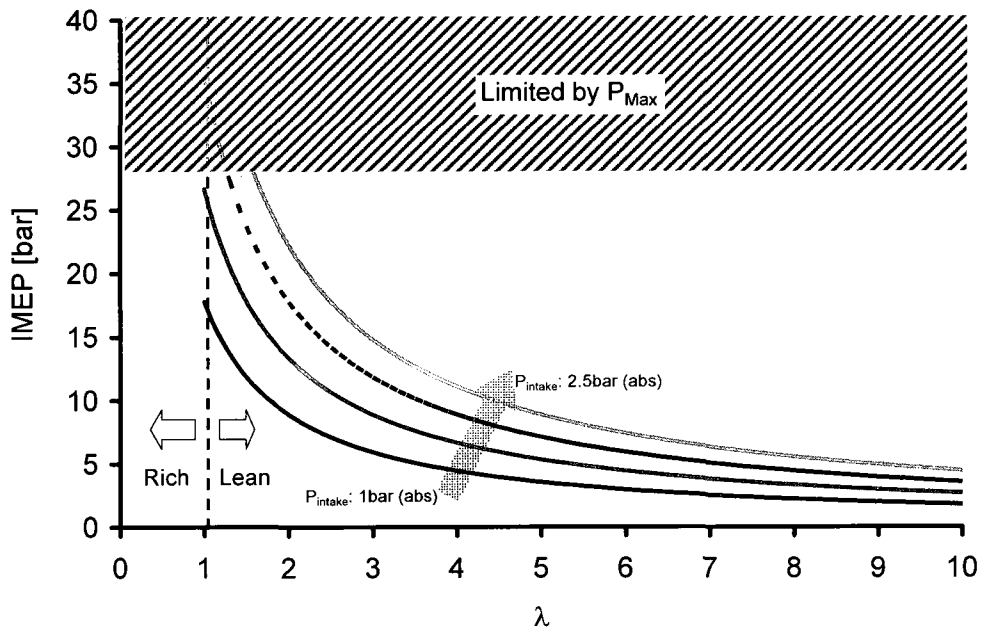
Figure 2-11: Effect of λ and boost pressure on IMEP at 0% EGR.

40
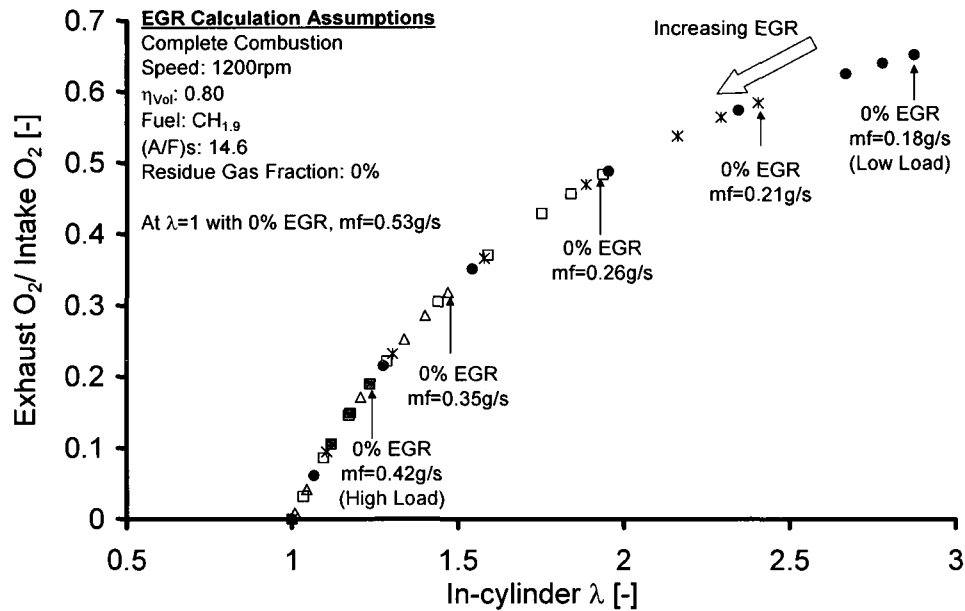
Figure 2-12: Oxygen ratio across the engine vs. in-cylinder mixture strength.

In addition to the relative load, the λ is also an indicator of the load level but is affected by the EGR and boost levels. In stark contrast, the O_2 ratio and CO_2 ratio across the engine also indicate the engine load while largely independent of boost and EGR levels (Figure 2-12).

2.2.2 Evaluating the Energy Released

To calculate the mass fraction burnt in spark ignition engines, the burn rate is usually applied to the combustion data (Stone 1999). In diesel engine applications, on the contrary, the heat-release analysis is normally applied. This evaluates how much heat would have to be added to the cylinder contents so as to produce the observed pressure variations. When the power producing cycle of the engine is of interest, the effect of the gaseous exchange process may be neglected and the heat-released is evaluated during the compression and expansion strokes up to the maximum total cumulative energy.

Assuming that the cylinder contents are fully mixed, the first law of Thermodynamics can be applied during the IVC and EVO (i.e. closed system of this control volume) in which there is no mass transfer. The heat released by combustion δQ_h is given by (Stone 1999):

$$\delta Q_{hr} = dU + \delta W + \delta Q_{ht} \qquad\qquad \text{Equation 2-19}$$

where δQ_{ht} is the heat transfer with the combustion chamber walls. Evaluating each of the terms in Equation 2-16:

$$dU = mc_v dT \qquad\qquad \text{Equation 2-20}$$

From the Equation of State for an ideal gas (pv=mRT)

$$mdT = \frac{1}{R}(pdV + Vdp) \qquad\qquad \text{Equation 2-21}$$

Substitution gives

$$dU = \frac{c_v}{R}(pdV + Vdp) \qquad\qquad \text{Equation 2-22}$$

Further substitution and noting that $\delta W = pdV$ gives on an incremental angle basis

$$\frac{Q_{hr}}{d\theta} = \frac{c_v}{R}\left(p\frac{dV}{d\theta} + V\frac{dp}{d\theta}\right) + p\frac{dV}{d\theta} + \frac{dQ_{ht}}{d\theta} \qquad\qquad \text{Equation 2-23}$$

The final simplified form for the heat-release analysis becomes

$$\frac{dQ_{hr}}{d\theta} - \frac{dQ_{ht}}{d\theta} = \frac{dQ_n}{d\theta} = \frac{1}{(\gamma-1)} \times \left[\gamma p\frac{dV}{d\theta} + V\frac{dp}{d\theta}\right] \qquad\qquad \text{Equation 2-24}$$

where $dQ_{hr}/d\theta$ is the heat release rate by combustion, $dQ_{ht}/d\theta$ the heat transfer rate with the cylinder wall, $dQ_n/d\theta$ is the net heat released, θ is the engine crank angle, γ the ratio of specific heats, and p and V the instantaneous cylinder pressure and volume, respectively. The normalised heat-release rate obtained from Equation 2-24 was compared with that obtained by other techniques including an in-house programme which

considers heat transfer and variable charge properties (Zheng & Reader 1996). The

phasing was found to be within ±1°CA and the results were in reasonable agreement

(Zheng 2006a). The heat-release rates presented in this dissertation were, therefore,

normalised by the maximum cumulative energy that was evaluated from the IVC to EVO

as shown in Figure 2-13.
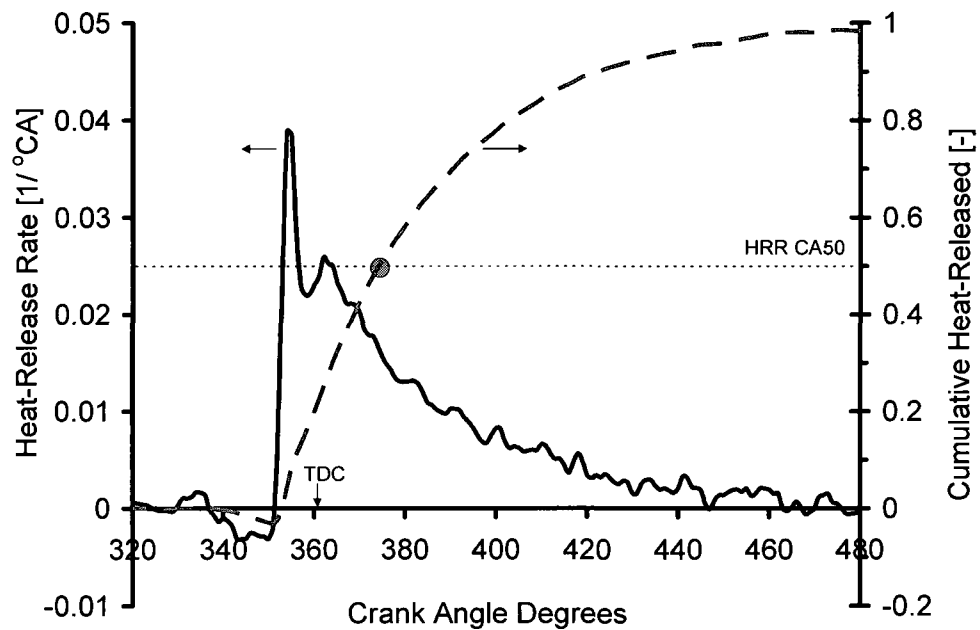
Figure 2-13: Normalised heat-release rate for a 4-stroke CI engine.

The heat-release analysis could be directly employed to evaluate the efficiency and the

effect of the combustion process. Furthermore, the heat-release analysis could be utilised

to assess the production of soot thus correlated to the emissions control strategies.

2.3 Aspects of Spark-Ignited Engines

Since the early internal combustion engine development in the 1600s improvements have

been made that involved increased power output, fuel economy and thermal efficiency

and reduced emissions, among others. Conventional internal combustion engines are the SI for instance gasoline or petrol engines and the CI such as diesel engines.

In SI engines, a premixed fuel/air mixture is compressed in the cylinder and a spark introduced near TDC that initiates a flame and subsequent mixture combustion as earlier discussed. These engines are operated at/near stoichiometric conditions and thus in-cylinder formation of NO_x is high but soot/PM formation is low due to premixed combustion. In-cylinder CO and UHC formation is also high due mainly to crevice volume and wall quenching effects, however, tail-pipe emissions of SI engines in automotive applications are mitigated through the use of flow-through TWC converters. The operation of the TWC is threefold, as the name suggests:

- Oxidation of the CO to CO_2.

- Oxidation of the UHC to produce CO_2 and H_2O.

- Chemical reduction of NO to produce N_2.

To achieve efficient operation of the TWC converter, SI engines are operated in a cyclic rich/lean mode. In the lean mode, the excess oxygen is utilised to oxidise the CO and UHC over a platinum/rhodium catalyst. Catalyst light-off in SI engines is achievable with relative ease because the exhaust gas temperatures are comparatively high as shown in Figure 1-6. Conversely, in the rich mode i.e. oxygen-deficient environment, the catalyst promotes the chemical reduction of NO_x by reactions involving HC and CO. The governing chemical equations for the complete oxidation of HC and CO are shown in

Equations 2-25 and 2-26 and those for the chemical reduction of NO_x in Equations 2-27 and 2-28 (Stone 1999).

$$4HC + 5O_2 \rightarrow 4CO_2 + 2H_2O \qquad \text{Equation 2-25}$$

$$2CO + O_2 \rightarrow 2CO_2 \qquad \text{Equation 2-26}$$

$$4HC + 10NO \rightarrow 4CO_2 + 2H_2O + 5N_2 \qquad \text{Equation 2-27}$$

$$2CO + 2NO \rightarrow 2CO_2 + N_2 \qquad \text{Equation 2-28}$$

The close control is achieved by electronic fuel injection (EFI) systems, with a lambda sensor to provided feedback by measuring the oxygen concentration in the exhaust. Stone (1999) reported that a typical air/fuel perturbation of ±0.25 (or ±0.02ϕ) from stoichiometric is employed.

2.4 Aspects of Compression-Ignited Engines

In CI engines on the other hand, air is drawn into the cylinder, compressed to relatively high compression ratios and diesel fuel injected near TDC. Combustion is initiated by auto-ignition and mainly dictated by diffusion processes and thus leading to increased in-cylinder NO_x and soot formation. In-cylinder NO_x formation is generally reduced by EGR and injection-timing retard while PM is reduced by enhanced premixed combustion but the challenge still exists due to the NO_x/PM formation trade-off. The use of TWCs as after-treatment devices for diesel engines is met with two main challenges namely relatively lower exhaust temperatures to effect catalytic light-off and availability of

oxygen that would impede the chemical reduction of NO_x. Instead, other devices are being researched and some are already in use as discussed below.

Selective Catalytic Reduction (SCR) techniques utilise ammonia (NH_3) or urea ($CO(NH_2)_2$) injection into the exhaust stream. The primary selective reaction in the SCR systems is expressed in Equation 2-29, which is believed to be promoted by the catalyst over the competitive reaction of NH_3 with the abundant O_2 (Ecopoint Inc. 2007). The main advantage of the SCR systems is the high NO_x conversion efficiency reaching up to 90% (Stone 1999). The disadvantages of the SCR systems, however, include high capital and operating cost, space requirements, generation of ammonia emissions (ammonia slip) and fouling of equipment with ammonium sulphate, which is a hazardous waste (Ecopoint Inc. 2007).
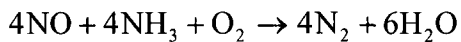
$$4NO + 4NH_3 + O_2 \rightarrow 4N_2 + 6H_2O \qquad\qquad \text{Equation 2-29}$$

In large stationary diesel engines, which usually operate at steady-state conditions, the SCR systems have been successfully adapted to ameliorate the tailpipe NO_x emissions. Conversely, the transient driving characteristics in mobile applications require a sophisticated active SCR system which would include accurate NO_x sensing technology, high reductant dispersion technology (urea/ammonia atomiser) and a wide catalyst operability range. Furthermore, the reductant fuelling infrastructure has to be available. Table 2-1 summarises typical active SCR component malfunctions with their respective immediate implications on the tailpipe emissions. Noted, a maldistribution of the

CHAPTER II – INTERNAL COMBUSTION ENGINES

reductant and no catalytic light-off (mainly due to low operation temperatures) would result in the NO_x emissions and reductant slipping to the environment.

Table 2-1: Active SCR component malfunction and tailpipe emission implications.

Active SCR Component	Component Malfunction	Affected Characteristics	Tailpipe Emissions
NO_x sensor	Lower NO_x reading.	Lowered reductant injection rate.	NO_x slip.
	Higher NO_x reading.	Increased reductant injection rate.	Reductant slip.
Atomiser	Poor reductant dispersion.	Poor chemical reduction process.	• NO_x slip. • Reductant slip.
Catalyst	Low temperature.	No catalytic light-off.	• NO_x slip. • Reductant slip.

Lean NO_x Trap (LNT) where the TWC is combined with a NO_x-absorbing material (Barium Carbonate, $BaCO_3$) to store the NO_x when the engine is operating in lean-burn mode. When the engine operates under rich conditions the NO_x is released from the storage media and chemically reduced by the TWC (Stone 1999). However, it is uncommon for diesel engines to operate under rich conditions hence supplemental fuel may be injected in the exhaust to achieve the rich condition under active flow after-treatment strategies as shown in Figure 2-14 where CDPF stands for Catalytic Diesel Particulate Filter (Zheng *et al*. 2005). The use of supplemental fuel may result in a fuel consumption penalty.
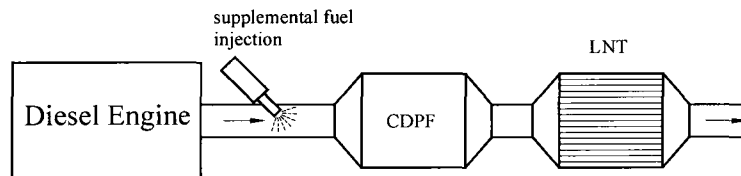
Figure 2-14: Unidirectional flow LNT (Zheng *et al*. 2005).

DENOx Catalysts use the hydrocarbons present in the exhaust stream to chemically reduce NO in a passive configuration. Active DENOx catalysts on the other hand use fuel injection, in-cylinder late post or supplementation in the exhaust stream, to promote chemical NO reduction.

The DPF physically traps the particulate as in conventional filtration systems. The DPF substrate is made from either Cordierite or Silicon Carbide for wall flow filters, metal fibres for flow-through filters and paper for disposable units used especially in coal mines. For non-single use filters, in addition to collecting the particulate a method should also exist to clean up the filter. This cleaning up process is called DPF regeneration. A typical illustration of the external fuel injection for wall-flow DPF regeneration is shown in Figure 2-15 (Zheng *et al*. 2005).
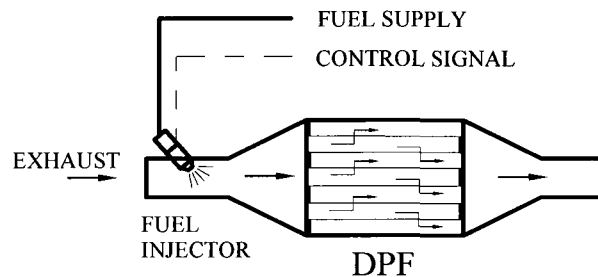
Figure 2-15: Fuel injection for wall-flow DPF regeneration (Zheng *et al*. 2005).

In recent years, more stringent measures have been introduced to reduce emissions of pollutant species from combustion processes especially those involving hydrocarbon fuels. The main engine-out pollutants from diesel engines are NO_x and PM. While recent improvements in diesel engine design and calibration have greatly reduced both NO_x and PM emissions, they are still high to meet future legislative requirements without after-

treatment devices such as SCR, LNT and DPF (Helmantel 2004). Nonetheless, diesel after-treatment systems still have a number of durability and servicing concerns that need to be resolved. Consequently, there is need for continued research in both in-cylinder and after-treatment emission control strategies because the technology in both areas is still improving. Some of the improvements include advanced injection systems, optimised combustion chamber designs, cleaner diesel and alternative fuels and energy-efficient after-treatment systems, among others.

CHAPTER III

LITERATURE REVIEW

As discussed in Chapter I, the diesel engine has benefited from tremendous improvements in all the areas where it was traditionally weak such as noise, smoke and power output while its key advantage of being more efficient has been further improved. However, more stringent measures have been introduced to reduce the emissions of toxic species from combustion processes especially those involving hydrocarbon-based fuels. The main engine-out pollutants from diesel engines are NO_x and soot/PM. Helmantel (2004) noted that while recent improvements in diesel engine design and calibration have greatly reduced both NO_x and PM emissions, they are still high to meet future legislative requirements without after-treatment devices such as LNT and DPFs. Nonetheless, the after-treatment systems have durability and servicing concerns, which presents a motivation for continued research in in-cylinder combustion strategies. Clean diesel combustion strategies are thus being pursued that should simultaneously reduce engine-out NO_x and PM emissions by the year 2010 and beyond. An interesting option is the diesel LTC mode such as HCCI-enabling technologies and smokeless diesel combustion.

3.1 Diesel High Temperature Combustion

Figure 3-1 is a schematic representation of the direct fuel injection in diesel engines. As discussed in Chapter I, in diesel engines, air is introduced into the cylinder and compressed. Near TDC, liquid diesel fuel is injected, usually in the piston bowl, and undergoes physical and chemical preparation before it auto-ignites. A variety of structures have been proposed describing the nature of the combustion processes in diesel

engines. Flynn *et al.* (1999) employed laser diagnostics, chemical kinetics and empirical validation to propose a structure for the diesel combustion process. They presented a thin diffusion flame surrounding the burning plume where complete oxidation would occur, yielding products of complete combustion CO_2 and H_2O. Because the temperatures at the diffusion flame interface are high, an ideal environment for NO_x formation reactions on the lean side of the reaction zone would exist. However, on the rich side of the reaction zone, products of incomplete combustion CO, UHC and PM would be formed which may be oxidised at the diffusion flame interface. It appears that no free oxygen is available inside the diffusion flame sheath and that the constituents and temperatures existing inside the sheath are ideal for the formation of diesel particulates (Borman & Ragland 1998, Flynn *et al.* 1999, Hiroyasu & Arai 1990, Hiroyasu *et al.* 1990, Stone 1999, Turns 2000, Zhao *et al.* 1996, Zheng 2002, 2004, 2006b).
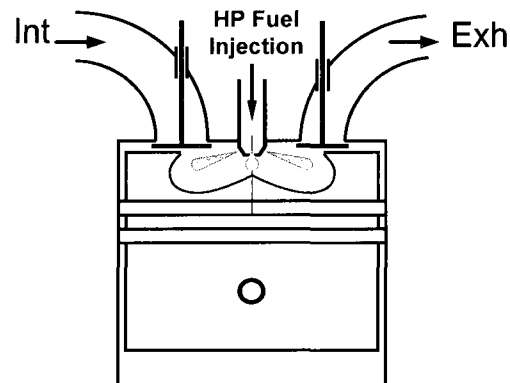
Figure 3-1: Schematic representation of diesel engine direct fuel injection.

3.2 Diesel Low Temperature Combustion

Figure 3-2 is a generalised schematic diagram describing the HTC and LTC strategies in diesel engines (Bessonette 2007, Christensen *et al.* 1999, Flynn *et al.* 1999, Helmantel

2004, Helmantel & Denbratt 2004, 2006, Hiroyasu *et al.* 1990, Jacobs *et al.* 2005, Kodama *et al.* 2007, Miles 2006, Najt 1983, Stanglmaier & Roberts 1999, Zheng 2002, 2006a, 2006b, 2007b, 2007c, 2007e). Previous work indicates that the lowered combustion temperature in diesel engines is capable of reducing NO_x and soot simultaneously. This can be implemented by the heavy use of EGR (EGR-incurred LTC) or the HCCI-enabling technologies.
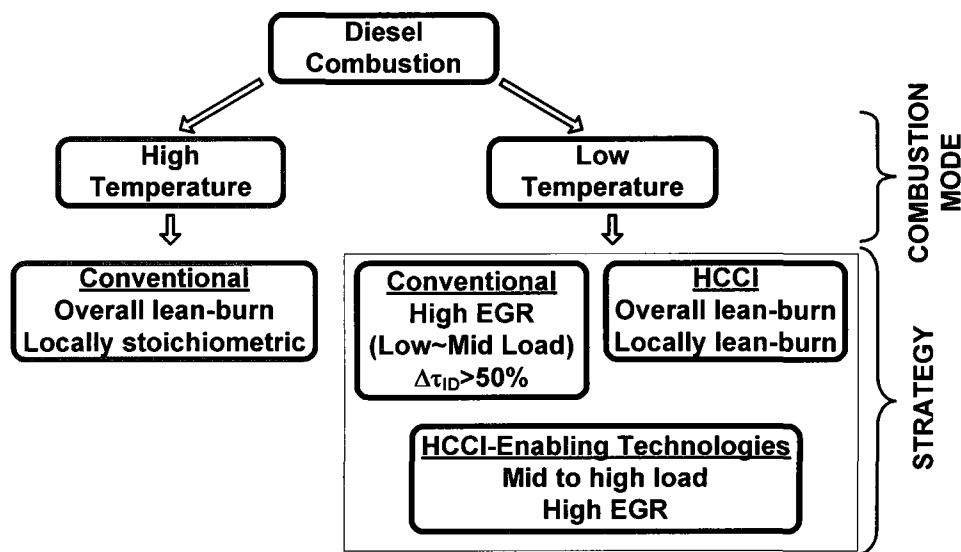
Figure 3-2: A generalised description of diesel HTC and LTC strategies.

A fuel-lean cylinder charge of high homogeneity commonly proceeds to LTC in diesel engines from low to medium load operations (Bessonette *et al.* 2007, Chen *et al.* 2000, Christensen *et al.* 1999, Helmantel & Denbratt 2004, 2006, Jacobs *et al.* 2005, Kodama *et al.* 2007, Kumar *et al.* 2007, Miles 2006, Mulenga *et al.* 2003c, Najt 1983, Stanglmaier & Roberts 1999, Su *et al.* 2005, Thring 1989, Zheng 2002, 2006a, 2006b, 2007b, 2007c, 2007e). The high homogeneity is however more difficult to realise as the engine load, and thus the fuelling rate, increases. The surplus oxygen depletes with higher fuelling rates

and the weighing of the premixed fuel reduces within the given ignition delay duration.

Table 3-1 summarises the fuel-strength scenarios that may be found in early-injection

diesel LTC mode i.e. diesel HCCI combustion.

Table 3-1: Fuel-strength scenarios in diesel HCCI combustion.

Scenario	Characteristics
Excessively lean	May cause misfire or elevated UHC and CO emissions.
Appropriately lean	Will help to initiate HCCI combustion but the phasing of the heat-release rates tend to be advanced thereby reducing engine cycle fuel efficiency.
Insufficiently lean	May result in increased combustion noise and even detrimental knocking.

Commonly, EGR is applied to withhold the cylinder charge from ignition, which gains

time for further fuel/air mixing. Furthermore, EGR weakens the strength of the

spontaneous diesel HCCI combustion that needs to be contained to limit the maximum

cylinder pressure and pressure rise rate.

Because diesel fuels commonly have high ignitability, one of the challenges of achieving

diesel homogeneous LTC is the issue of mixing and holding, especially if multiple early

injections are employed. There has to be sufficient fuel/air mixing so that fuel-rich

pockets are minimized in order to keep the soot levels low. Concurrently, the mixture

should not prematurely auto-ignite i.e. the mixture should be held long enough from

ignition until an appropriate engine crank angle position is reached for optimum engine

performance and emissions control. The preferred location is to have the crank angle of

50% heat-released (HRR CA50) near TDC, as shown in Figure 3-3. The main factors

affecting mixture holding when diesel early injection is employed are the mixture

strength (excess air-to-fuel ratio) and/or O_2 concentration, charge dilution with EGR and/or CO_2, local temperature and pressure.
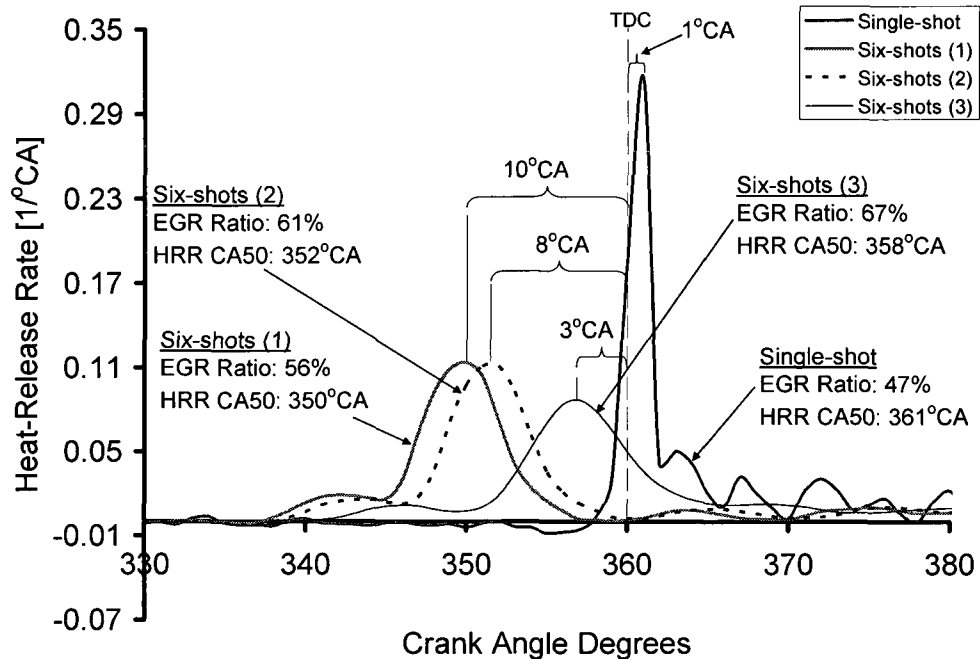
Figure 3-3: Effect of EGR on heat-release phasing in diesel HTC and LTC modes.

Figure 3-4 shows the indicated engine-out pollutant species for the HTC and LTC tests of Figure 3-3. Ultra-low levels of NO_x and soot were simultaneously attained in the LTC cases. Even though the CO and THC emissions increased with increasing EGR, the thermal efficiency did not decrease as seen in Figure 3-5. This may be attributable to improved combustion phasing as the EGR was increased.
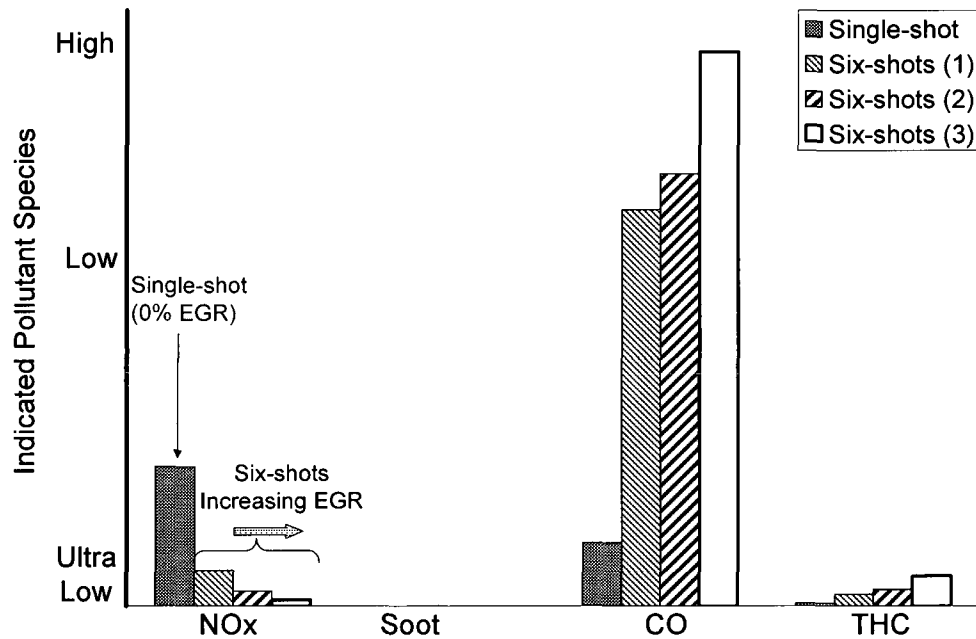
Figure 3-4: Indicated pollutant species in diesel HTC and LTC modes.
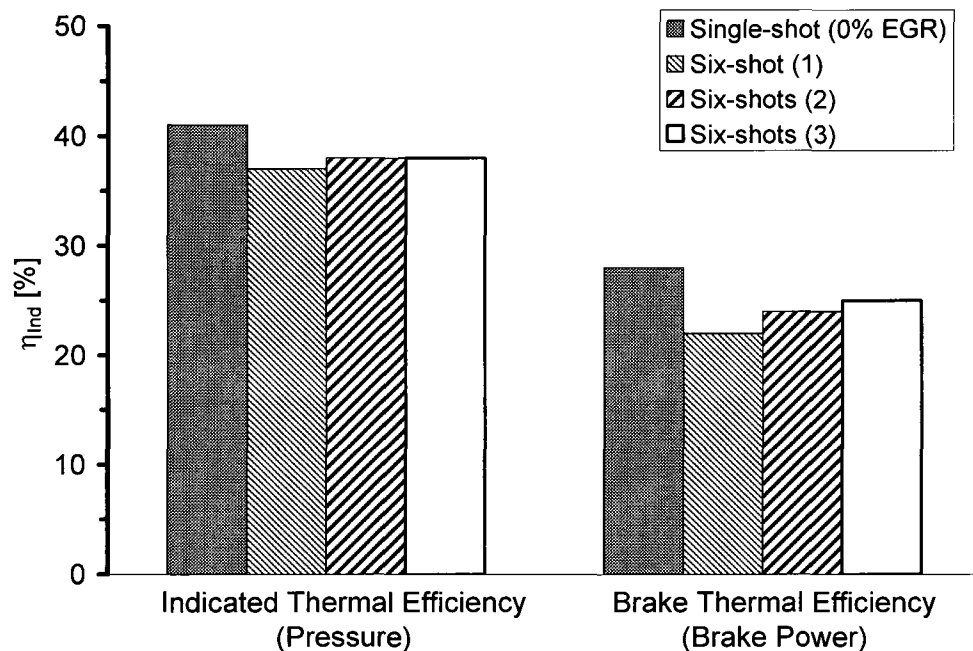
Figure 3-5: Thermal efficiencies in diesel HTC and LTC modes.

Figure 3-6 shows the variation of CO, THC and thermal efficiency with NO_x for a typical diesel LTC case. A deep-dive into the analysis of Figure 3-6 yields a new trade-off, shown in Figure 3-7, in engine-out species and engine performance that is established

when the diesel LTC mode is applied in conventional diesel engines. Noted, SOF

represents the soluble organic fraction of diesel particulates (Ecopoint Inc. 2007), which

includes heavy hydrocarbons derived from the fuel and from the engine lubricating oil.
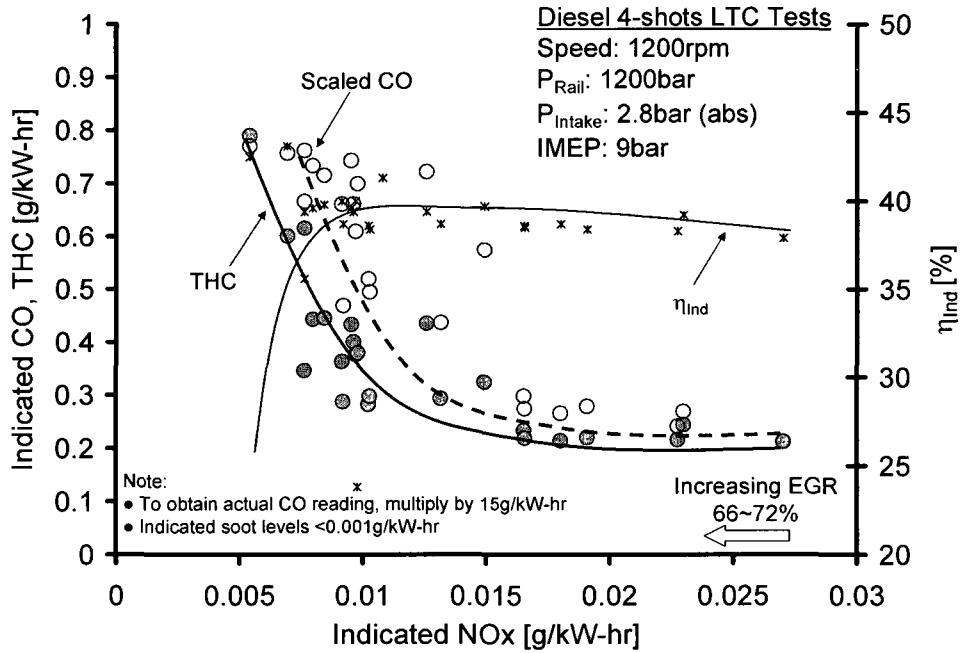
Figure 3-6: Indicated CO, THC and efficiency vs. indicated NO_x for diesel LTC mode.
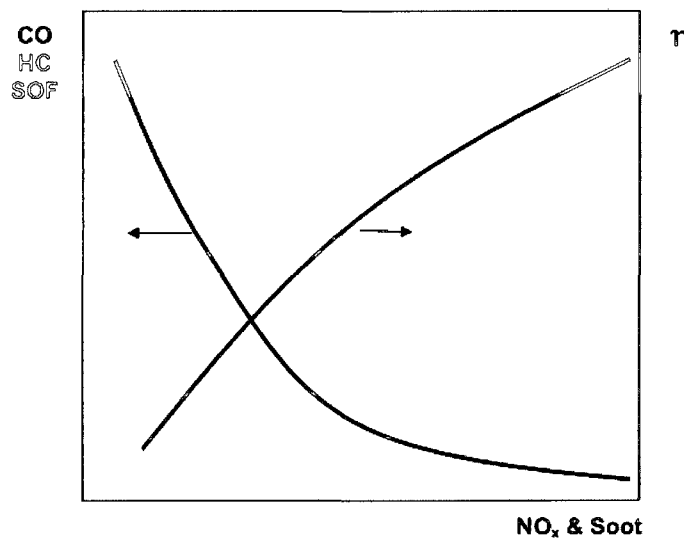
Figure 3-7: New trade-off during diesel LTC mode.

The diesel LTC results presented from Figure 3-3 to Figure 3-6 were acquired in the Clean Diesel Engine Research Laboratory at the University of Windsor using an advanced common-rail diesel engine with a compression ratio of conventional diesel HTC of 14~17. The author's contribution includes participating in the experimental preparation, data recording and analysis, among others. The results were presented at the 12th Diesel Engine-Efficiency and Emissions Reduction (DEER) Conference in Detroit, MI, USA in August 2006 by Zheng *et al.* (2006b).

A review of the benefits, challenges and future engine application of LTC such as HCCI has been discussed by Stanglmaier and Roberts (1999). It is noted that ignition-timing control, thus combustion phasing, could be achieved by altering either the fuel/air mixture's reactivity or its time-temperature history. Altering mixture reactivity could be accomplished by blending two/more fuels, fuel pre-conditioning or using fuel additives, while altering mixture time-temperature history by modulating intake temperature, in-cylinder injection timing, water injection, variable compression ratio, variable valve timing (VVT) or EGR, among others. The strategies mentioned above, which could also be implemented in combination, are already being investigated and some examples, and suggestions for improvement, are given below.

3.2.1 Altering Mixture Reactivity

3.2.1 (a) Blending Two or More Fuels

Christensen *et al.* (1999) demonstrated that almost any liquid fuel could be used in an HCCI engine using variable compression ratio. Under this particular experimental

investigation, different proportions of the primary reference fuels (PRF) iso-octane (Octane 100) and normal heptane (Octane 0) were employed; thus any octane number fuel between 0 and 100 could be investigated. While using inlet port injection for different octane numbers, the inlet air temperature and compression ratio were adjusted to obtain mixture auto-ignition at TDC. Secondly, different mixtures of gasoline (RON 98) and diesel (CN 54) were investigated from pure gasoline to pure diesel and the conclusions were that for HCCI operation, diesel fuel was quite challenging due to increase in smoke emissions because of poor atomisation and vaporisation leading to increased diffusion combustion.

With the advent of piezo-electric injectors in common-rail injection systems, the use of sequential direct high-pressure injections starting very early in the compression stroke is gaining lots of ground (Bosch 2005, Helmantel 2004, Helmantel & Denbratt 2004, 2006, Siemens 2003). Piezo-electric injectors operate much faster and more precisely than the conventional solenoid valves, and provide an even more finely controlled fuel supply to the cylinders. In-cylinder multiple injections, coupled with high levels of EGR to suppress peak in-cylinder temperatures, thus increasing the ignition delay period, would enhance homogeneous are/fuel mixture formation leading to simultaneous reduction of NO_x and PM in diesel engines.

In order to achieve heavy duty HCCI engine operation at practical loads and speeds, some researches have opted to change the fuel properties from the conventional gasoline and diesel fuels (Bessonette 2007). As reported by Bessonette *et al.* (2007), fuels in the

gasoline and diesel boiling range were designed and blended to cover a broad range of ignition quality, fuel chemistry and volatility, with nearly independent variation. At a compression ratio of 12:1, it was found that fuels with ignitability intermediate between conventional gasoline and diesel fuels provided maximum high load operability.

3.2.1 (b) Using Fuel Additives

Because gaseous fuels such as natural gas may easily form a homogeneous air/fuel mixture, unlike diesel fuel (compare the fuel properties shown in Table A-1), Chen *et al.* (2000) experimentally investigated natural gas CI in a homogeneous charged engine. However, the "easiness to auto-ignite" for natural gas is lower than that of most fuels (e.g. CN < 6) and thus to promote mixture auto-ignition without the use of high inlet temperatures and pressures, additives with low boiling points and high CN are usually employed and in this regard, various proportions of dimethyl ether (DME) were used. The conclusions drawn were that a finite amount of DME was necessary to achieve ignition and that compared to directly injecting the diesel fuel, there was increased thermal efficiency when DME proportion was optimised and reduced NO_x emissions, however, emissions of total UHC were high.

A numerical analysis of homogeneous natural gas/diesel/air mixture, which could be formed when small amounts of diesel pilot are used in a diesel dual fuel engine or when using natural gas/diesel dual-fuel HCCI combustion, was conducted by this author and the results reported (Mulenga *et al.* 2003c). For the cases considered, it was found that increasing the pilot diesel fuel may advance the ignition closer to TDC thereby increasing

peak cylinder pressure and gross IMEP. Increasing the diesel pilot may also result in early decomposition of the fuel consequently advancing the production of OH intermediate radicals that would oxidise the CO. For the same fuel/air mixture strength, increasing the pilot fuel may increase the NO_x production due to increased peak temperature, residence time and availability of O_2. When using leaner mixtures and small amounts of diesel pilot to promote/advance ignition, however, peak cylinder temperatures may be reduced and hence comparatively reducing engine-out NO_x emissions.

3.2.2 Altering Mixture Time-Temperature History

3.2.2 (a) In-cylinder Injection Timing

Helmantel and Denbratt (2004) investigated HCCI operation of a passenger car common-rail DI diesel engine with early injection of conventional diesel fuel. In their approach, up to 5 injection events were introduced in the cylinder during the compression stroke while using compression ratios of 13.4:1 and 11.5:1 so that a homogeneous diesel/air mixture could be formed before the start-of-ignition. Due to the low compression ratio and high EGR rates, commencement of the high-temperature reactions was delayed to near-TDC. Both NO_x and soot emissions were reduced to near-zero levels, however, UHC and CO levels increased significantly thereby reducing combustion efficiency.

At high load conditions, using boost pressure could assist in reducing the UHC and CO emissions. Furthermore, at low to mid load conditions, use of multiple injections may not be necessary because the single-shot technique has been shown to simultaneously reduce NO_x and soot with comparatively less penalty in the fuel efficiency (Zheng & Reader

2006a, Zheng *et al.* 2006b, 2007b, 2007c). Furthermore, adaptive control strategies are being sort to stabilise and enable the LTC operation from mid to high load conditions when high boost and EGR are applied (Zheng & Reader 2006a, Kumar *et al.* 2007).

3.2.2 (b) Variable Valve Timing and EGR

Kodama *et al.* (2007) conducted full-load diesel HCCI operation with a variable valve actuation system in a heavy-duty DI diesel engine. Using early single-injection and appropriate selection of the EGR ratio, intake manifold temperature, air-to-fuel ratio and intake valve closing timing the diesel HCCI operation range was extended to 20bar IMEP with ultra-low NO_x levels while maintaining the smoke level at 0.1BSU. It is noted that the use of a DOC and DPF in the after-treatment system may reduce the tail-pipe emissions of the HC, CO and PM. An intake manifold pressure of 4bar (abs) was employed resulting in maximum cylinder pressures and pressure rise rates of 175bar and 18bar/°CA, respectively, which, at the time of this dissertation, were just about the upper limits for most production engines.

3.3 Properties of Diesel Fuel

Diesel fuel is a complex mixture of hydrocarbons. Petroleum-derived diesel fuel comprises about 75% saturated hydrocarbons (primarily normal-, iso- and cyclo-paraffins) and 25% aromatic hydrocarbons (including napthalenes and alkybenzenes) (Chevron 2007). Figure 3-8 shows the typical carbon number distribution for No. 2 diesel fuel while Table 3-2 depicts the composition and CN of representative diesel fuel hydrocarbons where * is the primary reference material for CN scale (Chevron 2007).
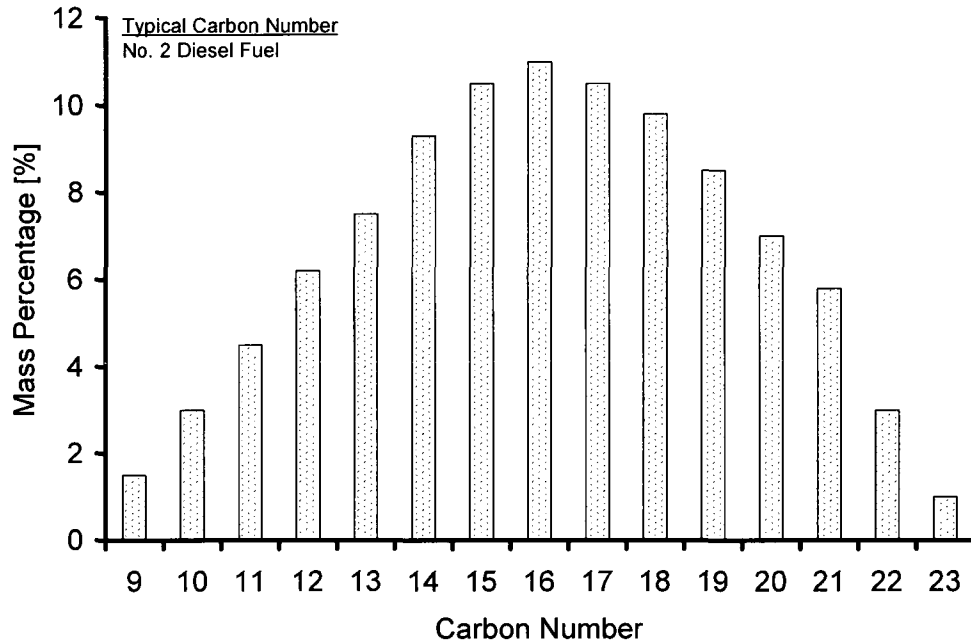
Figure 3-8. Typical carbon number distribution for diesel fuel (Chevron 2007).

Table 3-2: Composition and CN for a representative diesel fuel (Chevron 2007).

Compound Name	Hydrocarbon Class	Chemical Formula	Cetane Number
n-Decane	n-Paraffin	$C_{10}H_{22}$	76
n-Pentadecane	n-Paraffin	$C_{15}H_{32}$	95
n-Hexadecane (Cetane)*	n-Paraffin	$C_{16}H_{34}$	100
n-Eicosane	n-Paraffin	$C_{20}H_{42}$	110
3-Ethyldecane	Iso-Paraffin	$C_{12}H_{26}$	48
4,5 Diethyloctane	Iso-Paraffin	$C_{12}H_{26}$	20
Heptamethylnonane*	Iso-Paraffin	$C_{16}H_{34}$	15
8-Propylpentadecane	Iso-Paraffin	$C_{18}H_{38}$	48
7,8 Diethyltetradecane	Iso-Paraffin	$C_{18}H_{38}$	67
9,10-Dimethyloctane	Iso-Paraffin	$C_{20}H_{42}$	59
Decalin	Naphthalene	$C_{10}H_{18}$	48
3-Cyclohexyhexane	Naphthalene	$C_{12}H_{24}$	36
2-Methyl-3-cyclohexylnonane	Naphthalene	$C_{16}H_{32}$	70
2-Cyclohexyltetradecane	Naphthalene	$C_{20}H_{40}$	57
1-Methylnaphthalene*	Aromatic	$C_{11}H_{10}$	0
n-Pentylbenzene	Aromatic	$C_{11}H_{16}$	8
Biphenyl	Aromatic	$C_{12}H_{10}$	21
1-Butylnaphthalene	Aromatic	$C_{14}H_{16}$	6
n-Nonylbenzene	Aromatic	$C_{15}H_{24}$	50
2-Octylnaphthalene	Aromatic	$C_{18}H_{24}$	18
n-Tetradecylbenzene	Aromatic	$C_{20}H_{24}$	72

Table 3-3 is a summary of the effects of hydrocarbon class on the fuel properties. Normal paraffins have excellent CN, but very poor cold flow properties and low volumetric heating values. Aromatics have very good cold flow properties and volumetric heating values, but very low CN. Iso-paraffins and naphthalenes are intermediate, with values of these properties between those of normal paraffins and aromatics (Chevron 2007, Stone 1999).

Table 3-3: Relationship of hydrocarbon class to fuel properties (Chevron 2007).

Property of fuel	n-Paraffin	iso-Paraffin	Naphthalene	Aromatic
Cetane number	+ +	0/+	0/+	0/-
Low temperature operability	-	0/+	+	+
Volumetric heating	-	-	-	+

Table Legend
+ indicates a positive or beneficial effect on fuel property.
0 indicates a neutral or minor effect.
- indicates a negative or detrimental effect.

While diesel fuel has been used extensively, its application in HCCI could be met with two main difficulties: vaporisation and significant cool combustion chemistry. Diesel fuel has a higher boiling point than most neat fuels and thus makes it difficult to evaporate and form a homogeneous fuel/air mixture without substantial inlet pre-heating. The end result is increased diffusion combustion at high loads leading to increased NO_x and soot/PM formation. Using inlet pre-heating could assist in vaporisation of the fuel and formation of a homogeneous mixture, however, while soot/PM formation would be reduced, temperature-sensitive NO_x formation would be increased. The significant cool flame chemistry of diesel fuel leads to rapid auto-ignition once compression temperatures exceed 800 K subsequently causing overly advanced combustion phasing.

3.4 Alternative Diesel Fuels

A list of neat alternative fuels is given in Table A-1 of APPENDIX A. Fuel properties such as boiling point and CN, among others, have a crucial effect on HCCI combustion. The properties affect fuel/air mixing, ignitability and subsequent emissions formation. In this section, only the alternative diesel fuels Fischer-Tropsch and biodiesel are discussed. A brief description of DME is given in APPENDIX A.

3.4.1 Fischer-Tropsch Diesels

Fischer-Tropsch (FT) fuels are synthetic hydrocarbon fuels made by synthesising coal, natural gas or biomass using Gas-to-Liquid (GTL) processes (Alleman *et al*. 2004). This involves partial oxidation of a hydrocarbon fuel to produce synthesis gas (CO and H_2) which is then reacted over an FT catalyst (usually iron or cobalt based) to produce a range of hydrocarbon fuels. The resulting fuel is composed of almost entirely straight-chain paraffinic molecules and is free of sulphur, olefins, nitrogen and aromatics resulting in a high-cetane distillate. Sasol Oil (pty) Limited has successfully implemented this technology using coal as feedstock in the Republic of South Africa since 1955 while Royal Dutch Shell plc uses similar technology by converting natural gas into middle distillates such as gas oil, kerosene and naphtha (Shell Middle Distillate Synthesis, SMDS, with the first plant in Malaysia). In the United States of America, the Environmental Protection Agency (EPA) has classified FT diesel as a clean alternative fuel and several oil companies are researching its large scale production. In particular, Syntroleum Corporation based in Tulsa, OK, developed Syntroleum S-2, a synthetic diesel fuel using the FT synthesis process (Syntroleum 2007). Tests conducted at South

West Research Institute compared Syntroleum S-2 diesel with EPA#2 diesel, California

Air Resource Board (CARB) diesel and Swedish city diesel. It was deduced from the

tests that the synthetic diesel produced the lowest engine-out toxic emissions, was cleaner

(neither sulphur nor aromatics) and had better cold-starting capabilities. However, the

slightly lower energy density caused a small penalty in fuel economy. Figure 3-9 shows a

comparison of the exhaust pollutant species between the synthetic diesel and CARB

diesel.
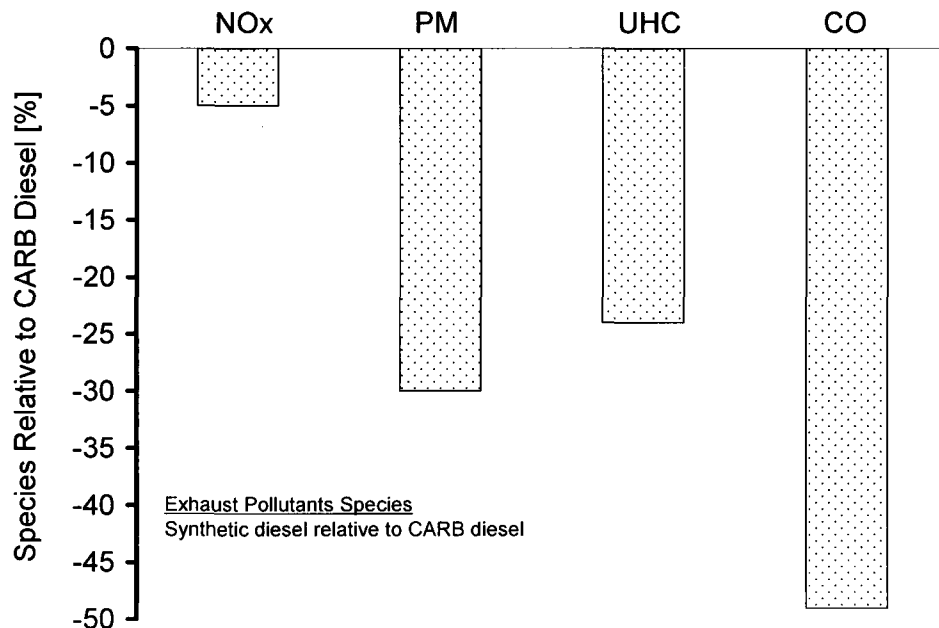
Figure 3-9: Emissions from FT diesel relative to CARB diesel (Syntroleum 2007).

Other examples of GTL activity in North America include ConocoPhilips and Rentech

Inc. ConocoPhilips with head quarters in Houston, TX, uses GTL processes based on FT

technology to convert natural gas to liquid petroleum products diesel, naphtha and waxes.

Rentech Inc. with Corporate offices in Denver, CO, plan to convert their methanol Sank

Creek Energy plant into a GTL processing plant that could supply commercial quantities

of high value fuel including cleaner burning sulphur and aromatic free diesel fuel.

Unfortunately, one of the problems of FT diesels is the formation of waxes (long paraffinic molecules) at low temperatures giving rise to cold-starting difficulties when high levels of FT diesel are employed. However, this could be alleviated by hydro-cracking and upgrading the fuel to produce higher percentage of cyclo-paraffins (naphtha), which improve low-temperature characteristics as mentioned earlier (Alleman *et al.* 2004, Chevron 2007, Syntroleum 2007).

Limited HCCI experimental work with neat FT diesel has been reported in the literature. This may be attributable to the challenging issue of mixture holding because of the high fuel CN and the exorbitant price of FT fuels. Stanglmaier *et al.* (SWR Institute 2006) conducted experiments with FT naphtha and compressed natural gas (CNG) fuel blends in heavy-duty diesel engines. Results from these experiments showed that FT naphtha had low levels of NO_x and PM formation, double the power output compared to diesel fuel (operating in HCCI mode) and operated on ambient intake temperatures i.e. without intake pre-heating.

3.4.2 Biodiesel Fuel

Biodiesel fuel, as a variety of fatty acid alkyl esters derived from agricultural products or recycled fat, is a renewable alternative for petroleum-derived diesel fuels (Boeman *et al.* 2004, Choi *et al.* 1997, 1999, Dorado *et al.* 2003, EMO 2006, Krisnagkura *et al.* 2006, Lin & Lin 2006, McCrady *et al.* 2007, Monyem *et al.* 1999, 2001, NB Board 2007, NRCan 2007, Patterson *et al.* 2006, Rosca *et al.* 2005, Tat *et al.* 2003a, 2003b, Tate *et al.* 2006a, 2006b, US DOE 2007a, 2007b, Weall & Collings 2007, Yamane *et al.* 2001,

Yuan *et al.* 2005, Zheng *et al.* 2006c, 2007b, 2007c). In comparison with conventional diesel fuels, the fuel-borne oxygen in biodiesels, which could be over 10% by mass, is capable of reducing engine-out emissions of PM, CO and UHC in modern four-stroke compression-ignition engines. However, a slight increase in emissions of NO_x, which could be partially caused by the fuel property incurred combustion-timing variations, has been observed in the use of oxygenated fuels in general (Murayama *et al.* 1995). Nevertheless, as discussed above, the LTC modes offer a promising solution to simultaneously reduce the in-cylinder formation of NO_x and soot/PM in diesel engines.

In recent years, the concern over depleting world reserves of fossil fuels and more stringent emission regulations have led to the resolute efforts in searching for renewable alternative fuels and low emission combustion strategies. Biodiesel fuel, which is identified as one of the future contenders to the fossil diesel fuels, has become commercially available in a number of countries. However, the long-term impact in modern common-rail injection systems still needs to be identified. Additionally, biodiesel is known to degrade up to four times faster than diesel fuel (Monyem 1999, 2001). The products of biodegrading could have detrimental effects on the injection components especially the high pressure fuel pump. In the short-term one of the disadvantages of biodiesel is its higher production cost. Table 3-4 summarises the key advantages and disadvantages of neat (100%) biodiesel fuels in comparison with conventional diesel fuels.

Table 3-4: Key aspects of biodiesel in comparison with conventional diesel fuels.

Characteristic	Advantages	Disadvantages
Renewable	• Can be made from domestically produced crop. • Alleviates dependence on foreign petroleum oil. • Decreases overall CO_2 emissions on a life-cycle basis.	Large scale use could raise concern for genetically modified crops, pesticide use, land-use impacts (wildlife habitat, soil erosion) and food crop competition, *inter alia*.
Non-toxic	• No serious health effects if ingested. • Environmentally friendly if spilled.	-
Oxygenated	• May provide more complete combustion of PM,UHC,CO. • Higher EGR rates may be employed without substantial penalty in efficiency.	May increase NO_x emissions in some engines.
Biodegradable (oxidative degradation)	Environmentally friendly if spilled.	• Products of degradation may damage the fuel injection equipment. • Increases viscosity and CN.
Higher viscosity	Improved lubricity.	Poor atomisation leading to poor air/fuel mixture preparation.
High boiling point	-	Increased cylinder wall condensation leading to increased oil dilution especially in LTC mode or when in-cylinder post injection is employed.
Low cloud point	-	At low temperature, may clog fuel injection systems, cause pump seizures etc.
High flash point	Safer to handle and transport (less flammable)	-
High CN	Reduced ignition delay may lead to weak air/fuel mixture preparation that burns in the premixed burning phase thus comparable NO_x emissions in some engines.	May cause early ignition thus off-phasing of the combustion event. This would compromise the engine efficiency.
Lower energy content	-	Higher fuel consumption especially at low loads.
No or low sulphur content (S≤15ppm)	May be readily used in stationary power plants with catalytic after-treatment systems currently using ≤S500ppm diesel.	-
High production cost	-	Expensive to produce and requires subsidies or tax incentives.

68

Biodiesel from vegetable oils, waste fats, or recycled restaurant greases (yellow grease) is usually produced through a process of base-catalysed transesterification of the oil with alcohol (NBB 2007, Yamane *et al.* 2001). Transesterification is the reaction of a fat or oil containing triglycerides with an alcohol to form esters and glycerol. Figure 3-10 is an illustration of the transesterification process showing a typical structure of the fatty acid alkyl ester, where R1, R2 and R3 are unsaturated mono-hydrocarbons (C_{11} to C_{17}) and R is a methyl or ethyl group (NBB 2007, Yamane *et al.* 2001).
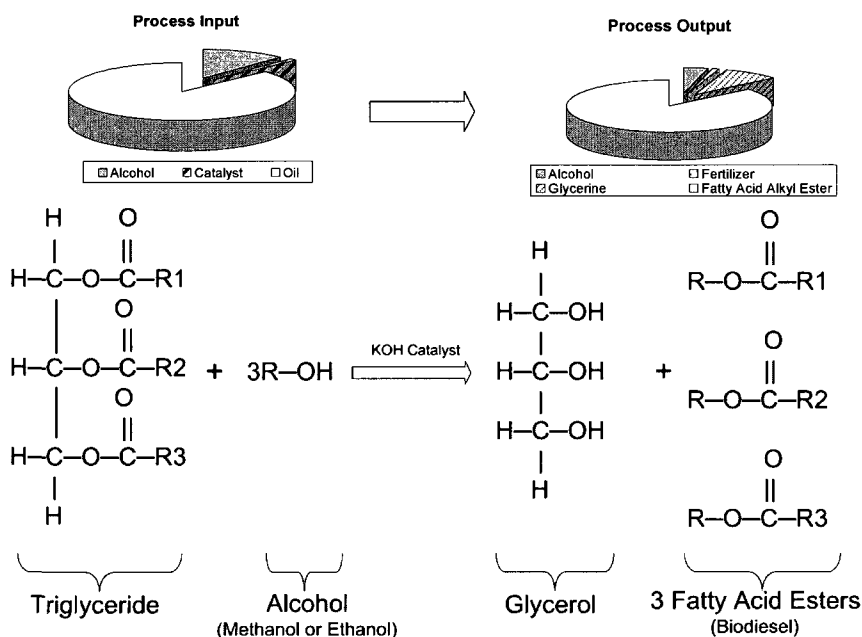
Figure 3-10: Base-catalysed transesterification of a fatty acid (NBB 2007).

The composition and thermo-physical characteristics of biodiesel fuels depend on the feedstock. Therefore, there are many different kinds of fatty acids that differ in carbon chain length and number of carbon-carbon double bonds (Tat 2003b). Table 3-5 shows the fatty acid composition of selected common vegetable oils, in weight percentage, as presented by Tat (2003b). The designation employed for the structure shows the number

of carbon atoms and double bonds. For instance, in Linoleic acid 18:2 stands for eighteen carbon atoms and 2 double bonds. Because fatty acids constitute almost 90% of the total mass of a triglyceride molecule, they have the greatest impact on the physical properties of biodiesel fuels. It has been demonstrated that biodiesel fuel viscosity increases with the increase in the chain length. Nevertheless, when the number of double-bonds increases, the viscosity decreases. To facilitate the characterisation of the fuel's physical properties, therefore, researchers have recommended that analysis of the fuels be conducted to determine their fatty acid composition.

The specification of the American Society for Testing and Materials International (ASTM) for neat biodiesel fuel (designated B100) is ASTM D6751-06 (ASTM 2007) that is shown in Table B-1 in APPENDIX B. Note that this specification does not include the density, C/H/O ratio and calorific value that have a direct impact on engine performance together with the viscosity and CN. However, the density is required for the determination of the sulphur content using the ASTM D5453 standard. In the European Union, the European Committee for Standardisation (*Comité Européen de Normalisation,* CEN) defines B100 through EN14213 and EN14214 as shown in Table B-2 (Knothe 2006). It is noted that both the ASTM and EN biodiesel standards do not require the determination of the fatty acid composition.

Table 3-5: Fatty acid composition in selected vegetable oils (Tat 2003b).

Fatty Acid	Structure	Formula	Cotton Seed	Rapeseed	Safflower	Soybean	Sunflower	Peanut
Myristic	14:0	$C_{14}H_{28}O_2$	0.00	0.00	0.00	0.00	0.00	0.00
Palmitic	16:0	$C_{16}H_{32}O_2$	28.33	3.49	8.60	11.76	6.08	11.38
Steari	18:0	$C_{18}H_{36}O_2$	0.89	0.85	1.93	3.15	3.26	2.39
Oleic	18:1	$C_{18}H_{34}O_2$	13.27	64.40	11.58	23.26	16.93	48.28
Linoleic	18:2	$C_{18}H_{30}O_2$	57.51	22.3	77.89	55.52	73.72	31.95
Linolenic	18:3	$C_{18}H_{28}O_2$	0.00	8.23	0.00	6.31	0.00	0.93
Arachidic	20:0	$C_{20}H_{40}O_2$	0.00	0.00	0.00	0.00	0.00	1.32
Behenic	22:0	$C_{22}H_{44}O_2$	0.00	0.00	0.00	0.00	0.00	2.52
Lignoceric	24:0	$C_{24}H_{48}O_2$	0.00	0.00	0.00	0.00	0.00	1.23

CHAPTER IV

METHODOLOGY

Figure 4-1 presents a schematic of the dissertation methodology. The engine modifications, data acquisition and fuel preparations constitute the experimental setup. The modelling work was performed in conjunction with the engine tests. The empirical investigation of the HTC and LTC comparison of conventional diesel and neat biodiesel fuels was the primary aspect of the dissertation work. The data analysis included the engine performance and emissions of NO_x, soot, THC and CO. Exhaust gas recirculation was extensively applied to initiate the LTC. The applicable range of the EGR was up to 80% for low load conditions thus requiring detailed analysis. Furthermore, an ignition delay correlation that takes into account the fuel CN and oxygen concentrations in the intake and fuel was investigated for steady-state operating conditions.
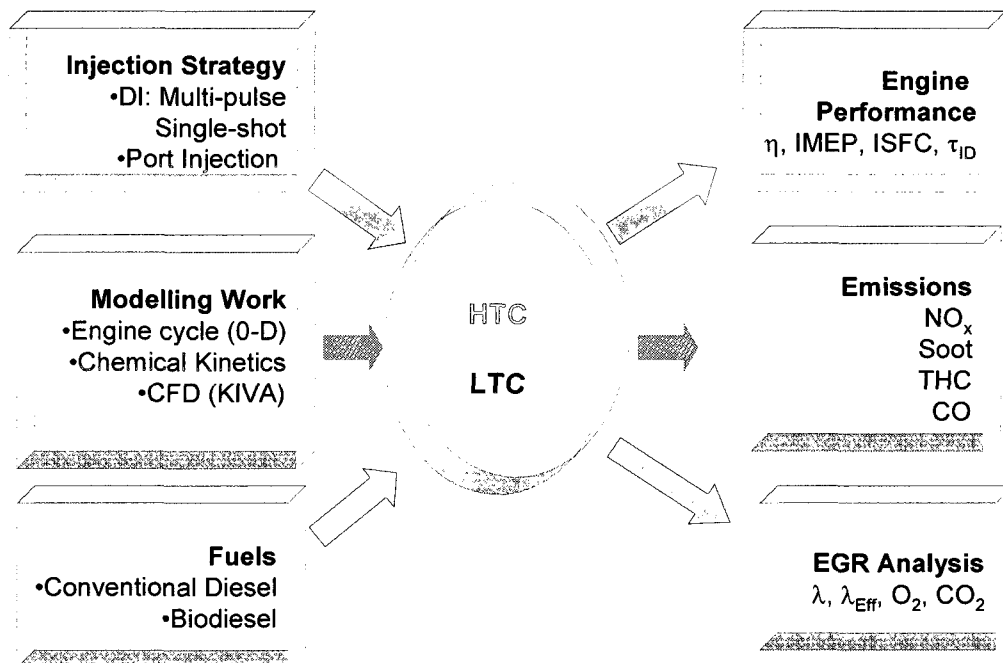
Figure 4-1: Schematic representation of the dissertation methodology.

4.1 Modelling Work

It is the general consensus that conducting engine simulations is cheaper and relatively less time consuming than performing the corresponding empirical investigations (Ogink 2004, Stone 1999). This is especially common if a proper model has been developed, calibrated and validated. Nonetheless, it should be emphasised that the processes that occur in an internal combustion engine are so complex that most cannot be modelled from the first principles. As a result, engine models rely strongly on experimental data and empirical correlations. The most common models employed in engine modelling are zero dimensional (0-D) and multi-dimensional in nature.

The 0-D models, also referred to as phenomenological models, commonly employ empirical heat-release models in which time is the only dependent variable. These models are relatively simple and have short calculation times. They could be used to estimate the engine efficiency, performance and emissions. Furthermore, these models are flexible and helpful in conducting parametric studies for instance one could specify a particular heat-release profile to obtain the expected pressure trace, engine performance and emissions (Zheng *et al.* 2007d, 2007e).

Multi-dimensional models numerically solve the fluid flow equations (mass, momentum, energy) and species conservation in three dimensions (Amsden 1985, 1993, 1998). They are generally called computational fluid dynamics (CFD) models and are helpful in understanding the physical phenomena taking place in internal combustion engines that include in-cylinder mixing history, temperature and species distribution when coupled to a detailed chemical kinetics mechanism. Noted, a compromise is usually made between

the computational resources and the phenomenon to be investigated. For instance, calculation times may be reduced by applying a 2-D mesh instead of 3-D, a relatively coarse grid and a simple chemistry model (Ogink 2004).

In this dissertation, the modelling aspect was primarily employed as a tool to assist in the interpretation of the empirical results. The modelling tools employed were engine cycle simulation (0-D), chemical kinetics and multi-dimensional (3-D).

4.1.1 Engine Cycle Simulations (0-D)

Engine cycle simulation tools SAES (Zheng & Reader 1996), an in-house programme, and GT-Power (Gama Technologies 2001), a commercial software package, were available at the institution for the study of the thermodynamic engine cycles of the fuels. These tools are zero-dimensional in nature and could be employed to estimate engine efficiency, performance and emissions.

4.1.2 Chemical Kinetics Modelling

The CHEMKIN software package (Kee *et al.* 2000) was available for the investigation of the temporal evolution of the chemical species. Because diesel fuel is a complex mixture of hydrocarbon fuels, it becomes too intricate to be modelled using a comprehensive chemical reaction mechanism. To simulate diesel fuel Curran's n-heptane detailed chemical kinetics mechanism (Curran *et al.* 1998) developed to study oxidation of C_7H_{16} in flow reactors, shock tubes and rapid compression machines, was employed. Normal heptane, with CN of 56, was selected for the investigation because it is the closest match

to diesel fuel among the accessible reaction mechanisms. Curran's n-heptane mechanism, consisting of 544 species and 2446 elementary reactions is available for download from the Lawrence Livermore National Laboratory website (2002) however, nitrogen chemistry is not included. To facilitate simulation of NO_x emissions, a detailed NO_x mechanism from University of California - San Diego (2003), also available for download, was incorporated and the resulting mechanism with 558 species participating in 2498 elementary reactions was finally used (Mulenga *et al.* 2003b).

To simulate larger alkyl esters, Fischer's Methyl Butanoate (Methyl Butyrate, $nC_3H_7C(=O)OCH_3$ i.e. $C_5H_{10}O_2$) detailed chemical kinetics mechanism (Fischer *et al.* 2000), a model compound for biodiesel fuels, was employed. Typical biodiesel molecules contain long chains of carbon atoms numbering 12 or more. However, Methyl Butanoate which is a fatty acid belonging to aroma compounds and found in the environment or food systems, is long enough to represent biodiesel fuel in modelling because it has the basic chemical structure (compare $C_5H_{10}O_2$ with Table 3-5). In addition, its structure is large enough to allow fast RO_2 isomerisation reactions that are believed to be important in low-temperature chemistry that controls auto-ignition under conditions found in diesel engines (Fischer *et al.* 2000). To facilitate the simulation of NO_x emissions, the detailed NO_x mechanism reported above was incorporated and the resulting mechanism with 275 species participating in 1260 elementary reactions finally used (Zheng *et al.* 2007b).

4.1.3 Multidimensional Modelling

For consideration of in-cylinder in-homogeneities, a multi-dimensional simulation tool, KIVA 3V (Amsden *et al.* 1993, 1998), was employed. Figure 4-2 shows the programme flow for KIVA 3V. The *iprep* file contains the description of the mesh i.e. grid generation. If the intake and exhaust valve profiles are to be included, such as for a full engine cycle simulation, the *itape18* file must be included. The actual simulation input parameters, or in-cylinder definition, is described in the *itape5* file. The results of the simulation are given as a graphical post processor and in text file format. The KIVA simulations help to understand the homogeneity distribution and history.

KIVA 3V

Iprep K3prep ⟹ Otape17

Itape18

Itape5 ⟹ **KIVA 3V**

Otape9

K3post

Graphical Post Processor

- Dat.Thermo
- Dat.Dynamic
- Dat.Inject
- Dat.Turb
- Otape12

Grid Generation

Valve Definition (Itape8)

In-cylinder Definition (Itape5)

KIVA Simulation

Post Processing
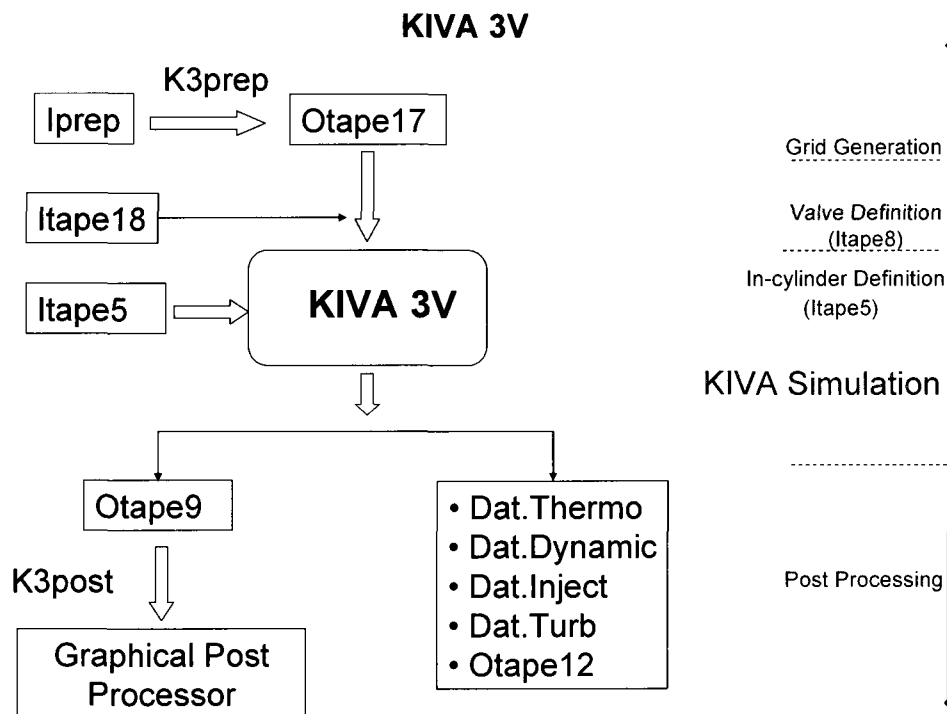
Figure 4-2: Schematic of the KIVA 3V programme flow.

As one could imagine, the KIVA code contains several sub-models to describe the combustion process. Notwithstanding, only the ignition and combustion models have

been discussed here because the author believes that they constitute the fundamental aspect of model calibration and validation. For a detailed description of the code, the reader is referred to the works of Amsden *et al.* (1993, 1998).

4.1.3 (a) Shell Auto-ignition Model

The Shell auto-ignition model, developed by Halstead *et al.*, is an 8-step kinetics model that has been implemented and proved valuable in predicting ignition of diesel and other fuels (Choi *et al.* 1997, Sazhina *et al.* 1999, Sazhin *et al.* 1999). The multi-step reactions of the model are presented below:

Initiation :

$$(1) \; RH + O \xrightarrow{k_q} 2R*$$ Equation 4-1a

Propagation :

$$(2) \; R* \xrightarrow{k_p} R* + P + Heat$$ Equation 4-1b

$$(3) \; R* \xrightarrow{f_1 k_p} R* + B$$ Equation 4-1c

$$(4) \; R* \xrightarrow{f_4 k_p} R* + Q$$ Equation 4-1d

$$(5) \; R* + Q \xrightarrow{f_2 k_p} R* + B$$ Equation 4-1e

Branching :

$$(6) \; B \xrightarrow{k_b} 2R*$$ Equation 4-1f

Termination :

$$(7) \; R* \xrightarrow{f_3 k_p} Out$$ Equation 4-1g

$$(8) \; 2R* \xrightarrow{k_t} Out$$ Equation 4-1h
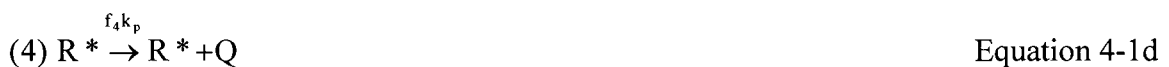
where RH is the hydrocarbon fuel ($C_nH_{2m}O_k$), R* is the radical formed from the fuel, B is the branching agent, Q is a labile intermediate species, and P is oxidized products consisting of CO, CO_2, and H_2O in specified proportions. The expressions for k_q, k_p,k_b, k_t, f_1, f_2, f_3, f_4 etc. are those originally given by Halstead et $al.$ in the publication of 1977 (Choi et $al.$ 1997, Sazhina et $al.$ 1999, Sazhin et $al.$ 1999). In addition, the local concentrations of O_2 and N_2 are needed to compute the reaction rates.

In the application of the Shell auto-ignition model, the reaction rate of reaction (4) (Equation 4-1d) is crucial to the ignition process and found to control the chemical ignition delay (Choi et $al.$ 1997) through the coefficient f_4 defined as:

$$f_4 = A_{f_4} \exp\left(-E_{f_4}/R_nT\right)[O_2]^{x_4}[RH]^{y_4} \qquad \text{Equation 4-2}$$

where R_n is the universal gas constant, A_{f4}, E_{f4}, x_4 and y_4 are the kinetic rate parameters fitted for each particular fuel.

4.1.3 (b) Combustion Model

Several combustion models have been employed in multidimensional simulation tools. Nonetheless, the laminar-and-turbulent characteristic time combustion model, of Reitz and Brocco, described by Chryssakis et $al.$ (2005) was utilised in this dissertation. In the model the rate of change of the mass fraction of species m, Y_m, due to chemical reaction is given as:

$$\frac{dY_m}{dt} = -\frac{Y_m - Y_m^*}{\tau_c} \qquad\qquad \text{Equation 4-3}$$

In Equation 4-3, τ_c is the characteristic time of combustion assumed to be the same for all species and Y_m^* is the local equilibrium mass fraction of species m. The characteristic time scale is assumed to be:

$$\tau_c = \tau_l + f\tau_t \qquad\qquad \text{Equation 4-4}$$

where τ_l and τ_t are the laminar and turbulent time scales, respectively, and f the weight function that simulates the influence of turbulence on combustion after ignition has occurred. In addition, because the model employs the eddy-break-up concept, the turbulent time scale is proportional to the eddy turnover time thus:

$$\tau_t = \frac{C_M k_t}{\varepsilon_t} \qquad\qquad \text{Equation 4-5}$$

where C_M is a variable to calibrate the different engines and their injection configurations.

4.2 Empirical Work

4.2.1 Experimental Setup

Two DI diesel engines were instrumented for the tests. The first is a naturally-aspirated, four-stroke, single-cylinder engine, Yanmar NFD170, coupled to a DC motoring dynamometer. The second is a modern common-rail DI diesel engine, Ford "Puma", coupled to an eddy current dynamometer. The LabVIEW programming environment

(National Instruments 2004) is utilised in the laboratory for equipment control and data acquisition and on-line monitoring of the pressures, temperatures and emissions, among others.

4.2.1 (a) Yanmar Single Cylinder DI Diesel Engine

The Yanmar NFD170 is a horizontal type, single cylinder DI diesel engine with the characteristics shown in Table 4-1. The original engine configuration, optimised to give the best efficiency with conventional diesel fuels, was modified to include independent control of EGR, sequential intake port injection, intake air pre-heating and throttling, which have been reported previously (Zheng *et al.* 2006c). Figure 4-3 is a schematic representation of the experimental setup and Figure 4-4 shows the fuel supply system in the laboratory.

Table 4-1: Geometrical characteristics for the Yanmar DI diesel engine.

Characteristic		Specification
Manufacturer injection configuration		Mechanical with single-shot@17°BTDC
Nozzle Opening Pressure (NOP) [bar]		204
Number of Injector Holes		4
Injector Hole Diameter [mm]		0.29
Injector Cone Angle [°]		150
Injector Inclination (Horizontal Axis) [°]		20
Piston Bowl Configuration		Mexican Hat
Displacement Volume [cm^3]		857
Bore [mm]		102
Stroke [mm]		105
Compression Ratio		17.8:1
Intake Valve Closing (IVC) [ATDC]		-135
Exhaust Valve Opening (EVO) [BBDC]		45
Rated Power		12.5kW@2400rpm
Load Level @ 1400rpm	Low	BMEP $\leq$ 4bar
	Medium	4 < BMEP < 7bar
	High	BMEP $\geq$ 7bar
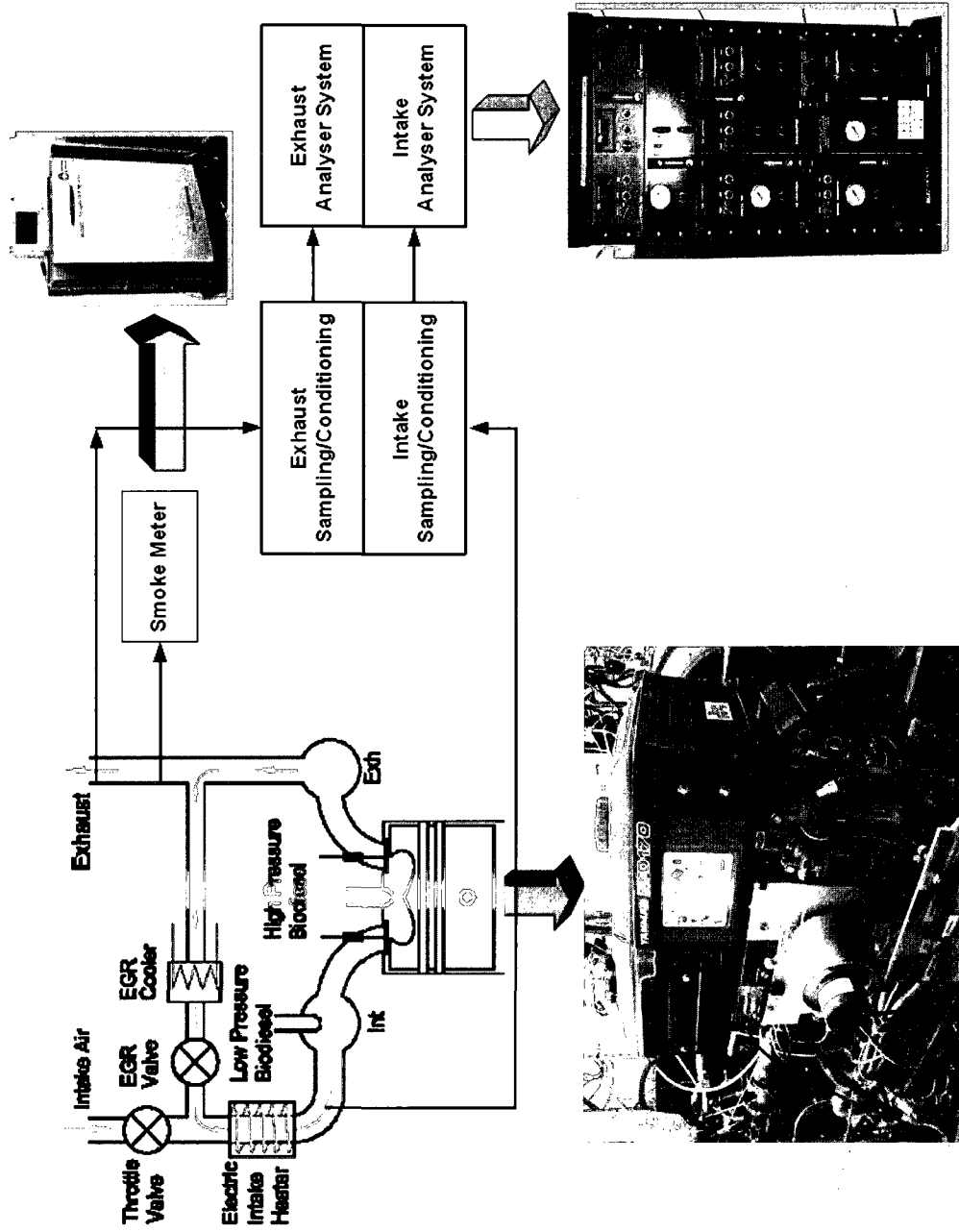
Figure 4-3: The Yanmar NFD170 single-cylinder DI diesel engine.
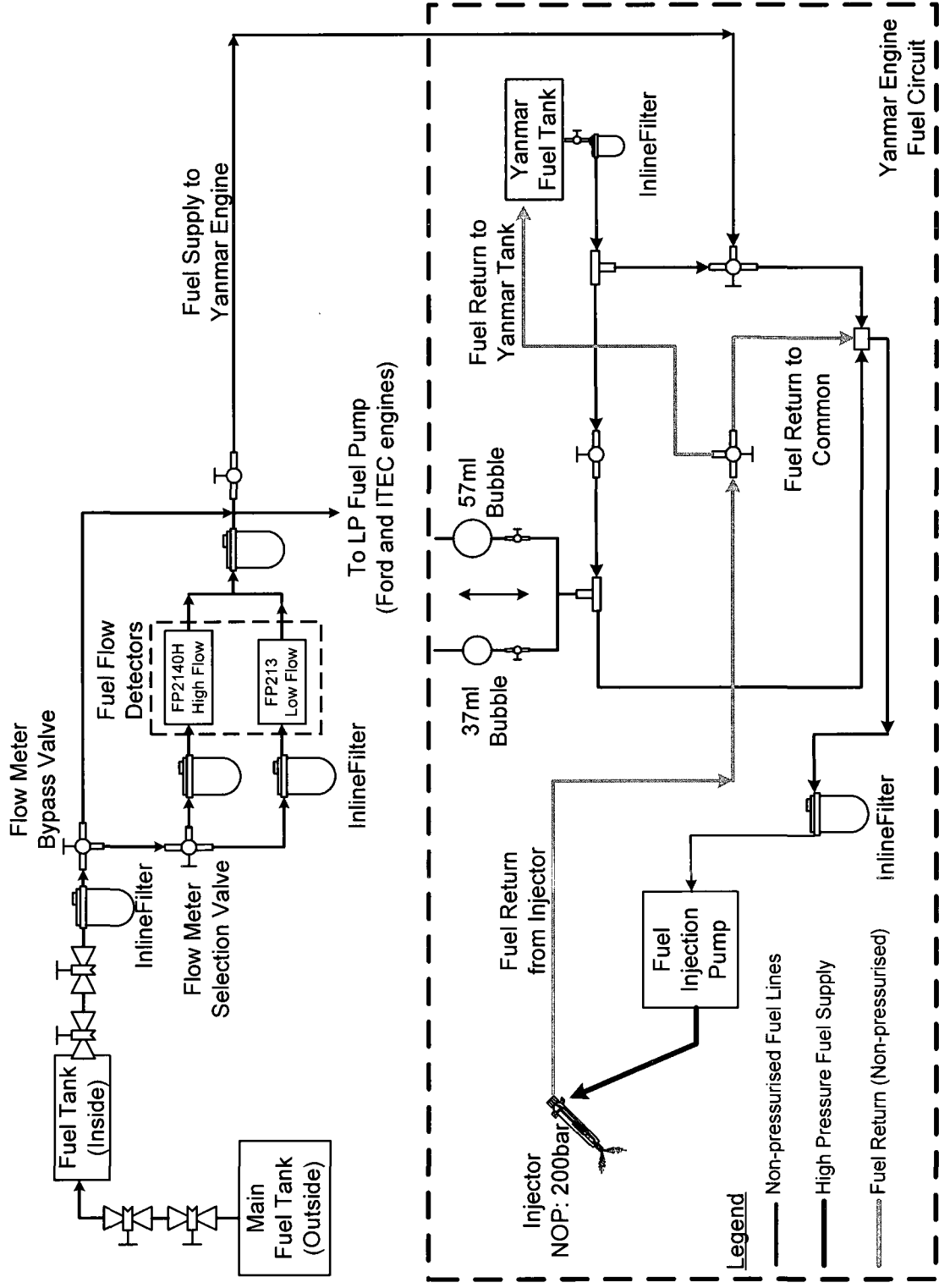
Figure 4-4: Schematic representation of the Yanmar engine fuelling system.

82

4.2.1 (b) Ford Common-rail DI Diesel Engine

The Ford ZSD-420 Duratorq is a 2.0L, 4-cylinder, common-rail DI diesel engine code name "Puma". The engine characteristics are shown in Table 4-2. The 4-cylinder Ford diesel engine, shown in Figure 4-5, running in single-cylinder mode was instrumented for the tests as shown in Figure 4-6 (Han *et al.* 2007, Zheng *et al.* 2007d). As described by Han *et al.* (2007), the 3 cylinders–to–1 cylinder configuration is a new exploration strategy that enables investigation of unstable combustion regimes with a non-motoring dynamometer. The 3 cylinders were operated in the conventional HTC mode at low load for stable engine operation. The combustion in Cylinder #1 was then pushed into the LTC cycles by independently controlling the EGR, boost and exhaust back pressures and fuel injection scheduling. An alternate to this strategy could be the use of a motoring dynamometer with the 3 cylinders operating under motoring conditions while the first cylinder is fired during the tests.

Table 4-2: Geometrical characteristics for the Ford C-R, DI diesel engine.

Characteristic	Specification
Number of Cylinders	4
Manufacturer injection configuration	Common-rail
Rail Pressure [bar]	300~1600
Displacement Volume [cm^3]	1998
Bore [mm]	86
Stroke [mm]	86
Compression Ratio	18.2:1
Connecting Rod Length [mm]	160
Rated Power	96kW, 330Nm (130hp, 244ft.lbf)

As shown in Figure 4-6, the engine was modified by separating Cylinder #1 from the other three cylinders. This, however, requires the intake and exhaust system of the single cylinder to be separated from the other three cylinders. Consequently, modifications were

made so that the engine could be operated under both one-cylinder and four-cylinder modes. A new intake manifold was constructed with the provision of running Cylinder #1 with either an independent intake system or using the same intake as the rest of the cylinders. A similar provision was also constructed on the exhaust side by separating the exhaust stream of Cylinder #1 from the rest of the cylinders. This was necessary because the exhaust gas from the single cylinder is required for measuring the emissions during the LTC tests (Han *et al.* 2007).

In order to command fuel injection precisely, a real-time controller embedded with a field programmable gate array (FPGA) device has been programmed to dynamically control the multiple events of in-cylinder fuel injection via reconfigurable solenoid- and piezo-electric-injector power drive units (Zheng & Reader 2006a). The FPGA generates the desired transistor-transistor logic (TTL) pulse patterns corresponding to the on-fly updated injection schedule. This TTL output signal is amplified using the injector power driver to execute the pulse trains, which are programmed to drive the injectors with the suitable voltage and current curves. In the laboratory, up to 8 fuel injection pulses per cylinder per cycle have been applied to modulate the homogeneity and the homogeneity history of the high load LTC operations under independently controlled levels of EGR, boost, and intake temperature.
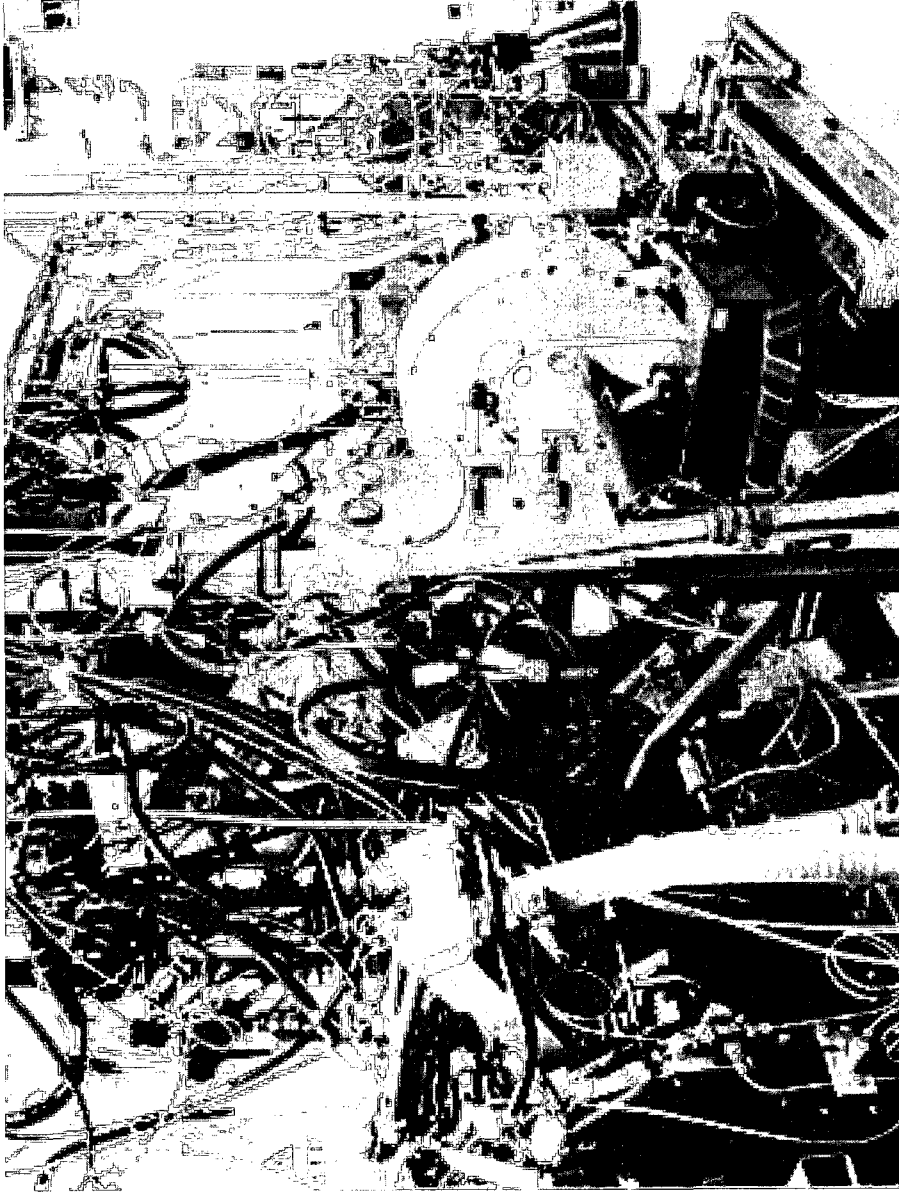
Figure 4-5: The Ford "Puma" common-rail DI diesel engine in the test cell at the University of Windsor.
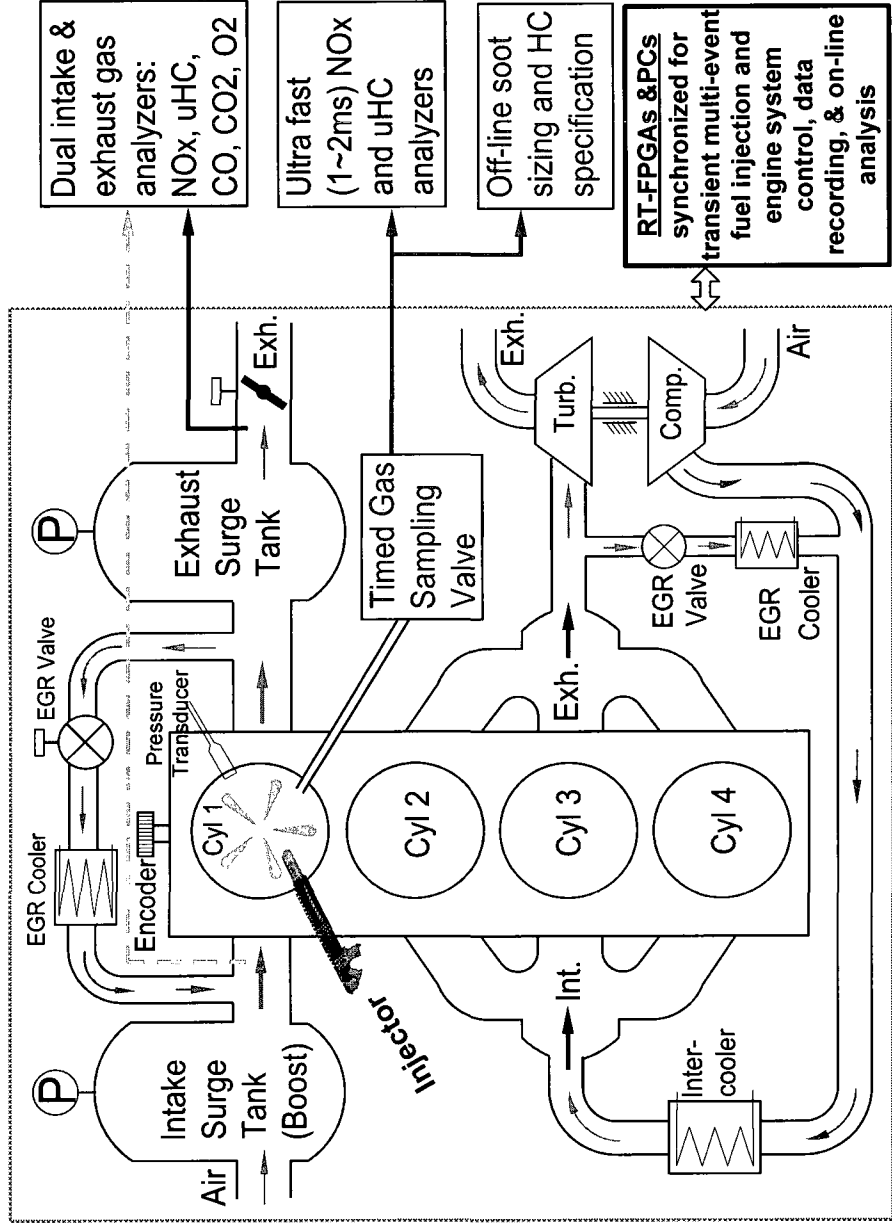
Figure 4-6: Schematic representation of the Ford common-rail DI diesel engine (Zheng *et al.* 2007d).

4.2.2 The Test Fuels

An ultra-low sulphur diesel fuel with the properties presented in Table 4-3 is used in the laboratory. Neat (i.e. 100%) soybean oil, Canola oil and yellow grease derived commercial biodiesel fuels from biodiesel producers in Canada were analysed by an established research institution following the ASTM D6751 standard, a test specification for neat biodiesel fuel B100 shown in Table B-1 of APPENDIX B. Additionally, ASTM D5291 was applied to obtain the C/H/O ratios and ASTM D4809 for the energy content.
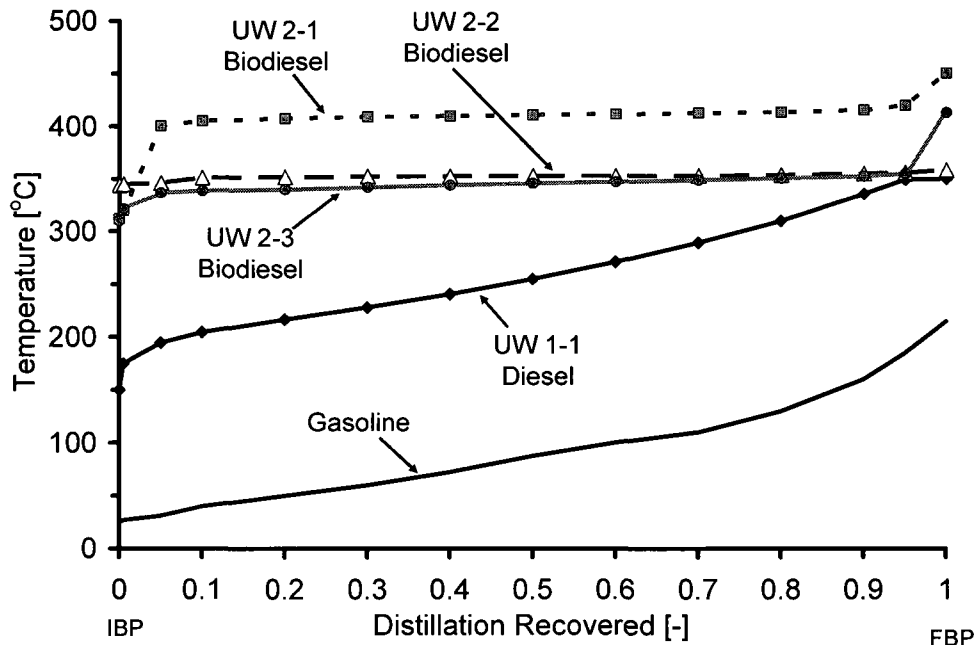
Figure 4-7: Distillation profiles for the test fuels (Zheng *et al.* 2007b).

Figure 4-7 shows the distillation profiles for the test fuels where gasoline has been included for the comparison of the fuel volatility. In comparison with the diesel fuel, the biodiesel fuels have lower volatility, are more viscous but have a narrow boiling range. Such biodiesels can readily be burnt in diesel engines through in-cylinder fuel injection,

87

although the higher CN for the biodiesel fuels UW2-2 and 2-3 would cause the start of ignition (i.e. SOC) to advance.

In order to achieve the homogeneous cylinder charge with diesel fuels, a variety of fuel delivery strategies have been devised and tested in the Clean Diesel Engine Research Laboratory at the University of Windsor, as shown in Figure 4-8. The intake port injection strategy has been reported previously (Zheng *et al.* 2006a), in which multi-pulse sequential injection and intake charge heating were applied to improve the cylinder charge mixing. The EGR fuel reforming technique, which helps to produce a stream of gaseous fuel from the liquid diesel supply, has been documented separately (Zheng *et al.* 2007a). The in-cylinder injection techniques are primarily discussed in this dissertation.
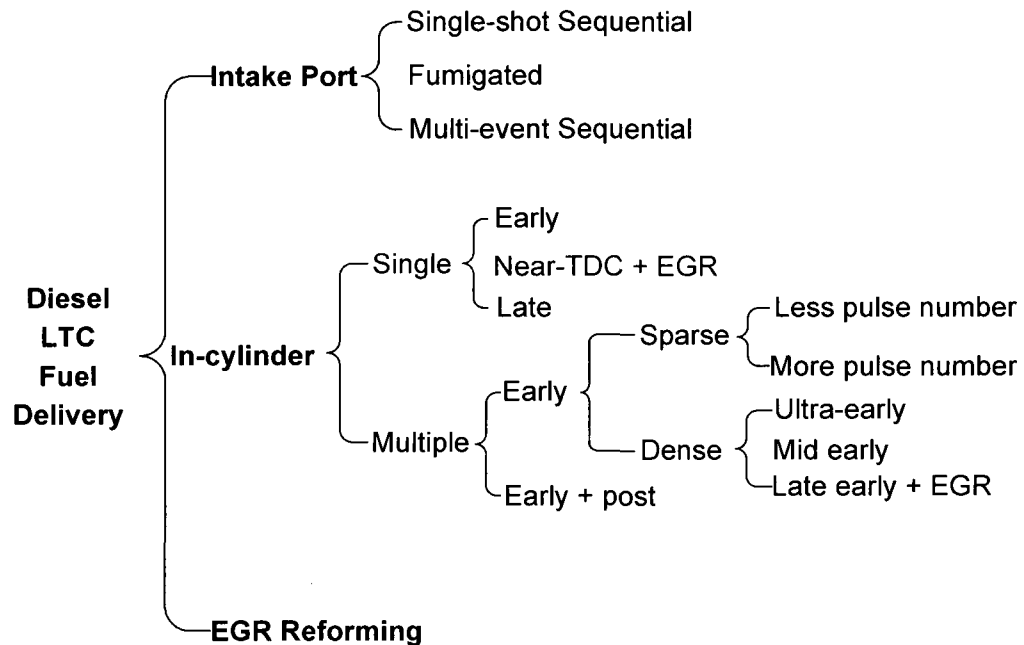
Figure 4-8: Fuel mixing strategies implemented at the University of Windsor.

Table 4-3: Characteristics of the test fuels.

Characteristic	ASTM Test Method	Diesel Fuel UW No. 1-1	Biodiesel Fuel UW No. 2-1	Biodiesel Fuel UW No. 2-2	Biodiesel Fuel UW No. 2-3
Feedstock	-	Petroleum Oil	Soy	Canola	Yellow Grease
Description	D975 (Diesel) D6751 (Biodiesel)	Ultra-low Sulphur	B100	B100	B100
Density [kg/m^3] @15°C	D1298	835.8	883.3	883.8	876.1
Cetane Number	D613	50.2	50.6	53.6	61.2
Kinematic Viscosity [cSt] @40°C	D445	1.5	4.1	4.4	4.8
Distillation Temperature [°C] (up to 95% distillation)	D86 (Diesel) D1160 (Biodiesel)	175~350	312~420	344~356	321~353
LHV [MJ/kg]	D4801	42.9	37.6	37.8	37.3
LHV [MJ/l]		35.9	33.2	33.4	32.7
Total Sulphur [ppm]	D5453	<4	6	2	15
Reduced Chemical Formula (based on C/H/O)	D5291	$CH_{1.9}$	$CH_{1.82}O_{0.11}$	$CH_{1.88}O_{0.11}$	$CH_{1.95}O_{0.11}$
Stoichiometric A/F (mass)	D5291	14.57	12.34	12.44	12.54

4.2.3 In-cylinder Pressure

In-cylinder pressures were acquired using a flush-mounted water-cooled KISTLER pressure transducer for the Yanmar engine. With respect to the Ford engine, an AVL pressure transducer mounted through the glow-plug slot was used. In the laboratory, the pressures are normally recorded for 200 cycles at 0.1°CA (degree crank angle) resolution with the help of Gurley rotary incremental encoders (Gurley Precision Instruments 2005). The 0.1°CA resolution is used to provide accurate ignition delay periods and thus phasing of the heat-release rates during the on-line monitoring of the combustion event. During the post-processing phase, pressures are averaged to 1°CA to calculate the IMEP, net heat-release rate and the cumulative heat-released. Furthermore, the 200 cycles are used to calculate the coefficient of variance (CoV) of the IMEP and other parameters. The net heat-release rate was evaluated as discussed in Chapter II.

4.2.4 Exhaust Gas Recirculation

To extend the EGR applicability in the Yanmar engine, a digitally controlled intake throttle valve was actuated by an in-house developed PC-control system. The intake throttling was used to increase the pressure differential between the exhaust and the intake thereby extending the EGR ratio in some cases. The amount of EGR could be estimated from Equation 4-6, where $\dot{m}_e$ is the mass flow rate of the recycled gases, $\dot{m}_a$ is the mass flow rate of the fresh air and $\dot{m}_f$ the mass flow rate of the fuel (specific to intake port-injection systems).

$$\text{EGR Ratio} = \frac{\dot{m}_e}{\dot{m}_a + \dot{m}_f + \dot{m}_e} \approx \frac{\text{Intake } CO_2}{\text{Exhaust } CO_2} \approx 1 - \frac{MAF_{new}}{MAF_{initial}} \qquad \text{Equation 4-6}$$

Empirically, the amount of EGR could be evaluated with sufficient accuracy by measuring the CO_2 concentration in the intake and exhaust (Stone 1999, Helmantel 2004, Helmantel & Denbratt 2004, 2006, Zheng *et al.* 2004). Alternatively, under steady operating conditions, the EGR rate could be evaluated from the mass air flow (MAF) readings where MAF_{new} and $MAF_{initial}$ are the intake mass air flow readings with and without EGR application, respectively.

4.2.5 Gas Sampling and Analyser System

A dual-bank exhaust analyser system (NO_x, UHC, CO, CO_2, O_2, and soot) was instrumented for the tests; normally one for the exhaust emissions and the other for the intake gas concentrations (Figure 4-9). At the time of the dissertation write-up, an in-cylinder gas sampling system (ultra-fast direct gas sampling system) was being installed for temporal analysis of the NO_x and UHC formation. Table 4-4 summarises the types of emission analysers used in the laboratory where THC denotes total hydrocarbons. A description of the working principles for the analysers is given below.
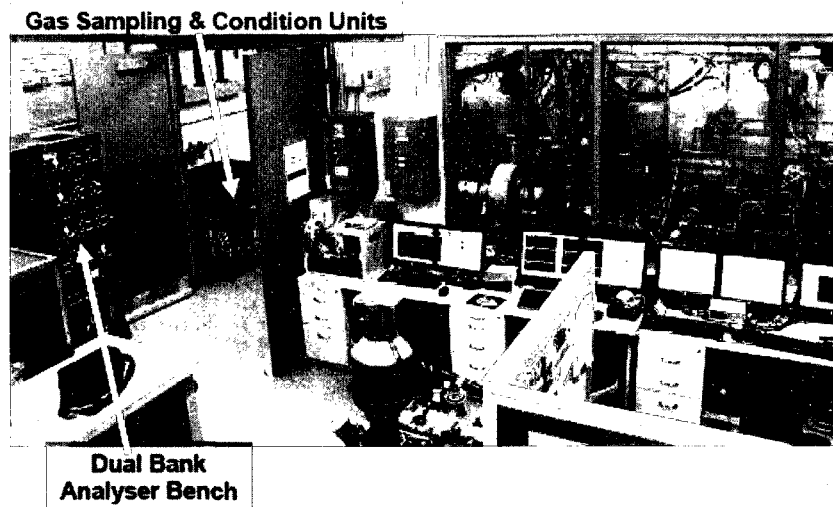
Figure 4-9: The dual bank gas analyser system.

Table 4-4: In-cylinder, intake and exhaust gas sampling analysers used in the laboratory.

Analyser Type	Species	Measured Unit	Manufacturer and Model No.
Dual Bank Emissions Bench (Intake/Exhaust)			
Non-Dispersive Infra-Red (NDIR)	CO	ppm	CAI Model 300
	CO_2	%	CAI Model 200 (Intake)
			CAI Model 602P Digital (Exhaust)
Paramagnetic	O_2	%	CAI Model 300 (Intake)
			CAI Model 602P Digital (Exhaust)
Heated Chemiluminescence	NO	ppm	CAI Model 600-HCLD Digital
	NO_2	ppm	
Heated-Flame Ionisation Detector (H-FID)	THC	ppm	CAI Model 300M-HFID
Variable sampling smoke meter	Smoke/Dry Soot	FSN (or mg/m^3)	AVL Model 415S
In-cylinder Direct Gas Sampling (Fast Sampling) Bench			
Heated Chemiluminescence	NO_x	ppm	CAMBUSTION /NO_x 400
Flame Ionisation Detector (FID)	THC	ppm	CAMBUSTION HFR 500 Fast FID

THC: Total Hydrocarbons (measuring C_1)

ppm: Parts per million

FSN: Filter Smoke Number

CAI: California Analytical Instruments, Inc.

AVL: AVL List GmbH

92

4.2.5 (a) Non-Dispersive Infra-Red (NDIR) System

As discussed by Stone (1999), infra-red radiation is absorbed by a wide range of gas molecules, each of which has a characteristic absorption spectrum. The fraction of radiation transmitted, τ_λ, at a particular wavelength is given by Beer's Law shown in Equation 4-7 where ρ is the gas density, α_λ is the absorptivity and L is the path length.

$$\tau_\lambda = \exp(-\rho\alpha_\lambda L) \hspace{4cm} \text{Equation 4-7}$$

The key components in the NDIR system include the infra-red source and the reference, sample and detector cells, among others. The detector cells are filled with the gas that is to be measured so that they absorb the radiation in the wavelength band associated with the gas (Stone 1999). The gas to be analysed flows through the sample cell and the reference cell is filled with air. If the relevant gas is present in the sample, infra-red will be absorbed in the sample cell and less infra-red will be absorbed in the detector cell resulting in a pressure differential in the detector cells. This pressure differential can then be measured and related to the gas concentration. In the CAI NDIR analysers, the differential pressure causes a slight gas flow between the two-chamber infra-red micro-flow detector (CAI 2000). This flow is detected by a mass flow sensor and converted to an AC signal which is then amplified and rectified into a DC voltage signal and ultimately supplied to the output terminal and digital panel meter. The electrical signal is, therefore, directly proportional to the concentration of the sample gas.

4.2.5 (b) Paramagnetic System

A number of O_2 analysers using various methods of operation are available. Nonetheless, the paramagnetic types are probably the most accurate (Stone 1999). Paramagnetism is a form of magnetism which occurs only in the presence of an externally applied magnetic field. It occurs in O_2 because two of the electrons in its outer shell are unpaired consequently the O_2 modelcule is attracted by a magnetic field (Stone 1999). Commonly, there are two main types of O_2 analysers using paramagnetic principle; thermomagnetic analysers and magneto-dynamic analysers.

The CAI analyser measures the paramagnetic susceptibility of the sample gas by means of a magneto-dynamic type measuring cell (CAI 2000). The cell consists of a dumbbell of diamagnetic material, which is controlled electronically at 50°C. The higher the O_2 concentration, the great the dumbbell is deflected from its rest position. This deflection is detected by an optical system connected to an amplifier. Surrounding the dumbbell is a coil of wire. A current is passed through this coil to return the dumbbell to its original position. The current applied is linearly proportional to the percent of O_2 concentration in the sample gas which is displayed on a digital panel meter.

4.2.5 (c) Chemiluminescence System

Chemiluminescence is the emission of electromagnetic radiation, most commonly generated by oxidation, during the course of chemical reactions. Therefore, the chemiluminescence technique depends on the emission of light. In Equation 4-8, NO

reacts with ozone (O_3) to produce nitrogen dioxide in an activated state (NO_2^*) which in due course can emit light as it reverts to its normal state (Stone 1999):

$$NO + O_3 \rightarrow NO_2^* + O_2 \rightarrow NO_2 + O_2 + photon \qquad \text{Equation 4-8}$$
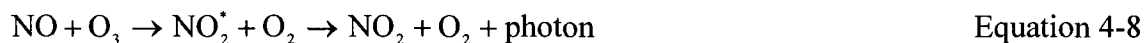
The CAI analyser utilises the principal of chemiluminescence for analysing NO or NO_x (CAI 2000). In the NO mode, the method is based upon the chemiluminescent reaction between O_3 and NO to yield NO_2 and O_2. This reaction produces light which has an intensity proportional to the mass flow rate of NO_2 into the chamber. The light is measured by means of a photodiode and associated amplifications electronics. In the NO_x mode, the $NO+NO_2$ is determined as above, however, the sample is first routed through the internal NO_2 to NO converter which converts the NO_2 in the sample to NO. The resultant reaction is then directly proportional to the total concentration of NO_x.

4.2.5 (d) Heated Flame Ionisation Detector (H-FID)

The flame ionisation method operates on the principle that when hydrocarbons are burnt, electrons and positive ions are formed. If the un-burnt hydrocarbons are burnt in an electric field, the current flow corresponds very closely to the number of carbon atoms present (Stone 1999).

The CAI analyser utilises the flame ionisation detection method to determine the total hydrocarbon concentration within a gaseous sample (CAI 2000). The analyser has an adjustable heated oven (60 to 200°C) which contains a heated pump and burner in which

a small flame is elevated and sustained by regulated flows of air and either pure H_2 or a 40/60 mixture of H_2 and He. The burner jet is used as an electrode and is connected to the negative side of a precision power supply. An additional electrode, known as the "collector" is connected to a high impedance, low noise electronic amplifier. The two electrodes establish an electrostatic field. When a gaseous sample is introduced to the burner, it is ionised in the flame and the electrostatic field causes the charged particles to migrate to their respective electrodes. The migration creates a small current between the electrodes. This current is measured by the precision electrometer amplifier and is directly proportional to the hydrocarbon concentration in the sample (CAI 2000).

4.2.5 (e) Smoke Meter

The soot emissions were acquired with the help of the AVL 415S smoke meter. This is a filter-type meter for measuring soot content in the exhaust of diesel and related internal combustion engines. The result of the measurement is displayed as FSN defined according to the ISO standard 10054 as the loss of reflectivity of filter paper after sampling an exhaust gas column of 405mm length (AVL 2002). Part of the exhaust gas flow is sampled by means of a probe in the exhaust line and drawn through a filter paper. The resultant blackening of the filter paper is measured by a reflectometer and represents a measure of the soot content in the exhaust gas. The blackening of the filter paper primarily depends on the soot concentration in the exhaust gas and the effective sampling length (exhaust gas volume in relation to the filter area). The unloaded, clean filter paper is given the value 0 and completely blackened, soot-coated filter paper or 100 %

blackening is given the value 10 FSN. The correlation between the filter paper loading

(FSN) and the soot concentration is shown in Equation 4-9 and plotted in Figure 4-10.

$$\text{Soot} \, [\text{mg/m}^3] = 13.11 \times \text{Loading} \, [\text{FSN}] \times \exp(0.31 \times \text{Loading} \, [\text{FSN}]) \qquad \text{Equation 4-9}$$
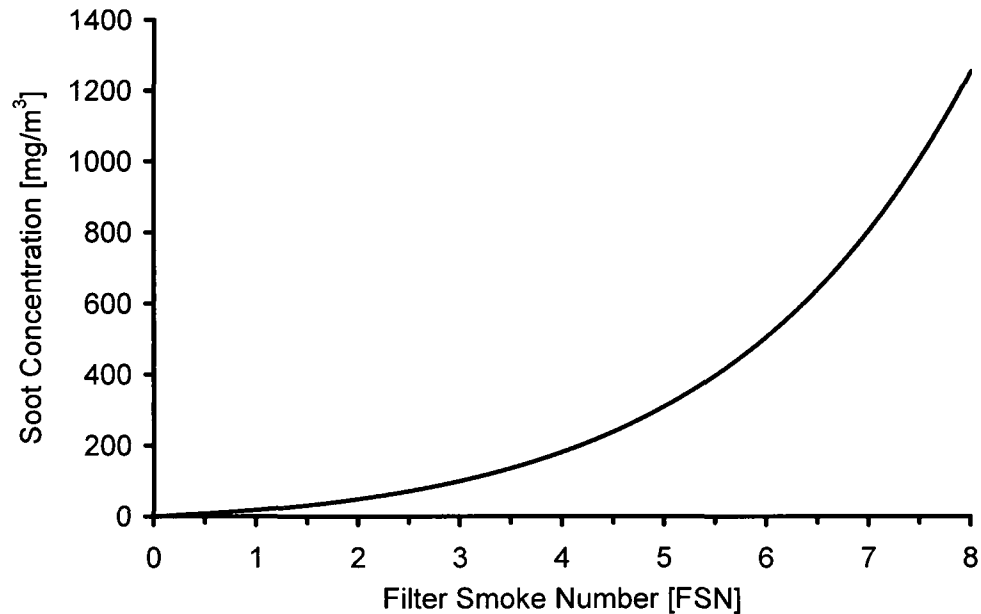
Figure 4-10: Correlation between soot concentration and filter loading.

The emissions of CO, THC and NO_x are acquired in ppm while the smoke is in FSN. The

regulation is to report them on a brake-specific basis in g/kW-hr. A discussion of how to

convert the emissions is given in APPENDIX D. Note also that multi-cylinder engines

are normally tested on a driving cycle therefore and the weighted emissions from each

mode are added and reported as composite emissions. The procedure to determine the

composite emissions is also presented in APPENDIX D.

CHAPTER V

EXHAUST GAS RECIRCULATION ANALYSIS

The most common technique to reduce the in-cylinder NO_x formation in diesel engines is the implementation of EGR. Exhaust gas recirculation brings back a portion of the products of combustion into the cylinder. This may be achieved by intake and exhaust valve profile adjustment to trap some of the gases after the combustion event (prompt EGR) or by physical piping (external EGR). The decrease in NO_x emissions with the increase of EGR rate is the result of mainly the thermal, dilution and chemical effects (Ladomatos *et al.* 2000, Zheng *et al.* 2004). In modern DI diesel engines, the external EGR is commonly employed as shown in Figure 5-1. Noticeably, at 0%EGR the mass flow rate of the fresh charge is equal to the total intake air flow rate i.e. $M_{air} = M_{in}$ at 0% EGR.

M_{air}: Mass flow rate of fresh air
M_{in}: Mass flow rate of air + recycled gases
M_{Fuel}: Mass flow rate of fuel into the engine
M_{out}: Mass flow rate of engine-out exhaust gases
X_{EGR}: Mass fraction of EGR
λ: Excess fresh air-to-fuel ratio
λ_{cyl}: In-cylinder air-to-fuel ratio
λ_{Exh}: Excess fresh air-to-fuel ratio evaluated from exhaust
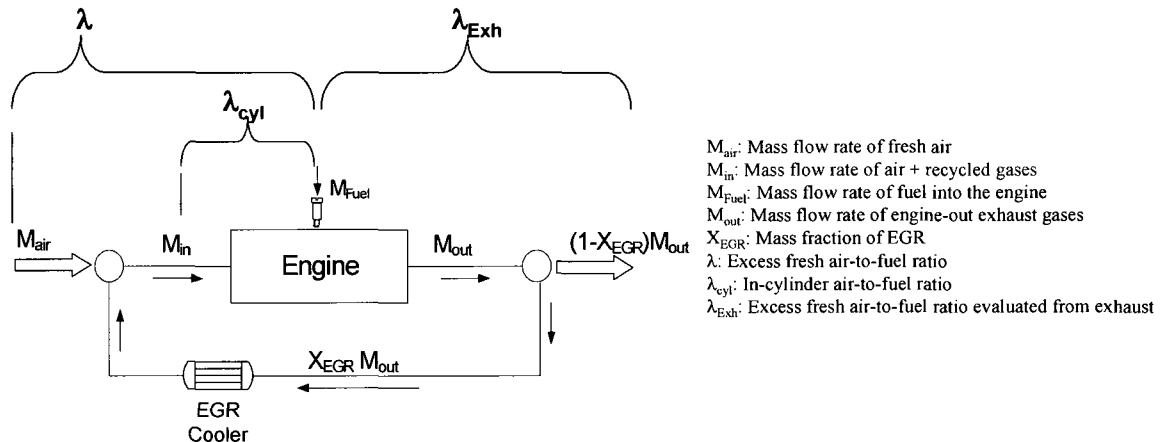
Figure 5-1: External exhaust gas recirculation system.

5.1 The Effects of EGR

At the same temperature, the constant-pressure molar specific heat capacity of gases increases with the number of atoms in the molecules (Heywood 1988, Turns 2000) i.e.

$Cp_{monatomic} < Cp_{diatomic} < Cp_{triatomic}$. In the thermal effects, therefore, the increase of inlet heat capacity due to higher specific heat capacity of re-circulated CO_2 and H_2O compared with O_2 and N_2 (at constant boost pressure) results in lowered in-cylinder peak compression and combustion temperatures.

With respect to the dilution effect, the diminished inlet O_2 concentration, whose main consequence is the deceleration of the mixing between O_2 and fuel, results in the extension of flame region. As a result, the gas quantity that absorbs the heat released is increased subsequently leading to a lower flame temperature. It is noted that one consequence of the dilution effect is the reduction of local temperatures which can also be considered as a local thermal effect. Furthermore, the dilution effect contributes to the reduction of the oxygen partial pressure and its effect on kinetics of the elementary NO formation reactions.

The re-circulated H_2O and CO_2 are dissociated during combustion. The dissociation of H_2O and CO_2, constituting the chemical effect, is believed to affect the combustion process and the NO_x formation. In particular, the endothermic dissociation of H_2O results in a decrease of the flame temperature.

Other effects include the increased soot formation and increased ignition delay with increasing EGR. In the HTC mode, the increase of soot formation with EGR results in an increase of the flame radiation thus decreasing the flame temperature. Furthermore, an increase of the ignition delay with EGR rate is generally observed. Consequently, the

whole combustion process would be shifted further into the expansion stroke, leading to lowered combustion temperatures.

5.2 The Evaluation of EGR

There are several ways of evaluating the EGR rate. As discussed in Chapter IV, the use of intake and exhaust CO_2 concentrations is commonly employed. Alternatively, especially when the EGR valve can be independently controlled, the mass air flow rate may be employed as shown in Equation 5-1 where m_0 and m_1 are the intake mass air flow rates (M_{air} in Figure 5-1) without and with EGR implementation, respectively. The variation of the fresh intake air flow rate with EGR is presented in Figure 5-2 for different boost levels. A η_{vol} of 86% was employed in the calculation, which represents an empirically evaluated average in the Clean Diesel Engine Research Laboratory at 1400rpm and 0% EGR rate.

$$r_{egr} = 1 - \frac{m_1}{m_0} \qquad\qquad \text{Equation 5-1}$$

Because the fresh mass air flow rate decreases with increasing EGR, the excess air-to-fuel ratio λ of Figure 5-1 could be evaluated thus:

$$m_0 r_{egr} = m_0 - m_1 \qquad\qquad \text{Equation 5-2a}$$

$$m_1 = m_0 \left(1 - r_{egr}\right) \qquad\qquad \text{Equation 5-2b}$$

From the definition shown in Equation 5-3, the expression for λ is given in Equation 5-4.

$$\lambda = \frac{\left(\dfrac{\dot{m}_{air}}{\dot{m}_f}\right)_{Actual}}{\left(\dfrac{\dot{m}_{air}}{\dot{m}_f}\right)_{Stoichionetric}}$$

Equation 5-3

$$\lambda = \frac{m_0\left(1 - r_{egr}\right)}{\left(\dfrac{\dot{m}_{air}}{\dot{m}_f}\right)_{Stoichiometric} \times \left(\dot{m}_f\right)_{Actual}}$$

Equation 5-4
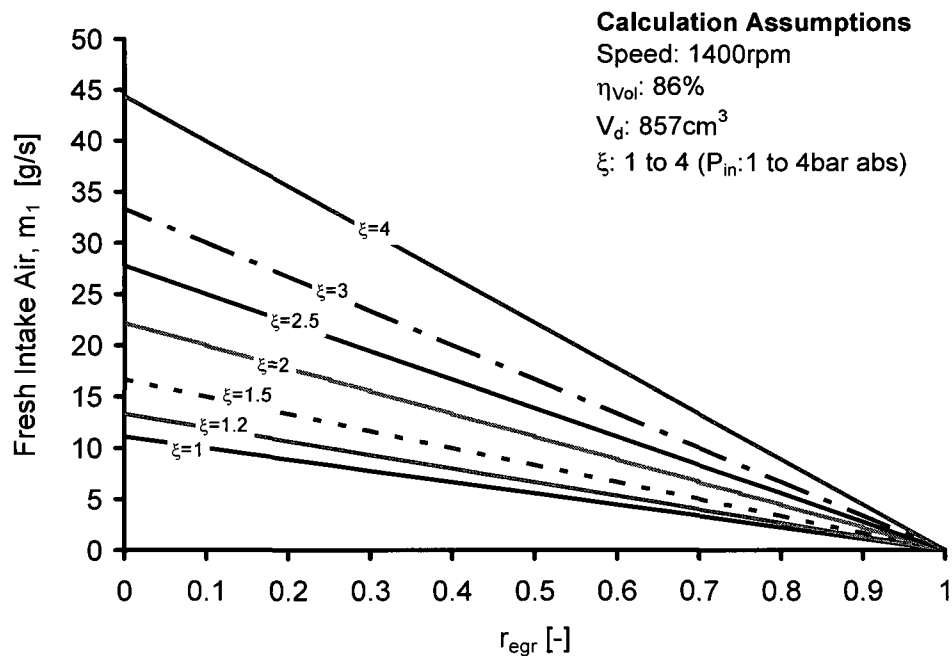
Figure 5-2: Effect of EGR rate on fresh intake air flow rate at different boost levels.

At constant fuelling rate, intake pressure and speed, as the EGR rate is increased the excess air-to-fuel ratio decreases as shown in Figure 5-3. Note that λ_0 is the excess air-to-fuel ratio at 0% EGR. Because diesel engines are inherently lean-burn systems, the excess air-to-fuel ratio has been truncated at stoichiometric conditions i.e. $\lambda=1$. Below this limit, the air/fuel mixture enters the rich conditions which are normally not attained during the power-producing cycles in modern diesel engines. Rich conditions may,

however, be employed to facilitate the effective operation of the after-treatment systems such as lean NO_x traps using in-cylinder post injection.
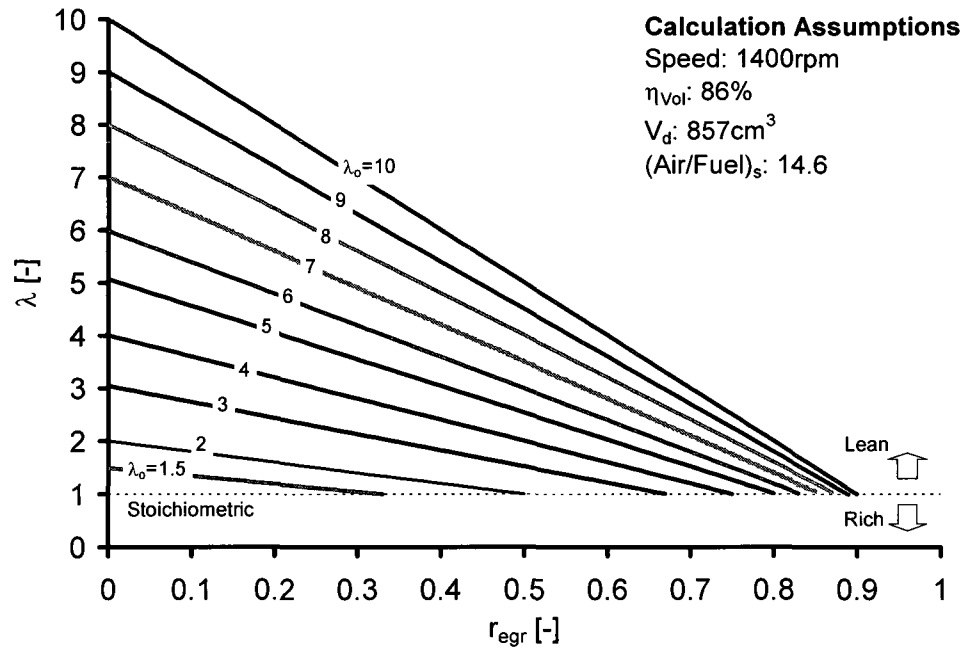
Figure 5-3: Effect of EGR rate on fresh air excess air-to-fuel ratio.

A molar-based analysis could provide helpful insight into the applicability of the EGR. The assumption of complete combustion of a lean hydrocarbon based fuel with fresh air yields Equation 5-5.

The reactants are :

$$C_\alpha H_\beta O_\gamma + \lambda \left(\alpha + \frac{\beta}{4} - \frac{\gamma}{2} \right)(O_2 + 3.762 N_2)$$
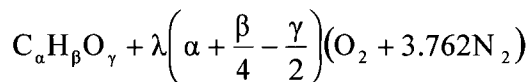
The products are :

Equation 5-5

$$\alpha CO_2 + \frac{\beta}{2} H_2O + \lambda \left(\alpha + \frac{\beta}{4} - \frac{\gamma}{2} \right) \times 3.762 N_2 + (\lambda - 1)\left(\alpha + \frac{\beta}{4} - \frac{\gamma}{2} \right)O_2$$
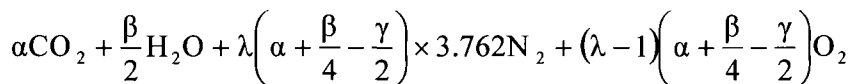
Evaluated from Equation 5-5, the variation of the volumetric composition of the exhaust gases with λ is shown in Figure 5-4. As the load decreases (decreasing fuelling rate at constant speed and boost), the exhaust concentration of CO_2 and H_2O also decreases. Consequently, at low load conditions the effect of the re-circulated gases on in-cylinder combustion may not be observed at low EGR rates. It is not uncommon to attain 50% EGR at low load conditions before appreciable in-cylinder effects are observed. Under such conditions, intake throttling is normally employed to increase the pressure differential between the intake and exhaust plenums thus enhancing the EGR.
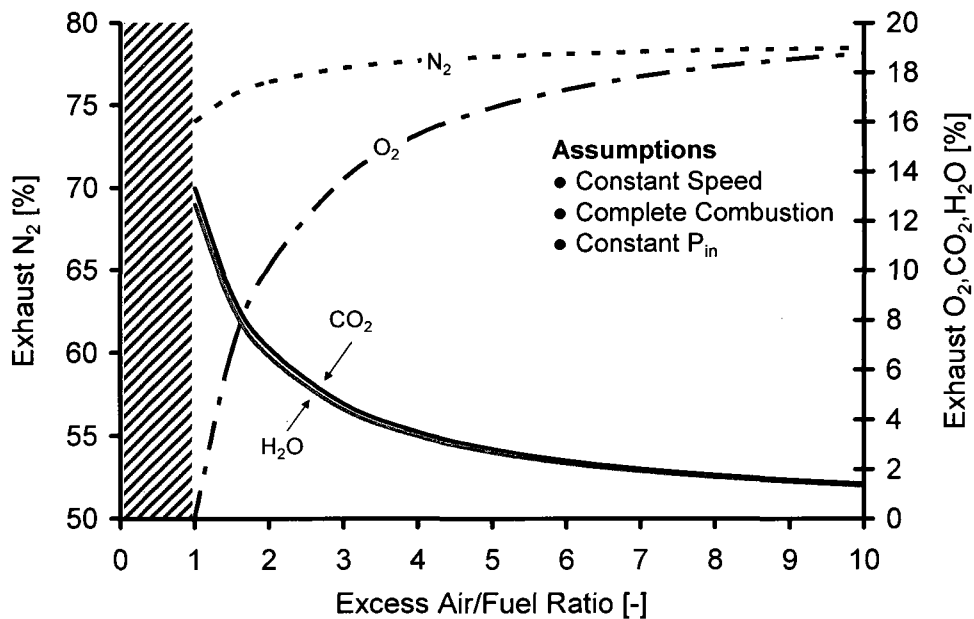
Figure 5-4: Variation of exhaust species concentrations with excess air/fuel ratio.

Because the EGR displaces the fresh intake air, Equation 5-5 can be extended as shown below, where it has been separated into the intake charge and exhaust gas compositions for clarity. The intake charge composition, which includes the fresh charge and recycled gases, can be evaluated from Equation 5-6:

$$\left(\lambda - r_{egr}\right) \times \left(\alpha + \frac{\beta}{4} - \frac{\gamma}{2}\right)O_2 + \lambda\left(\alpha + \frac{\beta}{4} - \frac{\gamma}{2}\right) \times 3.762N_2 + \alpha \times r_{egr}CO_2 + \frac{\beta}{2} \times r_{egr}H_2O \quad \text{Equation 5-6}$$

The intake molar species concentrations for O_2, N_2, CO_2 and H_2O are:

$$\chi_{Reac(O_2)} = \frac{\left(\lambda - r_{egr}\right) \times \left(\alpha + \frac{\beta}{4} - \frac{\gamma}{2}\right)}{\left(\lambda - r_{egr}\right) \times \left(\alpha + \frac{\beta}{4} - \frac{\gamma}{2}\right) + \lambda\left(\alpha + \frac{\beta}{4} - \frac{\gamma}{2}\right) \times 3.762 + \alpha \times r_{egr} + \frac{\beta}{2} \times r_{egr}} \quad \text{Equation 5-7a}$$

$$\chi_{Reac(N_2)} = \frac{\lambda\left(\alpha + \frac{\beta}{4} - \frac{\gamma}{2}\right) \times 3.762}{\left(\lambda - r_{egr}\right) \times \left(\alpha + \frac{\beta}{4} - \frac{\gamma}{2}\right) + \lambda\left(\alpha + \frac{\beta}{4} - \frac{\gamma}{2}\right) \times 3.762 + \alpha \times r_{egr} + \frac{\beta}{2} \times r_{egr}} \quad \text{Equation 5-7b}$$

$$\chi_{Reac(CO_2)} = \frac{\alpha \times r_{egr}}{\left(\lambda - r_{egr}\right) \times \left(\alpha + \frac{\beta}{4} - \frac{\gamma}{2}\right) + \lambda\left(\alpha + \frac{\beta}{4} - \frac{\gamma}{2}\right) \times 3.762 + \alpha \times r_{egr} + \frac{\beta}{2} \times r_{egr}} \quad \text{Equation 5-7c}$$

$$\chi_{Reat(H_2O)} = \frac{\frac{\beta}{2} \times r_{egr}}{\left(\lambda - r_{egr}\right) \times \left(\alpha + \frac{\beta}{4} - \frac{\gamma}{2}\right) + \lambda\left(\alpha + \frac{\beta}{4} - \frac{\gamma}{2}\right) \times 3.762 + \alpha \times r_{egr} + \frac{\beta}{2} \times r_{egr}} \quad \text{Equation 5-7d}$$

The exhaust gas composition can be evaluated from Equation 5-8:

$$\alpha\left(1 + r_{egr}\right)CO_2 + \frac{\beta}{2}\left(1 + r_{egr}\right)H_2O + \lambda\left(\alpha + \frac{\beta}{4} - \frac{\gamma}{2}\right) \times 3.762N_2 + \left(\lambda - r_{egr} - 1\right) \times \left(\alpha + \frac{\beta}{4} - \frac{\gamma}{2}\right)O_2 \quad \text{Equation 5-8}$$

The exhaust molar species concentrations for O_2, N_2, CO_2 and H_2O are:

$$\chi_{Prod(O_2)} = \frac{\left(\lambda - r_{egr} - 1\right) \times \left(\alpha + \frac{\beta}{4} - \frac{\gamma}{2}\right)}{\alpha\left(1 + r_{egr}\right) + \frac{\beta}{2}\left(1 + r_{egr}\right) + \lambda\left(\alpha + \frac{\beta}{4} - \frac{\gamma}{2}\right) \times 3.762 + \left(\lambda - r_{egr} - 1\right) \times \left(\alpha + \frac{\beta}{4} - \frac{\gamma}{2}\right)} \quad \text{Equation 5-9a}$$

$$\chi_{Prod(N_2)} = \frac{\lambda\left(\alpha + \frac{\beta}{4} - \frac{\gamma}{2}\right) \times 3.762}{\alpha\left(1 + r_{egr}\right) + \frac{\beta}{2}\left(1 + r_{egr}\right) + \lambda\left(\alpha + \frac{\beta}{4} - \frac{\gamma}{2}\right) \times 3.762 + \left(\lambda - r_{egr} - 1\right) \times \left(\alpha + \frac{\beta}{4} - \frac{\gamma}{2}\right)} \quad \text{Equation 5-9b}$$

$$\chi_{Prod(CO_2)} = \frac{\alpha\left(1 + r_{egr}\right)}{\alpha\left(1 + r_{egr}\right) + \frac{\beta}{2}\left(1 + r_{egr}\right) + \lambda\left(\alpha + \frac{\beta}{4} - \frac{\gamma}{2}\right) \times 3.762 + \left(\lambda - r_{egr} - 1\right) \times \left(\alpha + \frac{\beta}{4} - \frac{\gamma}{2}\right)} \quad \text{Equation 5-9c}$$

$$\chi_{Prod(H_2O)} = \frac{\frac{\beta}{2}(1 + r_{egr})}{\alpha(1 + r_{egr}) + \frac{\beta}{2}(1 + r_{egr}) + \lambda\left(\alpha + \frac{\beta}{4} - \frac{\gamma}{2}\right) \times 3.762 + (\lambda - r_{egr} - 1) \times \left(\alpha + \frac{\beta}{4} - \frac{\gamma}{2}\right)} \qquad \text{Equation 5-9d}$$

The above equations may be used for any complete combustion of a lean air/fuel mixture for fuel with composition $C_\alpha H_\beta O_\gamma$. Note that an iterative process is necessary to achieve convergence of the EGR rate. At the time of this dissertation, a manuscript detailing the EGR analysis in the Clean Diesel Engine Research Laboratory at the University of Windsor was being compiled for peer reviewed publications.

Figure 5-5 to Figure 5-7 shows the analysis for the fuels investigated in this dissertation. Note that at constant load, speed and boost conditions with 0% EGR, the assumption of complete combustion yields the same concentration of O_2 in the exhaust irrespective of the fuel. A similar result was observed for the exhaust CO_2 and H_2O. Because the biodiesel is oxygenated, more fuel has to be added to attain the same excess air-to-fuel ratio as that of diesel fuel (compare 0.76g/s for diesel UW1-1 and 0.90g/s for biodiesel UW2-1 at stoichiometric conditions with 1400rpm, 86% η_{Vol}, 857cm^3 V_d and ξ of 1). Therefore, the result is not surprising apropos of the assumptions made.
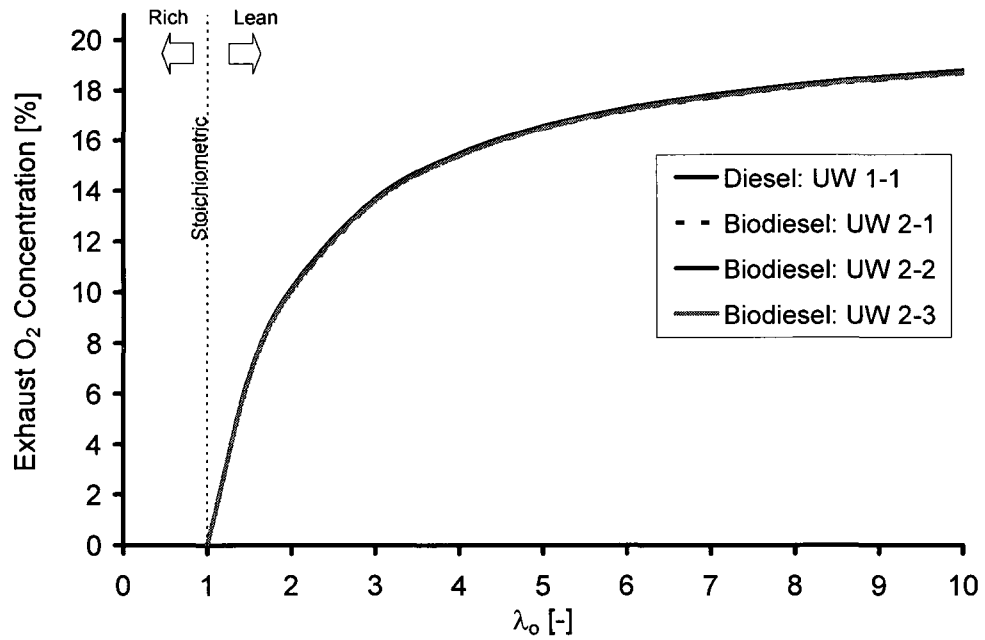
Figure 5-5: Variation of exhaust O_2 concentration with λ_o.
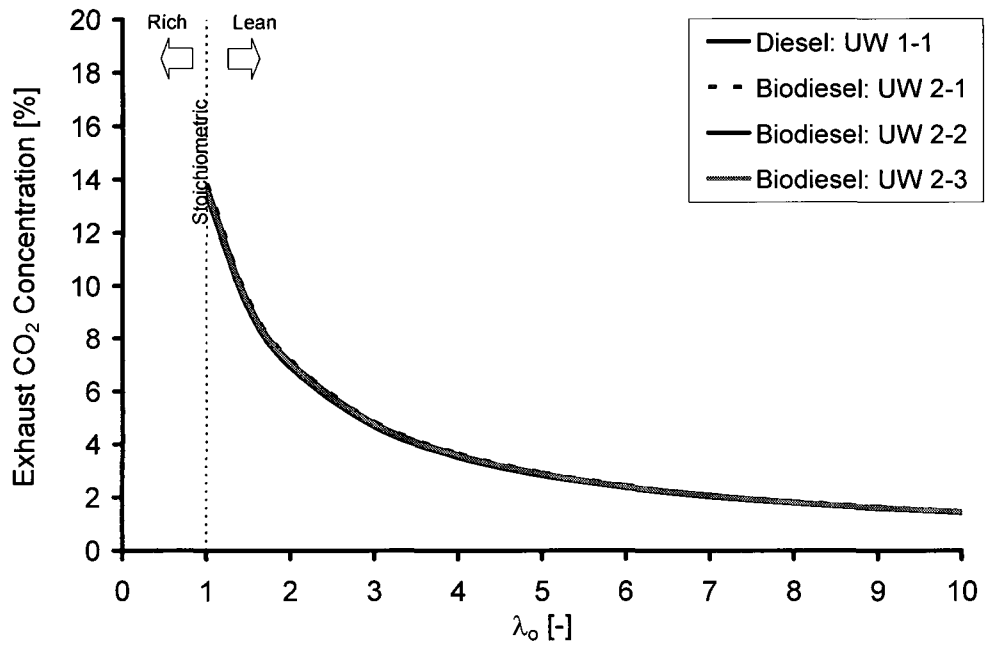
Figure 5-6: Variation of exhaust CO_2 concentration with λ_o.
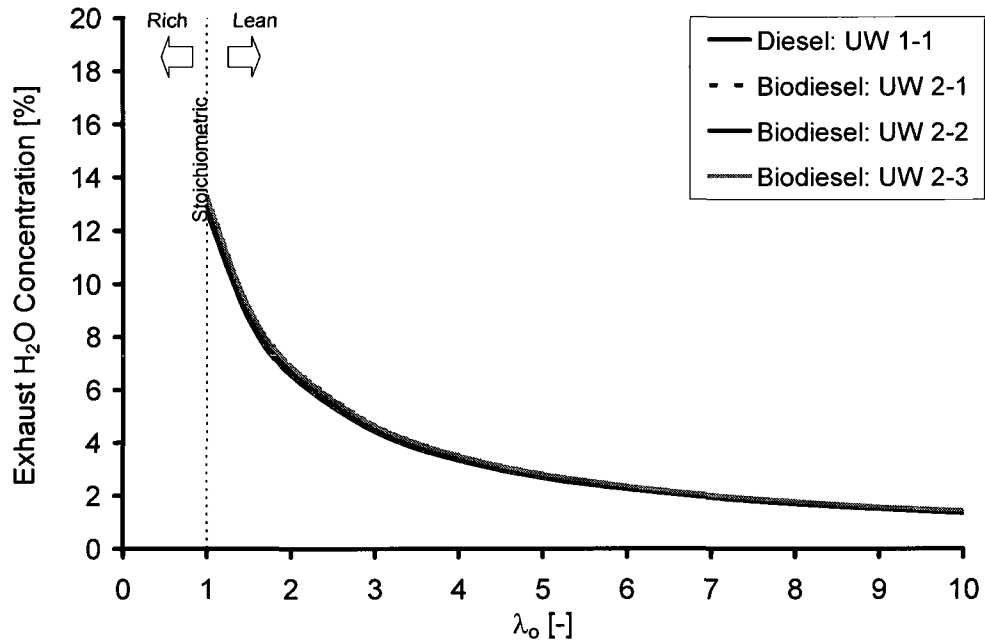
Figure 5-7: Variation of exhaust H_2O concentration with λ_o.

Nonetheless, the combustion of fuels in internal combustion engine applications does not follow the global reactions considered above. The combustion is, instead, believed to follow a sequence of complex chemical kinetic reaction mechanisms. If a multi-component fuel, such as diesel, is employed one could only imagine the intricacy of such mechanisms. As discussed in Chapter II, in the diffusion-controlled combustion process, the fuel strives to find the oxygen and *vice versa*, in order to form a combustible mixture. If the fuel is oxygenated and its molecular composition has an optimal structure that makes the oxygen accessible for combustion, then more complete burning of the fuel may be promoted (Mueller *et al*. 2003). Figure 5-8 is a schematic representation summarising the fuel/air mixture preparation process for oxygenated and non-oxygenated fuels. Because the biodiesel fuels contain oxygen atoms, they may promote a more complete combustion of the fuel compared to conventional diesel fuels. The effective reduction of the engine-out emissions of CO, UHC and PM by the fuel-borne oxygen in biodiesel

107

fuels has been well-characterised and the conclusion appears to be robust (EPA 2002). Consequently, at constant load, speed and boost conditions, the exhaust concentrations of O_2 shown in Figure 5-5 may not necessarily be the same for the biodiesel and diesel fuels. The same should be said about the exhaust concentrations of CO_2 and H_2O shown in Figures 5-6 and 5-7, respectively.
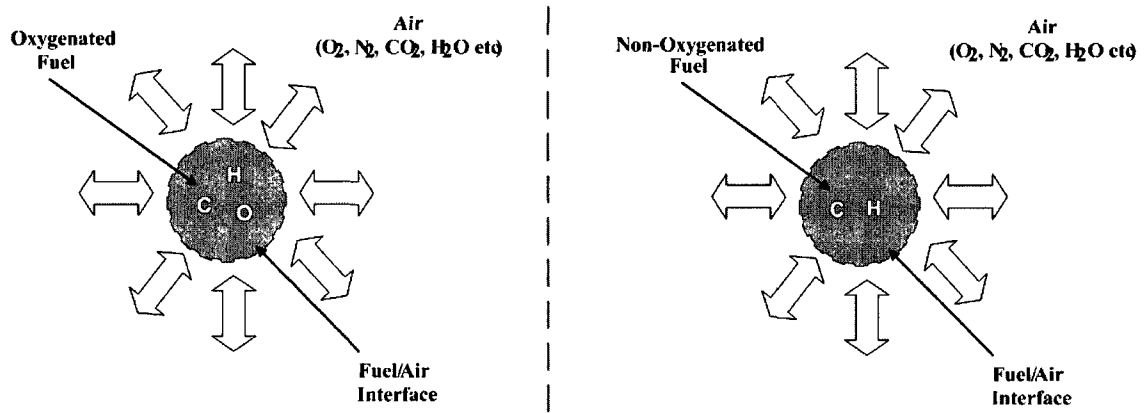
Figure 5-8: Schematic of oxygenated and non-oxygenated fuel/air mixing process.

When the intake oxygen concentration is known, the effective excess air-to-fuel ratio, also referred to as the in-cylinder excess air-to-fuel ratio ($\lambda_{Eff} = \lambda_E = \lambda_{Cyl}$), may be evaluated with the help of Equation 5-10 where [O_2] is the measured intake oxygen concentration in [%], MW_{O_2} and MW_{air} are the molecular weights for O_2 and air respectively and M_{in} is the total mass air flow rate into the cylinder (Zheng et al. 2007c).

$$\lambda_{Cyl} = \frac{\left(\left(\frac{[O_2]}{100} \right) \times \left(\frac{MW_{O_2}}{MW_{air}} \right) \times M_{in} \times 4.29 \right)}{\left(\frac{\dot{m}_{air}}{\dot{m}_f} \right)_{Stoichiometric} \times \left(\dot{m}_f \right)_{Actual}}$$

Equation 5-10

Apparently, one of the assumptions made in the application of Equation 5-10 is that for every gramme of O_2 there would be 3.29g of N_2 to constitute air i.e. 4.29g of air. The in-cylinder residual gases are therefore not considered.

Figure 5-9 shows the calculated results for the variation of the intake oxygen concentration and in-cylinder excess air-to-fuel ratio with fuelling rate for diesel and biodiesel fuels. The squares and circles represent the diesel and biodiesel fuels, respectively. Similar to the discussion above, at constant fuelling rate, speed and boost levels, the λ_{Cyl} for the biodiesel is expected to be higher than that for diesel fuel. Figure 5-10 and Figure 5-11 are the 3-D plots for diesel and biodiesel fuels, respectively, which show a clear indication of the mentioned trends.
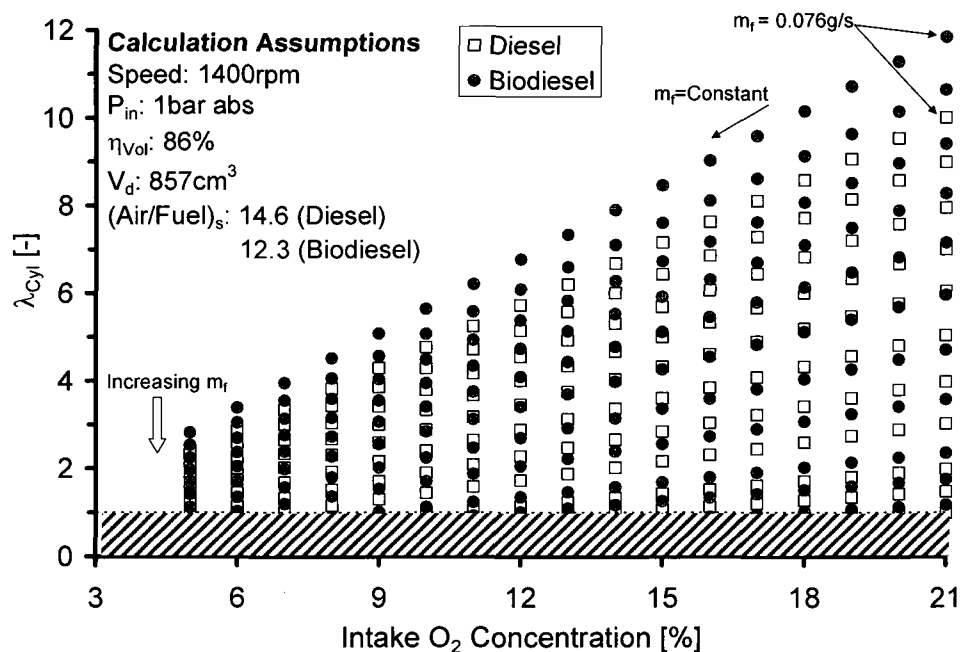
Figure 5-9: Variation of λ_{Cyl} with intake O_2 concentration.
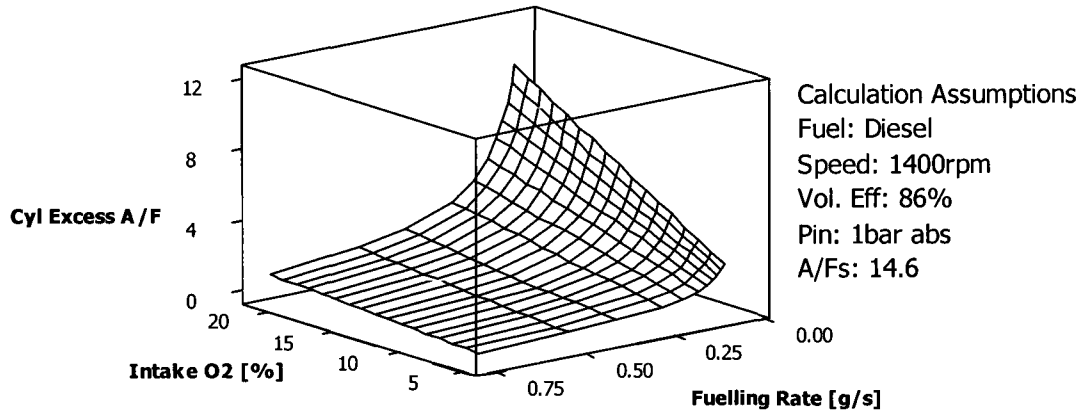
Figure 5-10: Variation of λ_{Cyl} with intake O_2 and fuelling rate for diesel fuel.
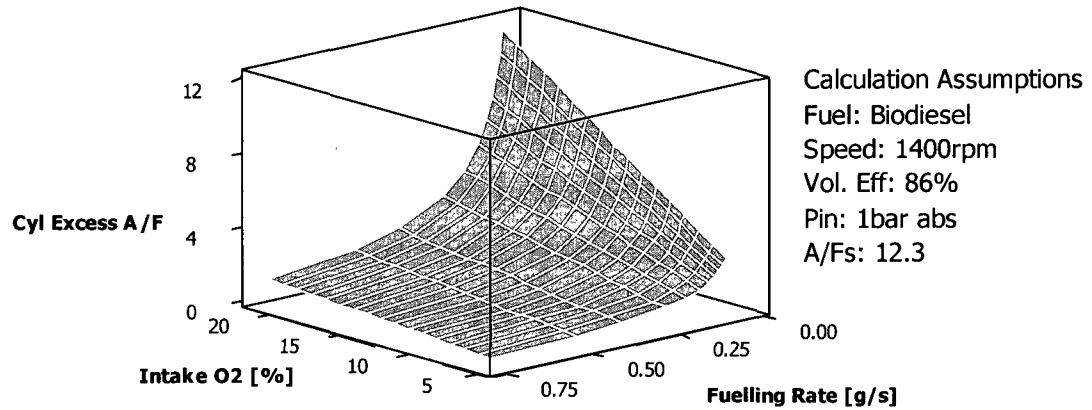
Figure 5-11: Variation of λ_{Cyl} with intake O_2 and fuelling rate for biodiesel fuel.

At 0% EGR, the excess air-to-fuel ratios λ and λ_{Cyl} would be the same. As the EGR rate is increased the ratios decrease. The λ would simply follow a linear relationship with the EGR rate so that at 0% EGR $\lambda_o=\lambda$, as shown in Equation 5-11.

$$\lambda = \lambda_o \left(1 - \lambda_o r_{egr}\right)$$ Equation 5-11

On the other hand, the λ_{Cyl} would be comprised of the λ and the effect of oxygen from the re-circulated exhaust, ϑ, among others, as shown in Equation 5-12a. This is because

diesel engines are inherently lean-burn systems thus the re-circulated gases will also contain some oxygen. As a consequence, the λ_{Cyl} may not necessarily be a straight line as in the λ vs. r_{egr} relationship. It should also be noted that when the λ_{Cyl} attains the stoichiometric condition, there would be no oxygen in the exhaust to re-circulate. Accordingly, $\lambda_{Cyl} = \lambda$ at stoichiometric conditions.

$$\lambda_{Cyl} = \lambda + \lambda r_{egr} + \vartheta \qquad \qquad \text{Equation 5-12a}$$

$$\lambda_{Cyl} = \lambda \; ; \text{at 0\% EGR} \qquad \qquad \text{Equation 5-12b}$$

$$\lambda_{Cyl} = \lambda = 1 \, ; \text{at stoichiometric conditions} \qquad \qquad \text{Equation 5-12c}$$

Combining Equation 5-12a with the boundary conditions shown in Equations 5-12b and 5-12c yields the relationship between the in-cylinder and fresh charge excess air-to-fuel ratios shown in Equation 5-13.

$$\lambda_{Cyl} = \lambda\left(1 + r_{egr}\right) - r_{egr} \qquad \qquad \text{Equation 5-13}$$

Figure 5-12 to Figure 5-14 show the variation of λ and λ_{Cyl} with the EGR rate for diesel and biodiesel fuels. Figure 5-15 shows similar trends obtained from the experimental investigations, in the Clean Diesel Engine Research Laboratory at the University of Windsor, with diesel fuel using the MAF-based EGR rate up to 70%. The results were in good agreement with the analysis. Because the combustion inefficiency in diesel HTC

mode is normally $\leq 2\%$ (Heywood 1988), the assumption that the diesel engine exhaust

gas in HTC is composed of N_2, CO_2, H_2O and O_2 is thermodynamically reasonable.
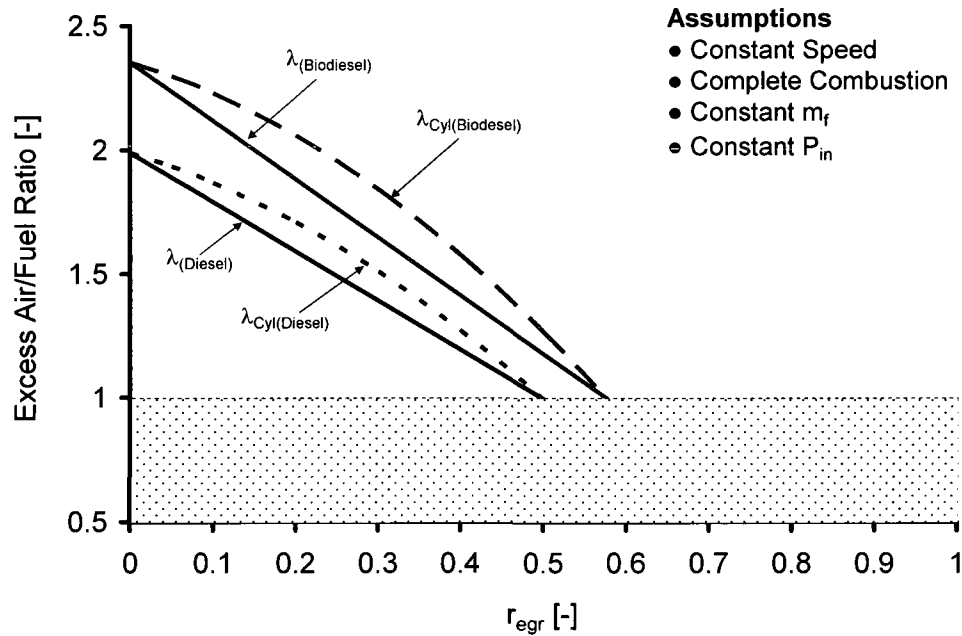
Figure 5-12: Variation of λ and λ_{Cyl} with EGR rate at medium-to-high load.
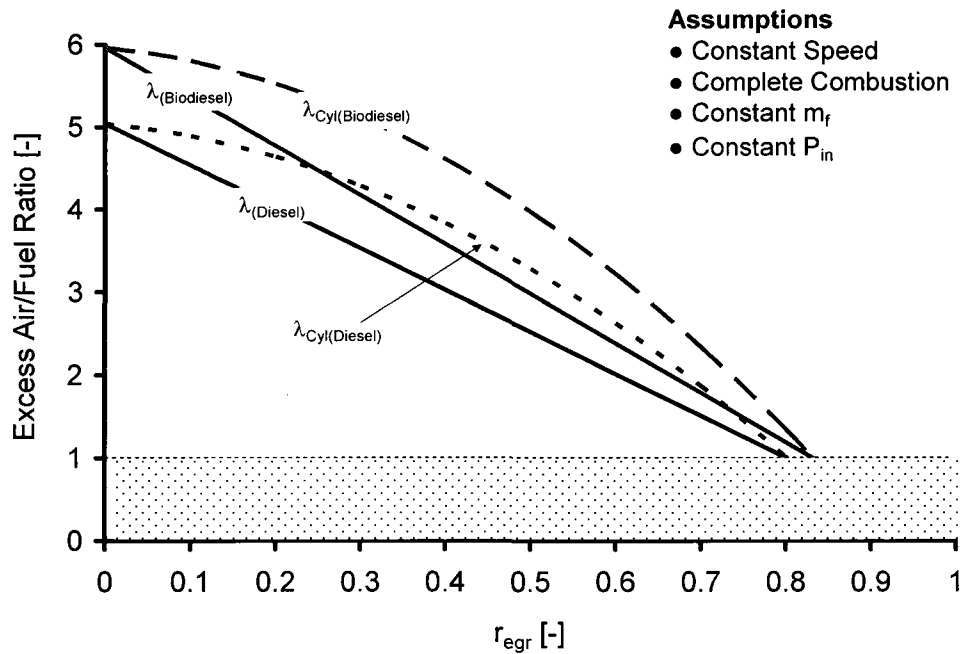
Figure 5-13: Variation of λ and λ_{Cyl} with EGR rate at low-to-medium load.
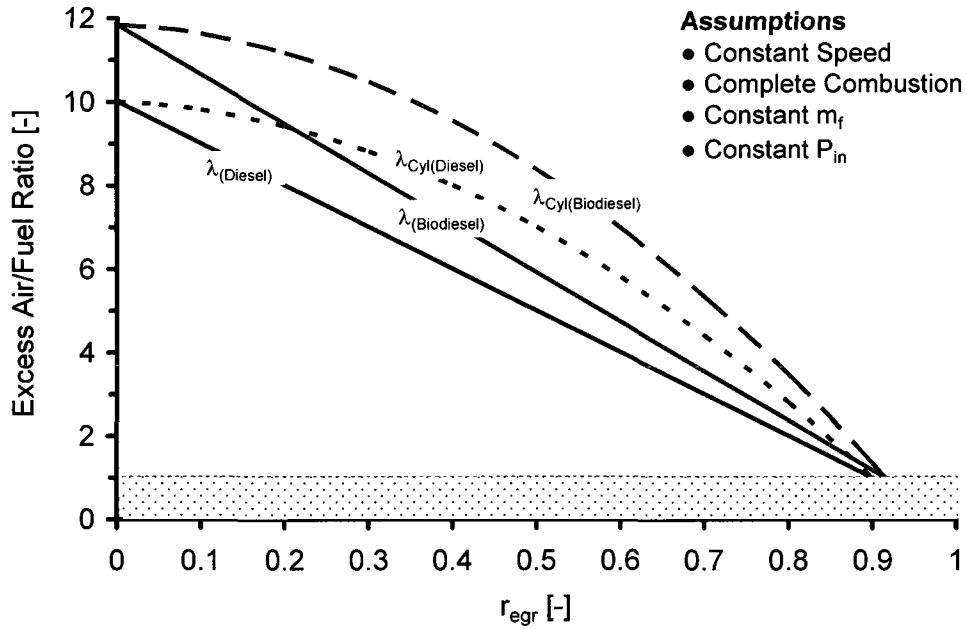
Figure 5-14: Variation of λ and λ_Cyl with EGR rate at very low load.
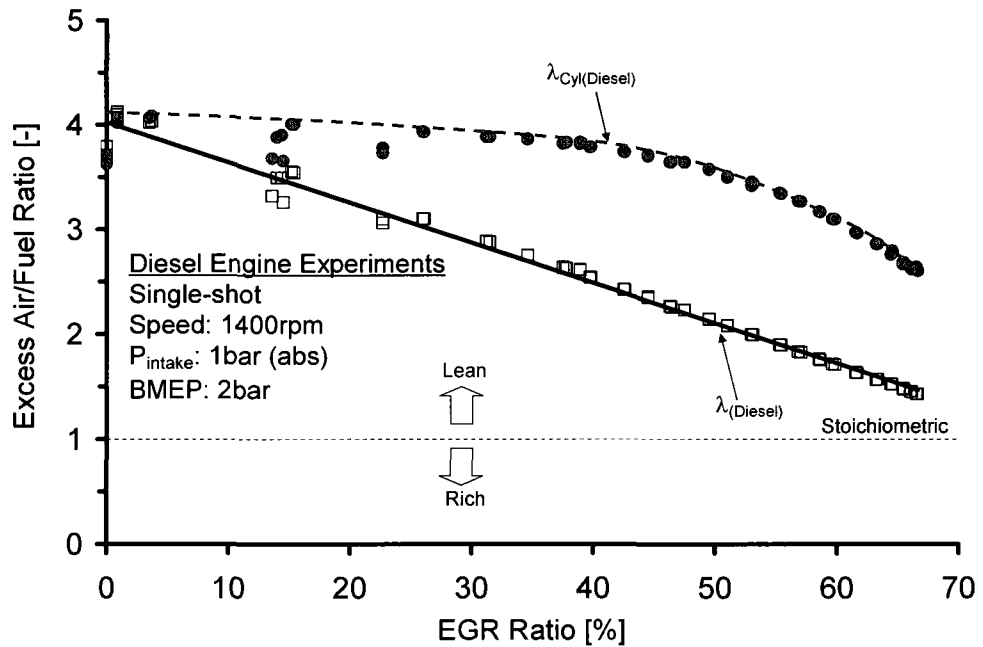
Figure 5-15: Experimental variation of λ and λ_Cyl with EGR rate at low load.

CHAPTER VI

MODELLING RESULTS AND DISCUSSION

6.1 Engine Cycle Simulation (0-D)

In general, the heat-release rates during the main stage of combustion in LTC mode appear to have a Gaussian-like shape (Ogink, 2004), which can also be observed in Figure 3-3. Therefore, an arbitrary Gaussian-like heat-release rate was specified as the input to the SAES programme and the SOC varied from 300 to 450°CA. Because the fuel/air mixtures in LTC mode are near-homogeneous, ignition occurs almost instantaneously at multiple sites resulting in shortened combustion durations. In the present study, a combustion duration sweep from 5 to 70°CA was investigated.

From Figure 6-1 to Figure 6-5 it can be deduced that rapid combustion would produce a higher rate-of-pressure rise thus increased combustion noise. However, it appears that changing the LTC combustion duration may have only minimal effects, if any, on the engine efficiency. Instead, the HRR CA50, i.e. crank angle of 50% heat-released, has significant influence on the thermal efficiency. For the cases investigated, the maximum engine cycle efficiency occurred at HRR CA50 370°CA, corresponding to a SOC of 360~365°CA.

As reported by Zheng et al. (2007d) who extended this study to include the effect of heat-release shaping, the trend of the simulation results largely agreed with the empirical observations of the diesel LTC operations that have a tendency of early combustion phasing. The gain in energy utilisation by the shortened apparent burning duration of

diesel LTC operations was quantified as making insignificant improvement in the thermal efficiency from the modelling analysis.

Furthermore, the engine cycle simulation could be considered as enlightening to help identify the influencing parameters of diesel LTC efficiency. The simulation indicated that the phasing had the strongest, the duration the medium and the shaping the weakest effects on diesel LTC thermal efficiency (Zheng *et al.* 2007d).
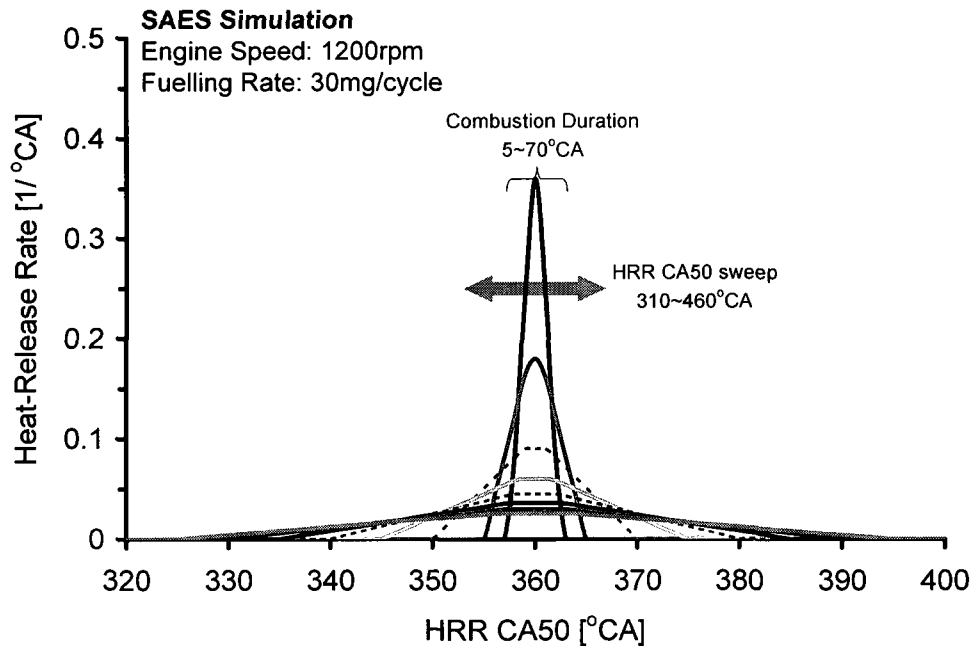
Figure 6-1: SAES simulation input for heat-release phasing and duration sweeps.
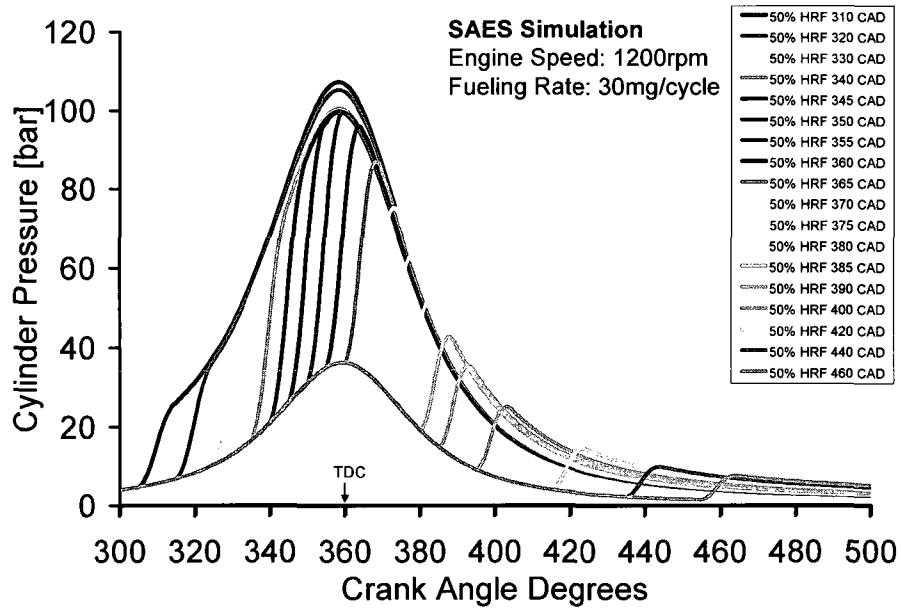
Figure 6-2: SAES simulation results showing pressure profiles for the CA50 sweep.
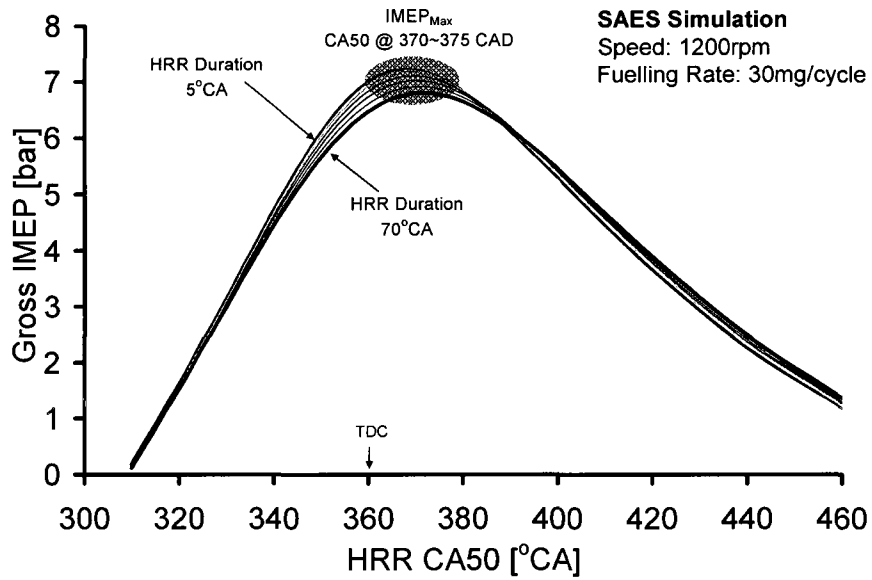
Figure 6-3: Effect of heat-release phasing and duration on IMEP - SAES.
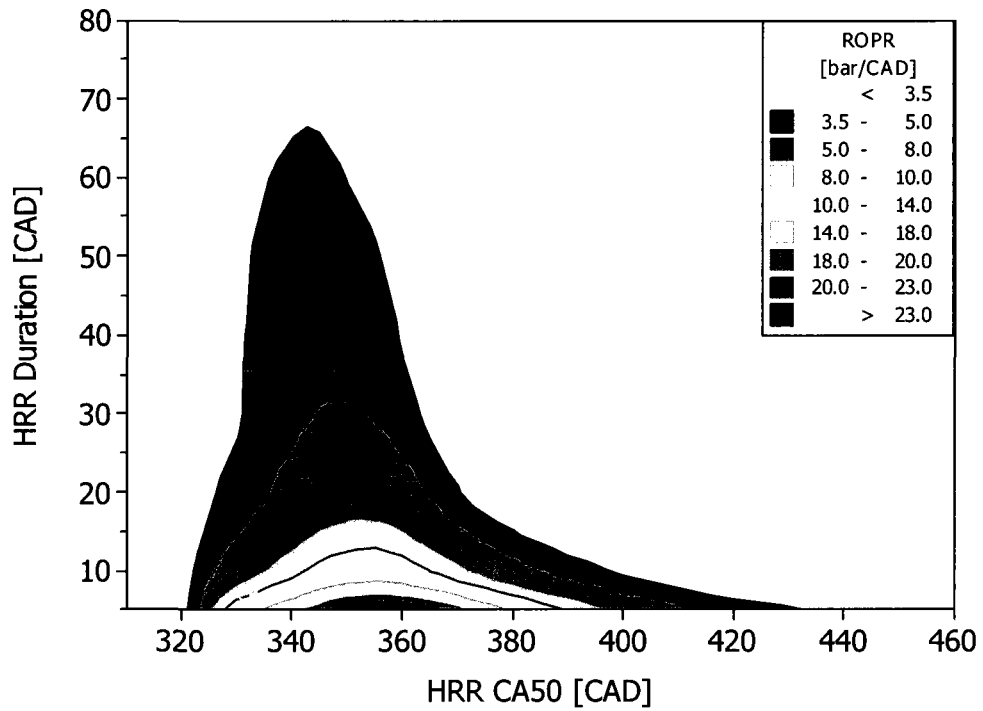
Figure 6-4: Effect of heat-release phasing and duration on dP/dθ$_{Max}$ - SAES.
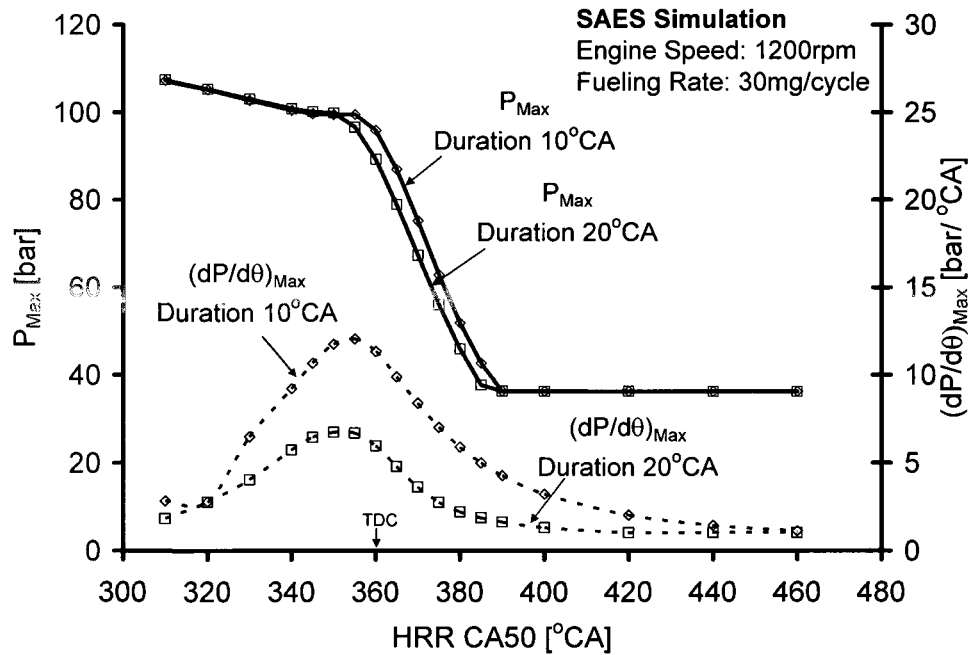
Figure 6-5: P$_{max}$ and (dP/dθ)$_{max}$ profiles for CA50 sweep - SAES.

6.2 Chemical Kinetics Modelling

To simulate diesel fuel, Curran's n-heptane mechanism was employed. The effect of EGR was simulated by diluting the homogeneous charge with CO_2 while keeping the fuelling rate constant. Table C-1 in APPENDIX C shows some of the properties of the model fuels and Table 6-1 shows the simulation input parameters. In order to attain ignition of the Methyl Butanoate/air mixture near TDC for the specified input conditions, the mixture temperature at IVC had to be set to 400K. Using the same temperature for the n-heptane/air mixture however resulted in extremely advanced auto-ignition. Therefore, the mixture temperature for the n-heptane/air at IVC was set to 300K.

Table 6-1: CHEMKIN Simulation input parameters.

Input Parameters	Values Used
Start of Computation [CAD ATDC]	-135
End of Computation [CAD ATDC]	135
Excess Air/Fuel Ratio (0% CO_2)	3
Estimated Fuelling [mg/cycle]	32, 23
Intake CO_2 [%]	0~8.5
Intake Pressure [atm (abs)]	1.2
Temperature @ IVC [K]	400, 300

Figure 6-6 to Figure 6-13 show the biodiesel and diesel model fuel results from the CHEMKIN simulations. For the conditions considered, the maximum peak cylinder temperature attained was 2000K and less than 1800K for model biodiesel and diesel, respectively. The peak cylinder temperatures reduced with the increase in the charge dilution. These temperatures were quite close to the thermal NO_x formation threshold of 1800K (Stone 1999, Turns 2000). Within this low-temperature homogeneous combustion mode, the engine-out NO_x levels are expected to be relatively low while soot levels, represented by the soot precursor (C_2H_2), would be near-zero if auto-ignition was

attained. Generally, the n-heptane produced more soot precursors per mg of fuel than the

oxygenated fuel.
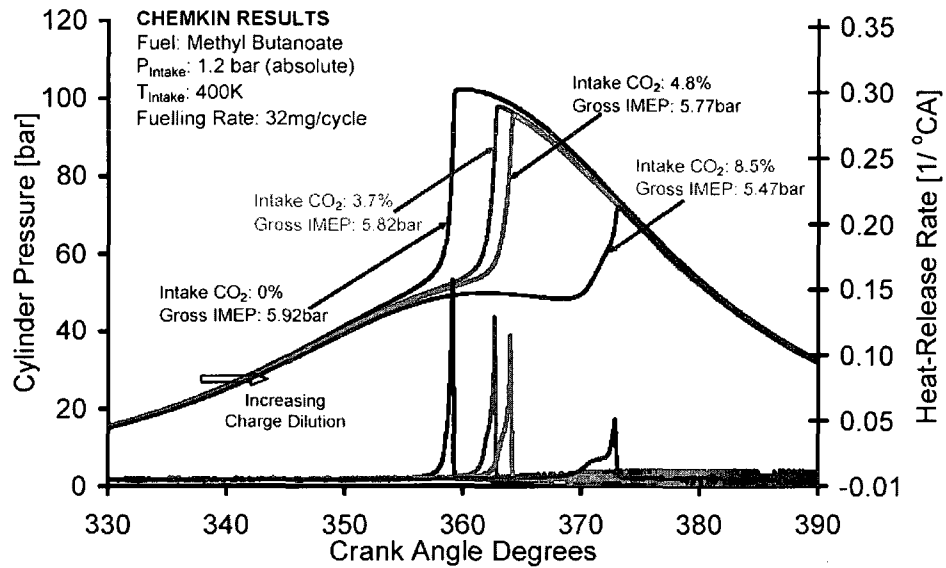
Figure 6-6: Effect of CO_2 on pressure and HRR for biodiesel - CHEMKIN.
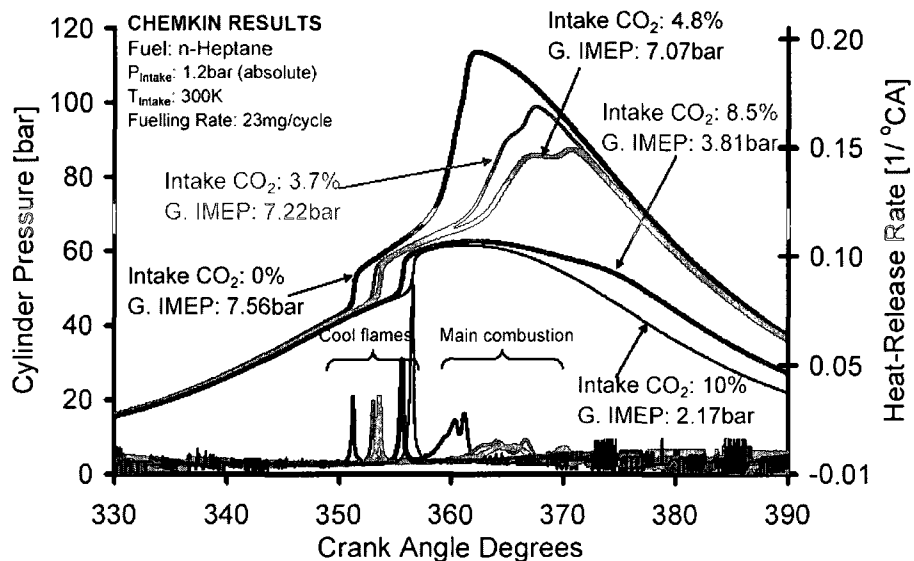
Figure 6-7: Effect of CO_2 on pressure and HRR for diesel - CHEMKIN.
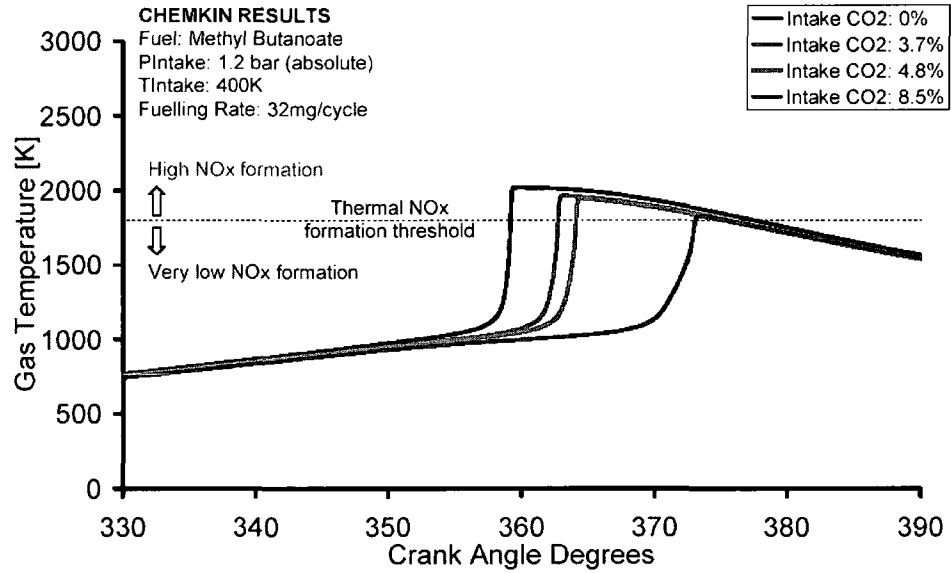
Figure 6-8: Effect of CO_2 on gas temperature for biodiesel - CHEMKIN.
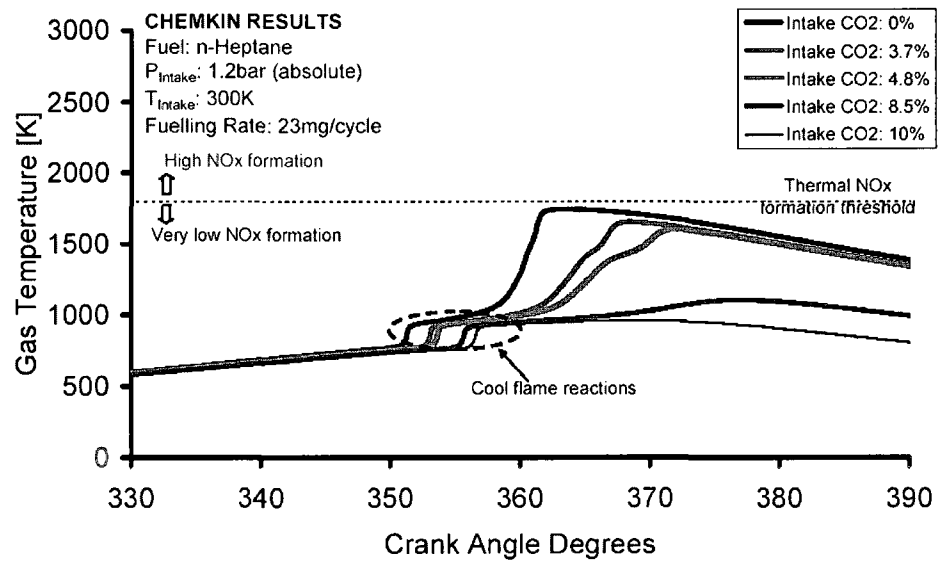
Figure 6-9: Effect of CO_2 on gas temperature for diesel - CHEMKIN.

CHEMKIN RESULTS
Fuel: Methyl Butanoate
P_{Intake}: 1.2 bar (absolute)
T_{intake}: 400K
Fuelling Rate: 32mg/cycle

Increasing charge dilution

0% Intake CO_2
G. IMEP: 5.92bar

3.7% Intake CO_2
G. IMEP: 5.82bar

4.8% Intake CO_2
G. IMEP: 5.77bar

8.5% Intake CO_2
G. IMEP: 5.47bar
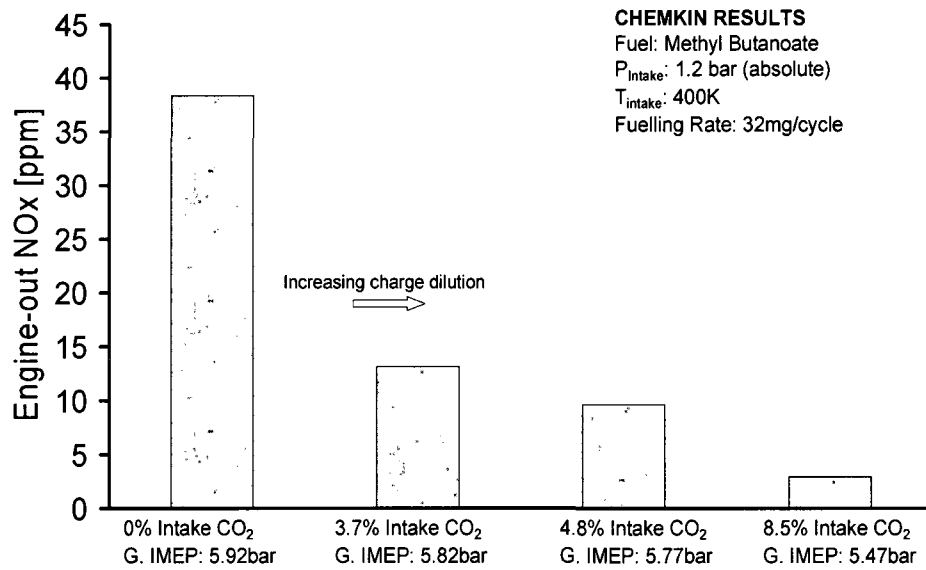
Figure 6-10: Effect of CO_2 on engine-out NO_x for biodiesel - CHEMKIN.

CHEMKIN RESULTS
Fuel: n-Heptane
P_{Intake}: 1.2bar (absolute)
T_{Intake}: 300K
Fuelling Rate: 23mg/cycle

Increasing charge dilution

ONLY Cool flame reactions observed.
No main combustion stage.

0% Intake CO_2
G. IMEP: 7.56bar

3.7% Intake CO_2
G. IMEP: 7.22bar

4.8% Intake CO_2
G. IMEP: 7.07bar

8.5% Intake CO_2
10% Intake CO_2
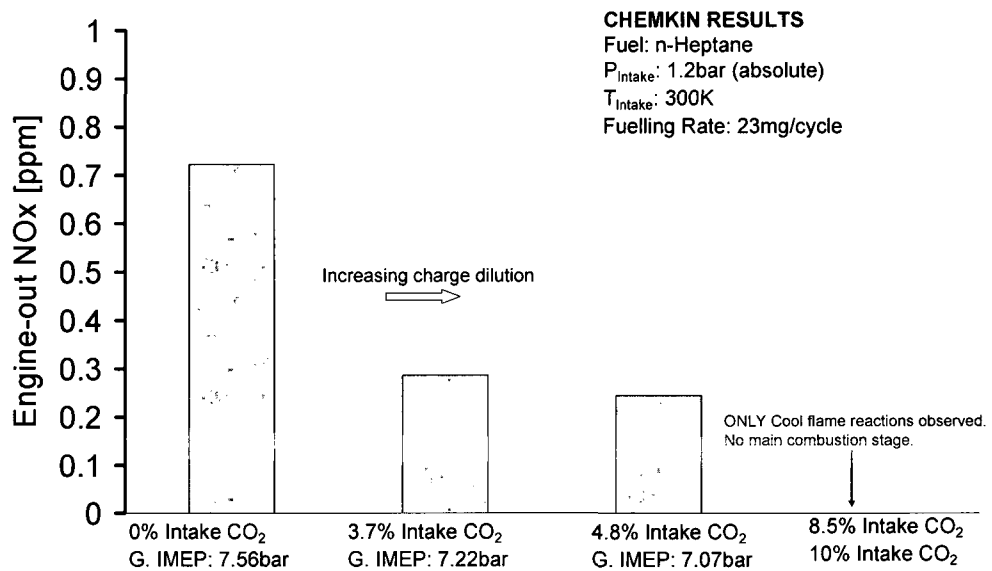
Figure 6-11: Effect of CO_2 on engine-out NO_x for diesel - CHEMKIN.

121
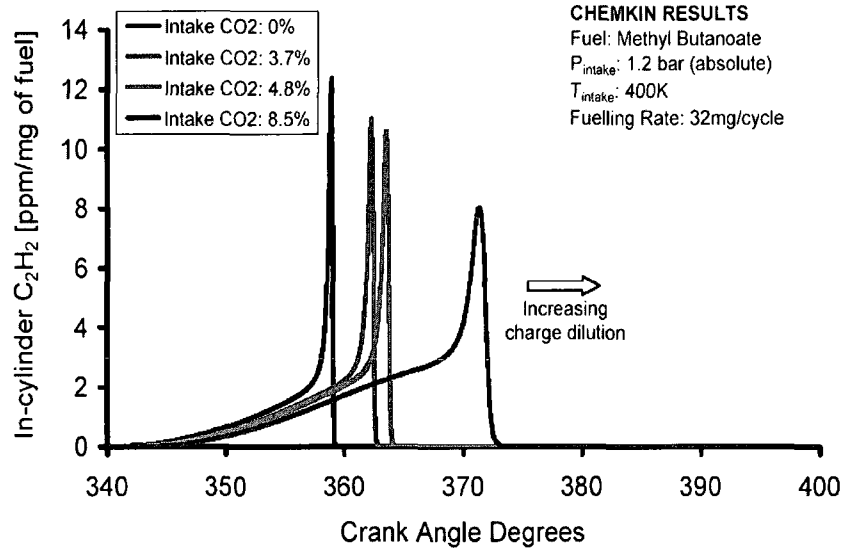
Figure 6-12: Effect of CO_2 on evolution of soot precursor for biodiesel - CHEMKIN.
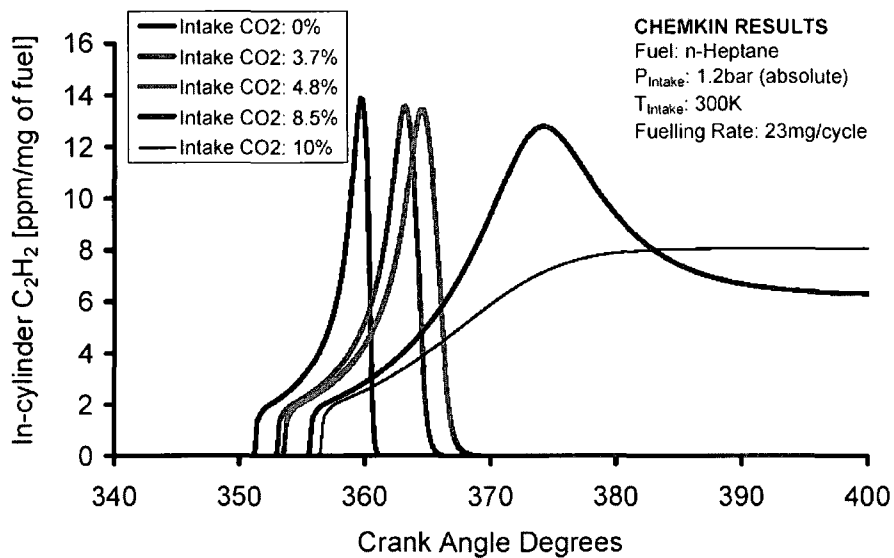
Figure 6-13: Effect of CO_2 on evolution of soot precursor for diesel - CHEMKIN.

6.3 Multidimensional Modelling

KIVA was utilised to provide insights into the combustion modes for the single-cylinder and modern common-rail multi-pulse DI diesel engines. The model fuel used was n-Tetradecane ($C_{14}H_{30}$), whose chemical composition is dissimilar from diesel fuel. As a consequence, a need to calibrate the model arises. The model was calibrated by matching

the experimental and simulated pressures and heat-release rate profiles. Table 6-2 shows the parameters used during the KIVA calibration process using an 18,000-cell 60° sector mesh while Figure 6-14 shows the results. The ignition delay was calibrated by adjusting the pre-exponential constant in the Shell Auto-ignition model while the premixed and diffusion burning phases were calibrated by adjusting the parameters in the Combustion Model.

Table 6-2: Parameters used during the KIVA calibration process.

Parameter		Empirical	KIVA
Fuel		UW1-1 Diesel	$C_{14}H_{30}$
Speed [rpm]		1200	1200
Intake Pressure [bar] (abs)		2.8	2.8
No. of Injections		1	1
P_{inj} [bar]		1200	1200
SOI [°CA aTDC]		-9	-9
Injection Duration	[°CA]	4.5	4.5
	[ms]	0.625	0.625
Fuelling Rate [mg/cycle]		36	36
Intake O_2 [%]		14.5	14.5
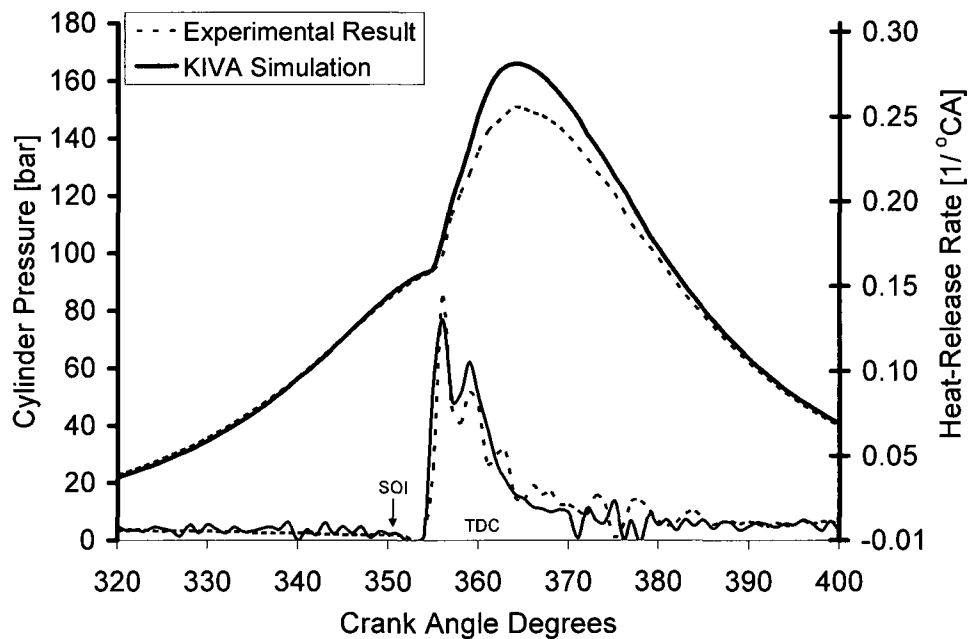
Figure 6-14: Pressure and heat-release rate for single-shot model calibration - KIVA.

Figure 6-15 presents the evolution of the injected liquid fuel. Note that the mass of the injected fuel is a sum of the liquid fuel and fuel vapour. The result indicates that all the injected liquid fuel had vaporised by the end of the premixed phase. This figure could be utilised to evaluate the in-cylinder fuel vaporisation and condensation process, which may be employed to qualitatively indicate the UHC emissions and thermal efficiency in some cases.
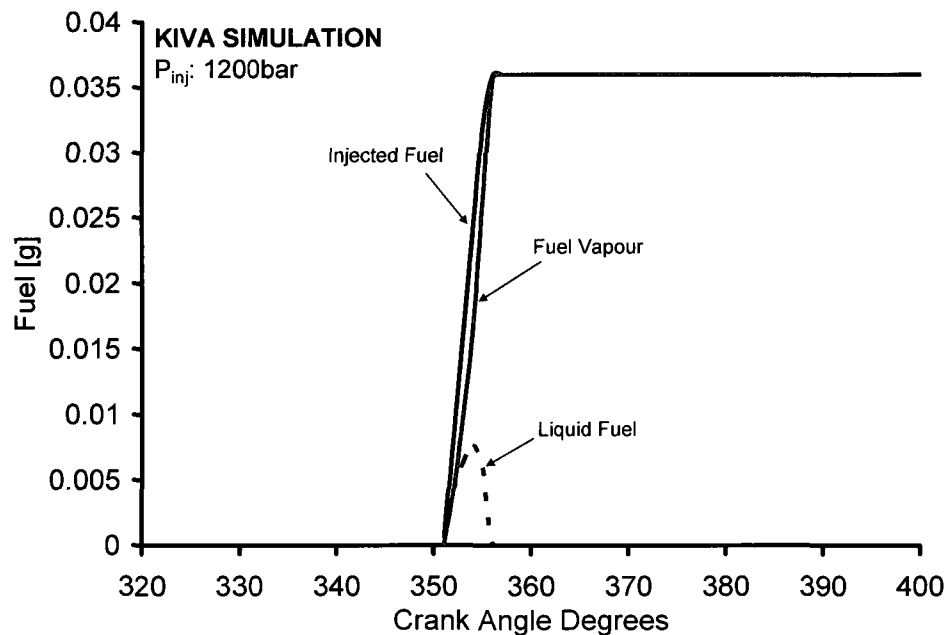
Figure 6-15: Fuel phase evolution for single-shot model calibration - KIVA.

The plot of equivalence ratio vs. local temperature, ϕ-T Plane, provides an intuitive framework for understanding the emission formation during combustion (Miles 2006). Figure 6-16 shows the KIVA ϕ-T planes for different injection pressures. In the figures, three main phases are apparent; fuel preparation, premixed burning and diffusion burning. Rich regions at elevated temperatures where high soot formation is expected to occur were observed at low injection pressures. As the injection pressure was increased,

the combustion process developed into lean premixed burning at elevated temperatures where high NO_x is expected to occur. Therefore, at fixed SOI, boost, fuelling rate and EGR level, increasing the injection pressure is expected to reduce the in-cylinder soot formation. On the other hand, the availability of O_2 and elevated temperatures would result in increased NO_x formation.

(a)

(b)

(c)

(d)
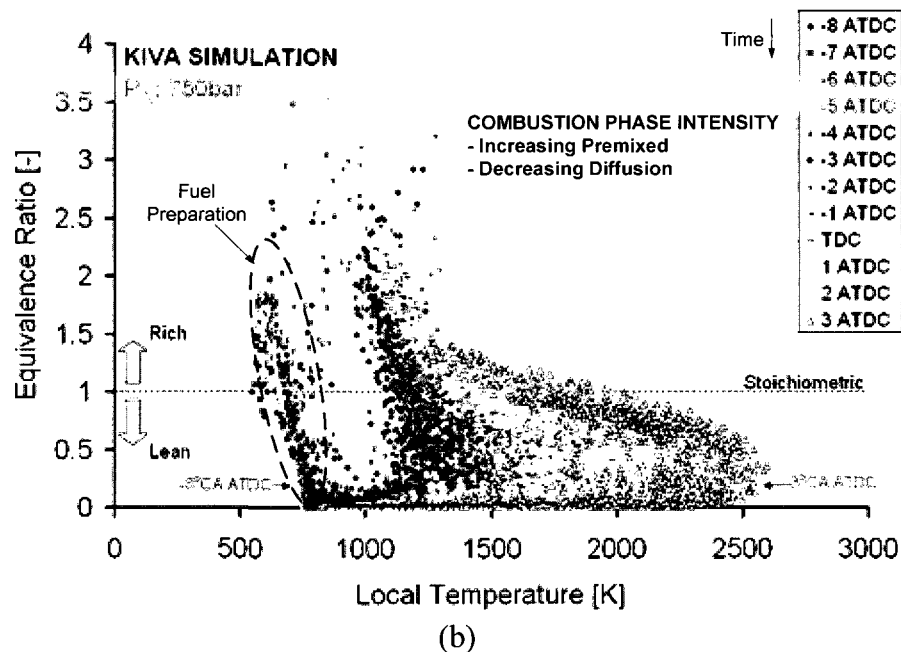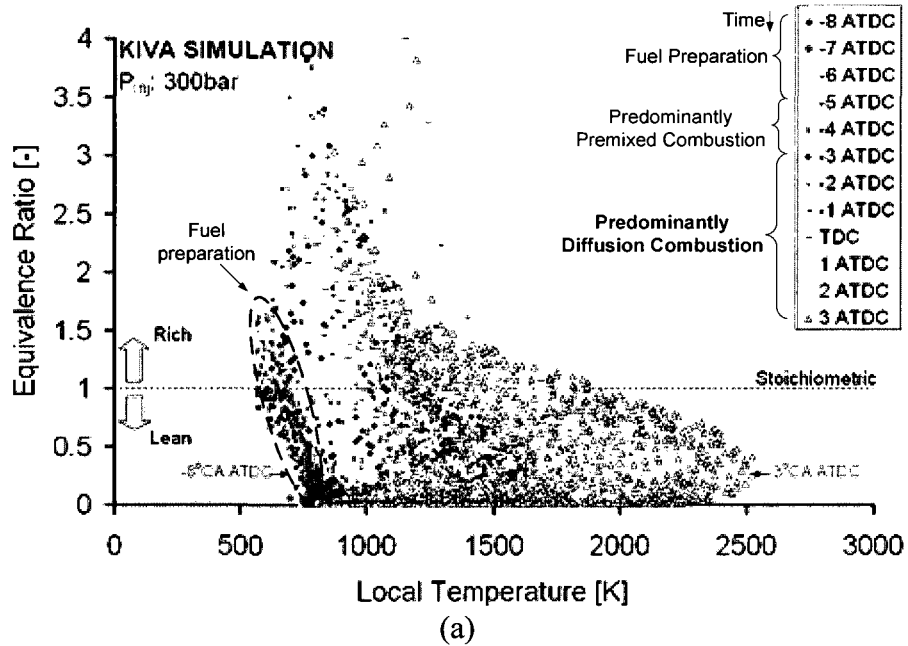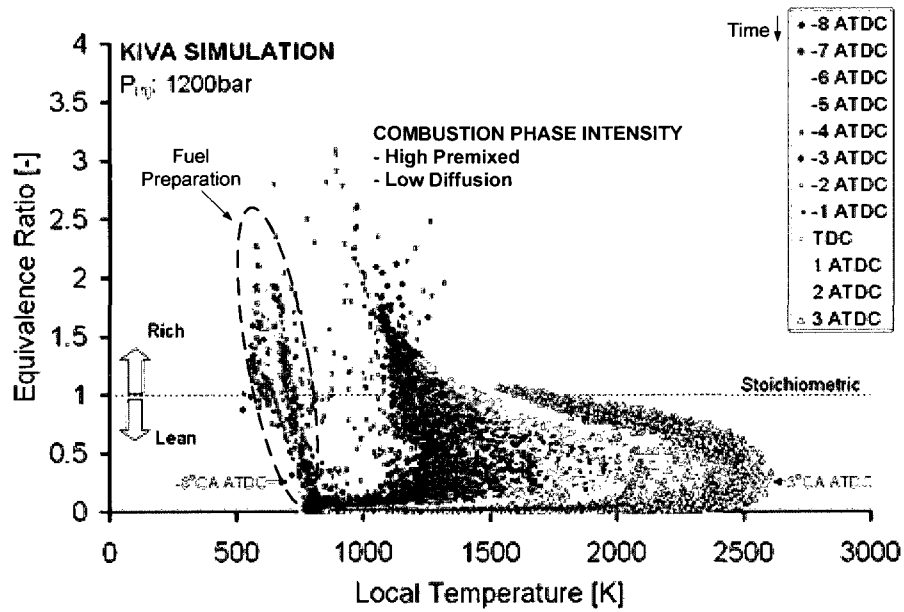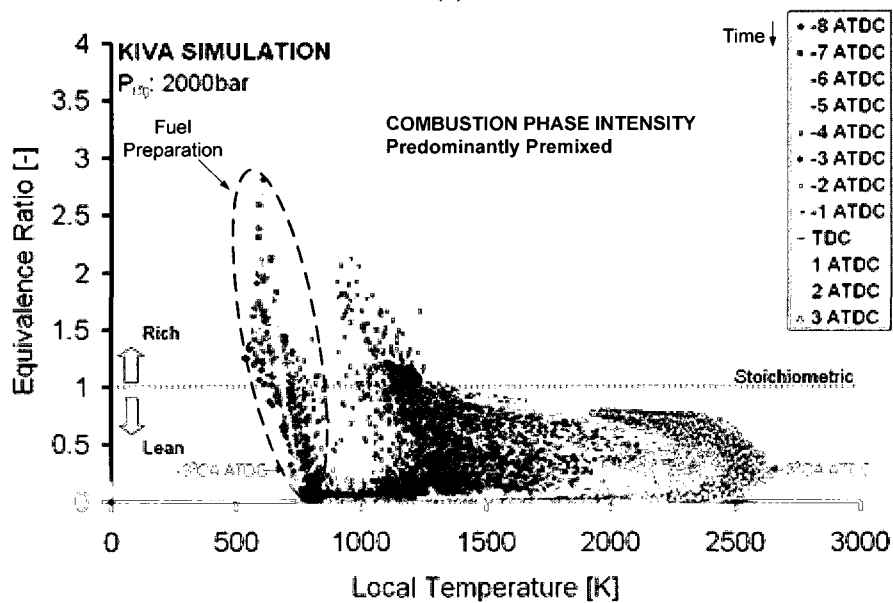
Figure 6-16: KIVA ϕ-T plane for P_{inj} (a) 300 (b) 750 (c) 1200 (d) 2000bar.

The resulting engine-out NO_x and soot emissions from the simulation are presented in Figure 6-17. Note that the KIVA simulated emissions have to be calibrated to match the empirical results. Nonetheless, Figure 6-18 shows that the trend in the KIVA and empirical results were in good agreement.
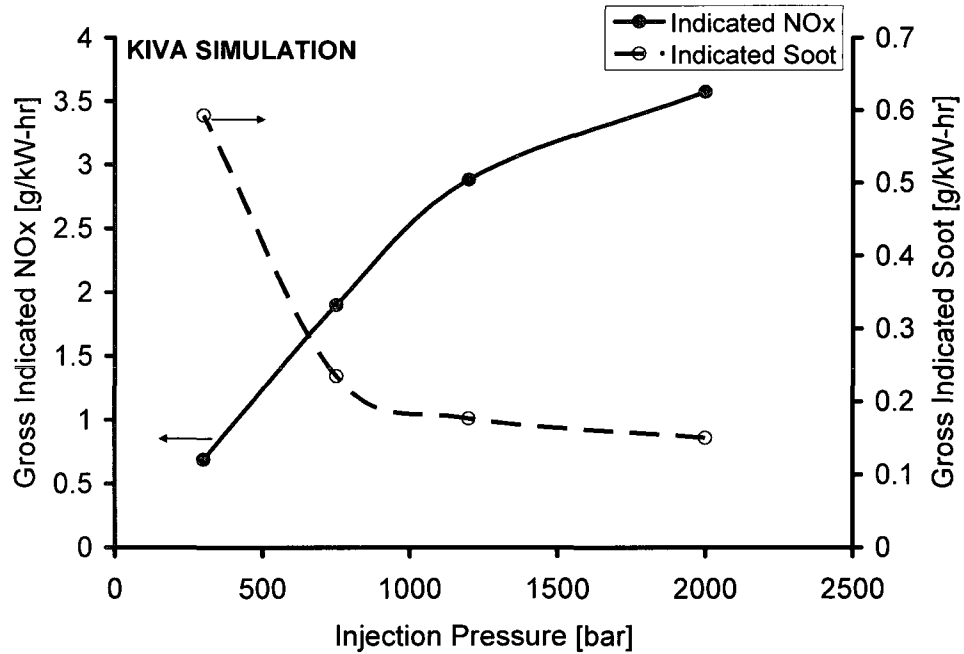
Figure 6-17: Effect of injection pressure on engine-out NO_x and soot - KIVA.
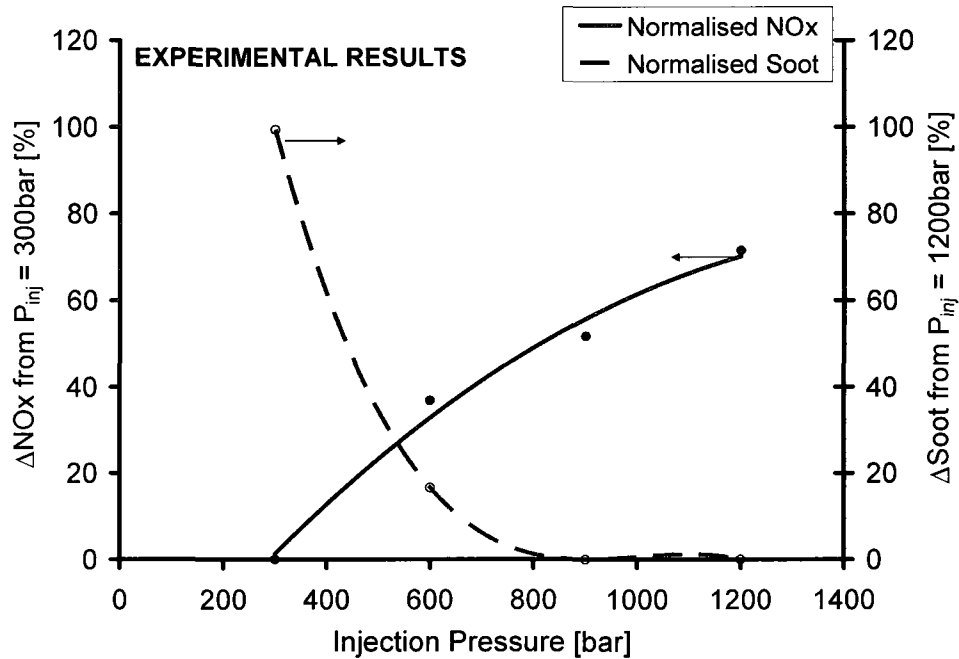
Figure 6-18: Effect of rail pressure on engine-out NO_x and soot - Empirical.

The effects of synthetic EGR, CO_2 dilution, for the single-shot injection are presented in Figure 6-19. As the intake CO_2 was increased, the diffusion portion of the heat-release

rates diminished. At high EGR rates the combustion became dominated by the premixed burning phase. However, the results of the emission indices (EI) of NO_x and soot, in Figure 6-20, do not capture the decrease in soot formation for the enhanced premixed combustion cases. A modification to the original soot model appears to be necessary to accurately represent the soot formation in diesel LTC mode. Liu *et al.* (2005) noted that the empirical soot models widely adopted in engine modelling have not been adequately validated to predict soot formation in multi-event injections, including the LTC mode. A multi-step phenomenological soot model was, therefore, proposed to replace the two-step model commonly employed for the diesel HTC mode. The soot model by Liu *et al.* included particle inception, surface growth, oxidation and particle processes of soot formation in diesel combustion. Compared to the original two-step soot model, the revised multi-step model successfully reproduced the measured soot emission dependence on the SOI.
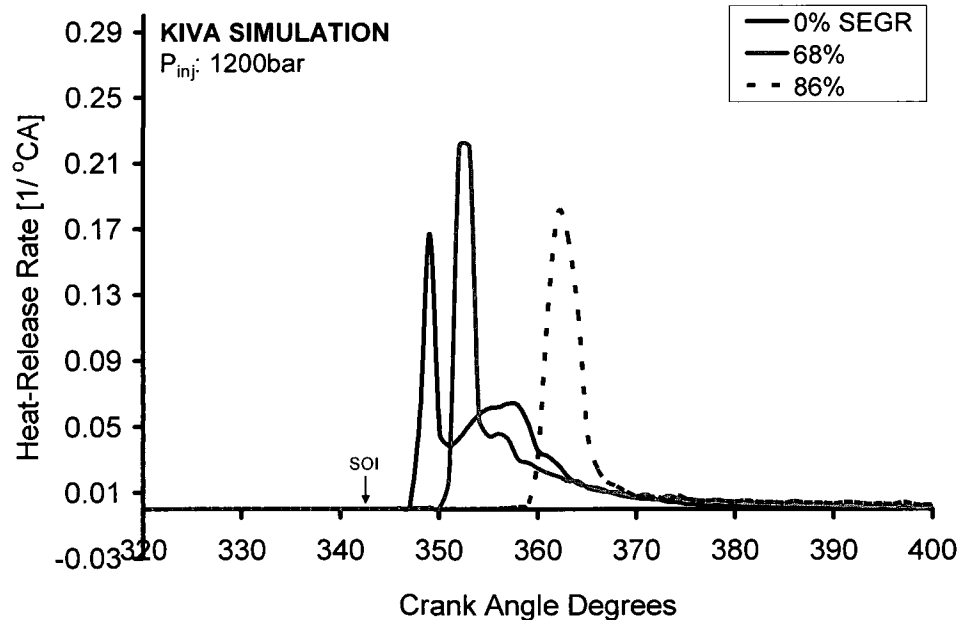
Figure 6-19: Effect of CO_2 dilution on heat-release rate - KIVA.
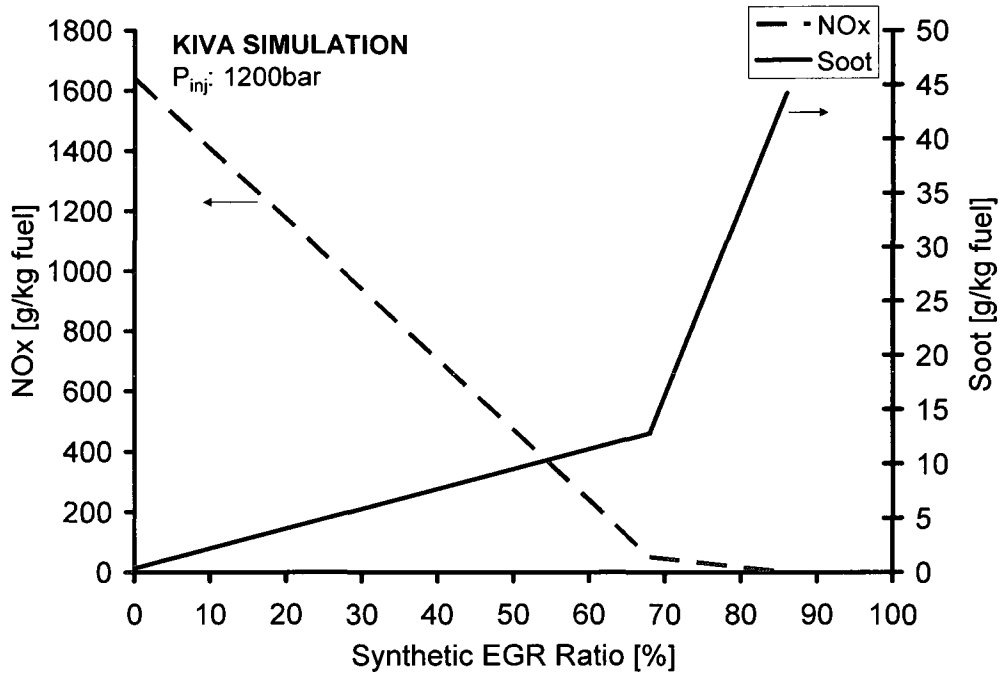
Figure 6-20: Effect of CO_2 dilution on EI NO_x and soot - KIVA.

The pressure and heat-release rate calibration for the multiple injections is shown in Figure 6-21. The empirical and KIVA simulated cylinder pressures were in good agreement though the KIVA simulation did not capture the cool flame reactions due to the limited chemistry in the model. The ϕ-T plane in Figure 6-22 shows the main stage of combustion being dominated by near-homogeneous lean-burning at elevated temperatures. Note, however, that the cylinder charge was not completely homogeneous, evident from the variation in the local temperature at the same engine crank angle position seen in Figure 6-23(a). At 364°CA, just after the SOC, the local temperature variation ranged from 700 to 2700K as seen in Figure 6-23(b).
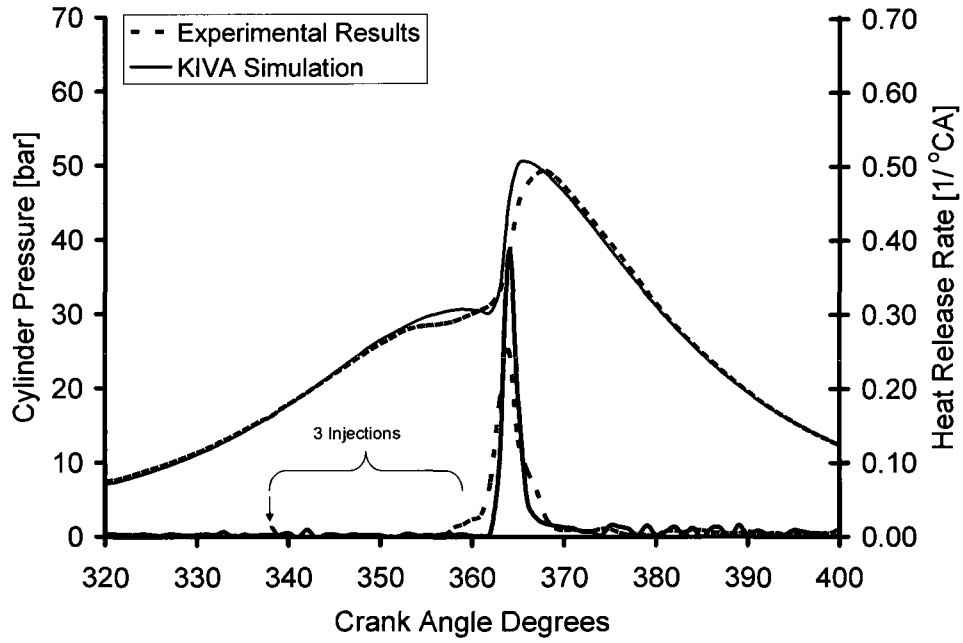
Figure 6-21: Pressure and heat-release rate for multi-shot model calibration - KIVA.
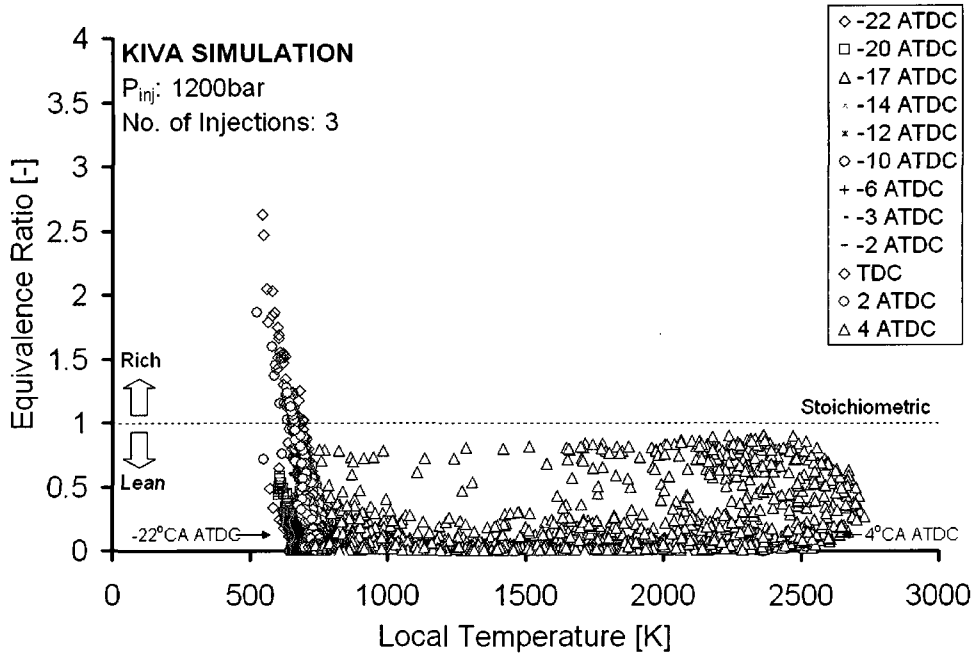
Figure 6-22: φ-T plane for multi-shot model calibration - KIVA.

(a)

(b)
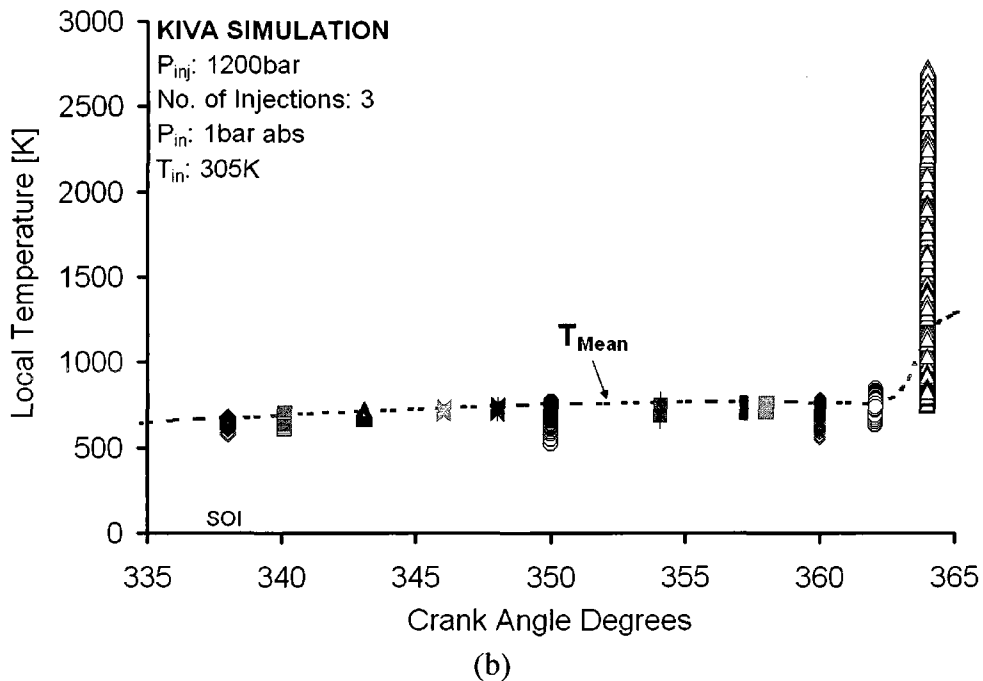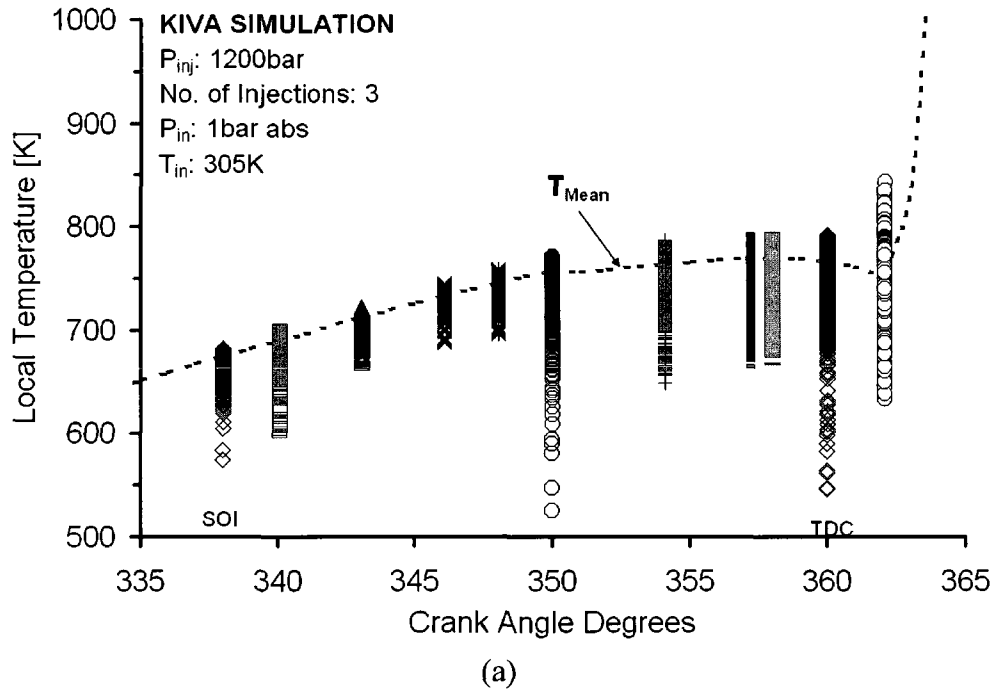
Figure 6-23: Local temperatures vs. CAD for multi-shot (a) before SOC (b) after SOC.

Figure 6-24 shows that most of the injected liquid fuel vaporised by 375°CA. Because the

injected fuel was directed into the piston bowl between 340 and 360°CA, most of the

combustion occurred inside the bowl thus minimal fuel condensation would occur. The

EI NO_x and soot were also relatively low (Figure 6-25) owing to the low fuelling rate.
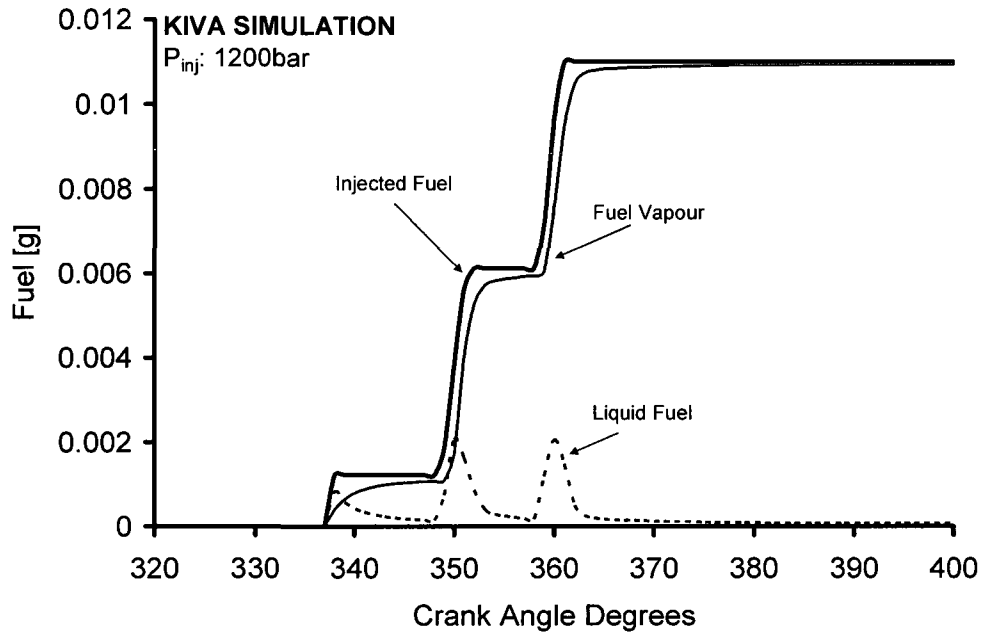
Figure 6-24: Fuel liquid phase evolution for multi-shot model calibration - KIVA.
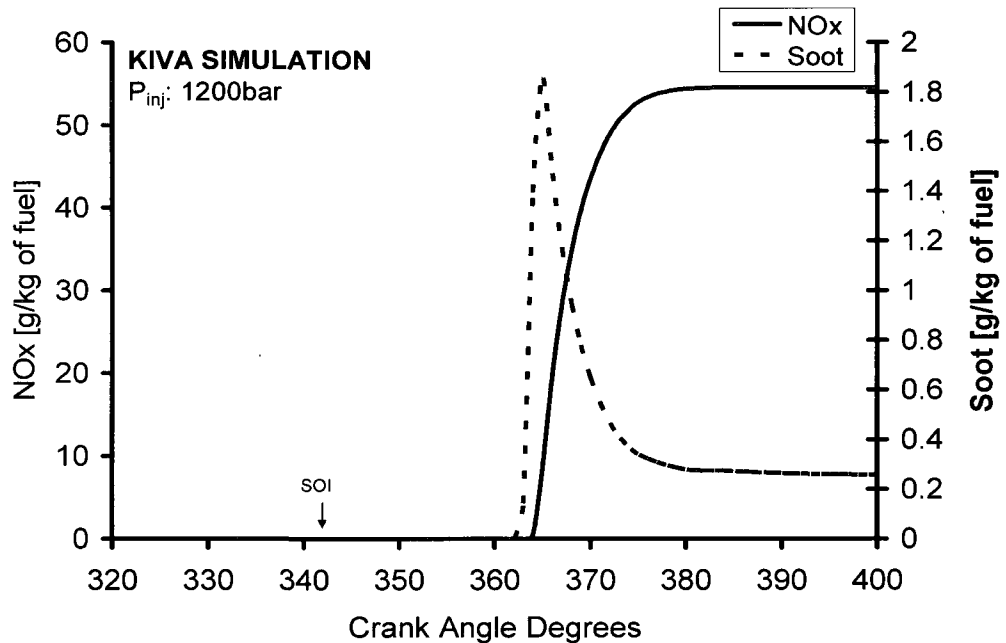
Figure 6-25: EI NO_x and soot for multi-shot model calibration - KIVA.

For a thoroughly mixed cylinder charge the tendency for soot formation is generally low whether the mixture is lean or rich. For instance, it is uncommon for a conventional gasoline engine that typically burns a homogeneous charge to emit black smoke. For a conventional diesel engine, however, the non-homogeneity makes the local cylinder charge vary from rich to lean. In the diesel HTC mode, the locally stoichiometric burning tends to produce very high flame temperatures that may also ignite the adjacent locally lean or rich mixtures. Consequently, in high load HTC processes, simultaneous NO_x and soot formation is inevitable (Zheng *et al*. 2007e). Exhaust gas recirculation, which is predominantly applied to lower the flame temperature thus the NO_x formation, also prolongs the ignition delay period. Hence, significantly improved mixing and eventual simultaneous soot and NO_x reduction may be achieved especially under light loads. The high homogeneity of a cylinder charge is, thus, a precursor to simultaneous NO_x and soot reduction, which also agrees with the essence of HCCI combustion.

CHAPTER VII

DIESEL TEST RESULTS AND DISCUSSION

This Chapter discusses the results for conventional diesel fuel experiments in LTC mode. First, the diesel LTC results using multi-pulse early injections at high load on a common-rail diesel engine are presented. Second, the LTC results utilising late single-injection with high levels of EGR at low load (EGR-incurred LTC) on the single cylinder engine with mechanical injection configuration are presented.

7.1 High Load Diesel Low Temperature Combustion

Low temperature combustion tests were conducted on the common-rail DI diesel engine using conventional diesel fuel UW1-1. The load levels investigated were from 6 to 10bar IMEP at fuel rail pressures of 1200bar and more.

Among the combustion phasing modulation techniques that include fuel injection scheduling and pressure, EGR, boost and intake temperature control, EGR is found the most effective as shown in Figure 7-1 where the fuelling rate was kept constant. However, the EGR phasing control requires high ratios of EGR that reduces the available intake oxygen and commonly causes CO and HC increase. From the LTC test results of Figure 7-1 and Figure 7-2, the IMEP was kept constant as the combustion phasing was shifted with EGR. An improvement in the indicated thermal efficiency (η_{Ind}) was also observed as the peak of the heat-release rate, which is almost at the same location as the HRR CA50 in LTC mode, approached the piston TDC. Nonetheless, compared with the

134

conventional diesel HTC case, the diesel LTC cycle efficiencies were lower as seen in

Figure 7-3.
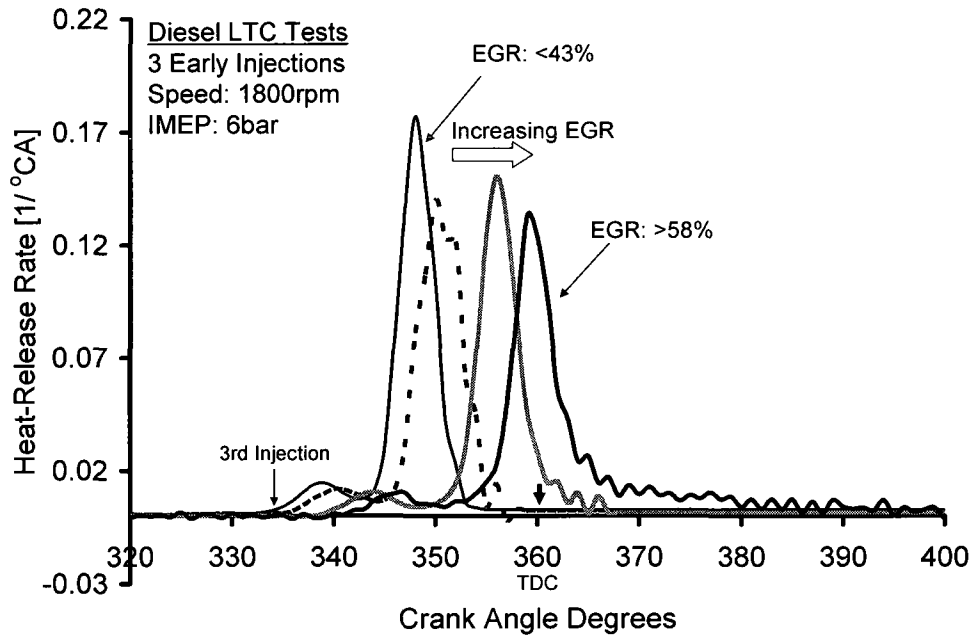
Figure 7-1: Heat-release phasing for diesel early injection multi-pulse LTC.
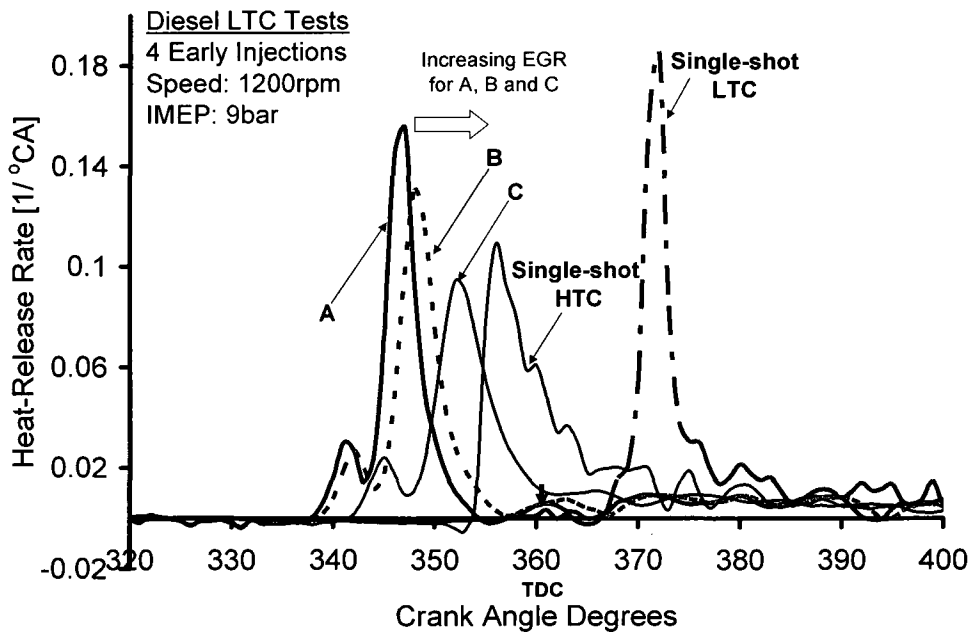
Figure 7-2: Comparison of diesel HTC and LTC heat-release rates.

135
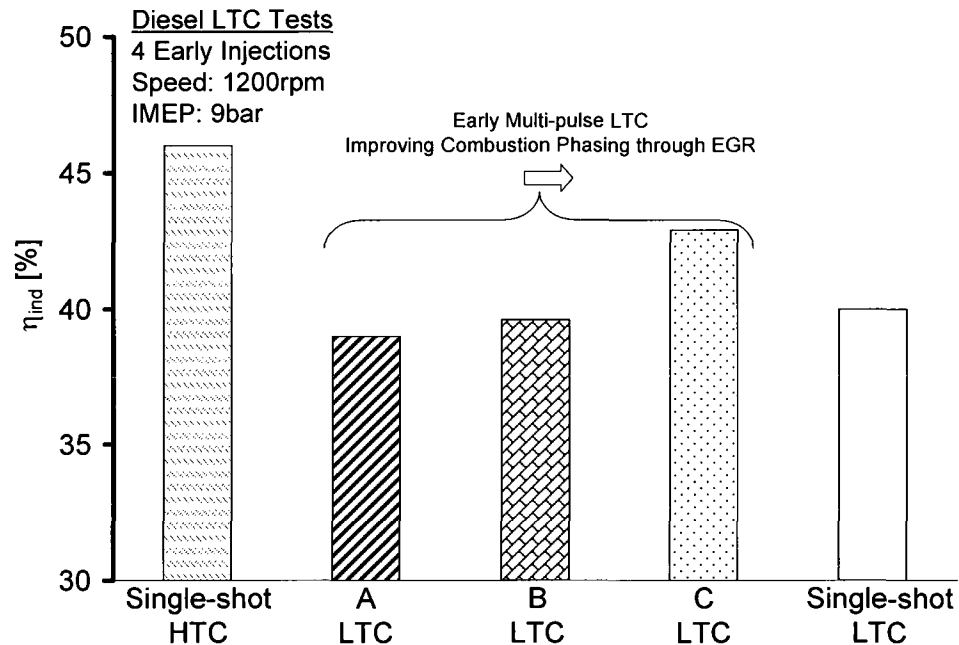
Figure 7-3: Comparison of diesel HTC and LTC η_{Ind}.

From Figure 7-4 to Figure 7-7, it is noted that both the early- and late-injection diesel LTC operation still produced positive net indicated work output per cylinder swept volume, i.e. IMEP, thus the engine should be able to produce reasonable effective power output when using a multi-cylinder configuration.

From medium to high load engine operations, the cylinder charge homogeneity can be improved via multi-event high-pressure fuel injection in the presence of heavy EGR and high boost (Kodama *et al.* 2007, Stanglmaier & Roberts 1998, Zheng *et al.* 2006b). The multi-pulse scheduling is necessary to prevent the occurrence of prevailing stoichiometric pockets in the cylinder charge that would otherwise cause premature ignition and elevated NO_x and soot. Up to 8 fuel injection pulses per cylinder per cycle have been applied at the laboratory to moderate the homogeneity history of high-load diesel LTC operations as seen in Figure 7-8 and Figure 7-9. In order to improve the fuel efficiency of

diesel LTC operation, the fuel injection can be controlled as such: low load use single-shot with prolonged EGR; medium load with 2~5 shots of late early-injection; and high load with 6~8 shots and EGR (Zheng 2006b).
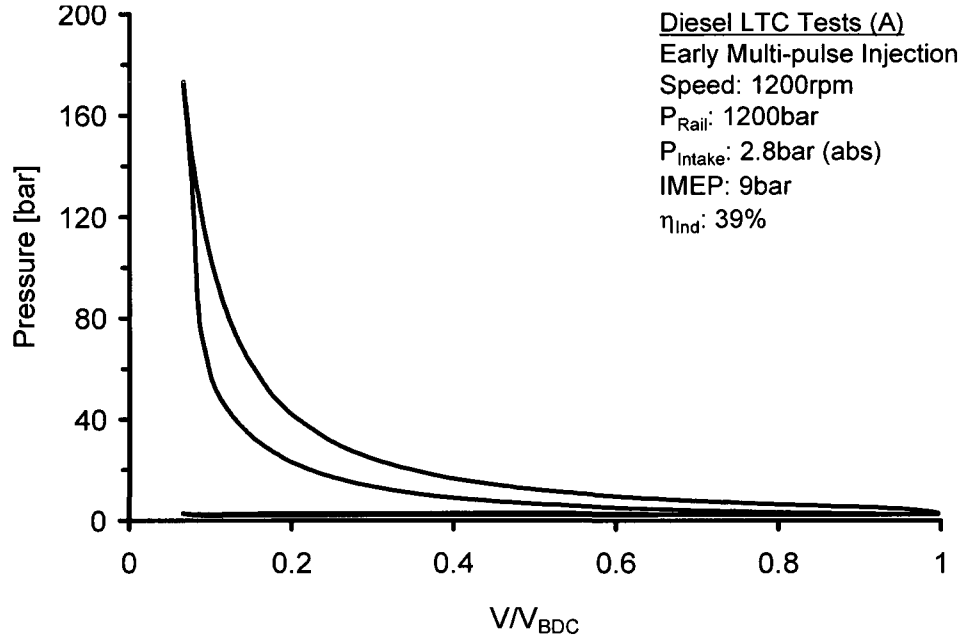
Figure 7-4: P-V trace for early diesel multi-shot LTC – High load.
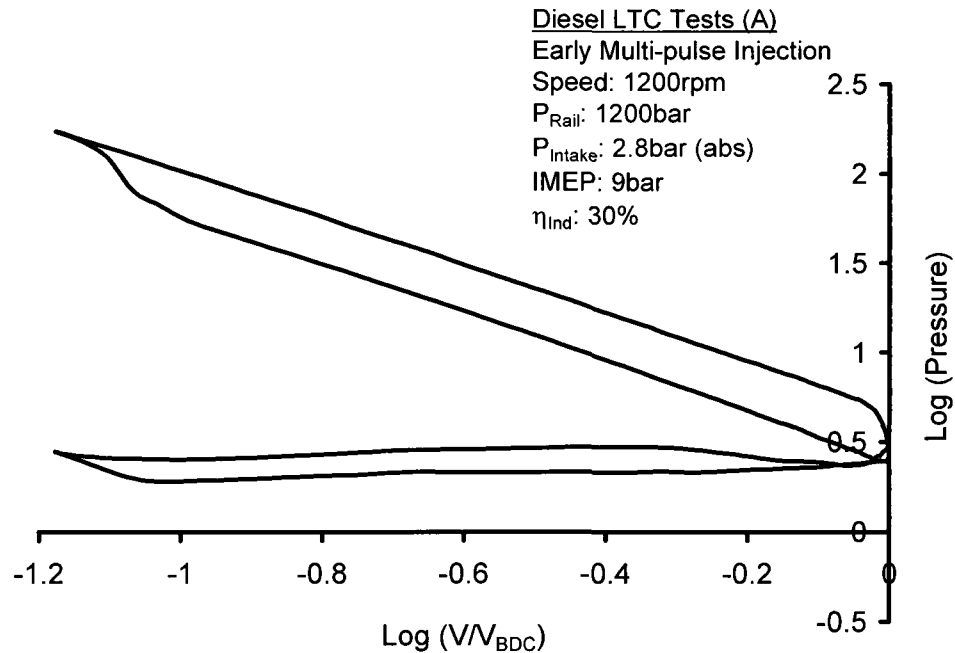
Figure 7-5: Logarithmic p-V trace for early diesel multi-shot LTC – High load.
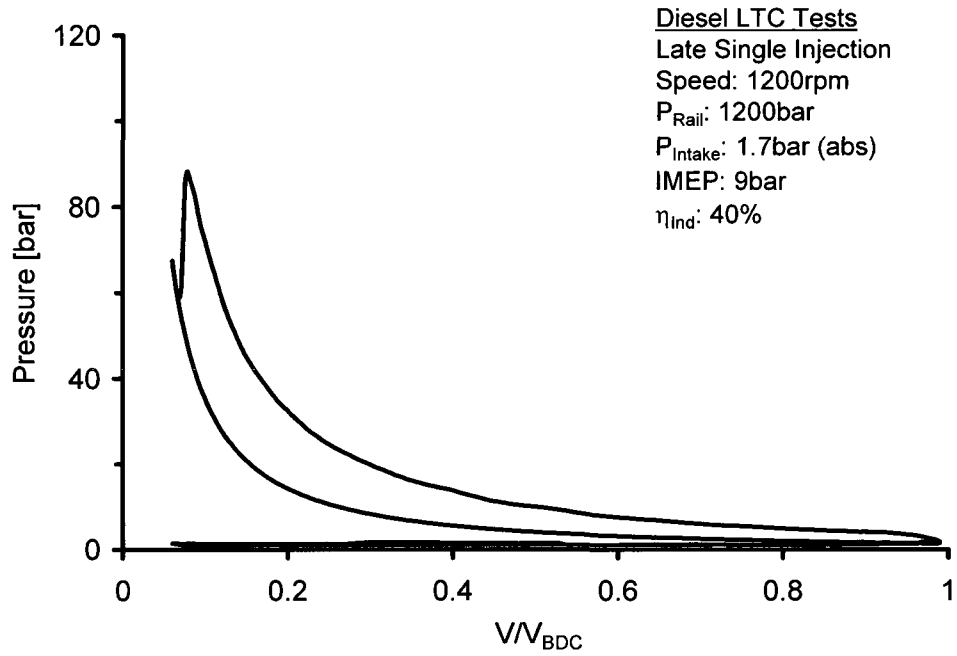
Figure 7-6: P-V trace for late diesel single-shot LTC – High load.
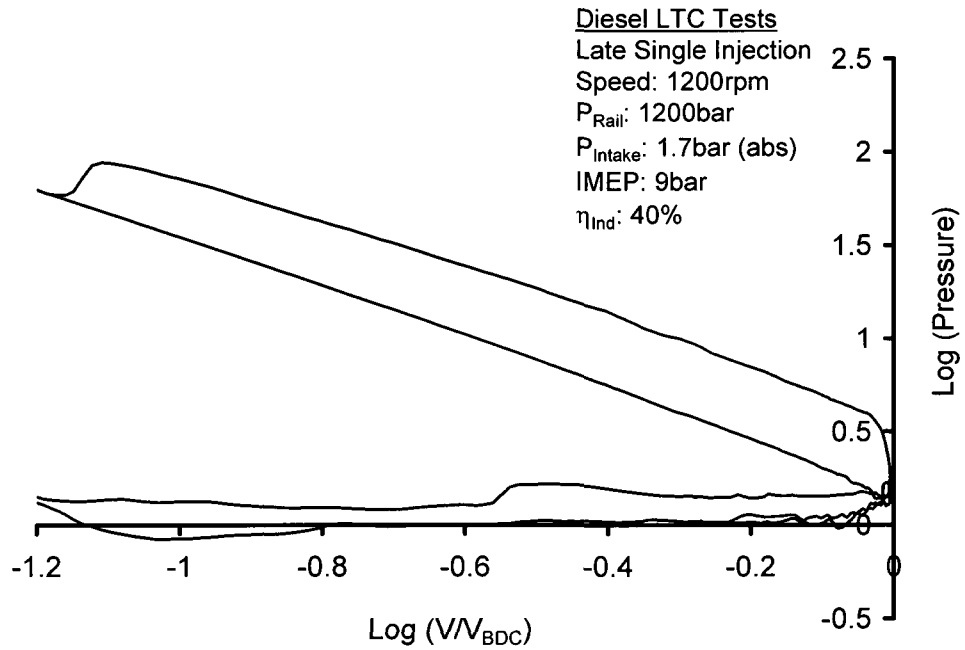
Figure 7-7: Logarithmic p-V trace for late diesel single-shot LTC – High load.

Diesel LTC Tests
Early Multi-pulse (8 shots)
Speed: 1800rpm
P_{intake}: 2bar (abs)
IMEP: 10bar
η_{ind}: 38%
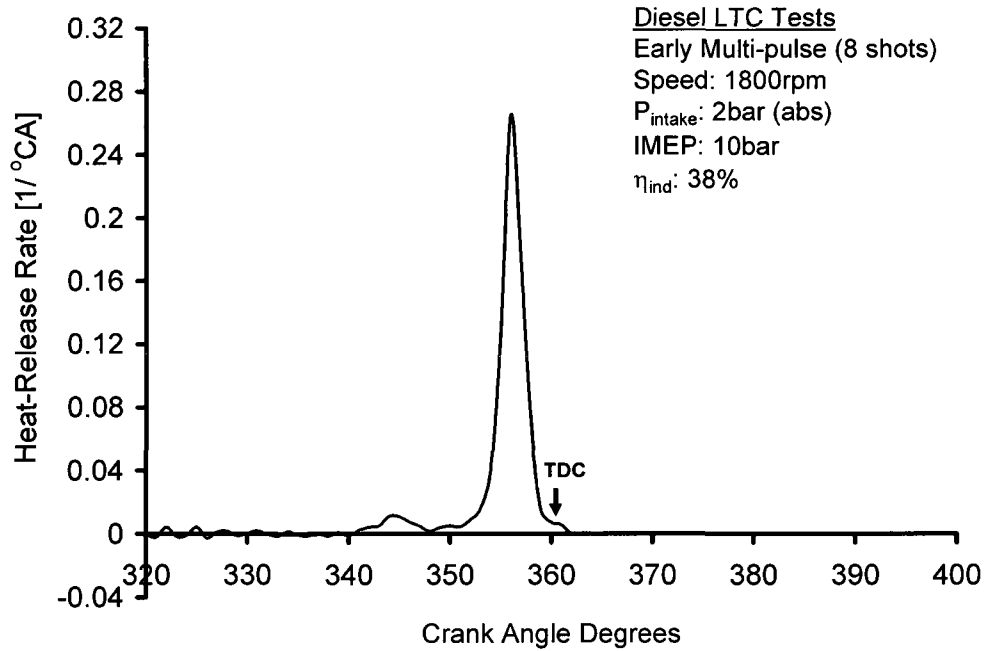
Figure 7-8: Heat-release rate for early 8-shots diesel LTC – High load.

Diesel LTC Tests
Early Multi-pulse (8 shots)
Speed: 1800rpm
P_{intake}: 2bar (abs)
IMEP: 10bar
η_{ind}: 38%
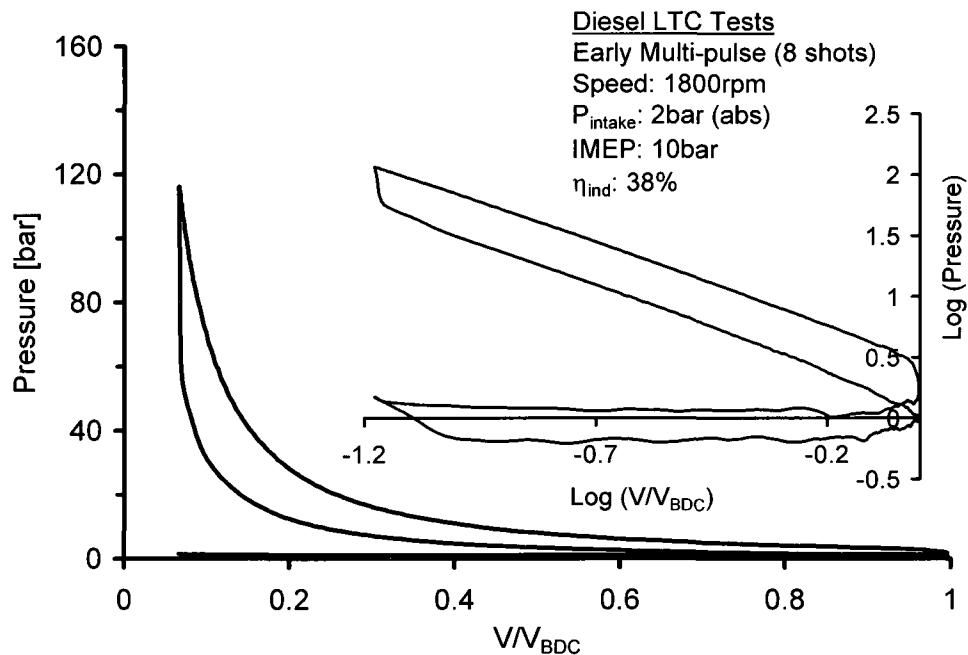
Figure 7-9: P-V (and log p-V) trace for early 8-shots diesel LTC – High load.

The fuel efficiency of LTC cycles is commonly compromised by high levels of UHC and

CO that drain substantial amount of fuel energy from the engine cycle. Therefore, it

becomes attractive to relate the energy contained in the engine-out UHC and CO to the in-cylinder fuel, HC_{Frc}, presented in Equation 7-1. The HC_{Frc} was evaluated on an energy basis from Equation 7-1(a) where χ_{THC} and χ_{CO} are the concentrations of total hydrocarbons (THC formula as $C_1H_\beta O\gamma$) and CO in ppm, respectively, MW_{THC} and MW_{CO} their respective molecular weights and E_{Frac} is the lower heating value (LHV) ratio of the input fuel to CO (4.3 and 3.8 for diesel and biodiesel fuels, respectively), $\dot{m}_f$ is the mass flow rate of the fuel into the cylinder and $\dot{m}_{Exh}$ the mass flow rate of the exhaust gas. Alternatively, the HC_{Frc} may be evaluated from the engine-out indicated-specific THC and CO emissions and the indicated-specific fuel consumption (ISFC) as shown in Equation 7-1(b). Noted, Equation 7-1(b) may also be employed if the brake-specific THC, CO and fuel consumption were known.

$$HC_{Frc} = \left(\frac{\left(\left(\frac{\chi_{THC}}{1 \times 10^6} \times \frac{MW_{THC}}{MW_{Exh}} \right) + \left(\frac{\chi_{CO}}{E_{Frac} \times 10^6} \times \frac{MW_{CO}}{MW_{Exh}} \right) \right) \times \dot{m}_{Exh}}{\dot{m}_f} \right) \times 100 \qquad \text{Equation 7-1a}$$

$$HC_{Frc} = \frac{\left(\text{Brake specific THC} + \dfrac{\text{Brake specific CO}}{E_{Frac}} \right)}{BSFC} \times 100 \qquad \text{Equation 7-1b}$$

Figure 7-10 shows the variation of the HC_{Frc} with EGR for a single-shot diesel LTC mode at medium to high load conditions. Note that the analysers had reached their measurement reading limits of 3000ppm THC and 5000ppm CO at EGR>75%. At such elevated EGR conditions, therefore, the HC_{Frc} was higher than 6.5%. A detailed

evaluation of the HC_{Frc} at different load levels is discussed in Chapter X. For the diesel LTC cases discussed above the engine-out NO_x and soot levels were near-zero.
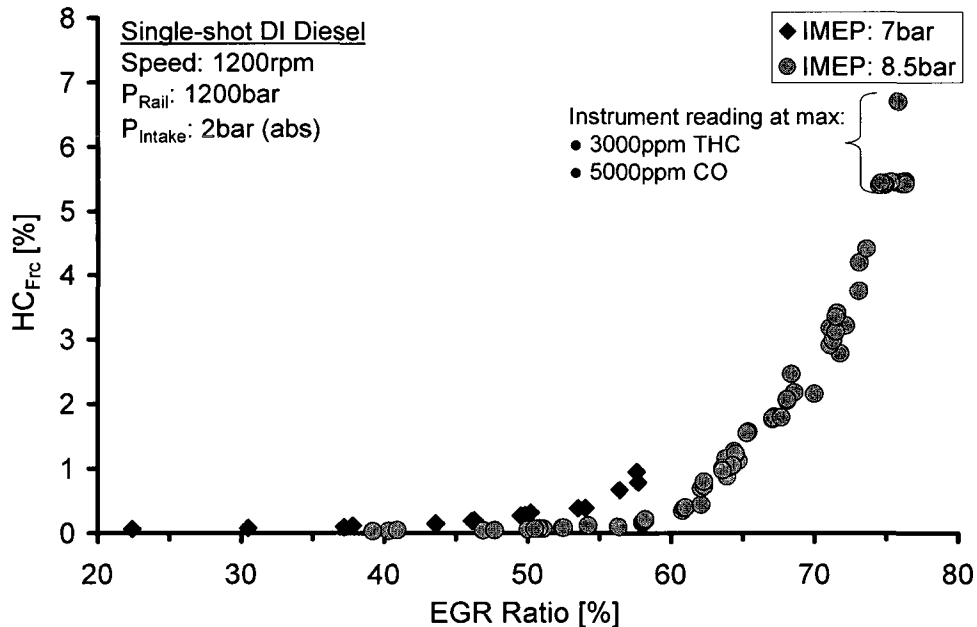
Figure 7-10: Exhaust HC_{Frc} vs. EGR for single-shot high-load LTC.

7.2 Low Load Diesel Low Temperature Combustion

Exhaust gas recirculation tests were conducted on the Yanmar NFD170 diesel engine using the UW 1-1 diesel fuel for single-shot DI at fixed SOI. Brake mean effective pressure sweeps from 2 to 4.5bar and EGR 0 to 90% were implemented at 1400rpm. Specific to the conditions investigated, BMEP levels of 2, 3 and 4.5bar correspond to IMEPs of 4, 5 and 6.5bar, respectively.

Figure 7-11 to Figure 7-22 show some EGR sweep results for the cylinder pressures and rate-of-pressure rise (ROPR), net heat-release rates, cumulative heat-released and logarithmic pressure vs. volume traces for the conditions investigated. Increasing the

141

EGR rate resulted in a decrease of the peak cylinder pressure and increased ignition delay. Note that at the low load level of 4bar IMEP, compared to the diffusion burning phase, a relatively high fraction of the energy was released during the premixed phase of combustion. Furthermore, at low EGR levels, the transition from the rapid burn phase (premixed) to the diffusion phase had a distinct boundary on all the cumulative heat-released traces. Conversely, under heavy EGR levels the heat-release rates were predominantly premixed burn and the transition was not observed. The heavy EGR levels were accompanied by a slight reduction of power output evident from the logarithmic pressure vs. volume diagrams. As shall be demonstrated in forthcoming figures, such elevated EGR levels lead to the diesel LTC mode for the conditions investigated.
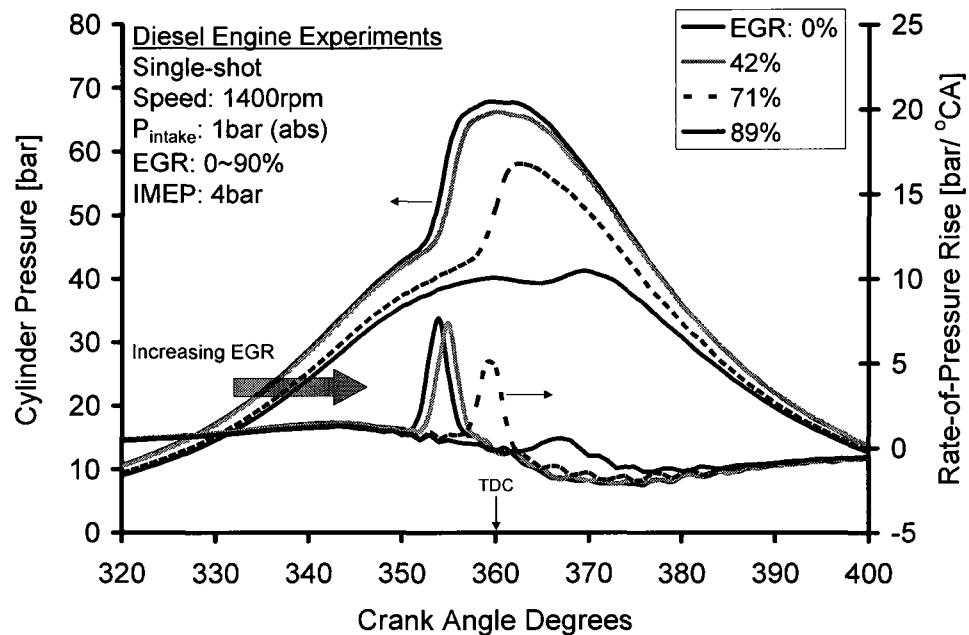
Figure 7-11: Effect of EGR on single-shot DI cylinder pressure at 4bar IMEP.
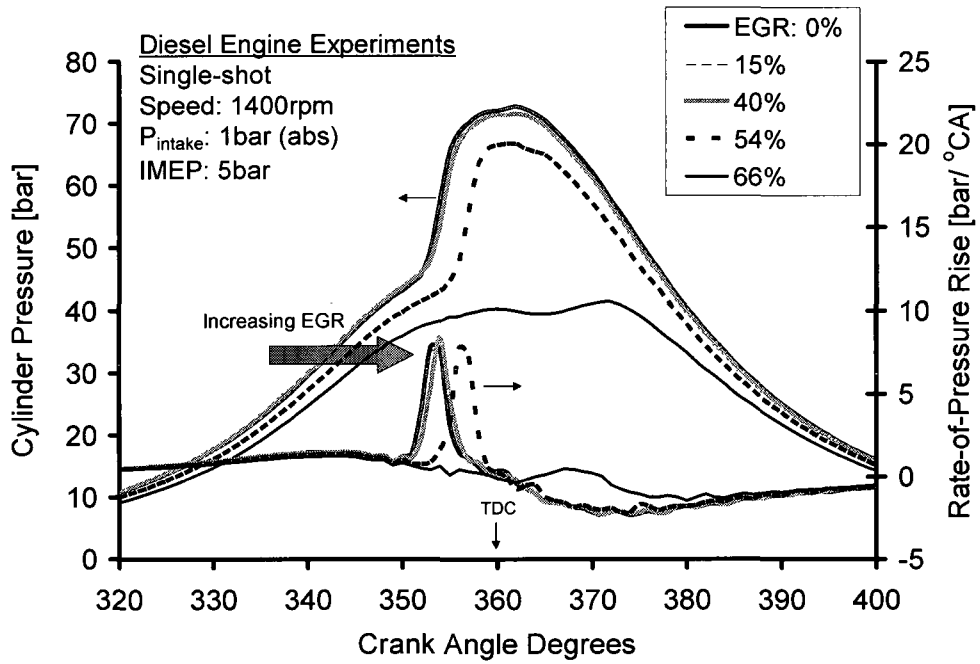
Figure 7-12: Effect of EGR on single-shot DI cylinder pressure at 5bar IMEP.
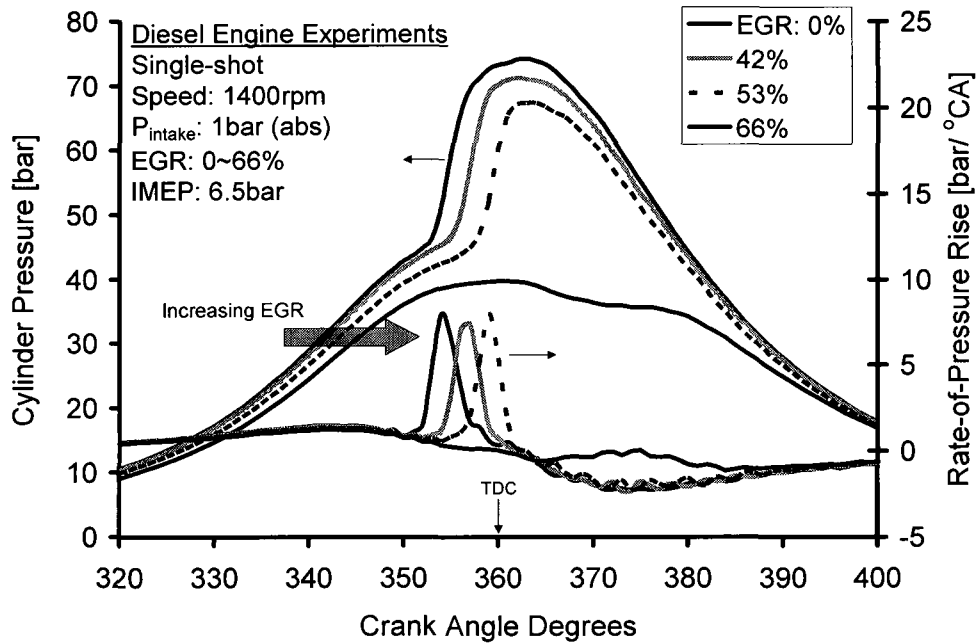
Figure 7-13: Effect of EGR on single-shot DI cylinder pressure at 6.5bar IMEP.
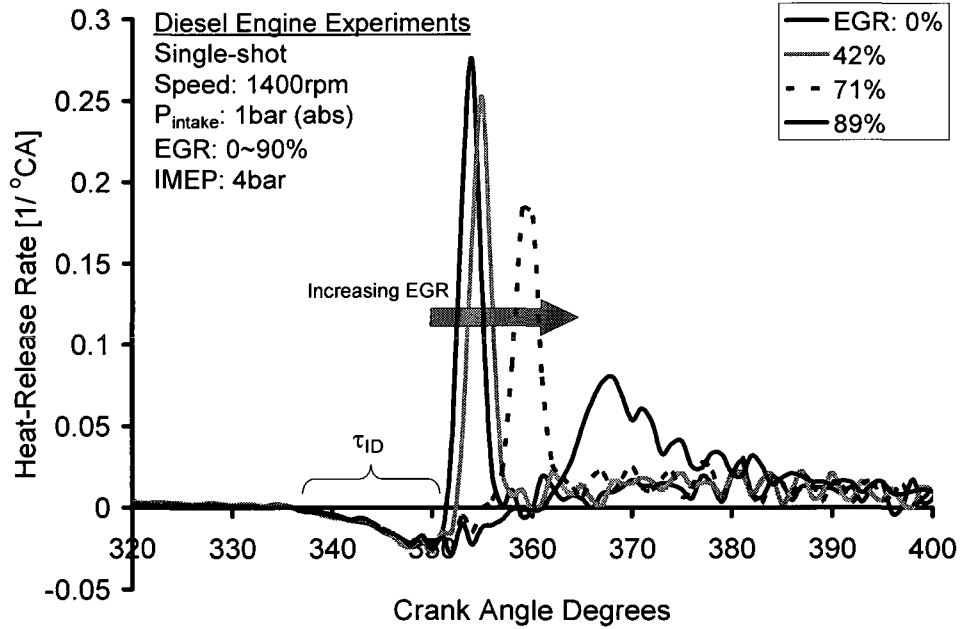
Figure 7-14: Effect of EGR on single-shot DI heat-release rate at 4bar IMEP.
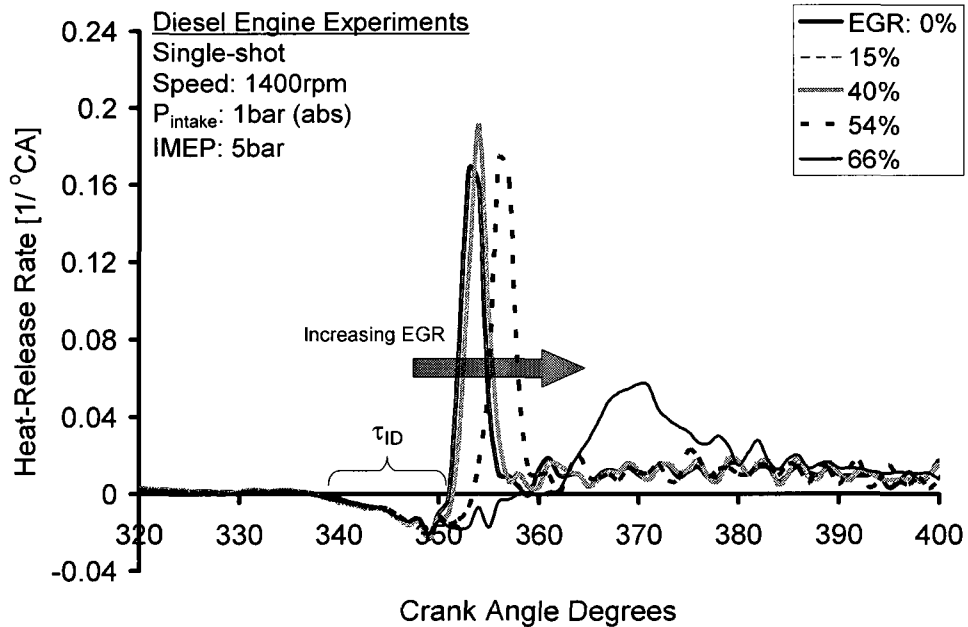
Figure 7-15: Effect of EGR on single-shot DI heat-release rate at 5bar IMEP.
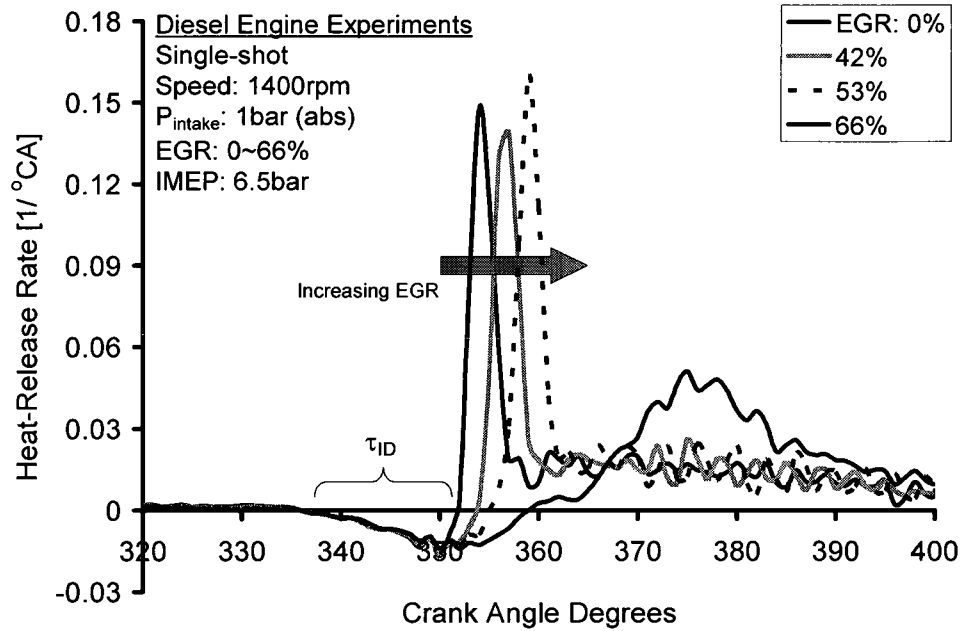
Figure 7-16: Effect of EGR on single-shot DI heat-release rate at 6.5bar IMEP.
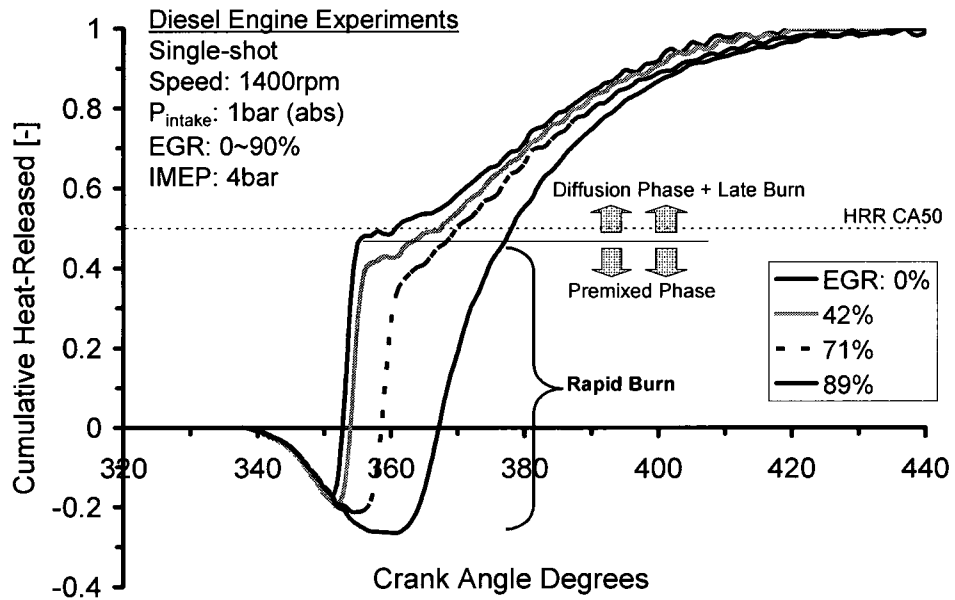
Figure 7-17: EGR effect on single-shot DI cumulative heat-released at 4bar IMEP.
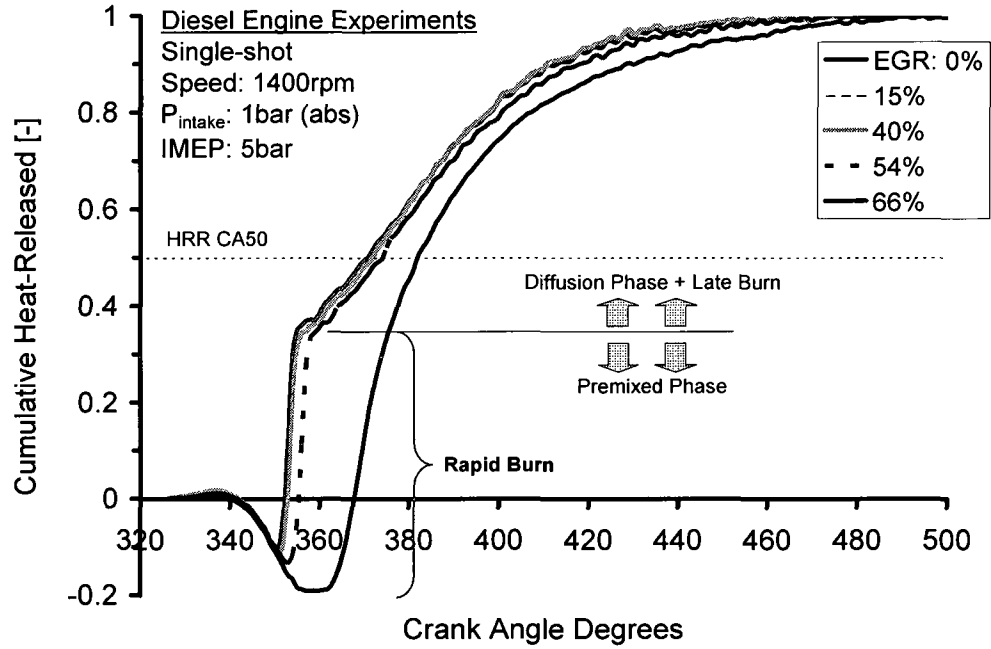
Figure 7-18: EGR effect on single-shot DI cumulative heat-released at 5bar IMEP.
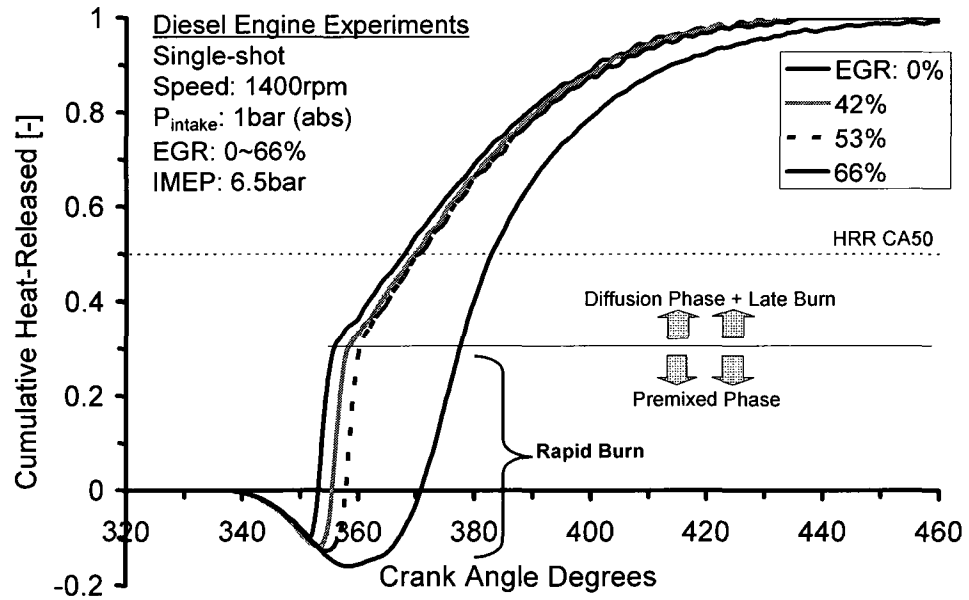
Figure 7-19: EGR effect on single-shot DI cumulative heat-released at 6.5bar IMEP.
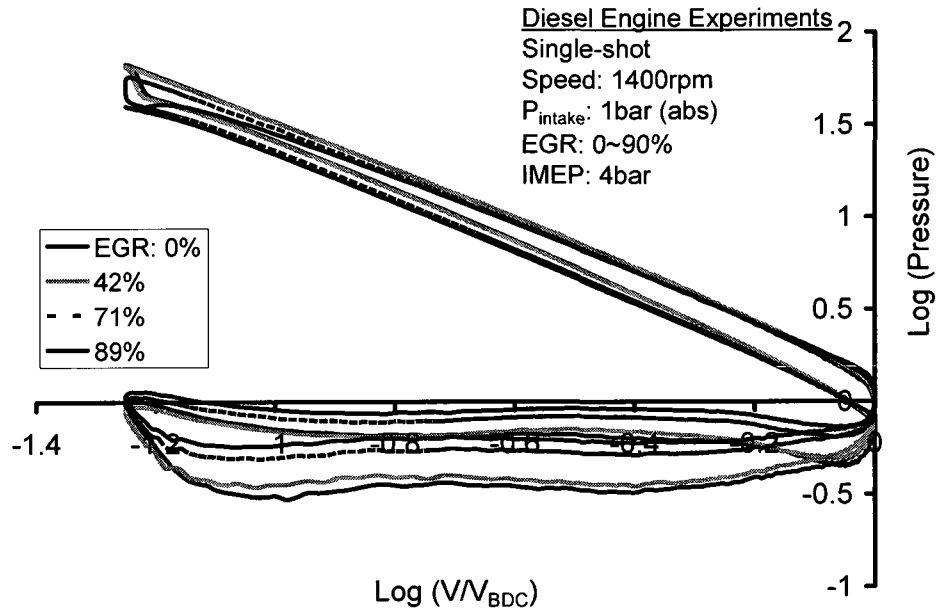
Figure 7-20: Effect of EGR on single-shot DI log p vs. log V at 4bar IMEP.
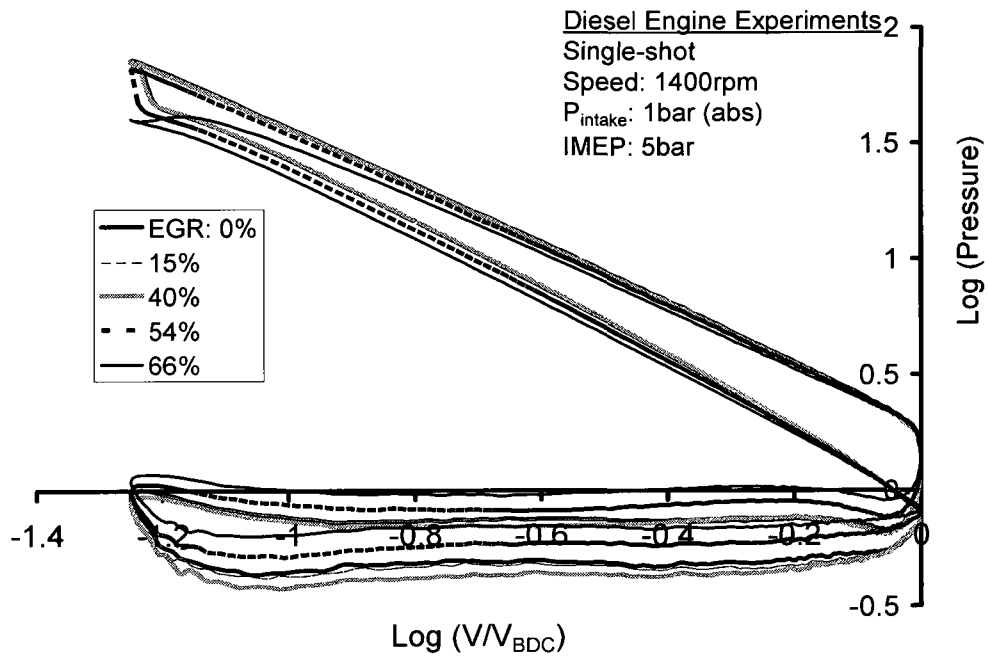
Figure 7-21: Effect of EGR on log p vs. log V for single-shot DI at 5bar IMEP.
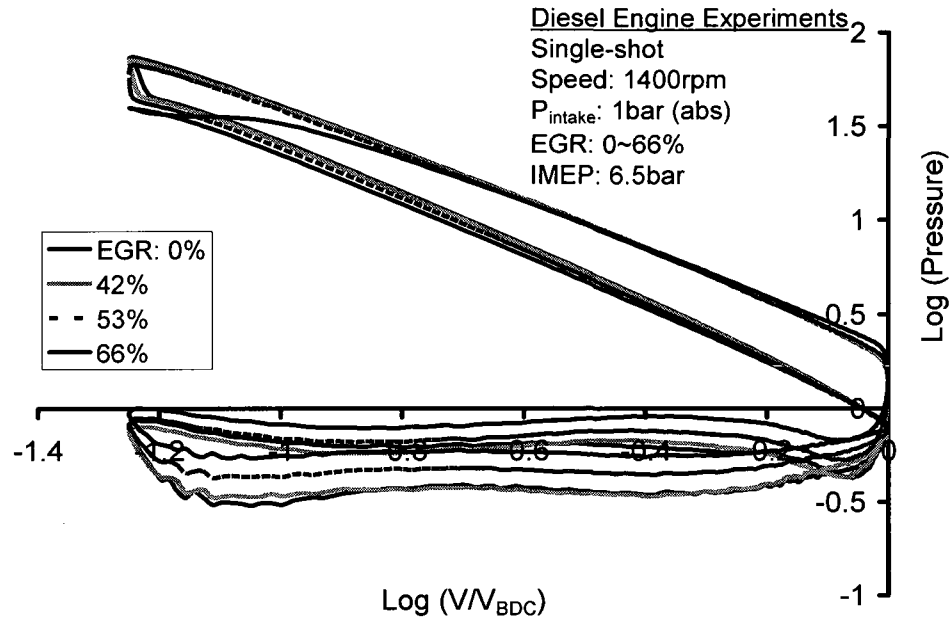
Figure 7-22: Effect of EGR on log p vs. log V for single-shot DI at 6.5bar IMEP.

The effect of EGR on the ROPR is presented in Figure 7-23. As the EGR level was increased, the ROPR was initially unaffected and remained constant at 8bar/°CA especially for the IMEP of 5 and 6.5bar. At EGR levels >50%, the ROPR decreased appreciably with increasing EGR. In the diesel LTC region the ROPR was <3bar/°CA, corresponding to a reduction of 63% compared to the conventional HTC mode. Under such conditions, the engine was running silently and the distinct diesel engine knocking sound was inaudible, especially at a ROPR of 1bar/°CA.
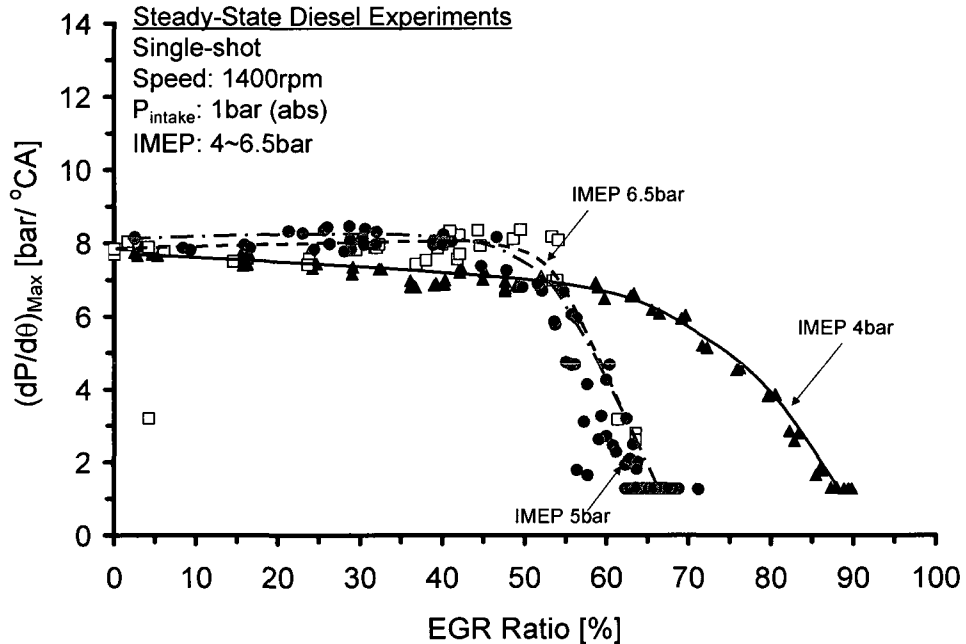
Figure 7-23: Effect of EGR on $(dP/d\theta)_{Max}$ for single-shot DI at different loads.

Figures 7-24 and 7-25 present the effect of EGR on engine-out NO_x and soot emissions for the conditions investigated. As the EGR was increased, the engine-out NO_x reduced monotonically. The soot production was almost constant at low EGR ratios but accelerated with further EGR increase. This mode of combustion is normally considered as HTC and the segment of the soot climbing curve is refered to as *Slope 1* of soot formation hereafter. As the EGR ratio was further increased, the soot level rapidly departed and fell from the peak soot value. As the soot production fell to a smokeless level, simultaneous ultra-low levels of NO_x and soot were achieved. This mode of combustion is normally considered as the LTC and the segment of soot dropping curve is referred to as *Slope 2* of the soot formation hereafter. The transition region between Slopes 1 and 2 is subjected to the stability of the entire engine operation. A slight change in the operating conditions may shift the combustion mode in either direction. A promising solution to the stability of LTC operation is discussed in Chapter IX.

(a)

(b)
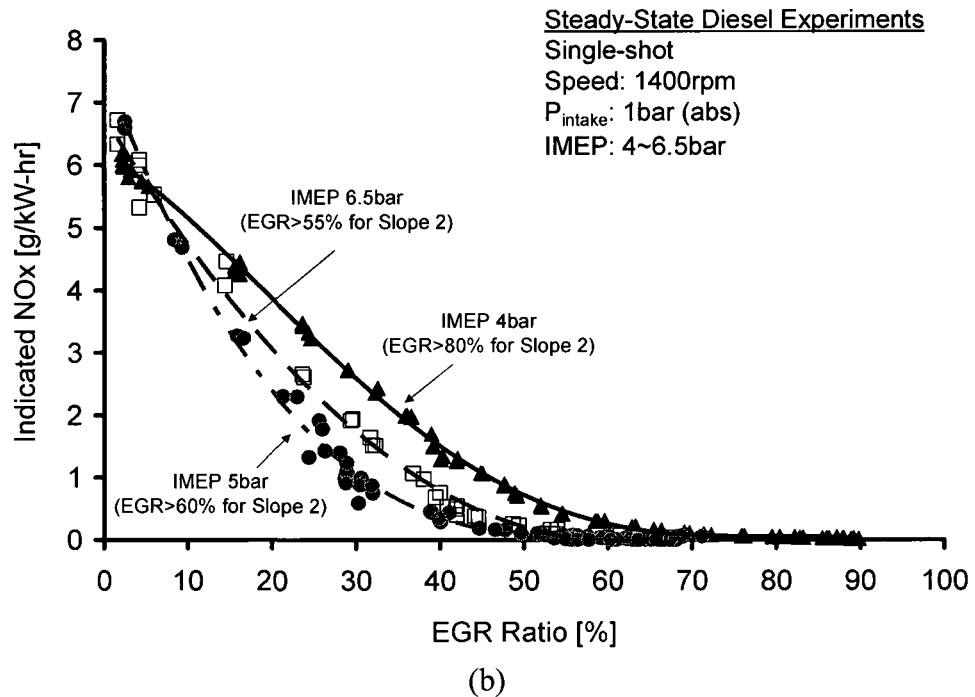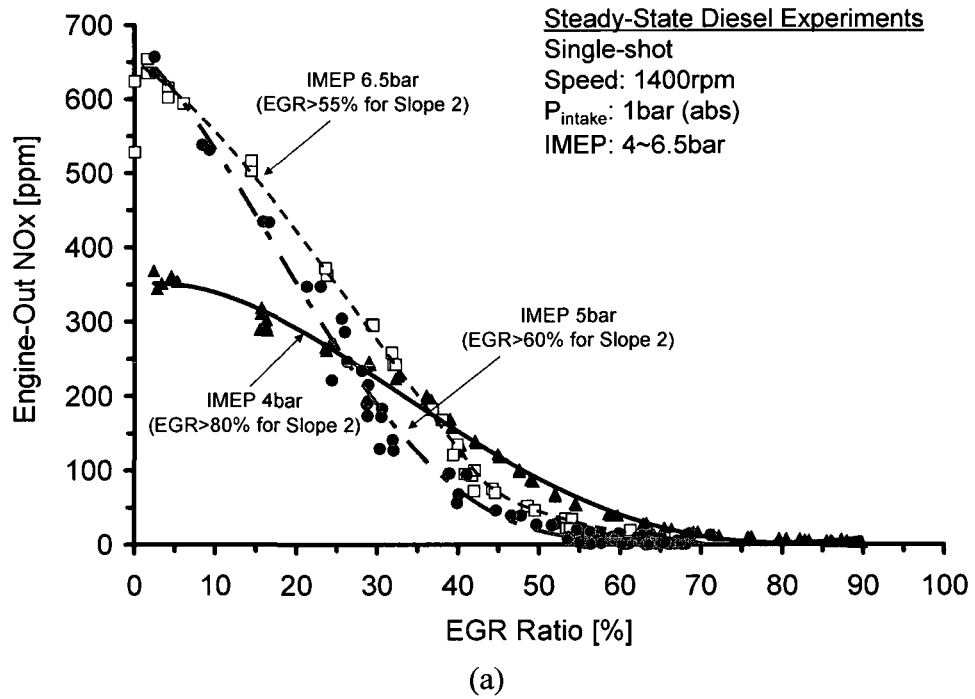
Figure 7-24: EGR effect on engine-out NO_x for single-shot DI at different loads
(a) concentration (b) indicated.
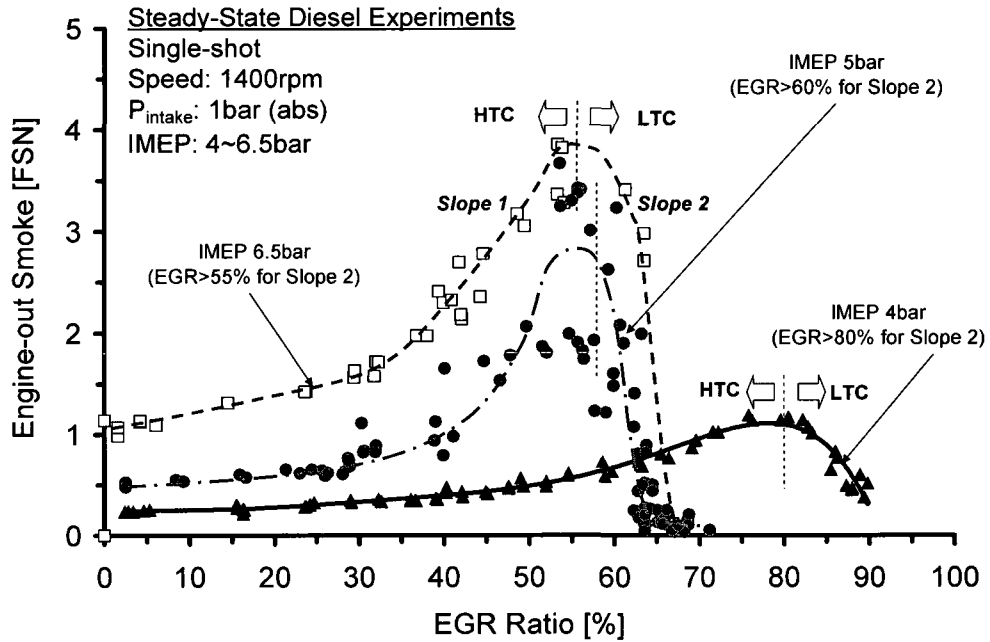
(a)
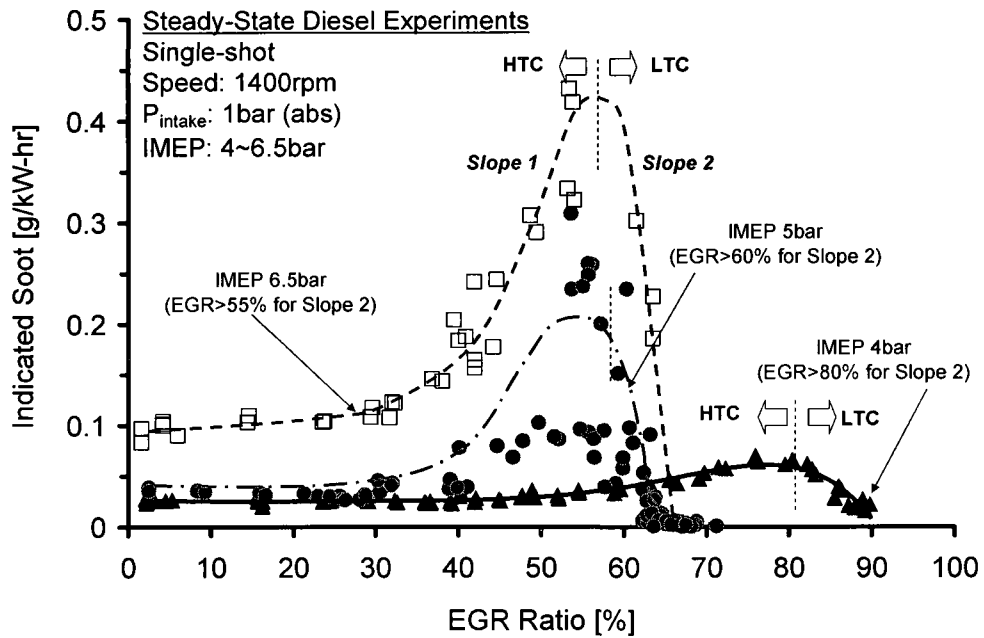
(b)

Figure 7-25: EGR effect on engine-out smoke for single-shot DI at different loads (a) smoke level (b) soot concentration.

During the LTC slope, the effective engine power output and fuel efficiency decreased

noticeably, Figure 7-26 and Figure 7-27, commonly accompanied with an increase in

UHC and CO emissions as shown in Figure 7-28 and increased cycle-to-cycle variation presented as the coefficient of variation in the IMEP (CoV$_{IMEP}$) in Figure 7-29. The CoV$_{IMEP}$ was determined from 200 consecutive cycles using Equation 7-2 where σ_{IMEP} is the standard deviation in the IMEP and $\overline{IMEP}$ is the 200 cycle-averaged IMEP. The standard deviation is the measure of the departure in the values of the data i.e. the spread of data about the mean. Equation 7-3 can be used to evaluate the deviation where x_1, x_2, $x_3...x_n$ are the individual values, $\overline{x}$ is the average value of x and n the number of data points (Easton and McColl 2007, NIST 2006).

$$CoV_{IMEP} = \frac{\sigma_{IMEP}}{\overline{IMEP}}$$

Equation 7-2

$$\sigma = \sqrt{\frac{(x_1 - \overline{x})^2 + (x_2 - \overline{x})^2 + (x_3 - \overline{x})^2 + (x_n - \overline{x})^2}{(n-1)}}$$

Equation 7-3
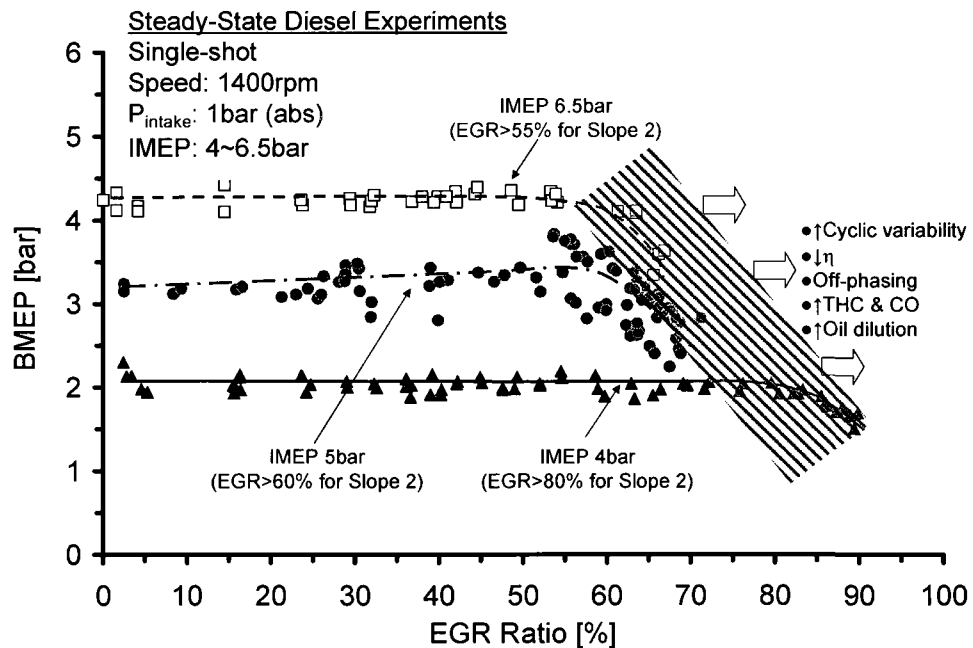
Figure 7-26: EGR effect on single-shot DI BMEP for different loads.
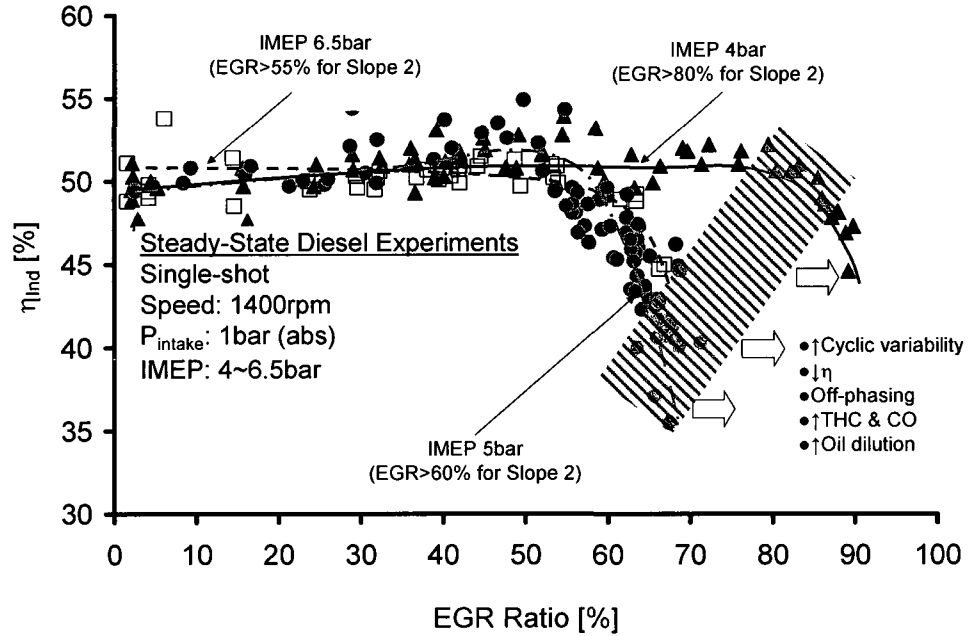
Figure 7-27: EGR effect on single-shot DI η_{Ind} for different loads.
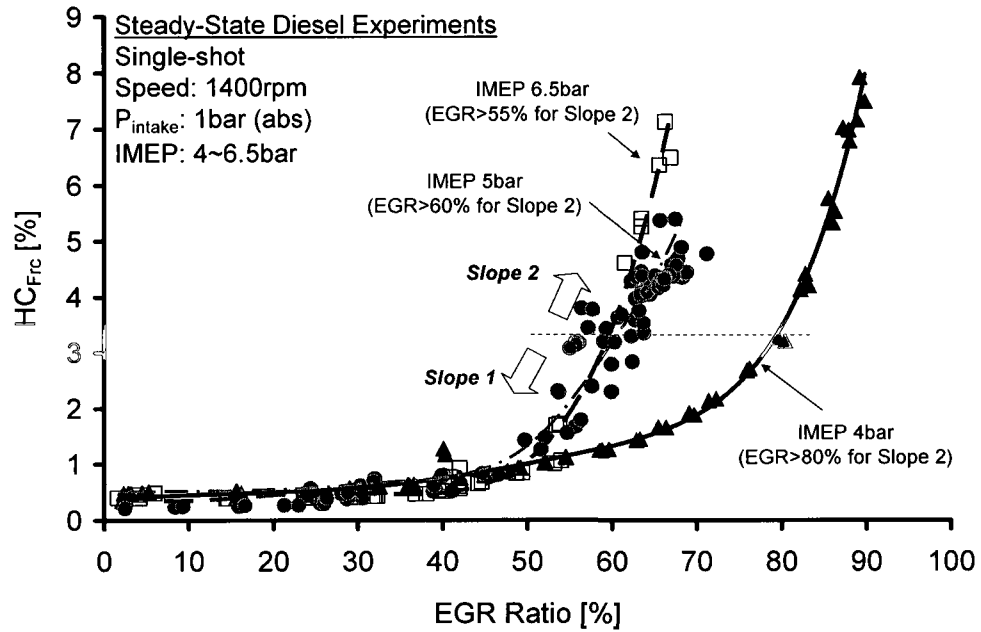
Figure 7-28: EGR effect on HC_{Frc} for single-shot DI at different loads.
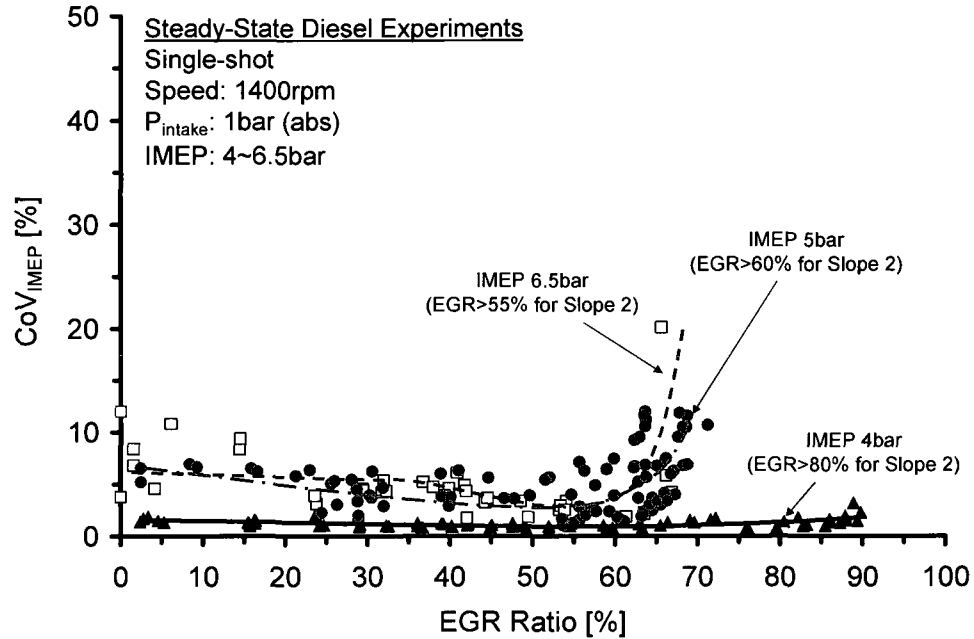
Figure 7-29: EGR effect on CoV$_{IMEP}$ for single-shot DI at different loads.

Though the decline in fuel efficiency and the rise in UHC come simultaneously, the UHC rise only accounts for a fraction of the power loss. The efficiency drop of Figure 7-27 is due to off-phasing of the combustion event, increased UHC and CO and the fuel condensation leading to oil dilution. The high UHC and CO emissions are highly attributed to the following reasons:

- The low volatility of diesel fuels;

- The lowered combustion efficiency of the lean and/or EGR diluted cylinder charge;

- The flame-out of the locally excessive lean mixture caused by the non-homogeneity of the cylinder charge;

- The fuel condensation and flame quenching on the surface of the combustion chamber.

Noted, such soot formation control mechanism only works under limited load levels and a heavy use of EGR is normally necessary to enact such smokeless LTC operations. Despite the use of elevated EGR levels, the overall air-to-fuel mixture strength was lean of stoichiometric for the conditions investigated, evident from the relatively high exhaust oxygen concentration presented in Figure 7-30 (see also Figure 5-15). The exhaust O_2 concentration was around 11 and 7% for the cases with IMEP levels of 4 and 6.5bar, respectively. With higher loads, the multi-pulse early injection provides more feasible LTC operations. The fuel efficiency attainable with the multiple shots is similar to the efficiency achievable with smokeless LTC operation in single-shot injection, which is indicated in Figure 7-27.
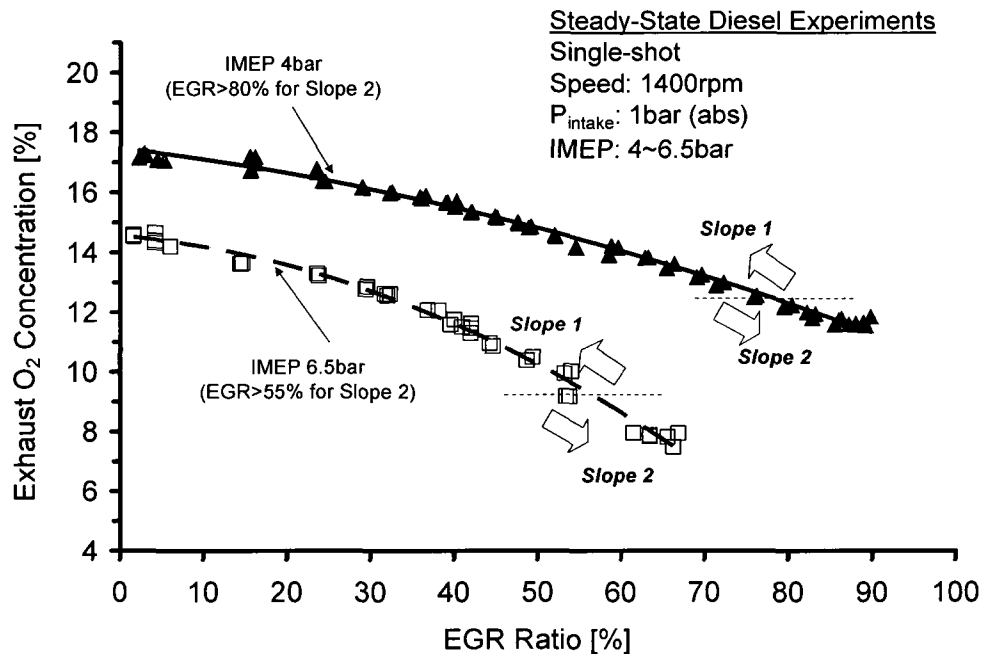
Figure 7-30: EGR effect on exhaust O_2 concentration for single-shot DI at different loads.

A detailed uncertainty analysis was not conducted in this dissertation. Instead, because the empirical data was obtained under steady-state conditions, the emission readings

reported were an average of at least 3 data points. Conducting an uncertainty analysis would have involved the consideration of all the instrumentation and method of data acquisition employed, resulting in digression from the dissertation objectives presented in Chapter I.

CHAPTER VIII

BIODIESEL TEST RESULTS AND DISCUSSION

(SINGLE CYLINDER DI DIESEL ENGINE)

This Chapter presents the results for the comparison of biodiesel and conventional diesel fuels in HTC and EGR-incurred LTC modes at fixed SOI on a single cylinder engine with mechanical injection configuration. The discussion includes analysis of engine-out NO_x and soot emissions, engine performance and ignition delay correlation under the influence of EGR at steady-state engine operating conditions.

8.1 Comparison of Diesel and Biodiesel Fuels in High Load

Using the Yanmar NFD170 engine, the conventional single-shot DI experiments, with no charge dilution, were conducted at high load conditions and the performance examined for the test fuels UW 1-1, 2-1, 2-2 and 2-3. For the high load condition, a BMEP level of 8bar was used, representing about 65% of the maximum rated power.

Figure 8-1 to Figure 8-4 show the cylinder pressures, ROPR, net heat-release rates, cumulative heat-released and logarithmic pressure vs. volume profiles for the test fuels at the high load condition while Table 8-1 summarises the results. Generally, the pressures and heat-release profiles for the test fuels were similar. However, inconsistencies were observed in the test results for the biodiesel fuel UW2-2. At the time of the fuel analysis, the fuel had a lower CN than that of biodiesel UW2-3. Nonetheless, the results of 8-month-later tests reveal that the UW2-2 fuel had advanced ignition, which is inconsistent with the fuel property analysis. A major reason for this could be that the fuel UW2-2 had

157

oxidised in storage generating peroxyl groups that have a profound effect on the CN and viscosity (Monyem 1999, 2001).

The net heat-release profiles showed the classical single-shot diesel DI modes of combustion consisting of a short premixed phase followed by a longer diffusion-controlled phase. In such combustion modes, also referred to as the HTC, the flames tend to initialise in and propagate to regions where the air/fuel ratios are near-stoichiometric, thus presenting an inherent NO_x/PM trade-off, as earlier discussed.
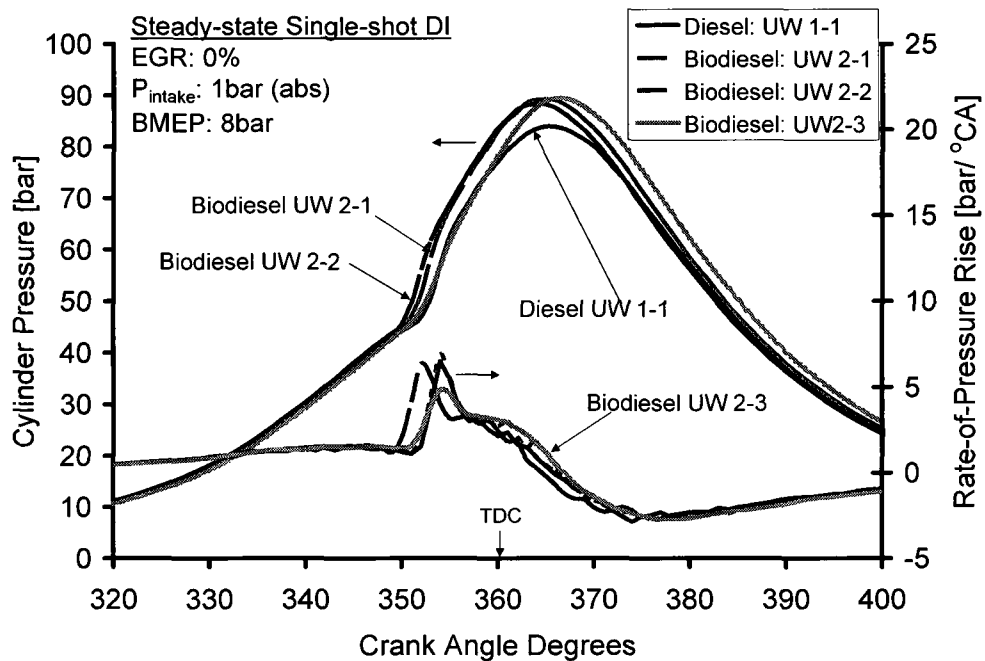
Figure 8-1: Comparison of diesel and biodiesel in-cylinder pressures at high load.
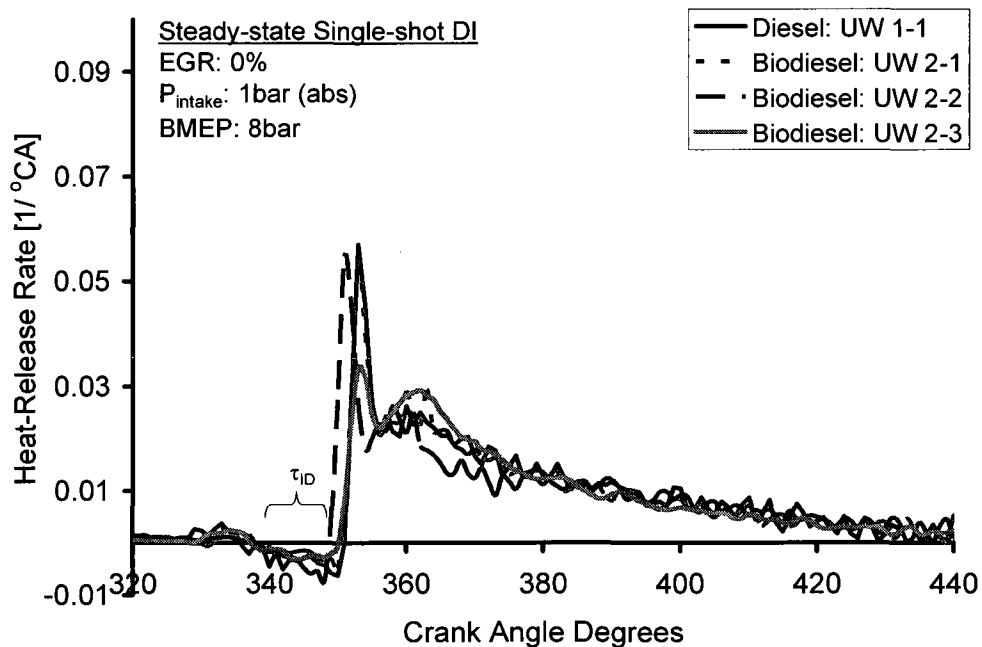
Figure 8-2: Comparison of diesel and biodiesel heat-release rates at high load.
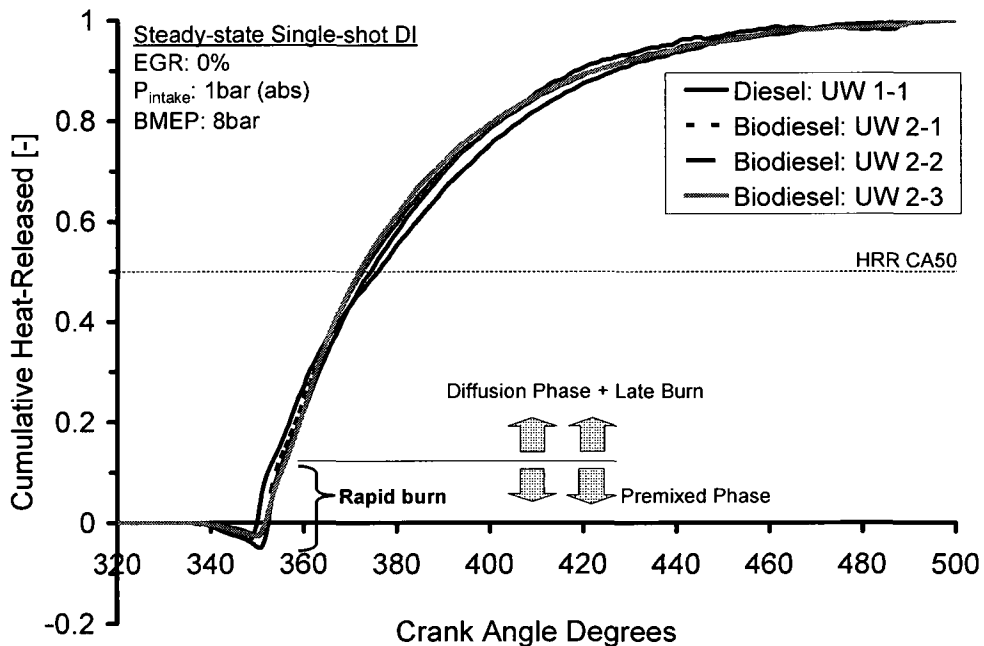
Figure 8-3: Comparison of diesel and biodiesel cumulative heat-released at high load.
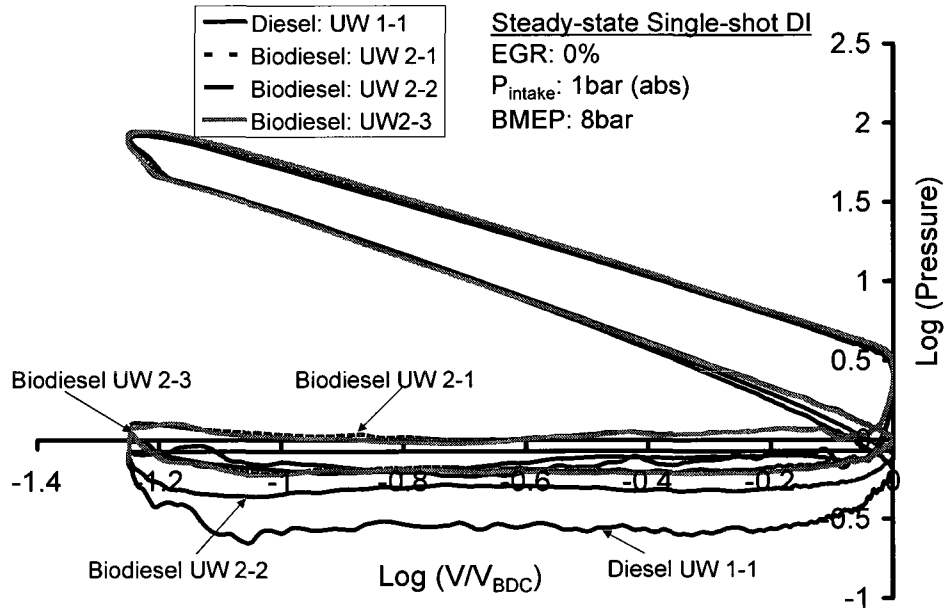
Figure 8-4: Logarithmic p-V traces for diesel and biodiesel fuels at high load.

The actual SOI for the biodiesel fuel was not experimentally determined in this investigation. Nonetheless, the engine crankshaft rotation required to reach injector NOP could be determined from Equation 8-1 (Tat & Van Gerpen 2003a, Rosca *et al.* 2005) where $P_{injection}$ is the injection pressure, B is the isentropic bulk modulus, v_p is the plunger velocity, A_p is the plunger area and V_f is the volume of the compressed fuel.

$$\theta = \frac{(NOP - P_o)V_f}{Bv_PA_P} = \frac{P_{injection}V_f}{Bv_PA_P}$$

Equation 8-1

160

Because of the higher viscosity and isentropic bulk modulus[1] of biodiesel fuels, the time required for the pressure wave in the injection system to reach the injector is expected to decrease, i.e. advanced injection timing. On the contrary, it was observed from the 200 cycle-averaged data that the start of fuel injection was consistent for all the fuels, which is supported by the dip in the net heat-release rate that coincides with the conventional single-shot SOI (Patterson *et al.* 2006, Stone 1999, Zheng *et al.* 2006c). A calculation, shown in Appendix E, revealed a difference of ±0.01ms (less than 0.1°CA at 1400rpm). Consequently, in the present study the SOI for all the fuels was considered to be at the same engine crank angle position of 17°CA BTDC.

Generally, the fraction of the energy released during the premixed phase was relatively lower for the high-CN fuel. The high-CN resulted in a shorter ignition delay period, τ_{ID}, (İçingür *et al.* 2003, Kidoguchi *et al.* 2000, Zheng *et al.* 2006c, 2007b) estimated from the SOI to the start of combustion (SOC). The SOC was taken as the crank angle position at which the net heat-release rate became positive after the initial dip coinciding with SOI. This was also checked by taking both the first and second derivatives of the cylinder pressure, $dP/d\theta$ (bar/°CA) and $d^2P/d\theta^2$ (bar/(°CA)^2), respectively. The τ_{ID} values were

---

[1] The isentropic bulk modulus for biodiesel fuels ranges widely from 1490 to 1670MPa or more while that for petroleum diesels is around 1370 to 1477MPa (Tat & Van Gerpen 2003, Rosca *et al.* 2005).

0.95ms for the diesel fuel UW1-1 and 0.91, 0.71 and 0.83ms for the biodiesel fuels UW2-1, 2-2 and 2-3, respectively. The effective excess air-to-fuel ratios, λ_E, shown in Table 8-1 were estimated from the intake oxygen concentration as described in Chapter V.

Table 8-1: Summary of the single-shot DI experimental results at high load.

Fuel UW	BMEP [bar]	IMEP [bar]	Fuelling [mg/cycle]	λ_E [-]	τ_{ID}		BSFC [g/kW-hr]	η_{Brake} [%]
					[ms]	[°CA]		
1-1	8.2	10.1	44	1.2	0.95	8.0	230	37
2-1	7.9	9.9	52	1.3	0.91	7.6	277	35
2-2	8.0	10	55	1.2	0.71	6.0	290	35
2-3	7.8	9.8	51	1.2	0.83	7.0	278	35

In the HTC mode the premixed phase is dominated by rapid or uncontrolled combustion determined by the fuel/air mixture that is formed during the ignition delay period (Stone 1999). Based on this premise, it is believed that this is where most of the in-cylinder NO_x would be formed, especially if the prepared air/fuel mixture was near-stoichiometric (Hiroyasu et al. 1990, Zhao et al. 1996, Zheng et al. 2004). This may explain the slightly lowered engine-out NO_x levels for biodiesel fuel UW2-3 compared with UW2-1, leading to comparable NO_x levels with diesel fuel shown in Figure 8-5. After the premix burning phase, the combustion progressed as mixing-controlled burning where the fuel-rich pockets struggle to find oxygen. However, the fuel-borne oxygen in the biodiesel may promote a more complete combustion resulting in comparatively reduced in-cylinder formation of soot, CO and THC as seen in Figure 8-5.
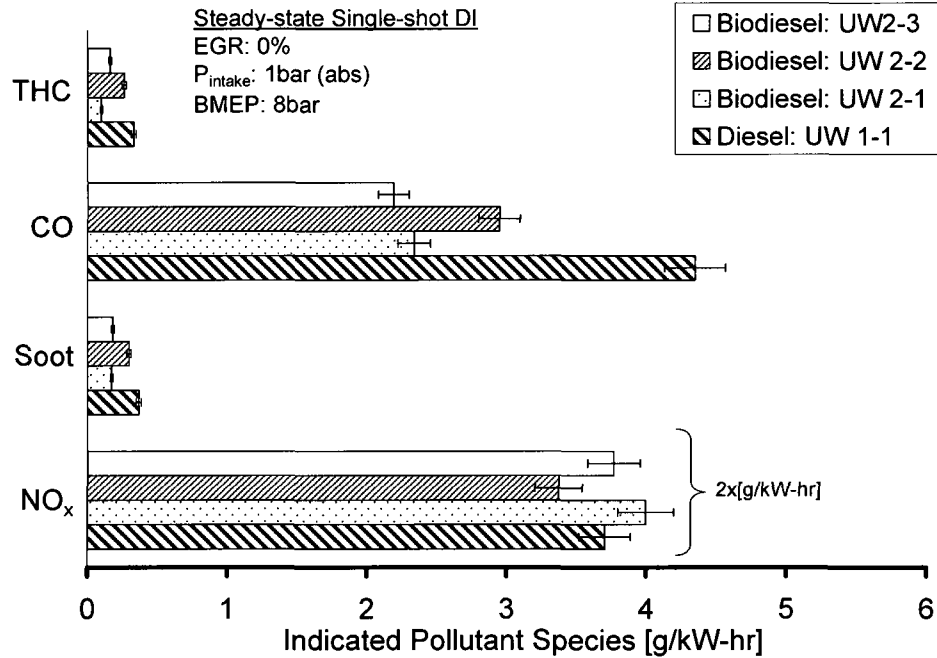
Figure 8-5: Comparison of diesel and biodiesel pollutants at high load.

For the same engine load level, the fuelling rate for the biodiesel fuels was higher, because of their lower energy content. Up to 23% increase in the BSFC was observed when the engine was fuelled with biodiesel. Based on the fuel energy conversion (i.e. LHV), however, up to 5% reduction in the η_{Brake} was observed when biodiesel was used. Nevertheless, for the same power output, the tested biodiesel fuels produced lower soot, CO and THC emissions.

8.2 Comparison of Diesel and Biodiesel Fuels under EGR

8.2.1 Engine Performance and Emissions

On the same Yanmar NFD170 engine, the conventional single-shot DI tests were also conducted with EGR sweeps at medium and low load conditions and the performance of the test fuels examined. The load levels investigated were 4.4 and 3.1bar BMEP corresponding to IMEPs of 6.4 and 5.1bar at medium and low loads, respectively.

The effects of EGR on biodiesel in-cylinder pressure, ROPR, heat-release rate, cumulative heat-released and logarithmic pressure vs. volume traces are shown in Figure 8-6 to Figure 8-9 while Table 8-2 summarises the engine performance. Similar to the observations in Chapter VII regarding the diesel fuel EGR sweep, the increase in the EGR rate reduced the peak cylinder pressure and maximum ROPR and increased the ignition delay period. The classical heat-release rate comprising the premixed and diffusion burning phases was not as evident in Figure 8-7 at such conditions in this engine. Nonetheless, it was observed that with the increase in EGR rate, the duration of the premixed phase increased, especially at high EGR levels. Conversely, an inspection of Figure 8-8 showed a rapid burning phase and a relatively slower burning phase. The former had characteristics consistent with the premixed phase and the latter the diffusion and late burning phase. At the investigated conditions, increasing the EGR rate from 0 to 60% had no perceptible effects on the burning rate (determined from the rate of change of the cumulative heat-released). Furthermore, the transition between the premixed and diffusion burning phases became less distinct at high EGR rates, similar to the observations in Chapter VII.

Table 8-2: Summary of the biodiesel single-shot DI test results at low load.

EGR [%]	BMEP [bar]	IMEP [bar]	Fuelling [mg/cycle]	λ_E [-]	τ_{ID} [ms]	τ_{ID} [°CA]	BSFC [g/kW-hr]	η_{Brake} [%]
2	3.1	5.1	25	2.6	0.95	8	322	28
33	3.2	5.2	25	2.3	1.07	9	308	29
45	3.2	5.2	25	1.9	1.43	12	309	29
64	2.9	4.9	25	1.4	1.76	15	327	27
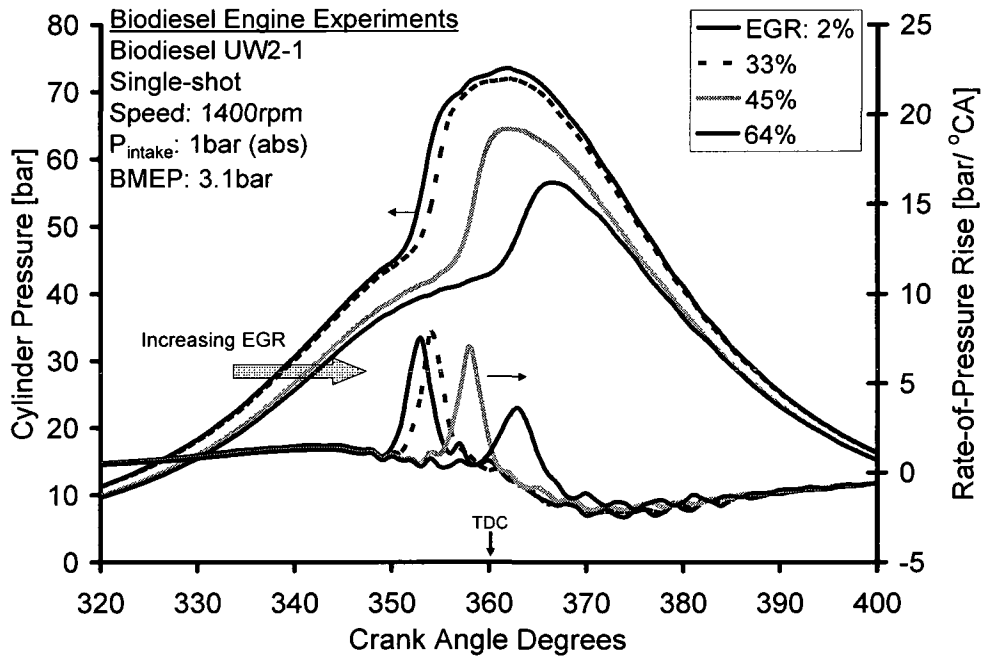
Figure 8-6: Effect of EGR on cylinder pressure and ROPR at low load.
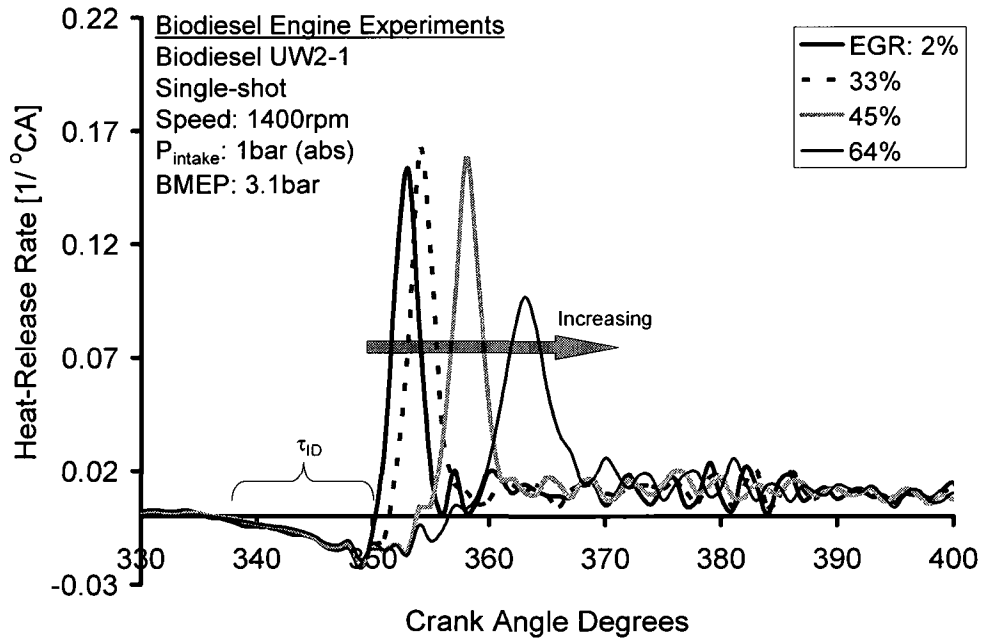
Figure 8-7: Effect of EGR on heat-release rate at low load.
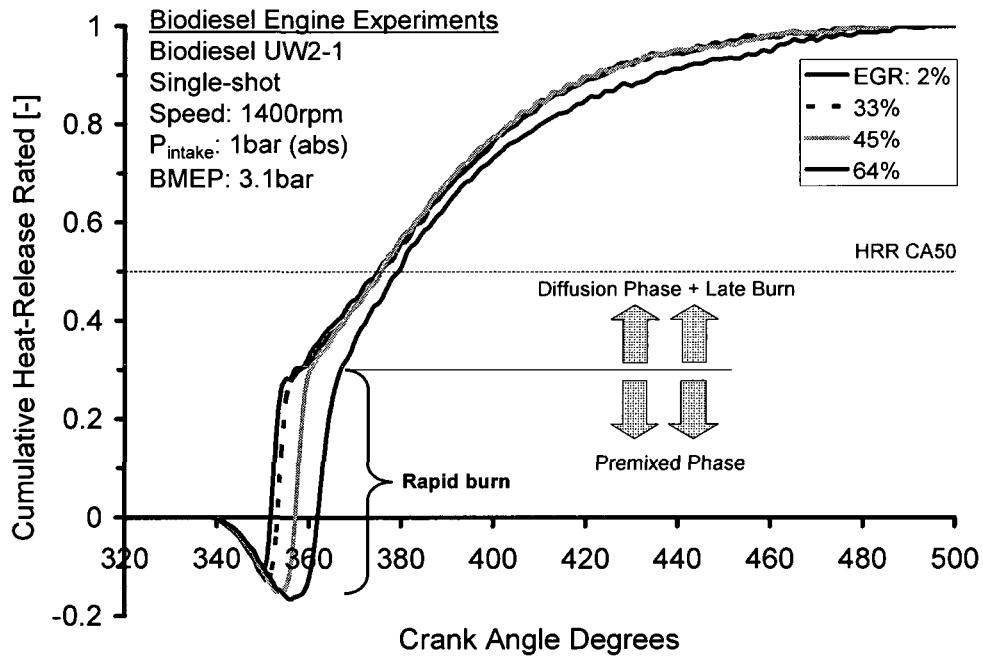
Figure 8-8: Effect of EGR on the cumulative heat-released at low load.
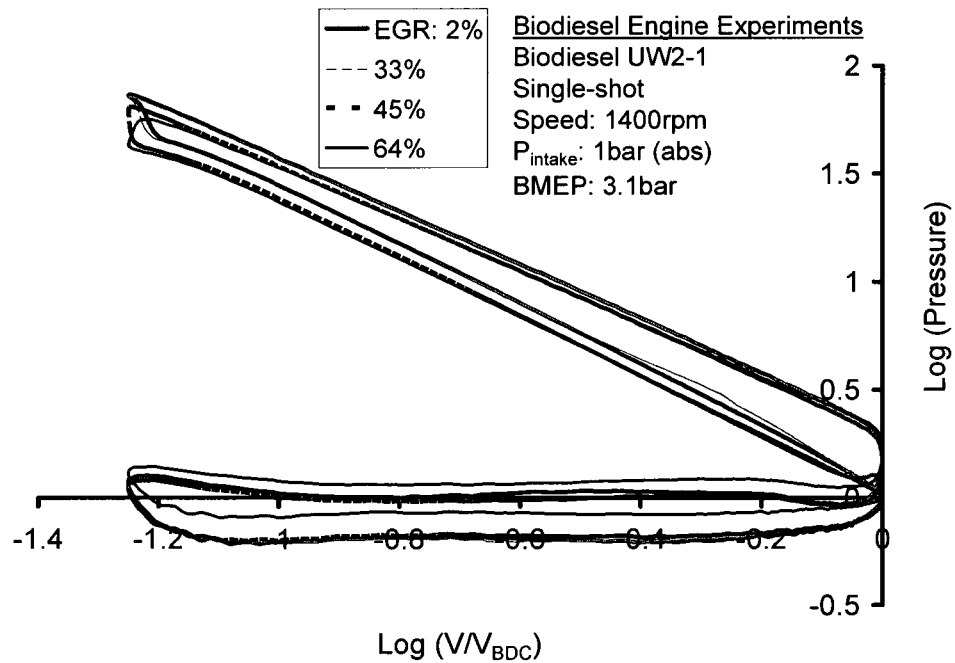
Figure 8-9: Logarithmic pressure vs. volume for biodiesel DI tests at low load.

Although increasing the EGR did increase the CO and THC as seen in Figure 8-10, the engine performance did not appreciably deteriorate. The logarithmic p-V trace of

166

Figure 8-9 showed only a slight decrease in the net work done on the piston by the gases i.e. IMEP. Note that the CO and THC could be oxidised using a DOC with relative ease. As a result, the following section only considers the comparison of diesel and neat biodiesel fuels with respect to the engine-out NO_x and soot emissions and the engine performance.
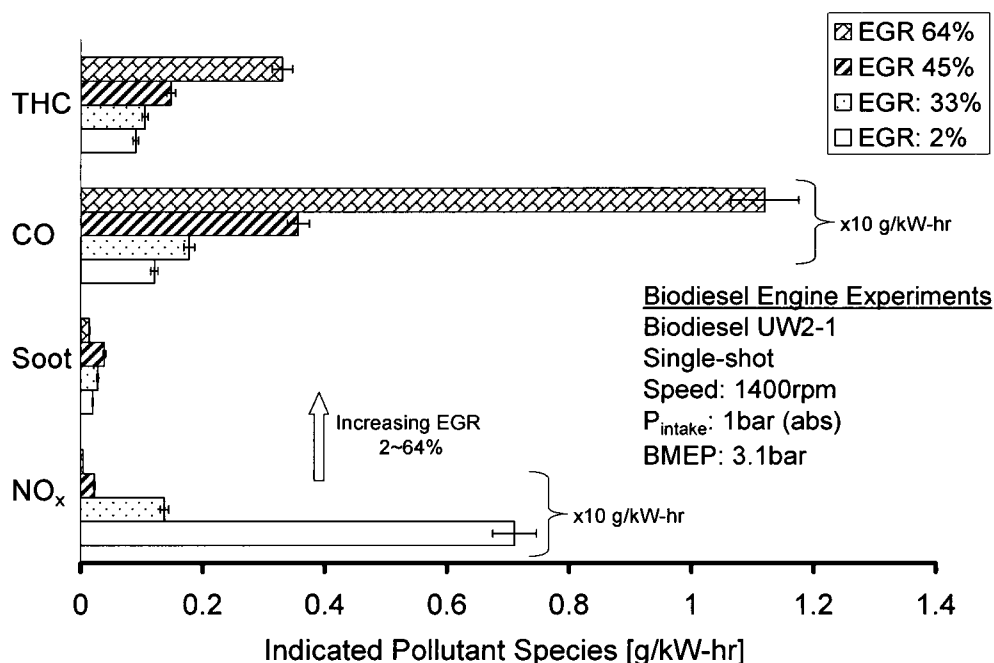
Figure 8-10: Effect of EGR on biodiesel engine-out species at low load.

8.2.1 (a) Comparison of NO_x Emissions

As discussed in Chapter I, when air is used as the oxidiser, the NO_x yield is affected primarily by the prevailing temperature, oxygen concentration and residence time during the reaction. Therefore, at steady-state conditions in diesel engines, as the EGR rate is increased the engine-out NO_x emissions would monotonically decrease as seen in Figure 8-11 and Figure 8-12. This is mainly due to the dilution, thermal and chemical effects of EGR, as discussed in Chapter V. The EGR dilutes the oxygen concentration of the working fluid. Concurrently, The EGR increases the specific heat capacity of the

working fluid thereby reducing the flame temperatures. Furthermore, the endothermic dissociation of the EGR constituents such as H_2O may contribute to the reduction in the flame temperatures.
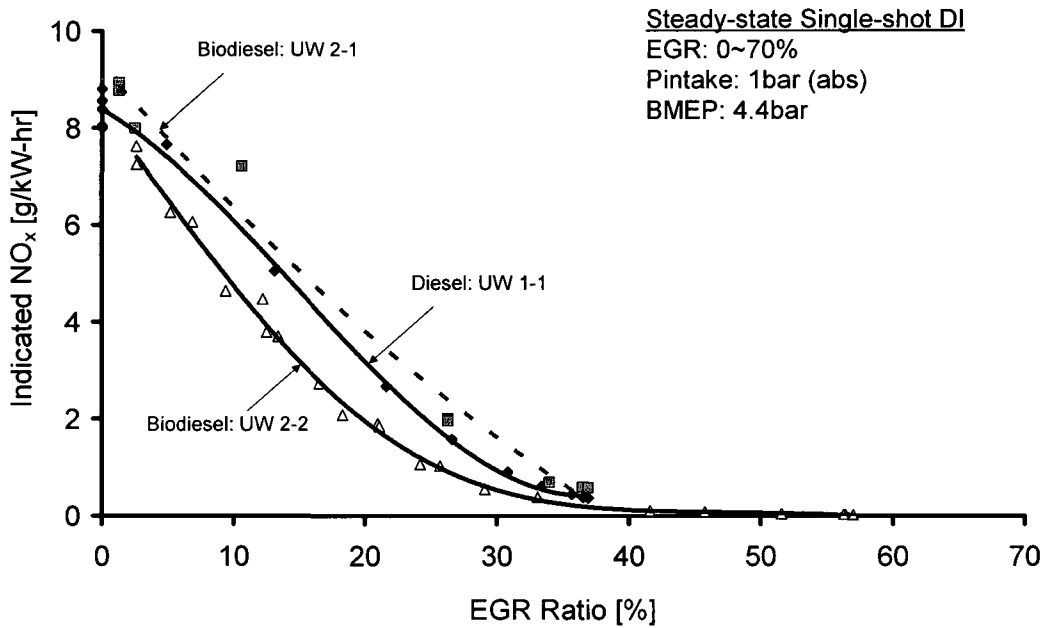
Figure 8-11: Effect of EGR on indicated NO_x at medium load.
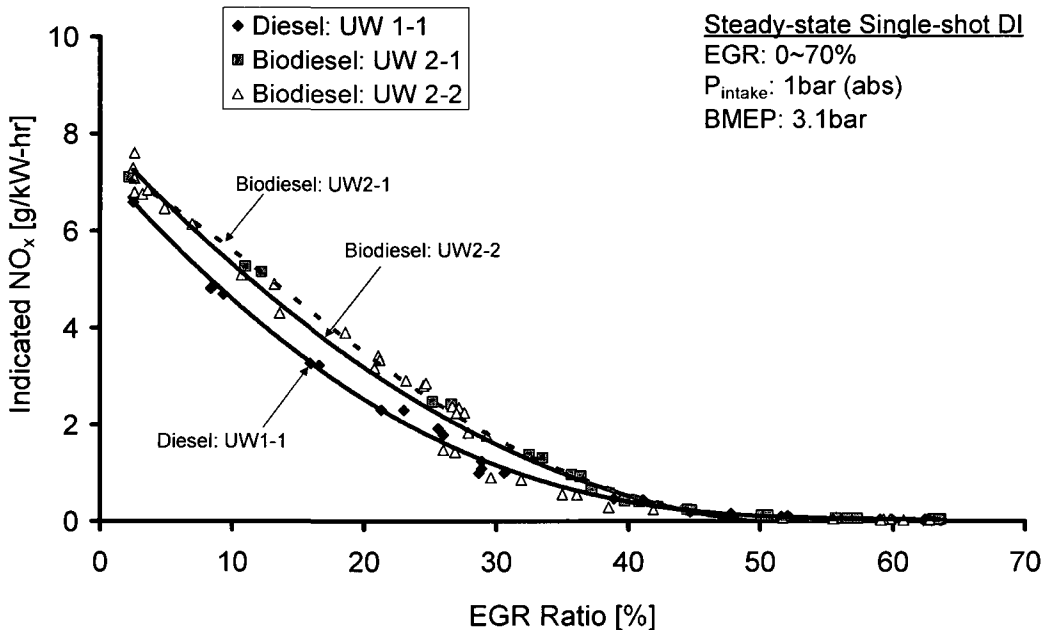
Figure 8-12: Effect of EGR on indicated NO_x at low load.

8.2.1 (b) Comparison of Soot Emissions

At steady-state conditions increasing the EGR rate results in an increased ignition delay period as demonstrated in Table 8-2. Figure 8-13 and Figure 8-14 show the effect of τ_{ID} (caused by increasing the EGR rate) on the engine-out soot. Similar to the results of Chapter VII, where the diesel-fuelled engine soot vs. EGR was investigated, the soot vs. $\Delta\tau_{ID}$ profile was observed to have two distinct slopes, *Slope 1* and *Slope 2*. In *Slope 1*, whose characteristics are consistent with HTC mode, the soot increased with increasing EGR until the τ_{ID} was prolonged by 50~70%. In *Slope 2*, consistent with HCCI-enabling technologies and smokeless diesel combustion i.e. LTC mode, the soot decreased with increasing EGR i.e. as the ignition delay was prolonged further.

Under *Slope 1*, the soot would increase with EGR particularly if the temperatures were high enough to initiate soot precursors in the existing fuel-rich pockets where the reduced oxygen environment would hinder the oxidation of the ensued soot. On the *Slope 2* side, however, the high rates of EGR and reducing cylinder temperatures during the expansion stroke would result in the increased τ_{ID} period and thus more mixing of the charge. Consequently, the heat-release rates would be dominated by the low temperature premixed phase of combustion thereby simultaneously reducing the in-cylinder NO_x and soot levels. To extend the EGR applicability, intake throttling was used to increase the pressure differential between the exhaust and the intake, especially at low load conditions. This was necessary because of the limited concentration of CO_2 produced at such conditions, as discussed in Chapter V.
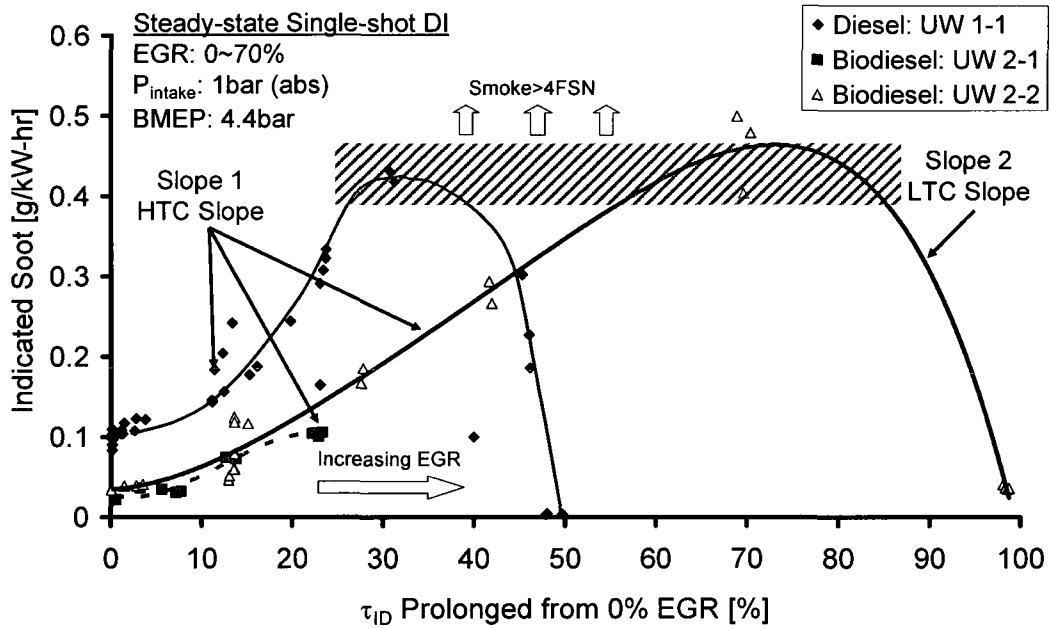
Figure 8-13: Effect of increasing τ_{ID} through EGR on indicated soot at mid load.
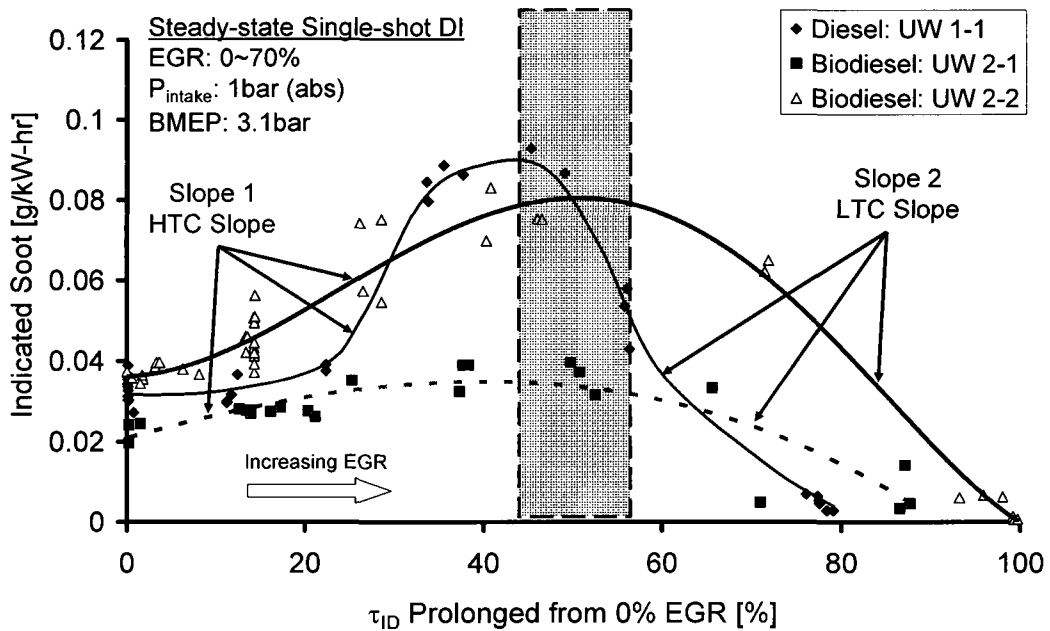
Figure 8-14: Effect of increasing τ_{ID} through EGR on indicated soot at low load.

8.2.1 (c) Comparison of Engine Performance

Note that the LTC slope is a narrow region obtained by prolonging the τ_{ID} by more than

80~100% through the use of EGR. A further increase of EGR beyond this point resulted

170

in increased CO and THC emissions and deterioration in the thermal efficiency represented by the loss of effective power in Figure 8-15 and Figure 8-16. At medium load conditions, the effective engine power loss was 18 to 23% while at low loads between 6 to 19% with the higher range being for the diesel fuel. However, this is a profound improvement in the engine performance compared to the biodiesel intake port injection tests that were reported previously (Zheng *et al.* 2006c). The port-injection tests had several setbacks including substantial engine oil dilution attributed to the fuel seeping through to the oil sump.

It was observed from Figure 8-17 that the cyclic variability of the biodiesel fuels was relatively lower than that of the diesel fuel at such elevated EGR levels. Consequently, the biodiesel fuels may sustain a further increase in the EGR rate before the cyclic variability becomes intorelable. This could be attributed to a combination of the biodiesels' fuel-borne oxygen which is accessible for combustion and relatively higher CN. In comparison with the conventional diesel fuel, the higher CN of the biodiesel fuels implies that at fixed pressure, temperature and load level the biodiesels would possess a higher propensity to auto-ignite. An inspection of the effective in-cylinder air/fuel mixture strength, λ_E, showed that the test conditions were stoichiometrically lean as seen in Figure 8-18, which presents a potential to further increase the EGR application limit for biodiesel fuels. Hence the biodiesel fuels with a higher CN than conventional diesel can sustain a broader range of engine loads in the EGR-incurred LTC mode.
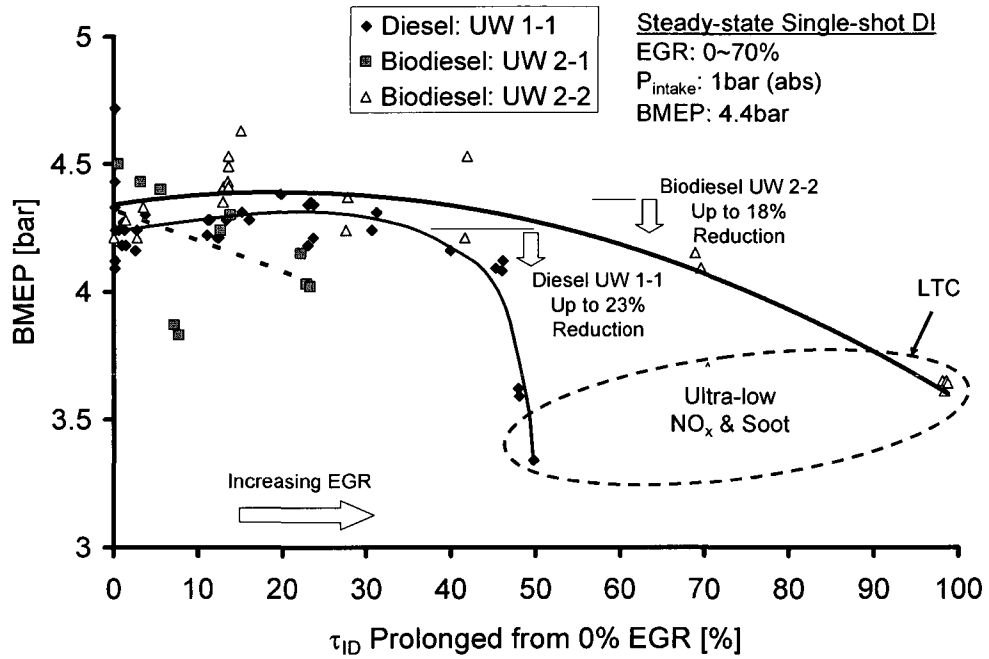
Figure 8-15: Effect of increasing τ_{ID} through EGR on BMEP at medium load.
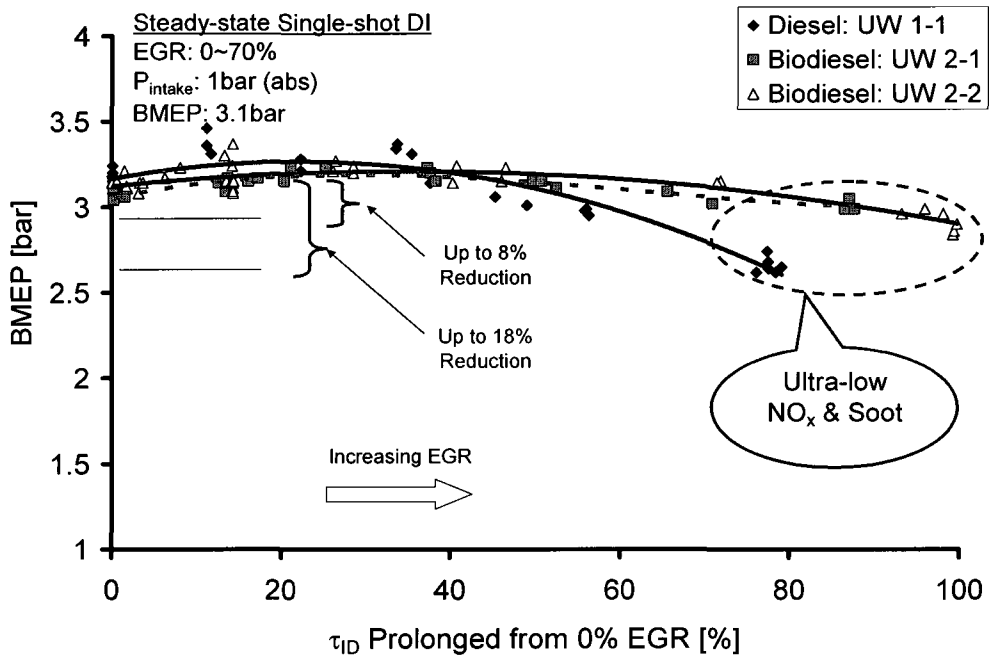
Figure 8-16: Effect of increasing τ_{ID} through EGR on BMEP low load.
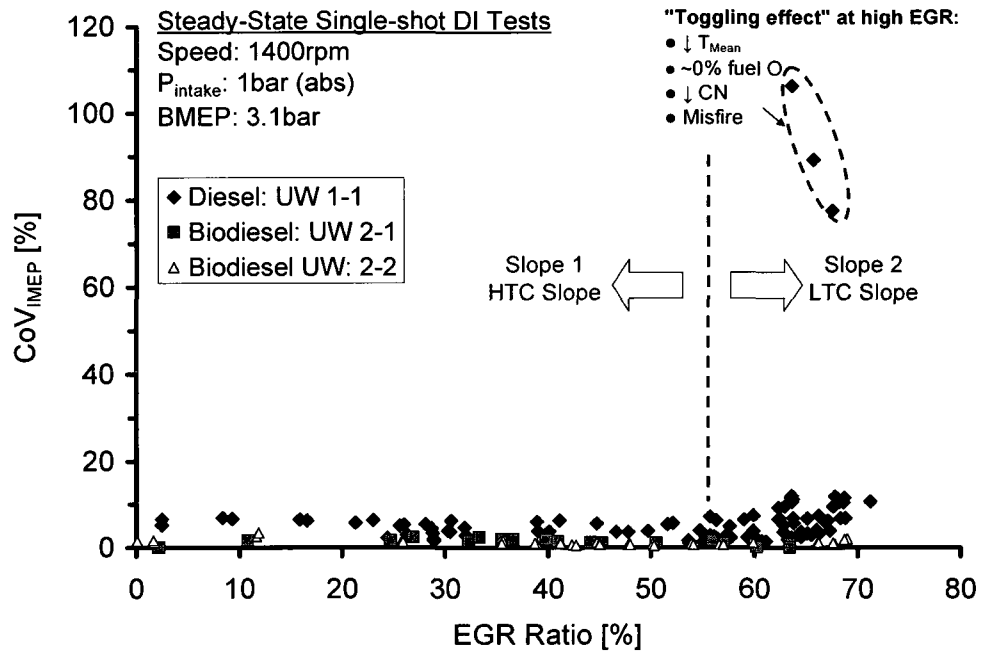
Figure 8-17: Effect of EGR on IMEP CoV at low load.
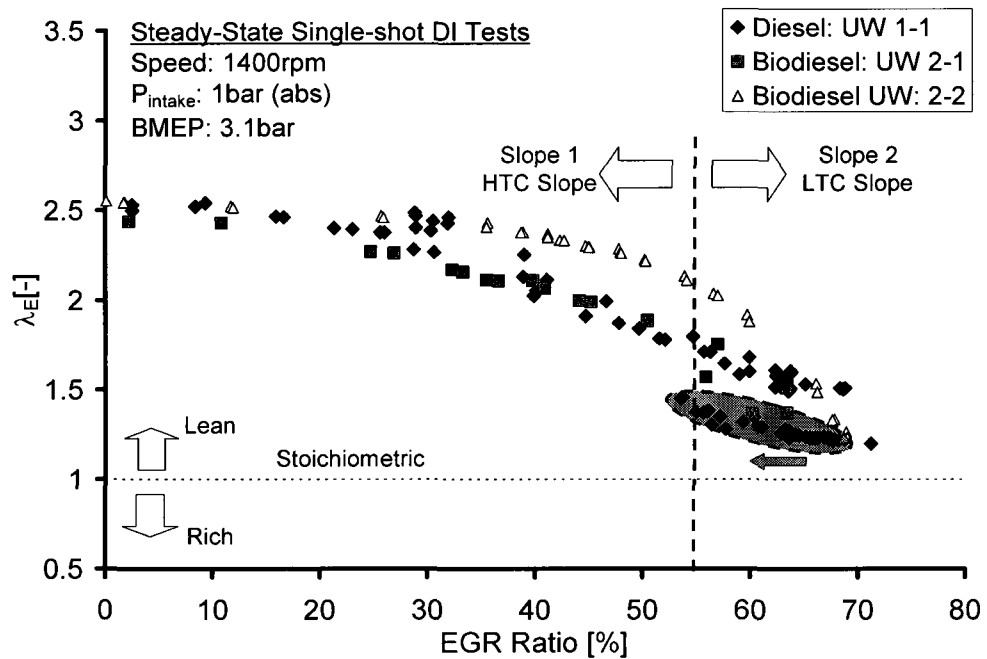
Figure 8-18: Effect of EGR on air/fuel mixture strength at low load.

8.2.2 Ignition Delay Correlation

For convenience in analyses, the ignition delay is usually correlated by an expression of the form shown in Equation 8-2 where E_a is the apparent activation energy, A, n are constants but functions of fuel type and air/fuel mixing/motion (Assanis *et al.* 2003, Stone 1999).

$$\tau_{ID} = AP^{-n} \exp\left(\frac{E_a}{R_u T}\right)$$

Equation 8-2

Several expressions for ignition delay have been proposed however the most common employed in diesel engines was deduced by Watson and is shown in Equation 8-3 (Stone 1999), where τ_{ID} is the ignition delay period (ms), P in (bar) and T in (K) are the mean pressure and temperature during the ignition delay period, respectively. The 'activation temperature' (E_a/R_u) for the No. 2 diesel fuel (D2) mixed with air was considered to be 2100K.

$$\tau_{ID} = 3.5P^{-1.022} \exp\left(\frac{2100}{T}\right)$$

Equation 8-3

Equation 8-3 was extended by Assanis *et al.* (2003) by considering the equivalence ratio, ϕ, as shown in Equation 8-4. The ignition delay was determined under a wide range of steady-state operating conditions from 5 to 100% load and 900 to 2100rpm. The pre-exponential coefficient was found to range from 2.6 to 3.8, as opposed to the Watson correlation where it is fixed at 3.45 over all operating points. However, it was interesting

to observe that the value employed by Watson translated into ϕ=0.116 which, the authors believed, may have been close to the actual mean fuel/air equivalence ratio during the ignition delay period (Assanis *et al.* 2003).

$$\tau_{ID} = 2.4\phi^{-0.2}P^{-1.02}\exp\left(\frac{2100}{T}\right)$$ Equation 8-4

Equation 8-4 could be modified to include the effect of extensive EGR application for single-shot low-temperature combustion. Furthermore, since biodiesel fuels seem to have similar ignition characteristics as diesel fuel, the expression could be used for this type of fuel as long as the effect of the CN was considered. Therefore, to account for the fuel CN, the activation energy could be modified by a factor 71.3/(CN+25) so that the baseline diesel D2 fuel with CN 46.3 would have a factor of unity (Choi & Reitz 1999). The final expression for ignition delay under the influence of EGR is shown in Equation 8-5 where $[O_2]_{in}$ and $[F_O]_{fuel}$ are the molecular and equivalent molecular oxygen mass fractions in the intake and fuel, respectively (Zheng *et al.* 2007c). Note that when the EGR is applied, the mean cylinder temperature during the τ_{ID} decreases. Figure 8-19 shows the effect of EGR, represented by the diminishing intake O_2 concentration, on the mean cylinder temperature during the ignition delay period. The mean temperature was estimated from the measured in-cylinder pressures, using the equation of state for an ideal gas.

$$\tau_{ID} = A([O_2]_{in} + [F_O]_{fuel})^{-k}P^{-n}\exp\left(\frac{2100\times[71.3/(CN+25)]}{T}\right)$$ Equation 8-5
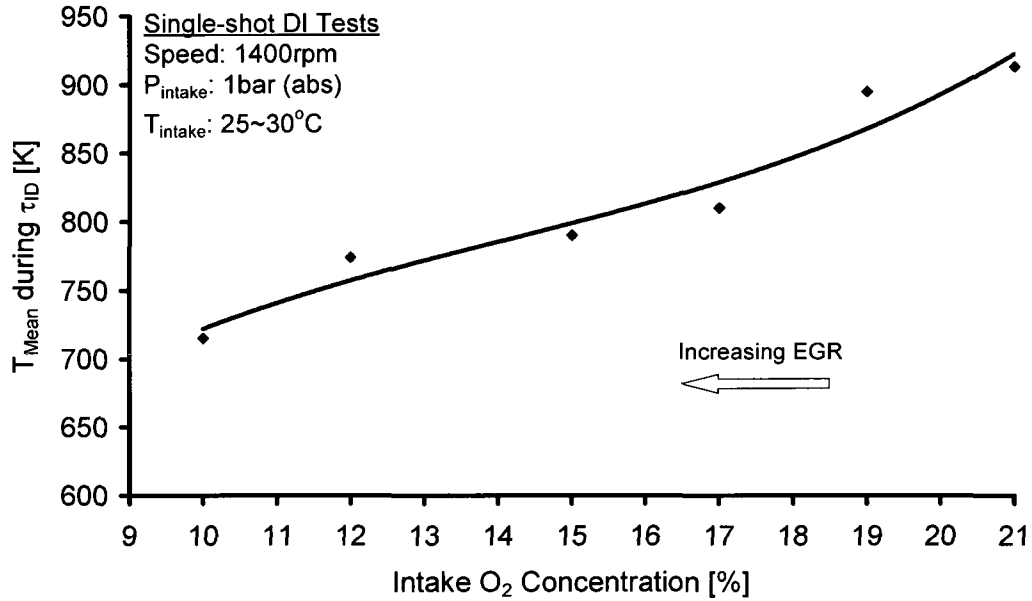
Figure 8-19: Variation of T_{Mean} with intake O_2 during τ_{ID}.

Figure 8-20 and Figure 8-21 present the results for the ignition delay correlation under the influence of EGR at steady-state conditions. The correlation captured the ignition delay trends estimated from the heat-release rate method with good agreement. A slight difference in the trends for the biodiesel UW2-2 was observed, which may be attributable to the oxidative degradation of the fuel as mentioned above. Note, however, that unlike the expressions given in Equations 8-3 and 8-4, the pre-exponential coefficient presented in the present work is a function of the oxygen concentrations in the intake air and fuel as shown in Figure 8-22 and Figure 8-23. Under the tested conditions, the coefficients were found to range from 4.3 to 4.5 for the diesel fuel and 3.9 to 4.2 for the biodiesel fuels. Because the coefficients are also dependent on the air/fuel mixing/motion, they may be different for different engines and engine operating conditions.
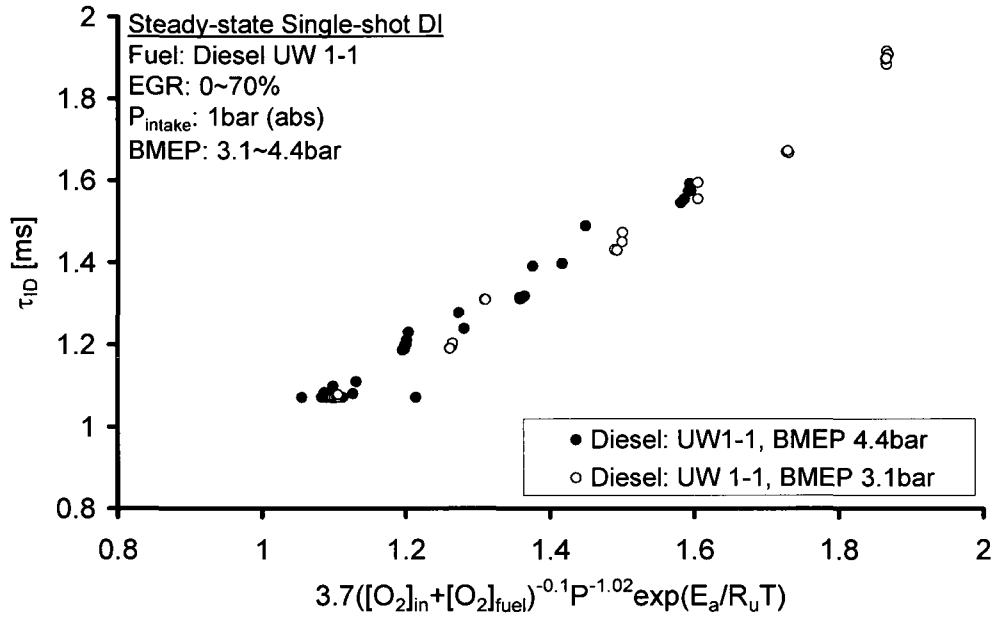
Figure 8-20: Steady-state τ_{ID} correlation under the influence of EGR for diesel.
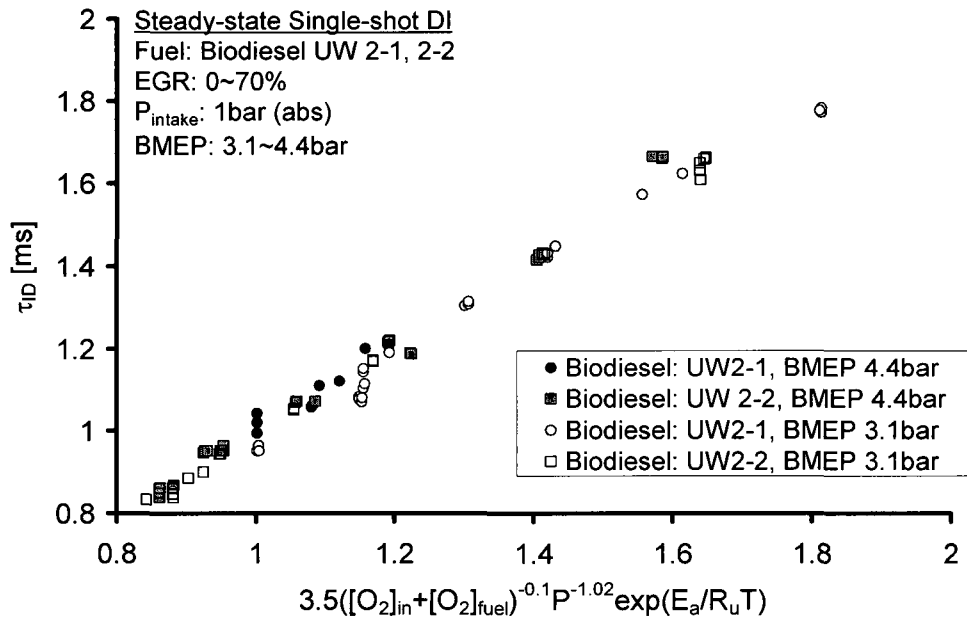
Figure 8-21: Steady-state τ_{ID} correlation under the influence of EGR for biodiesel.
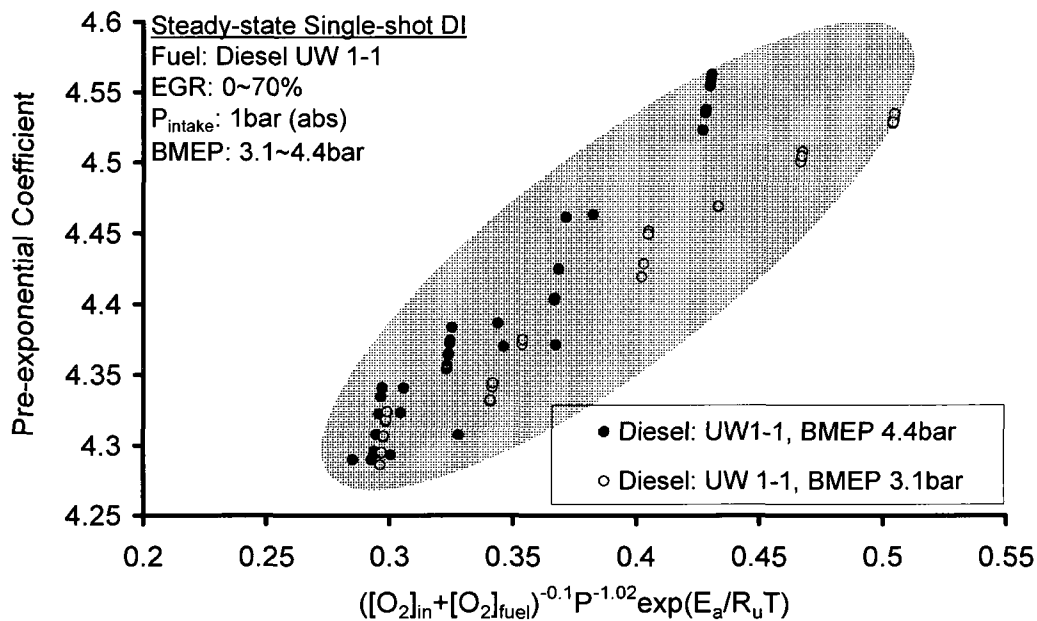
Figure 8-22: Steady-state pre-exponential factors for diesel fuel.
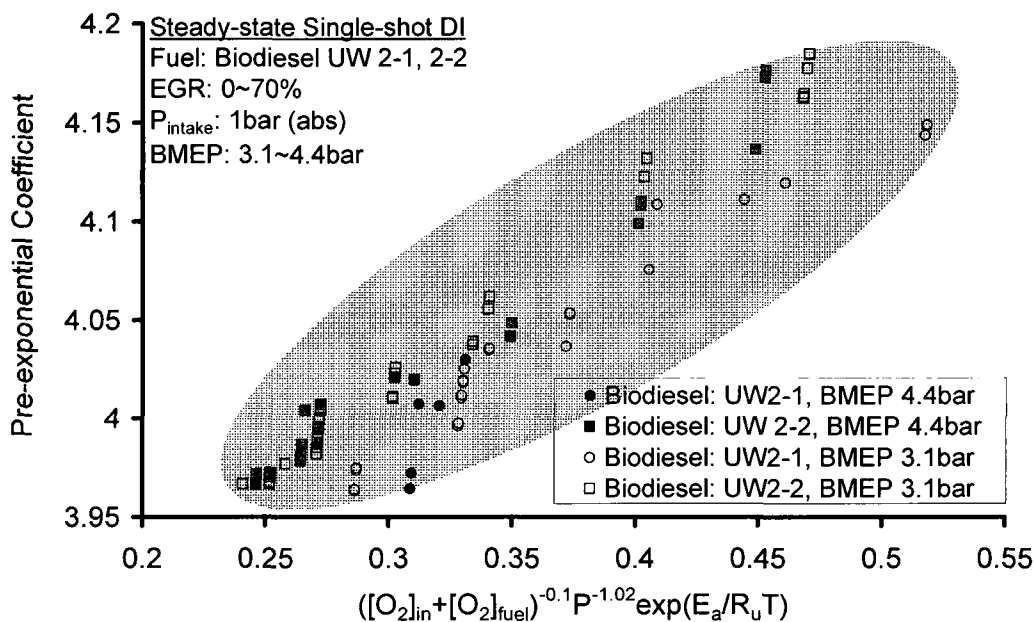
Figure 8-23: Steady-state pre-exponential factors for biodiesel fuels.

The NO_x data presented here comes from a small diesel engine with significant pre-mixed combustion. The results may be atypical of what one would see on a heavy-duty diesel engine, where diffusion combustion predominates. The percentage of premixed

combustion is affected by the fuel CN and other factors such as injection and boost

pressures. Installation of a common-rail injection system on the engine is planned for a

versatile set up allowing for independent control of the injection timing and quantity, thus

facilitating the optimisation tests for alternative fuels, such as neat biodiesels, to be more

effective.

CHAPTER IX

BIODIESEL TEST RESULTS AND DISCUSSION

(COMMON-RAIL DI DIESEL ENGINE)

The combustion and emission characteristics of a mixture of neat biodiesel fuels were investigated on the Ford "Puma" common-rail DI diesel engine. A blend of the fatty acid methyl esters derived from Canola oil, soybean oil, tallow and yellow grease was utilised under independently controlled levels of EGR, intake boost and exhaust backpressure. Furthermore, strategies that include single-shot with the commanded SOI sweeps, EGR sweeps and multi-pulse injection were applied to modulate the homogeneity history of the biodiesel LTC operations.

As described in Chapter IV, the fatty acid methyl esters derived from Canola oil, soybean oil, tallow and yellow grease, from biodiesel producers in Canada, were first analysed by an established research institution following the ASTM standards D6751, D5291 and D4809 for the B100 specification, C/H/O ratio and fuel energy content, respectively. Table 9-1 presents the characteristics of the fuels. The fuels were then mixed according to the approximate volumetric proportions as may be readily procured in Ontario Province of Canada (see Figure 9-1 and Figure 9-2). The final biodiesel fuel blend (hereafter called Biodiesel) was, however, not analysed. Therefore, the fuel characteristics shown in the last column of Table 9-1 were estimated from the fraction of the neat B100 fuels UW2-1 to 2-4 on a mass basis as shown in Equation 9-1.

Table 9-1: Estimated characteristics of the Biodiesel employed in the common-rail diesel engine.

Characteristic	ASTM Test	UW No. 2-1	UW No. 2-2	UW No. 2-3	UW No. 2-4	Biodiesel
Feedstock	-	Soy	Canola	YG	Tallow	Blend
Description	D6751	B100	B100	B100	B100	
Density [kg/m^3] @15°C	D1298	883.3	883.8	876.1	875.2	879
CN	D613	50.6	53.6	61.2	57.5	57.4
Kinematic Viscosity [cSt] @40°C	D445	4.1	4.4	4.8	4.8	4.6
Distillation Temperature [°C] (up to 95% distillation)	D1160	312~420	344~356	321~353	305~395	322~370
LHV [MJ/kg] LHV [MJ/l]	D4801	37.6 33.2	37.8 33.4	37.3 32.7	37.1 32.5	37.4 32.9
Total Sulphur [ppm]	D5453	6	2	15	18	11.3
Reduced Chemical Formula (based on C/H/O)	D5291	$CH_{1.82}O_{0.11}$	$CH_{1.88}O_{0.11}$	$CH_{1.95}O_{0.11}$	$CH_{1.97}O_{0.11}$	$CH_{1.92}O_{0.11}$
Stoichiometric A/F (mass)	D5291	12.34	12.44	12.54	12.48	12.48

$$B_{Biodiesel} = \sum_i^n (Y_i \times B_i) = (Y_{UW2-1} \times B_{UW2-1}) + (Y_{UW2-2} \times B_{UW2-2}) + \ldots\ldots (Y_{UW2-4} \times B_{UW2-4})$$ Equation 9-1

where $B_{Biodiesel}$ is the estimated property of the blended fuel, Y_{UW2-1} to Y_{UW2-4} are the mass fractions of the B100 fuels UW2-1 to 2-4

and B_{UW2-1} to B_{UW2-4} their respective ASTM-determined properties. The mass fractions of the B100 fuels in the blended Biodiesel were

determined from Equation 9-2.

$$Y_i = \frac{\rho_i \times V_i}{\sum_{i=UW2-1}^{n=UW2-4} (\rho_i \times V_i)}$$ Equation 9-2

2004 Canadian Potential Biodiesel Feedstock Availability
(NRCan, 2004)

□ Canola Oil	□ Marine Oils
☑ Soybean	☒ Tallow (Animal Fat)
□ Yellow Grease	
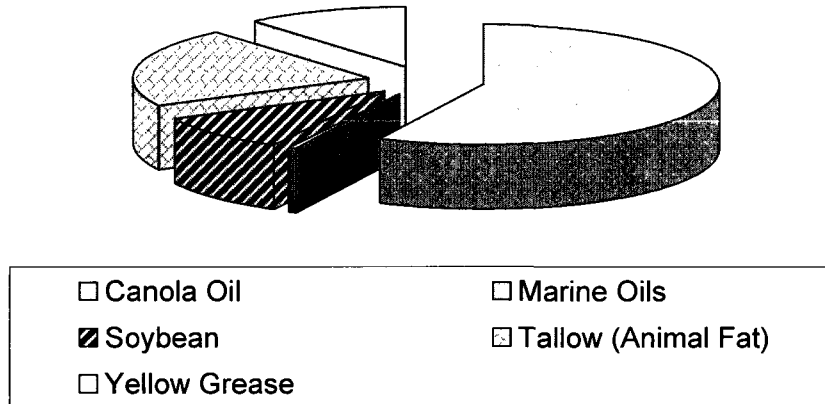
Figure 9-1: Canadian potential biodiesel feedstock availability, in tonnes, (NRCan, 2004).

B100 Fuel Mixture by Volume of Feedstock

Mostly supplied from Western Canada
(Including AB, BC, MB, SK)

Mostly supplied from Eastern Canada
(Including ON, QC)

□ Canola Oil ☑ Soybean ☒ Tallow □ Yellow Grease
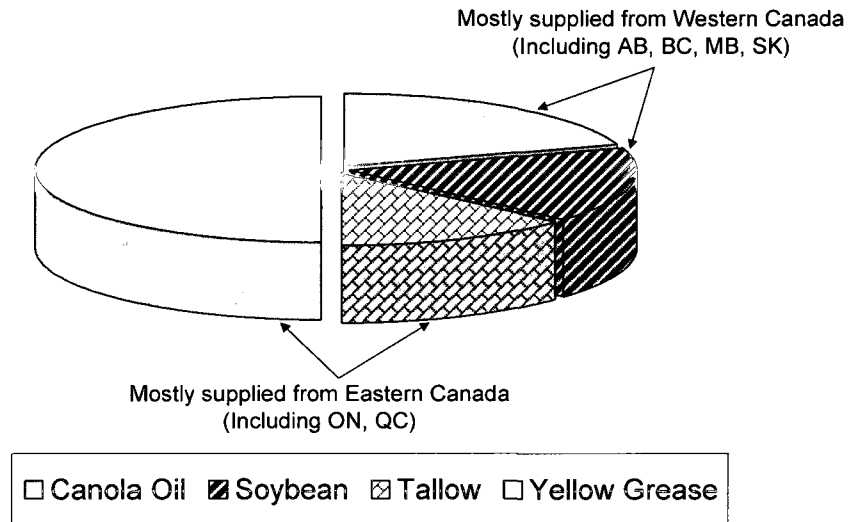
Figure 9-2: Biodiesel fuel mixture by volume of feedstock employed in the current study.

182

9.1. Commanded SOI Sweep

Figures 9-3 to 9-7 present the results for the variation of in-cylinder pressure, ROPR, heat-release rates, ignition delay and logarithmic pressure-volume profiles with the commanded SOI at 8bar IMEP and an absolute intake pressure of 1.2bar for the common-rail engine fuelled with Biodiesel. At a commanded SOI of 347.5°CA (i.e. -12.5°CA ATDC), the combustion process exhibited the classical HTC characteristics of premixed and diffusion burning phases.

Deduced from Figure 9-6, as the SOI was retarded the τ_{ID} was initially shortened during the compression stroke due to the increasing temperature and pressure. During the expansion stroke, however, because of the reducing temperature and pressure, a further retard of the SOI prolonged the τ_{ID}. Consequently, the combustion process entered a transition from the classical premixed and diffusion phase to the mainly premixed phase when the SOI was after the piston TDC. Because of the relatively high CN of the Biodiesel, its τ_{ID} was shorter than that of the diesel fuel for the conditions investigated. It is noted, from Figure 9-7, that the Biodiesel late injection still produced a positive IMEP, thus the engine should be able to produce reasonable effective power output when using a multi-cylinder configuration at such conditions.
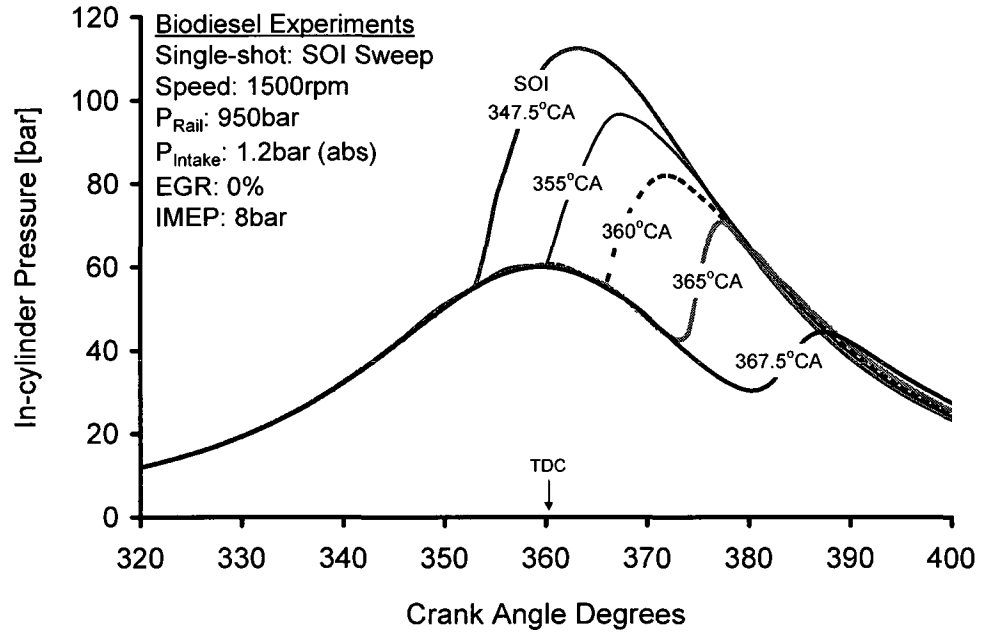
Figure 9-3: In-cylinder pressures for the SOI sweep at P_{Intake} of 1.2bar (abs).
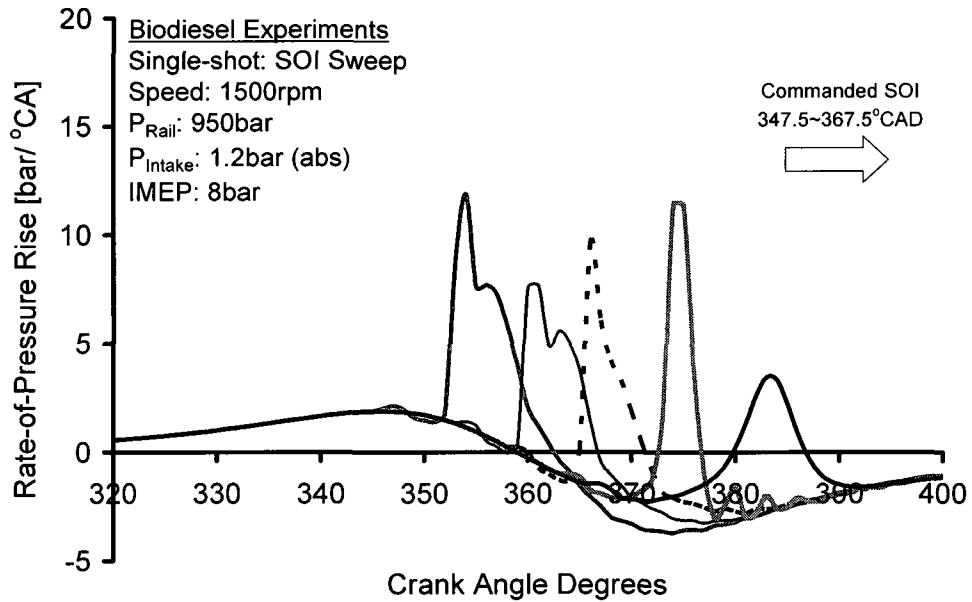
Figure 9-4: Rate-of-pressure rise for the SOI sweep at P_{Intake} of 1.2bar (abs).

184
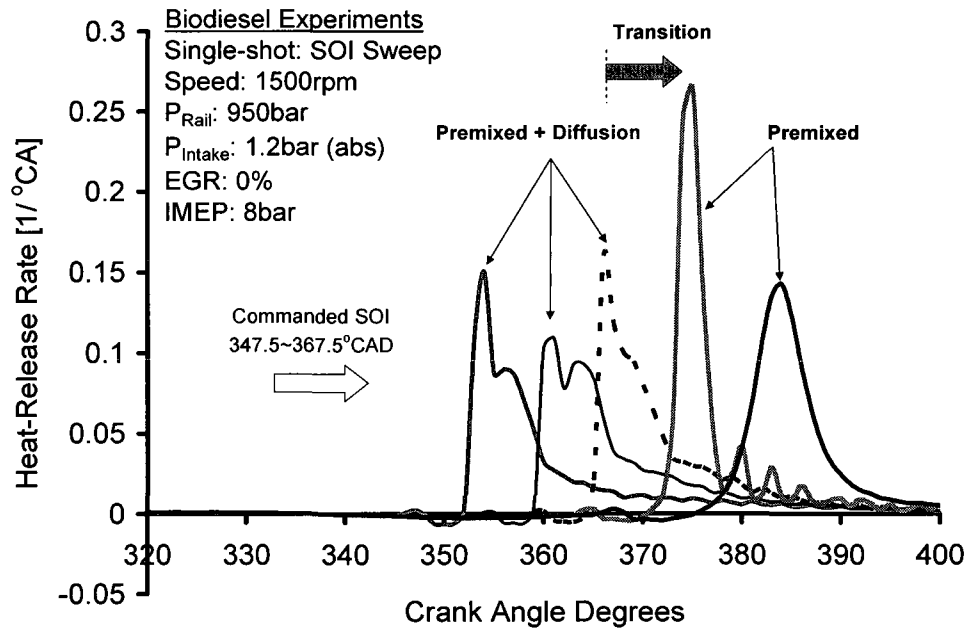
Figure 9-5: Normalised heat-release rates for the SOI sweep at P_{Intake} of 1.2bar (abs).
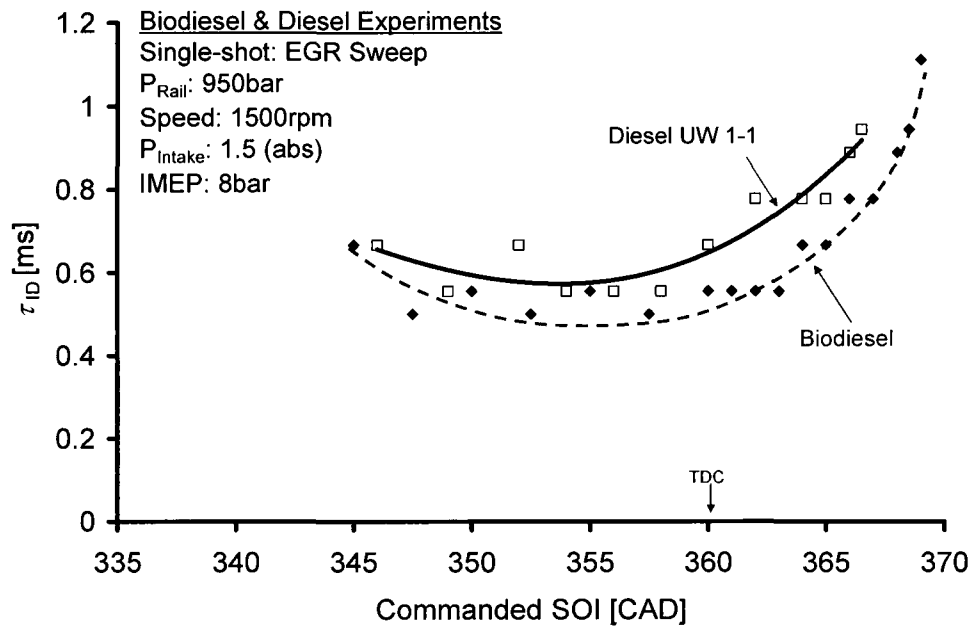
Figure 9-6: Variation of τ_{ID} with SOI at P_{Intake} of 1.5bar (abs).

Biodiesel Experiments
Single-shot: SOI Sweep
Speed: 1500rpm
P_{Rail}: 950bar
P_{Intake}: 1.2bar (abs)
EGR: 0%
IMEP: 8bar
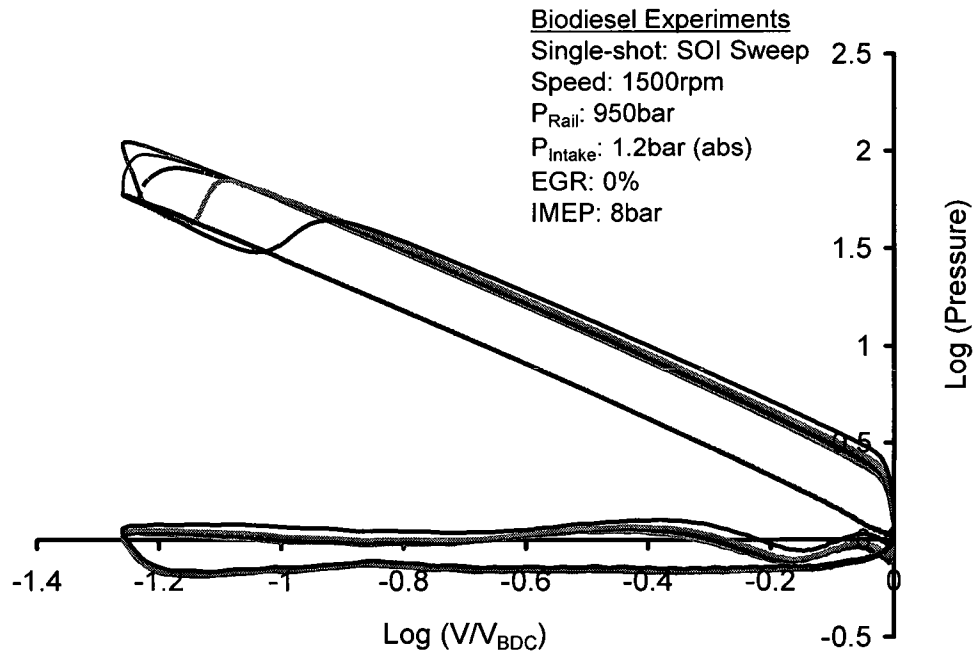
Figure 9-7: Logarithmic pressure vs. volume for SOI sweep at P_{Intake} of 1.2bar (abs).

Figures 9-8 and 9-9 present the effect of SOI on engine-out NO_x emissions for the single-shot DI tests at 8bar IMEP, where the Diesel UW1-1 fuel has been included for comparison. For the conditions investigated, there was only a marginal difference in the NO_x emissions between the Biodiesel and diesel fuels. Noted, it was possible to retard the SOI for Biodiesel further than that of the diesel fuel before the cyclic variability, determined from the CoV_{IMEP}, became intorelable (See Figures 9-11 and 9-12). One of the main reasons for this could be attributed to the relatively higher CN of the Biodiesel as disccused in Chapter VIII.
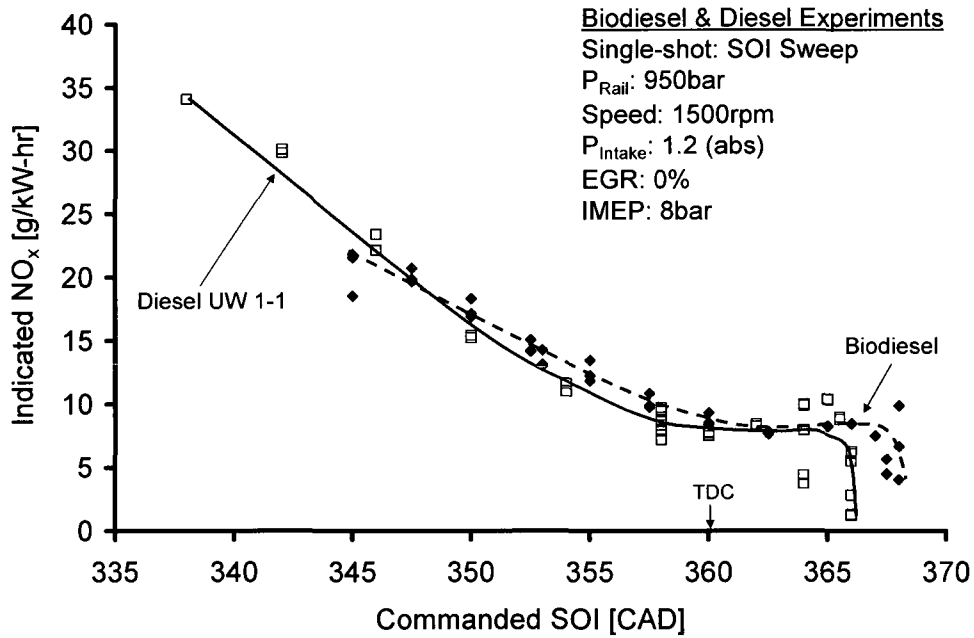
Figure 9-8: Indicated NO_x vs. SOI for Biodiesel and diesel at 8bar IMEP P_{Intake} 1.2 (abs).
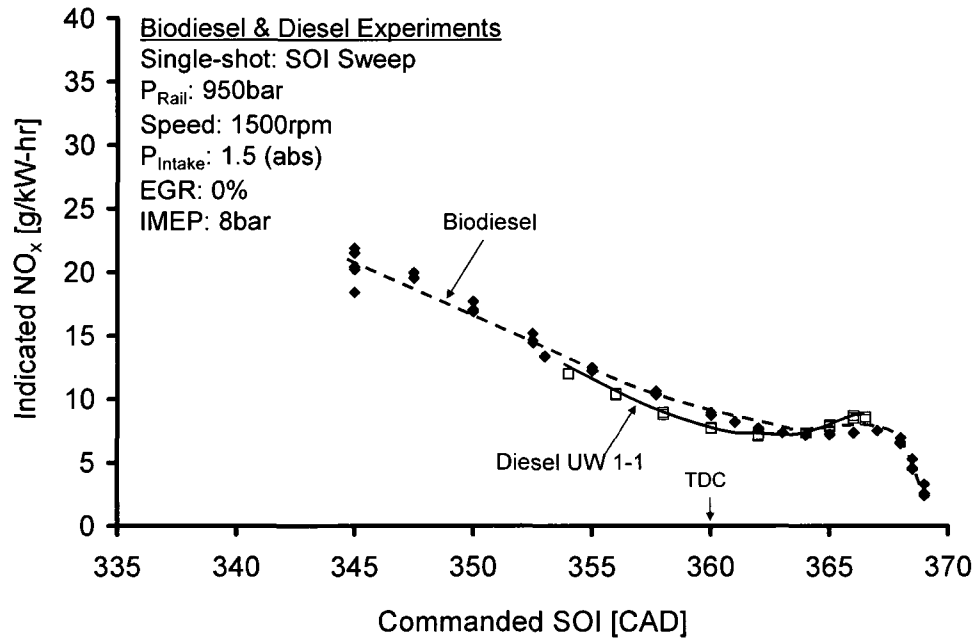
Figure 9-9: Indicated NO_x vs. SOI for Biodiesel and diesel at 8bar IMEP 1.5bar (abs).
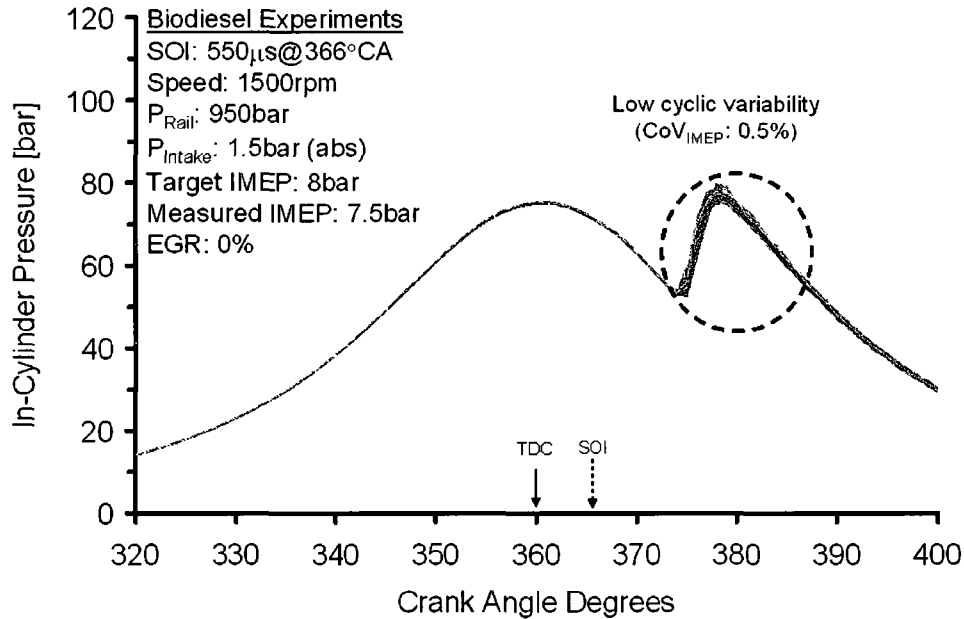
Figure 9-10: In-cylinder pressures at SOI 366°CA and P_Intake 1.2bar (abs) for Biodiesel.
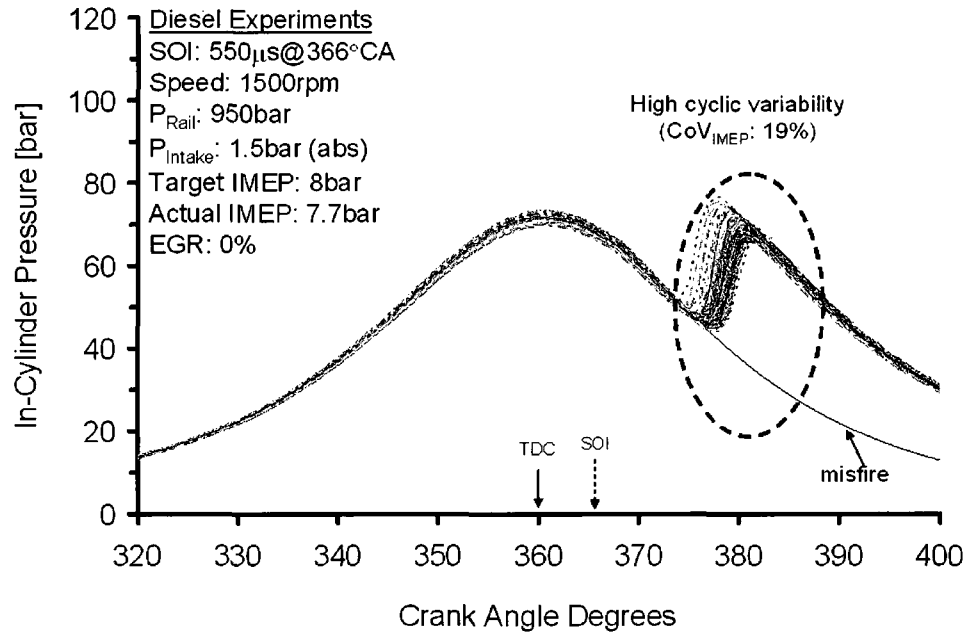
Figure 9-11: In-cylinder pressures at SOI 366°CA and P_Intake 1.2bar (abs) for diesel.

Figures 9-12 and 9-13 show the variation of the engine-out soot emissions with the SOI. Generally, the Biodiesel produced relatively lower soot levels than the diesel fuel in the

range 337<SOI<360°CA for the P_{Intake} 1.2bar (abs) case. Beyond this point, the diesel fuel seemed to enter the LTC slope of the soot formation curve, where simultaneous reduction of NO_x and soot is achieved. However, from Figures 9-8 and 9-9, ultra-low levels of NO_x were not achieved hence the LTC mode was not fully attained for the conditions considered. Nonetheless, increasing the injection and boost pressures in combination with adaptive control schemes (Kumar 2007), among other strategies, may facilitate the Biodiesel LTC mode with retarded SOI at medium to high load conditions.

Figures 9-14 and 9-15 show the variation of the HC_{Frc} at different commanded SOI for 8bar IMEP. During the classical HTC mode, the engine-out THC and CO emissions were unaffected by the SOI sweep with the Biodiesel producing relatively lower levels. As the SOI was retarded beyond the 365°CA position, however, the emissions of THC and CO rapidly increased mainly due to incomplete combustion from the falling temperatures during the expansion stroke.

Noted, to maintain a constant IMEP level, the fuelling rate had to be slightly reduced when the intake pressure was increased. Furthermore, because the energy content of Biodiesel is lower than that of the diesel fuel, a slightly higher ISFC, i.e. a slight penalty in η_{Ind} especially at P_{Intake} of 1.5bar (abs), was observed for the Biodiesel-fuelled engine as shown in Figures 9-16 and 9-17. Nonetheless, owing to the higher CN of the Biodiesel employed, there was no perceptible difference in the efficiency between the two fuels when the SOI was retarded after TDC. The increased fuel consumption after 365°CA is

mainly attributed to increased THC and CO emissions, off-phasing of the combustion

event and fuel condensation leading to oil dilution as discussed in Chapter VII.
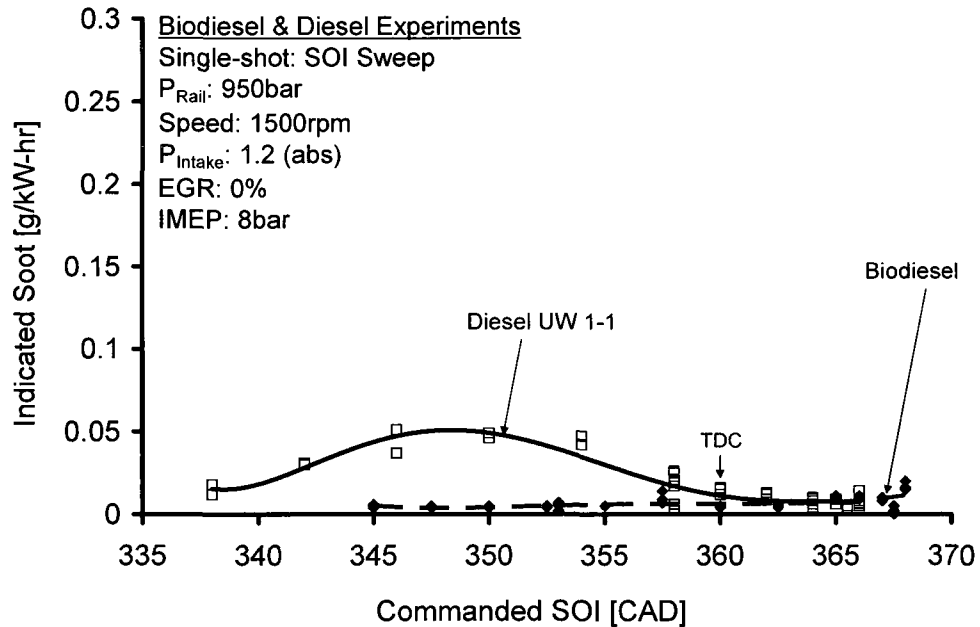
Figure 9-12: Soot vs. SOI for Biodiesel and diesel at 8bar IMEP P_{Intake} 1.2 (abs).
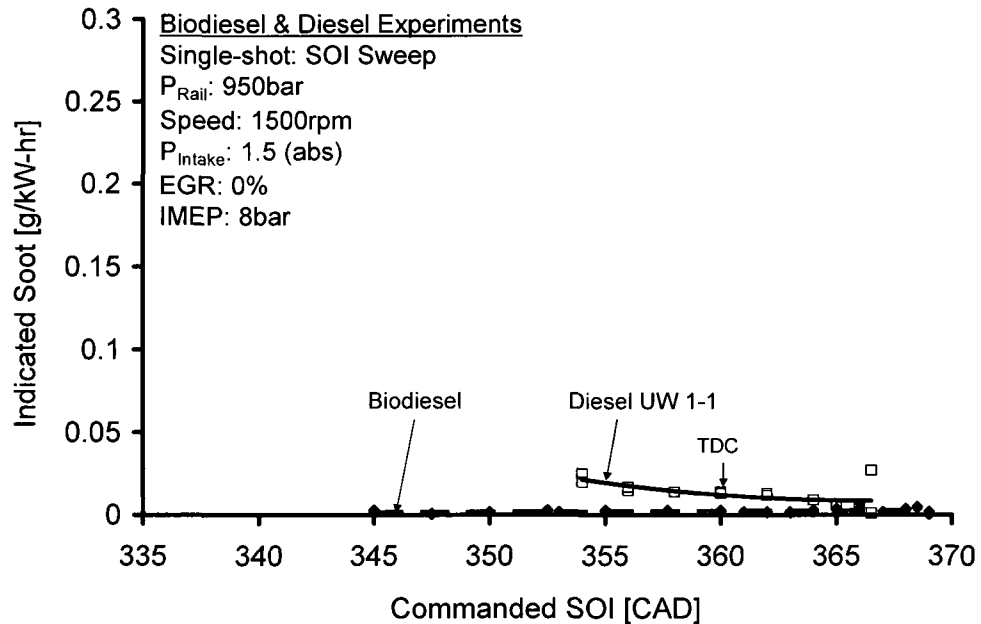
Figure 9-13: Soot vs. SOI for Biodiesel & diesel at 8bar IMEP P_{Intake} 1.5bar (abs).
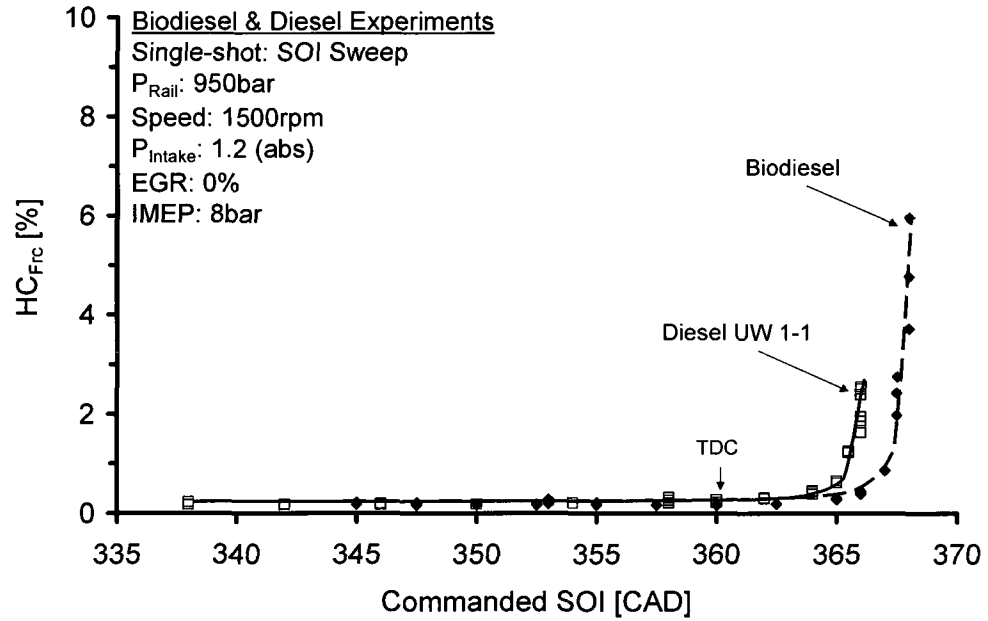
Figure 9-14: HC_{Frc} vs. SOI for Biodiesel & diesel at 8bar IMEP P_{Intake} 1.2bar (abs).
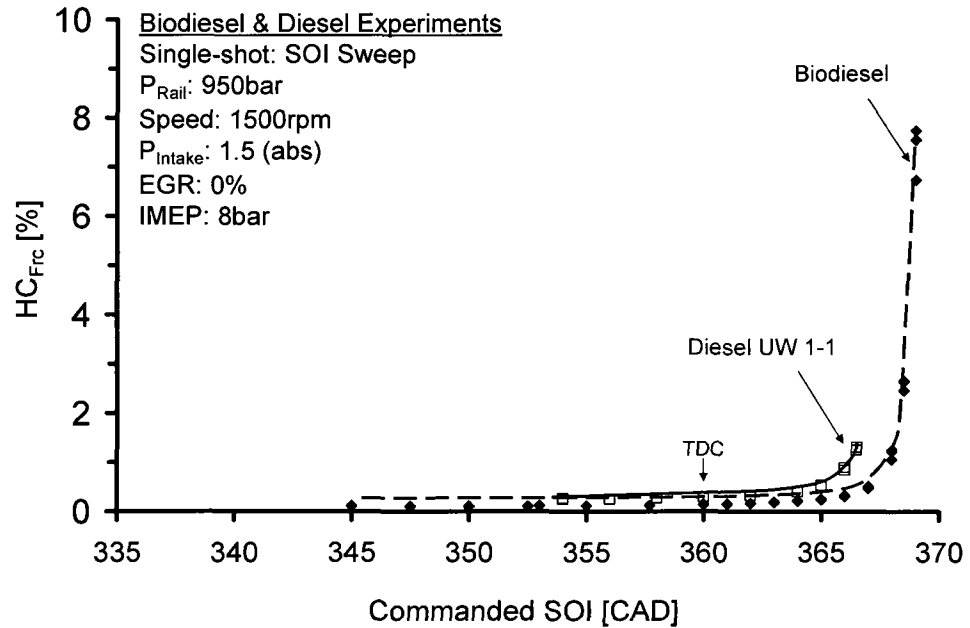
Figure 9-15: HC_{Frc} vs. SOI for Biodiesel and diesel at 8bar IMEP P_{Intake} 1.5bar (abs).
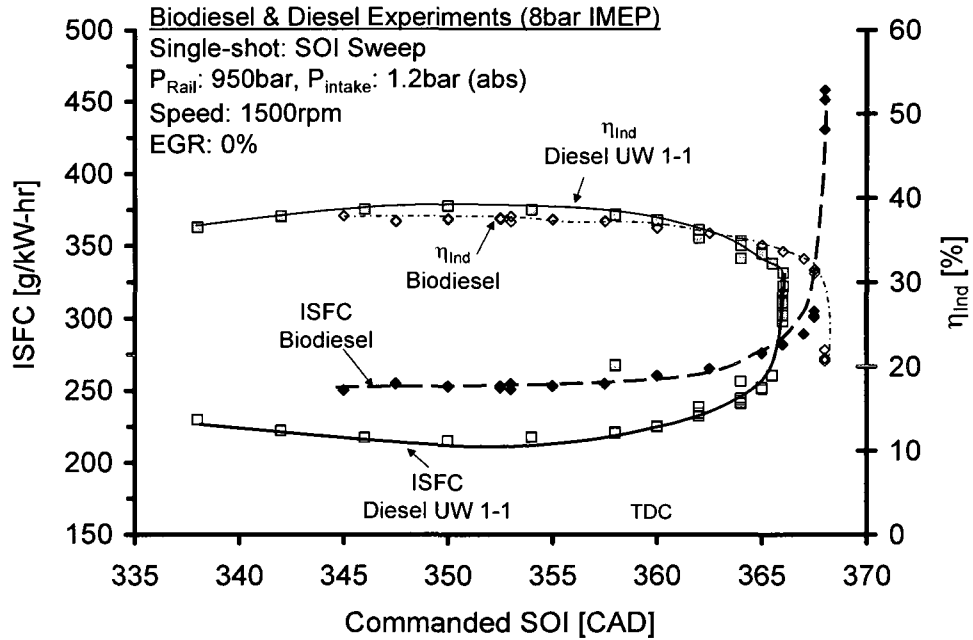
Figure 9-16: ISFC vs. SOI for Biodiesel and diesel at 8bar IMEP P_{Intake} 1.2bar (abs).
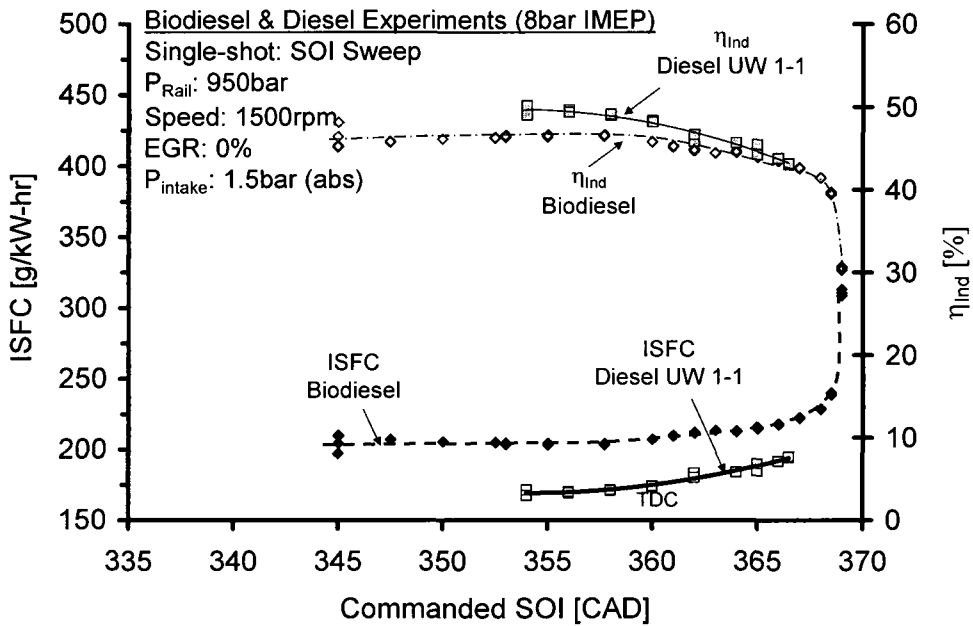
Figure 9-17: ISFC vs. SOI for Biodiesel and diesel at 8bar IMEP P_{Intake} 1.5bar (abs).

9.2 Biodiesel EGR Sweep

As discussed in Chapter VII, among the combustion phasing modulation techniques that include fuel injection scheduling and pressure, EGR, boost and intake temperature control, EGR is found the most effective. Furthermore, the use of EGR has been effective in reducing in-cylinder NO_x formation mainly because the thermal, dilution and chemical effects of EGR lower the flame temperature and oxygen concentration of the working fluid. However, the EGR phasing control requires high ratios of EGR that reduce the available intake oxygen and commonly cause increased CO and UHC emissions. Figures 9-18 to 9-21 show the effect of EGR on the engine-out emissions and engine performance of Biodiesel and diesel fuels at 8bar IMEP and a fixed SOI of 354°CA.

Not surprisingly, the engine-out NO_x level monotonically decreased with increasing EGR. The soot production was almost constant at low EGR ratios but accelerated with further EGR increase, which is consistent with *Slope 1*. As the EGR ratio was increased further, the soot level rapidly departed and fell from the peak soot value for the Biodiesel. At the conditions investigated, as the soot production fell to a smokeless level, simultaneous ultra-low levels of NO_x and soot were achieved for the Biodiesel as seen in Figure 9-19. This mode of combustion is normally considered as the LTC Slope of the soot formation i.e. *Slope 2*. On the contrary, the diesel fuel did not attain the soot descending curve under similar conditions. At 50% EGR the diesel-fuelled engine suffered from unstable combustion leading to misfire in some cases. Noted, at lower IMEP levels the EGR-incurred diesel LTC was achieved and the results were reported by Kumar *et al.* (2007).

193

From Figures 9-20 to 9-23, it was observed that the Biodiesel LTC process was accompanied by increased engine-out emissions of THC and CO, a noticeable drop in the fuel efficiency and a decrease in the maximum rate-of-pressure rise (also noticed when the characteristic diesel 'knocking' sound level was substantially decreased at $(dP/d\theta)_{Max}$ of 2.5bar/°CA).

Note that the Yanmar NFD170 is a stationary engine with mechanical injection configuration. Therefore, at fixed SOI and respective achievable injection pressure for such configuration the engine is optimised for best efficiency with conventional diesel fuels. The in-cylinder emission control strategies such as EGR, boost, injection strategy are not implemented in the manufacturer's original design. Consequently, in such applications tailpipe emissions are normally reduced by the use of after-treatment devices. Conversely, the Ford "Puma" is a common-rail diesel engine for passenger vehicle applications optimised for emissions compliant with Euro III. The manufacturer's combustion optimisation includes the use of pilot and main injections, rail pressures up to 1600bar (with respective injector configuration, piston geometry and swirl for fuel spray/air matching), EGR and variable geometry turbocharger, *inter alia*. The results of Chapters VII to IX would thus not be comparable because of major differences in the injection characteristics, combustion chamber design and the relatively high loads reported in Chapter IX. Nonetheless, the trends in *Slopes 1* and *2* were comparable. Similar to the conclusion in Chapter VIII, tests on the common-rail diesel engine showed that biodiesels with a higher CN than conventional diesel can endure higher EGR rates in the EGR-incurred LTC mode.
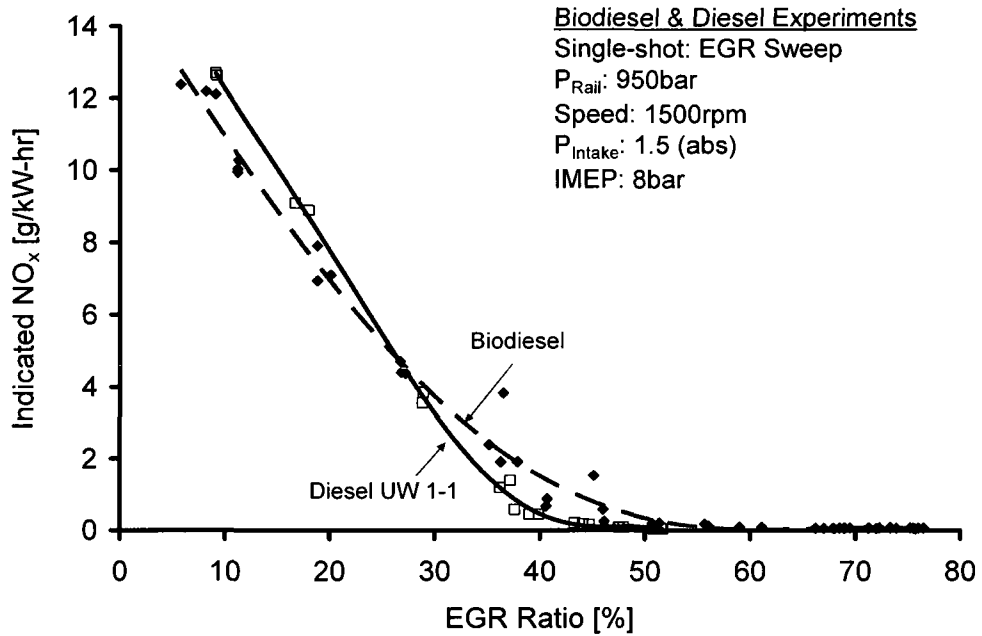
Figure 9-18: Indicated NO_x variation with EGR for Biodiesel and diesel at 8bar IMEP.
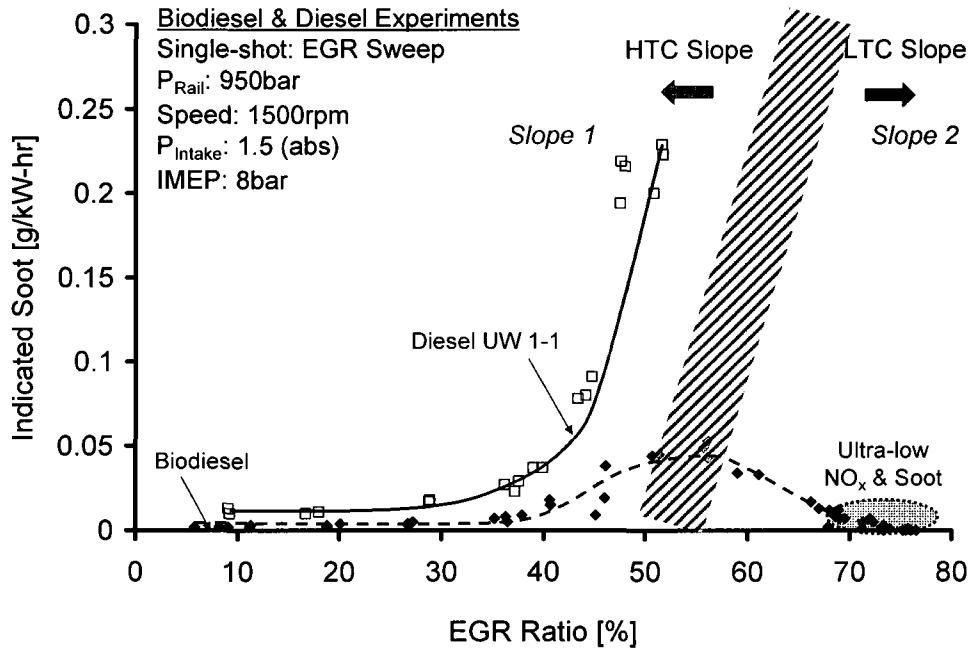
Figure 9-19: Indicated soot variation with EGR for Biodiesel and diesel at 8bar IMEP.
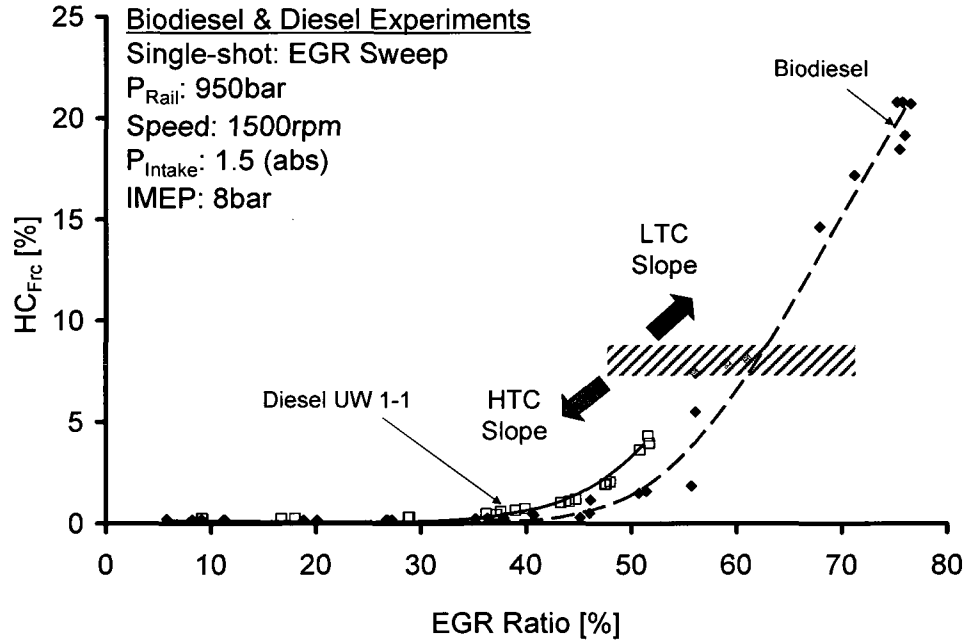
Figure 9-20: HC_{Frc} variation with EGR for Biodiesel and diesel at 8bar IMEP.
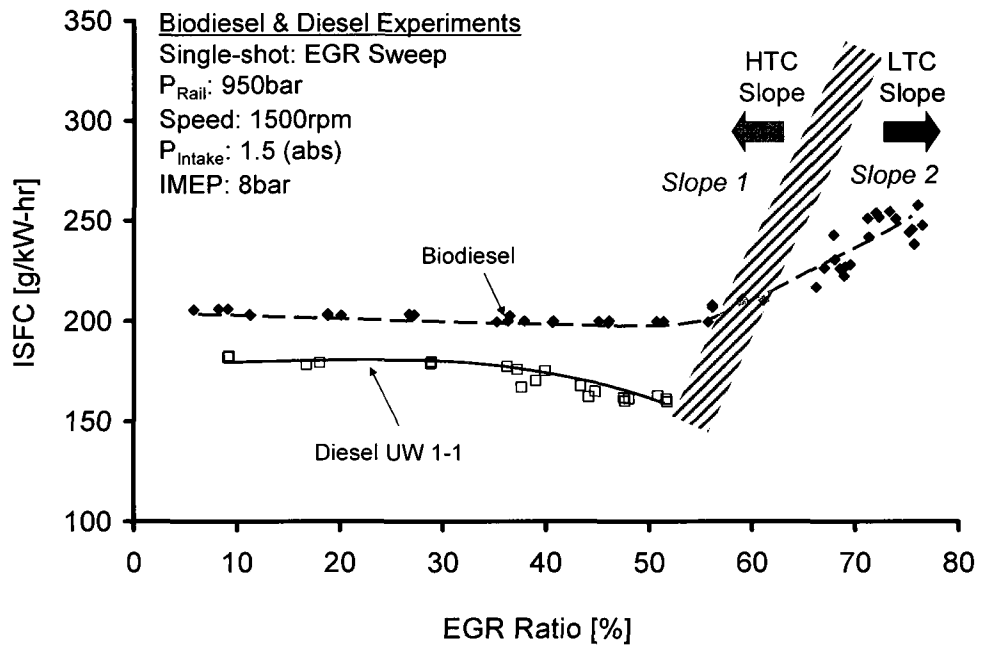
Figure 9-21: ISFC variation with EGR for Biodiesel and diesel at 8bar IMEP.
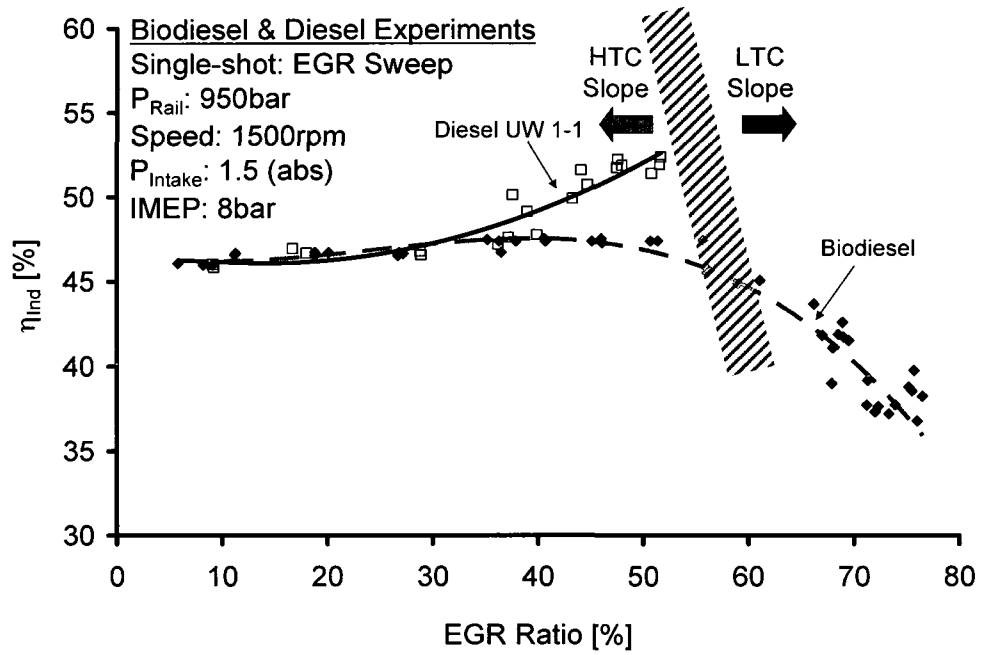
Figure 9-22: η_{Ind} variation with EGR for Biodiesel and diesel at 8bar IMEP.
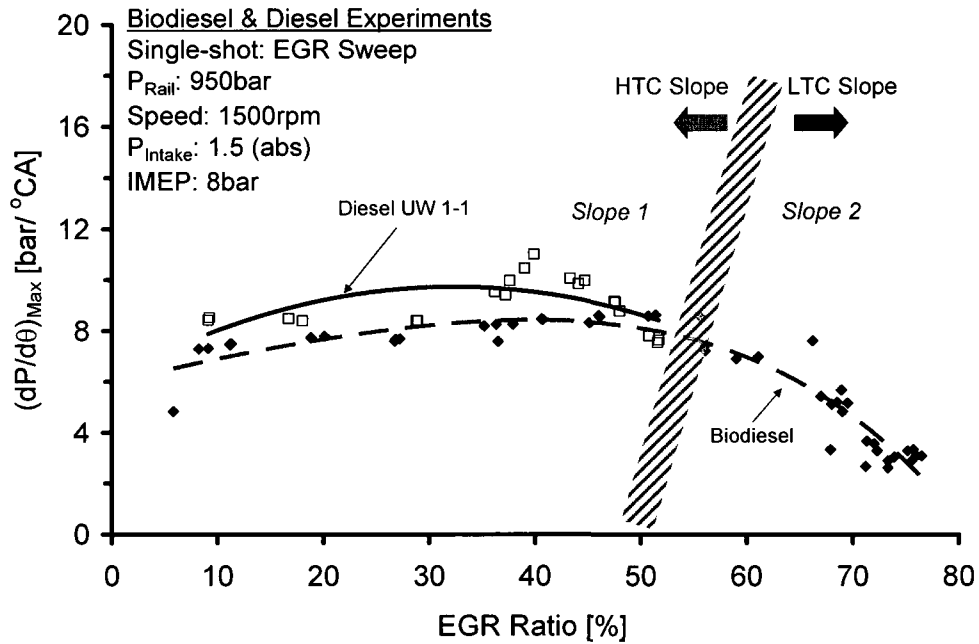
Figure 9-23: $(dP/d\theta)_{Max}$ variation with EGR for Biodiesel and diesel at 8bar IMEP.

197

9.3 Biodiesel Boost Sweep with EGR

As discussed in Chapter VII, the soot formation control mechanism in the EGR-incurred LTC only works under limited load levels and a heavy use of EGR. Figures 9-24 to 9-31 show the effect of EGR at different boost levels and constant IMEP. Intake pressures of 1.2, 1.35 and 1.5bar (abs) were employed at fixed SOI of 354°CA. Similarly, the fuelling rate had to be adjusted to maintain a constant IMEP of 8bar when the boost was changed. Deduced from Figures 9-24 and 9-25, the Biodiesel LTC mode was only attained for the $P_{Intake}>1.2$bar (abs). Note that the analysers had reached their reading limits in THC and CO at EGR>70%. At such conditions, therefore, it is expected that the HC_{Frc} was higher than 20% (Figure 9-26), an unacceptable result if this energy is allowed to go to the tailpipe. The EGR-incurred Biodiesel LTC process was accompanied by increased engine-out emissions of THC and CO, a noticeable drop in the fuel efficiency and a decrease in $(dP/d\theta)_{Max}$ (Figures 6-26 to 6-29).
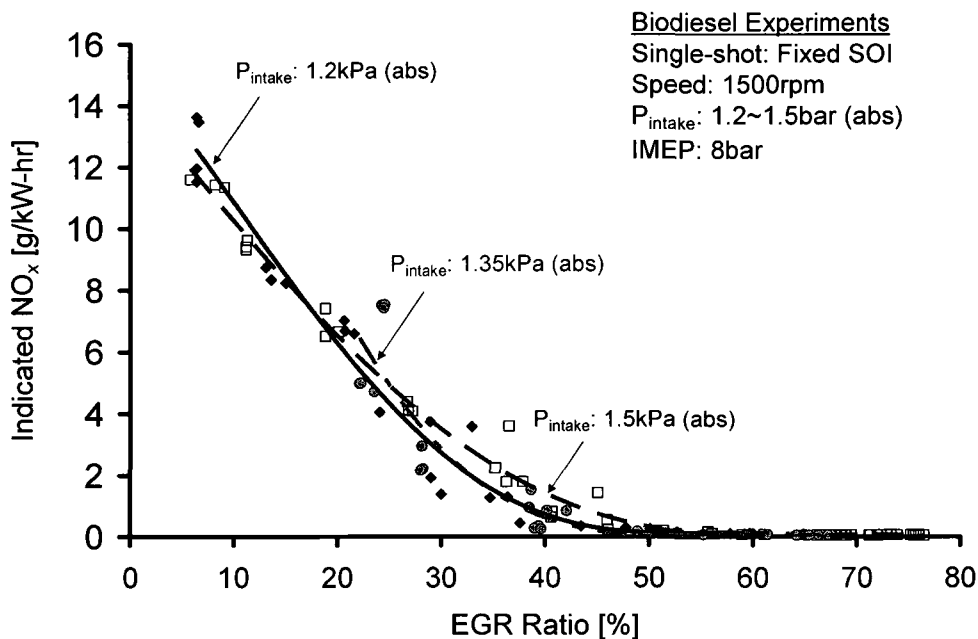
Figure 9-24: Biodiesel indicated NO_x vs. EGR for different boost at 8bar IMEP.
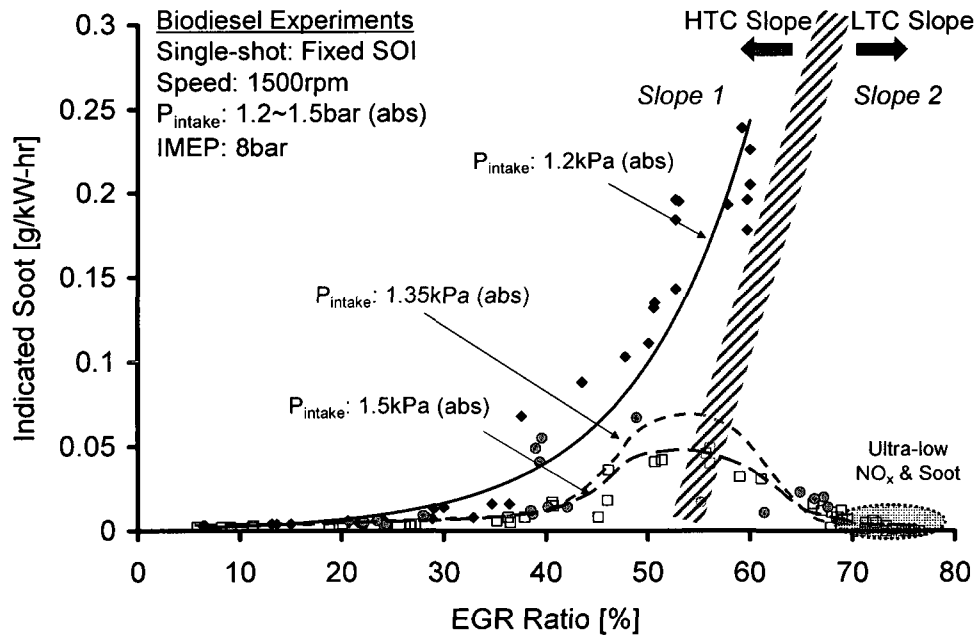
Figure 9-25: Biodiesel indicated soot vs. EGR for different boost at 8bar IMEP.
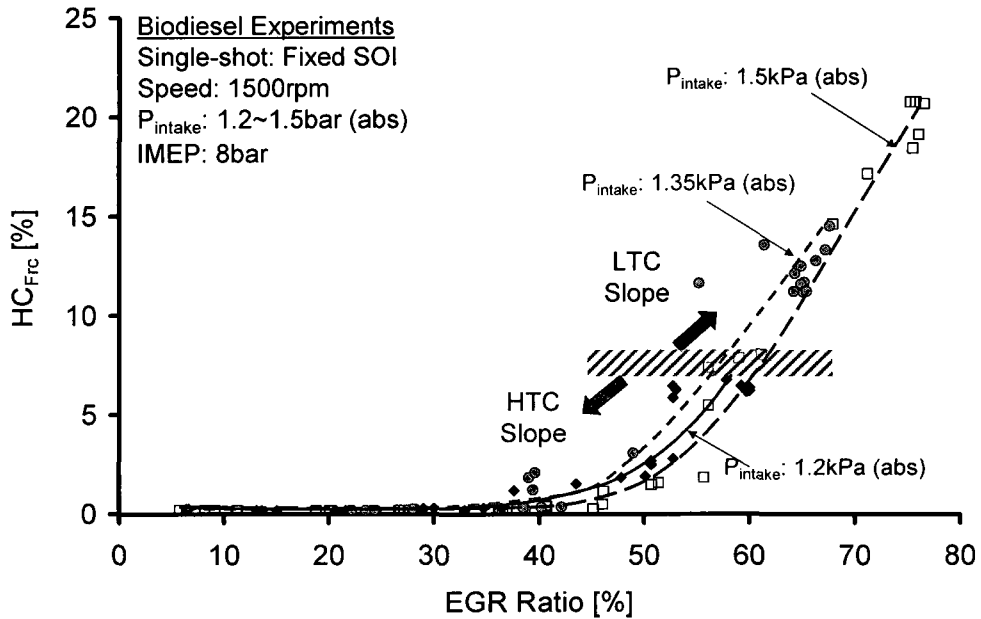
Figure 9-26: Biodiesel HC$_{Frc}$ vs. EGR for different boost at 8bar IMEP.
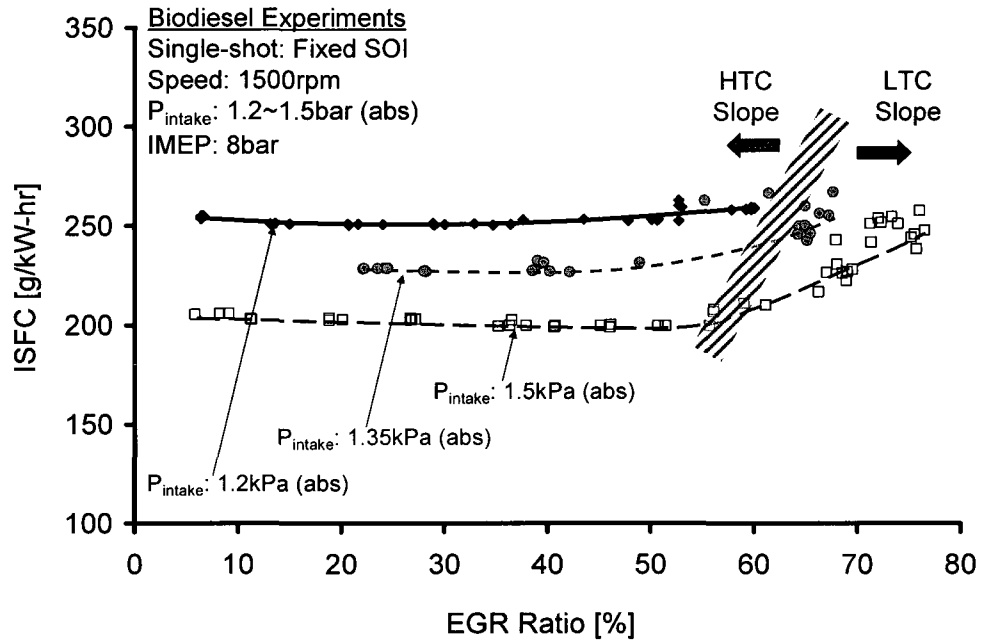
Figure 9-27: Biodiesel ISFC vs. EGR for different boost at 8bar IMEP.
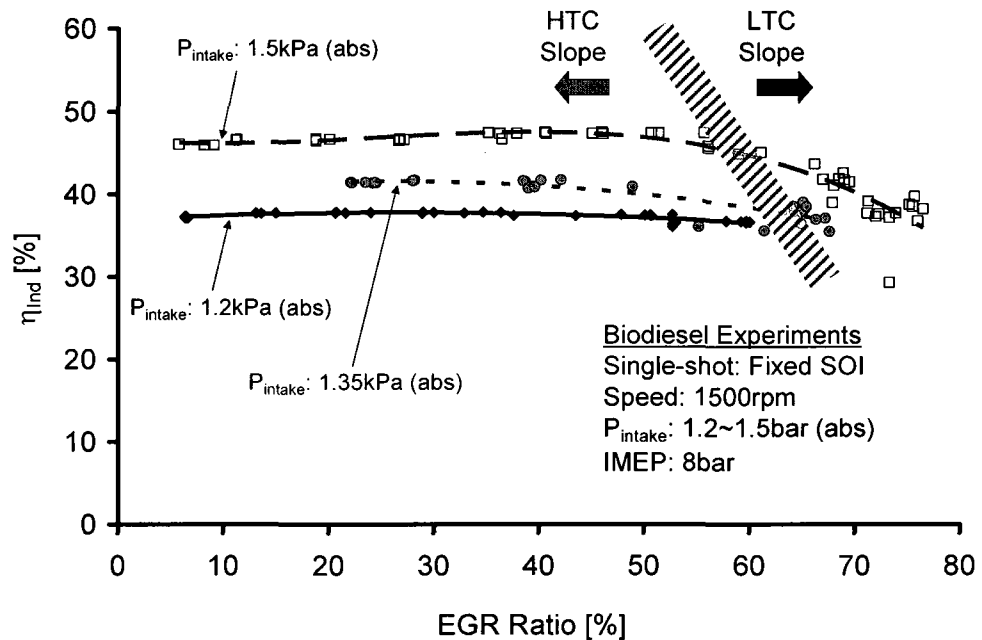
Figure 9-28: Biodiesel η_{Ind} vs. EGR for different boost at 8bar IMEP.
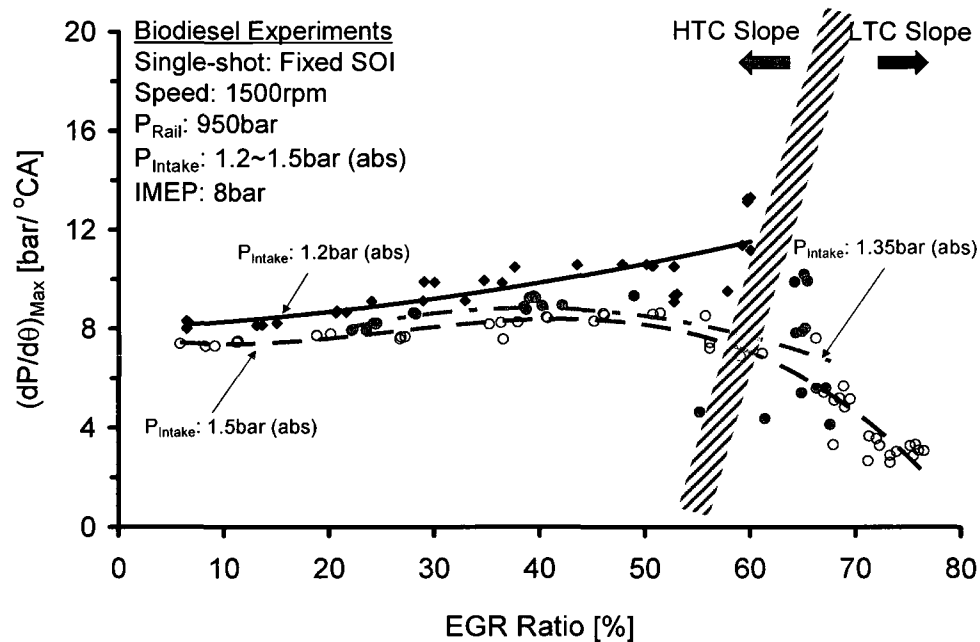
Figure 9-29: Biodiesel $(dP/d\theta)_{Max}$ variation with EGR for different boost at 8bar IMEP.

From Figure 9-30, as the EGR was increased beyond 60%, the peak cylinder pressure was essentially the engine compression pressure until the Biodiesel LTC mode suffered from unacceptably high cyclic variability as seen in Figure 9-31. Though the biodiesel LTC results with $HC_{Frc} > 20\%$ may not be encouraged for practical power generation, they do provide the constituents necessary for the aggressive regeneration of LNTs (Jacobs *et al.* 2005). The aggressive LNT condition could generate more CO for rapid regeneration, reduce the amount of time the engine runs rich and maintain a reasonable noise level. Furthermore, the HTC and LTC slopes present a platform for the model-based control in biodiesel-fuelled common-rail diesel engines.
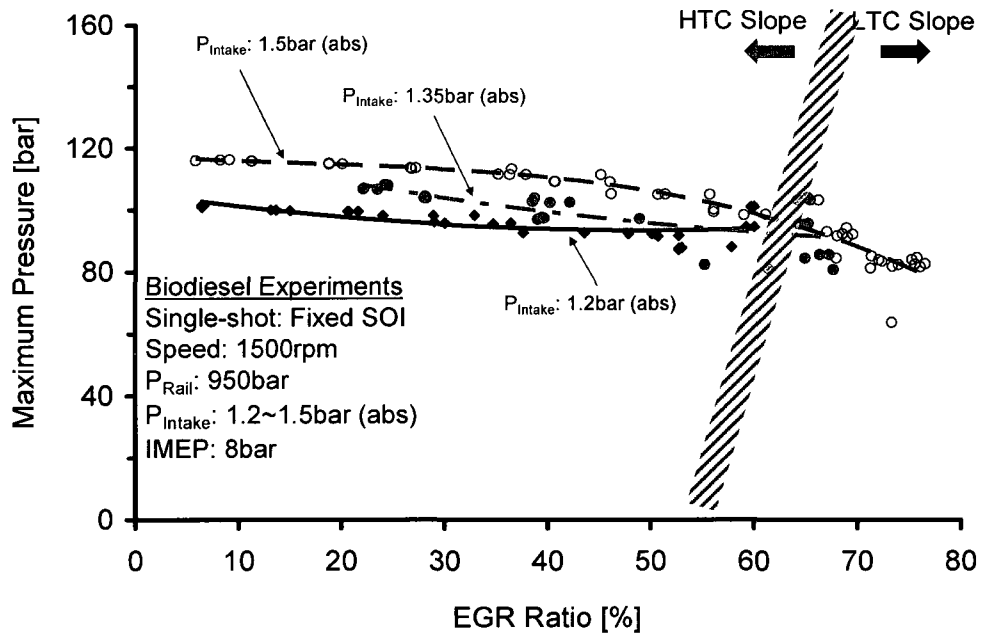
Figure 9-30: Biodiesel P_{Max} variation with EGR for different boost at 8bar IMEP.
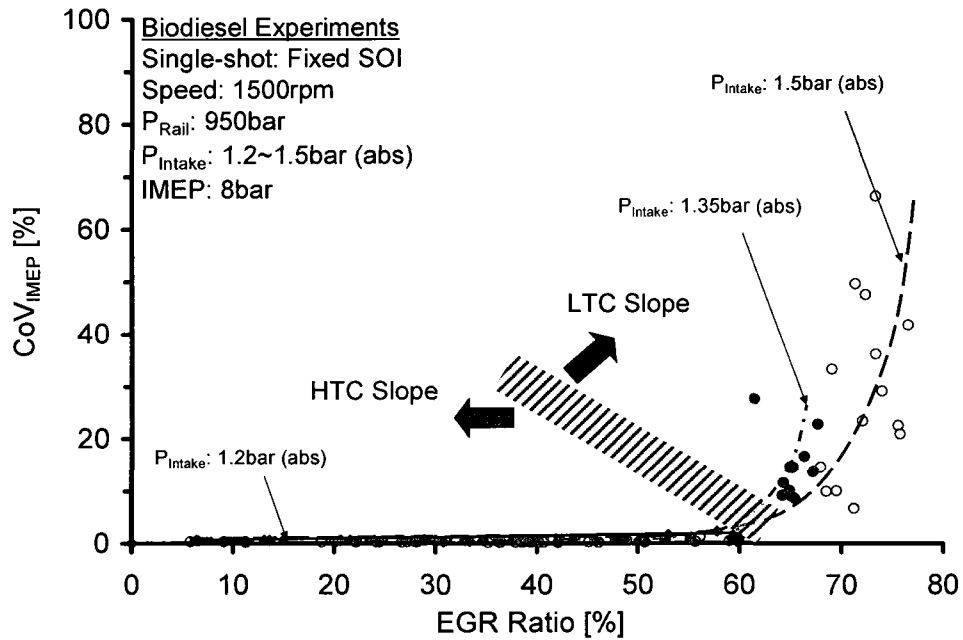
Figure 9-31: Biodiesel CoV_{IMEP} vs. EGR for different boost conditions at 8bar IMEP.

9.4 Biodiesel Multiple Injections

As discussed in Chapter VII, with higher loads, the multi-pulse early injection provides more feasible diesel LTC operations. Therefore, a preliminary investigation of Biodiesel early multiple injections was conducted at P_{Intake} 1.5bar (abs), P_{Rail} 950bar and a medium load of 6bar IMEP. Two- to five-early injections (during the compression stroke) were employed. The results are presented in Figures 9-32 to 9-39. Figure 9-32 is an image captured from a digital oscilloscope showing the online monitored commanded SOI signal, synchronised piston TDC signal from the encoder and the resulting acquired in-cylinder pressure trace from the pressure transducer.
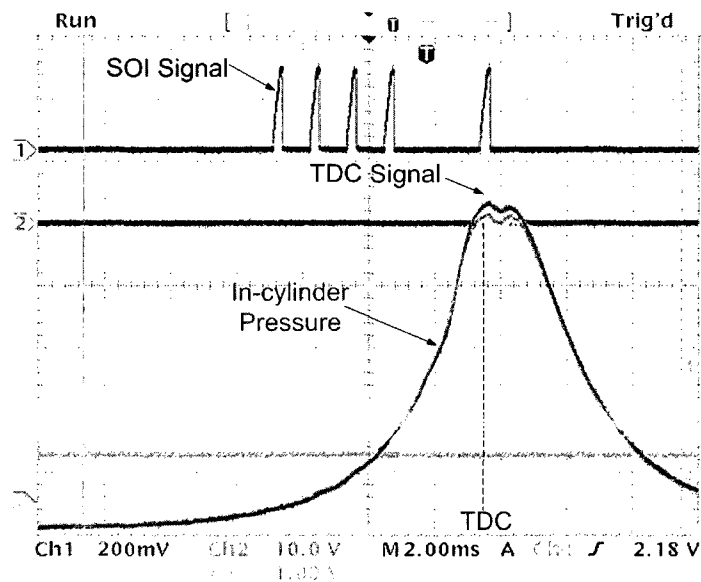
Figure 9-32: Oscilloscope image for Biodiesel early multi-pulse injection tests at 6bar IMEP and P_{Intake} 1.5bar (abs).
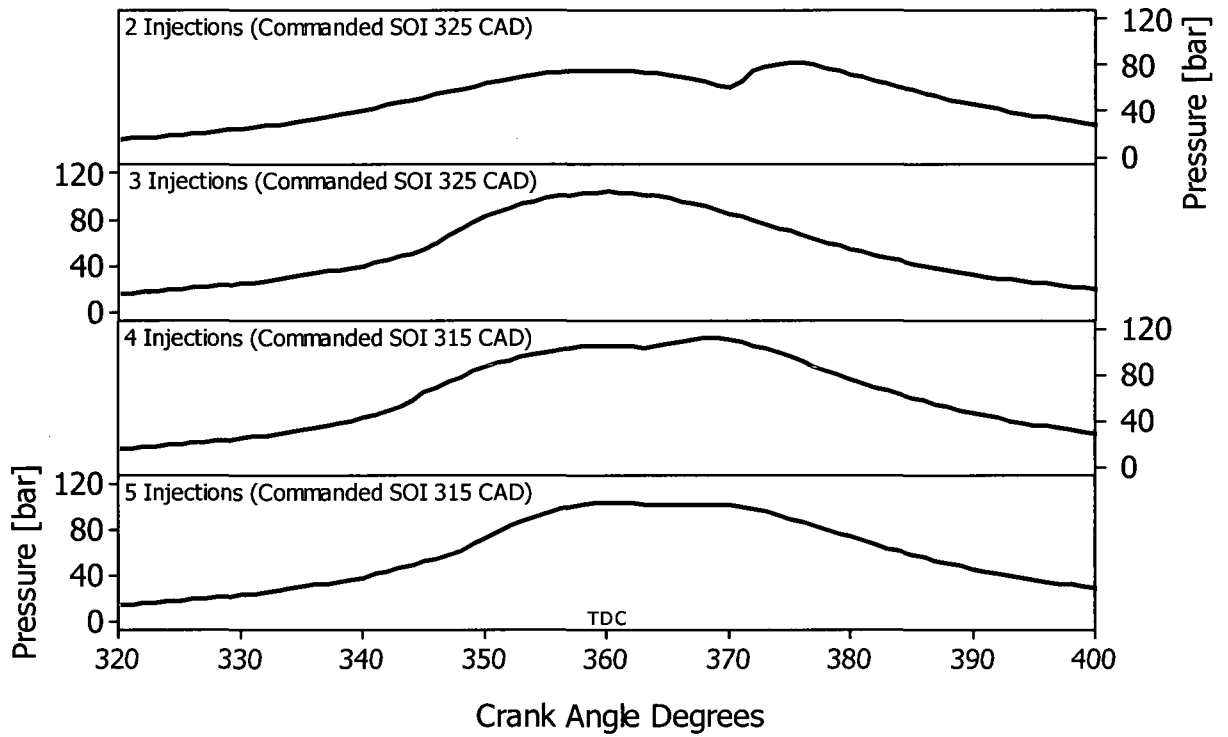
Figure 9-33: In-cylinder pressures for the Biodiesel multi-pulse injections at 6bar IMEP.
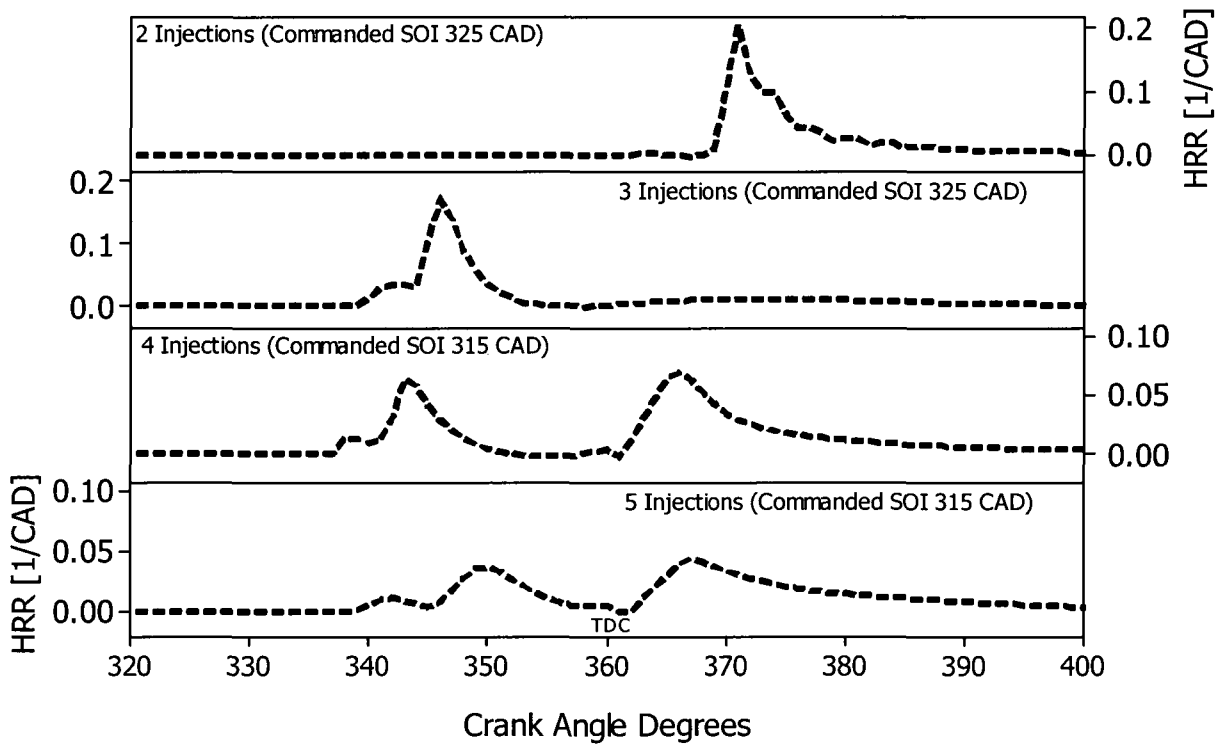
Figure 9-34: Heat-release rates for the Biodiesel multi-pulse injections at 6bar IMEP.

Figures 9-33 and 9-34 present the in-cylinder pressure and heat-release rate profiles for the Biodiesel multiple injections tests. The heat-release rates for the cases with very advanced SOI had double-humps, attributable to poor mixing and 'holding' characteristics of the fuel ('holding' refers to the ability to withhold the mixture from premature auto-ignition which is normally intrinsic in the CN). The low volatility and high viscosity and CN of the Biodiesel presented numerous challenges regarding the homogeneous mixture formation at the investigated conditions. Figures 9-35 to 9-38 demonstrate that the ultra-low NO_x emissions were achieved however the poor mixture preparation resulted in increased soot, CO and THC emissions with increasing EGR for the very advanced SOI cases, a situation consistent with the HTC mode. For the very advanced SOI cases, it appears that the temperatures were not high enough to maintain a fuel vapour phase at such conditions. Nevertheless, reducing the number of injections to two while retarding the SOI to -35°CA ATDC resulted in improved soot, CO, THC and ISFC. It should be emphasised that when the SOI was retarded from 315 to 325°CA, the fuelling rate was adjusted to maintain the same IMEP. The improvement in the engine performance was thus attributed to the enhanced combustion (due to the comparatively improved fuel/air mixing) and reduced fuelling rate shown in Figure 9-39.

Weall and Collings (2007) reported their investigations on highly homogeneous compression ignition in a DI diesel engine fuelled with diesel and biodiesel fuels at low load conditions. Using a B90 fuel blend from rapeseed oil methyl ester compliant with EN14214 and CN similar to the diesel fuel, the engine-out ultra-low levels of NO_x and soot emissions were achieved at a lowered compression ratio of 14.4:1 and P_{Rail} 900bar.

The effect of boost pressure was not demonstrated in their study because at low load and high EGR levels the achievable boost was negligible owing to the reduced available energy delivered to the variable geometry turbo charger (VGT). However, in the engine setup employed in the present dissertation, the EGR rate and boost level, among others, can be independently controlled. Thus, at higher load levels, future tests should include the use of enhanced premixed combustion strategies, such as increased boost (P_{Intake}>2bar abs) and injection (P_{Rail}>1200bar) pressures, at different compression ratios to study the in-cylinder simultaneous reduction of NO_x and soot in biodiesel-fuelled common-rail diesel engines. Because the CN of the diesel and biodiesel fuels is relatively high, the use of increased boost and injection pressures in diesel/biodiesel HCCI or LTC mode has to be combined with EGR to 'hold' the mixture from premature auto-ignition.
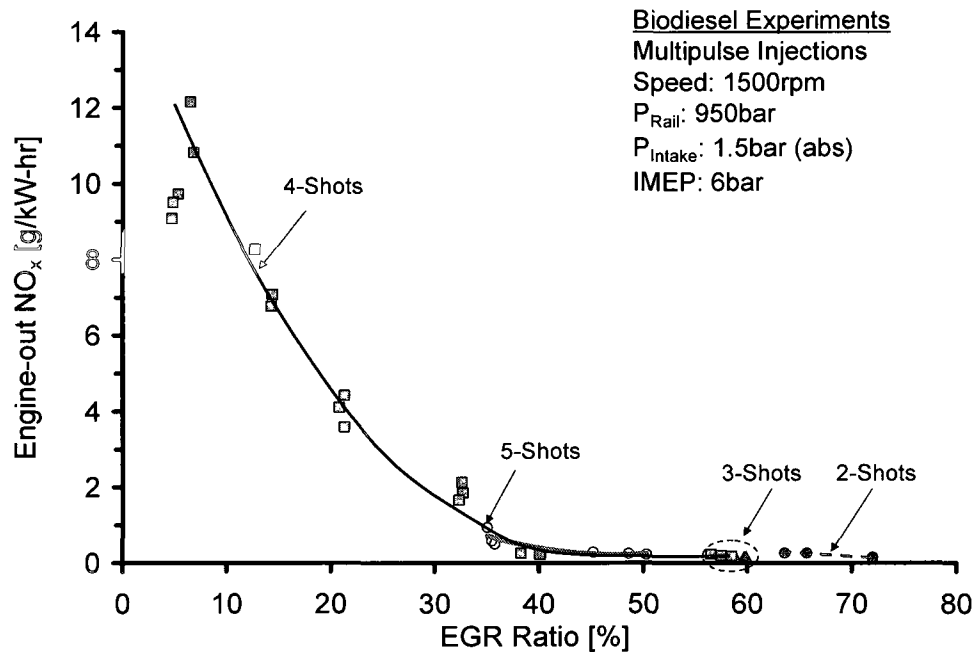
Figure 9-35: Engine-out NO_x for the Biodiesel multi-pulse injections at 6bar IMEP.
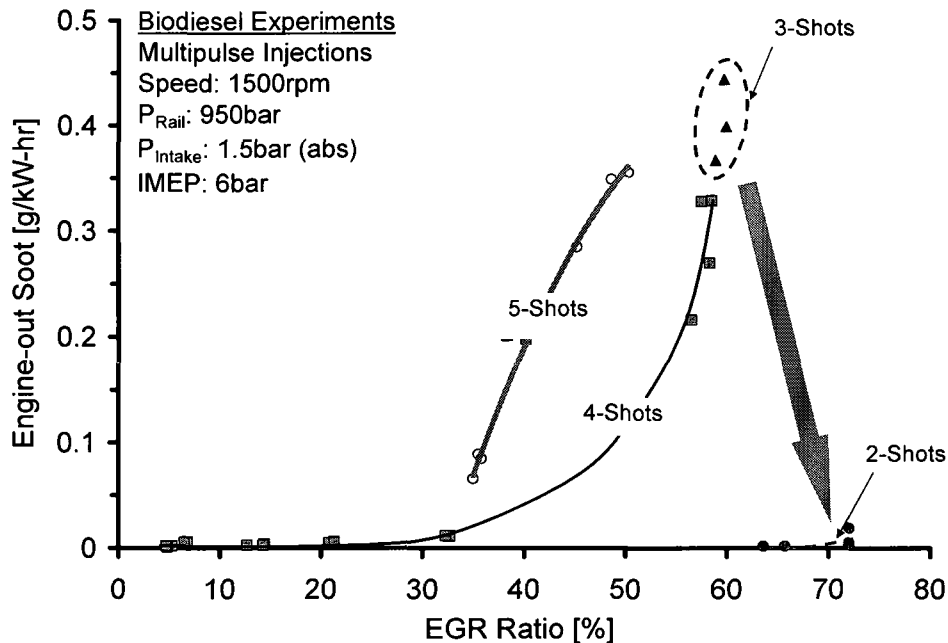
Figure 9-36: Engine-out soot for the Biodiesel multi-pulse injections at 6bar IMEP.
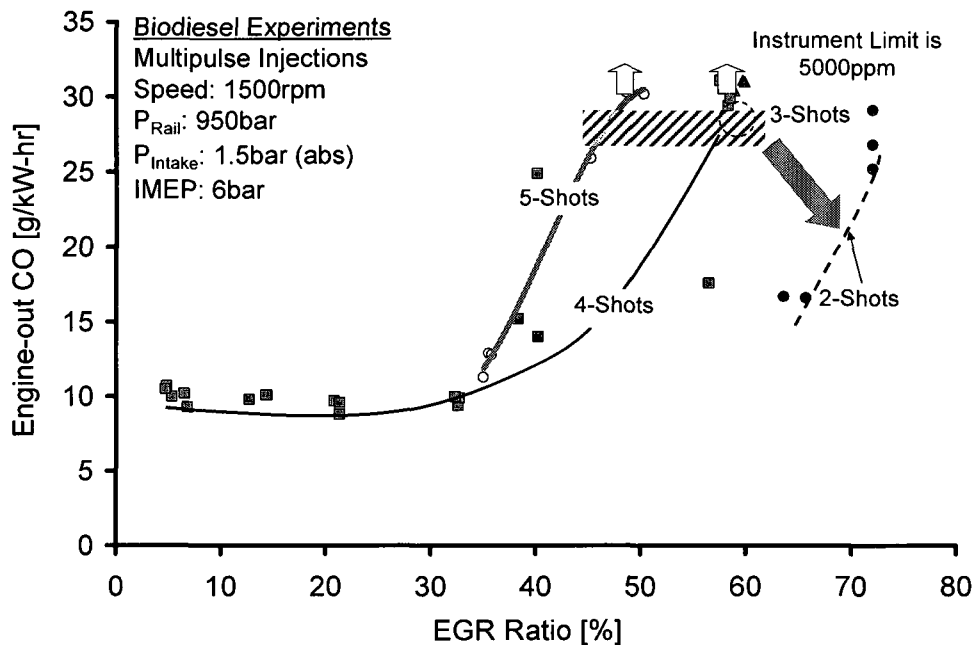
Figure 9-37: Engine-out CO for the Biodiesel multi-pulse injections at 6bar IMEP.

207
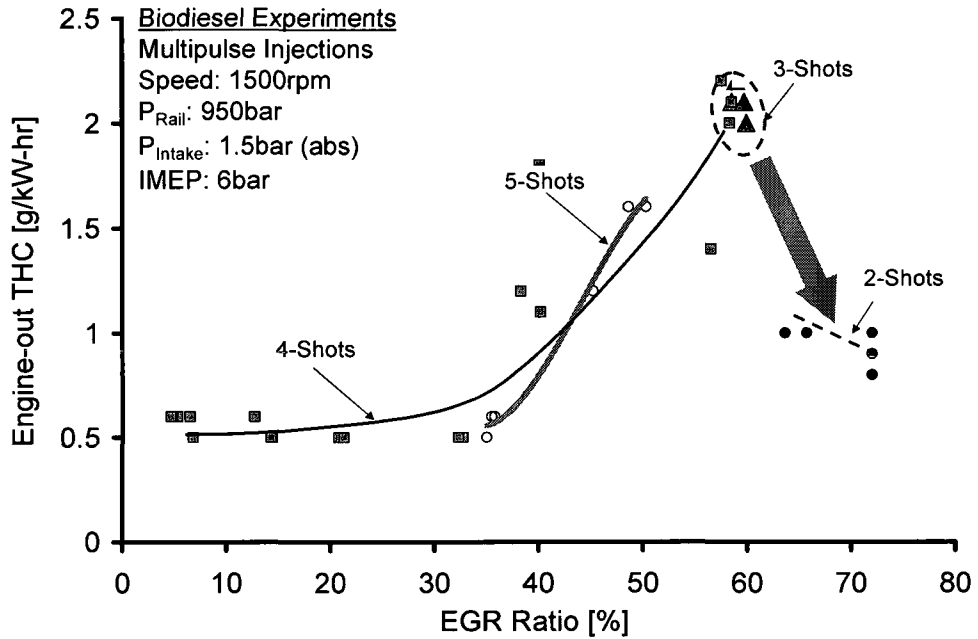
Figure 9-38: Engine-out THC for the Biodiesel multi-pulse injections at 6bar IMEP.
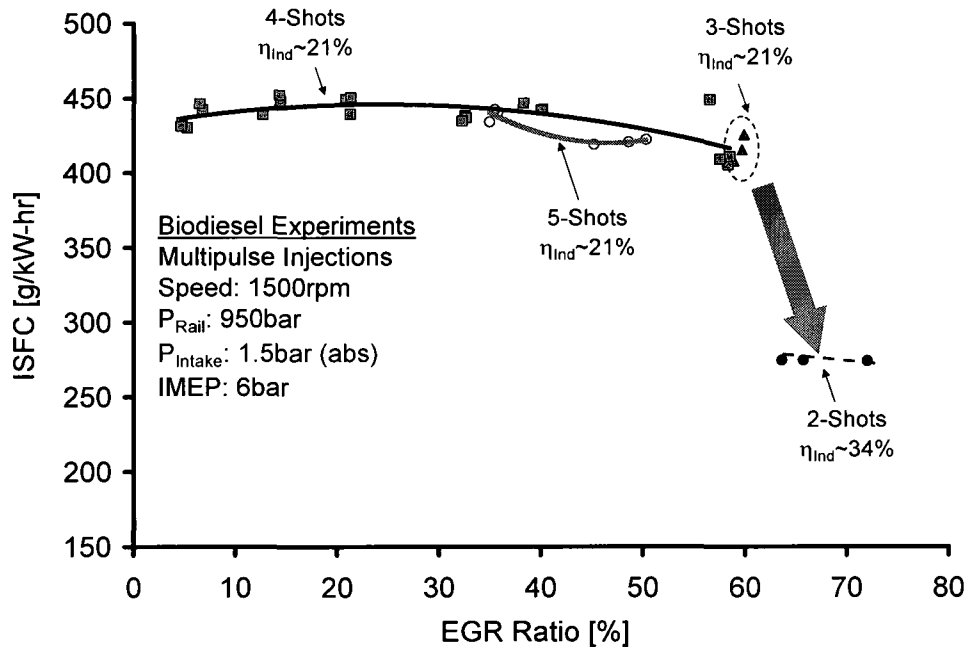
Figure 9-39: ISFC for the Biodiesel multi-pulse injections at 6bar IMEP.

Noted, during transients the actual levels of boost and especially EGR may substantially depart from the commanded values. Consequently, an adaptive fuelling control strategy

as indicated in Figure 9-40 has been developed in the Clean Diesel Engine Research Laboratory to adapt the EGR and boost discrepancies (Kumar *et al.* 2007, Zheng *et al.* 2007e). Using the cylinder pressure characteristics as a feedback signal, the diesel fuelling schedule was modulated promptly during transients by adaptively managing the control discrepancies in boost and EGR.

The extensive empirical tests in this dissertation indicated that the LTC mode could be applied to light-duty diesel- and biodiesel-fuelled engines to produce extremely low engine-out emissions of NO_x and soot. Nonetheless, the LTC modes including the HCCI are less robust than the conventional HTC modes and have a narrower range of operations. The cylinder pressure based adaptive diesel fuel-injection control strategy of Figure 9-40 could also be extended to stabilise the engine operation during the biodiesel LTC modes. As noted by Zheng *et al.* (2007e), the light-duty LTC application needs to be complemented with high-load HTC operations thus necessitating smooth mode switching between LTC and HTC, which could be facilitated with adaptive control schemes.
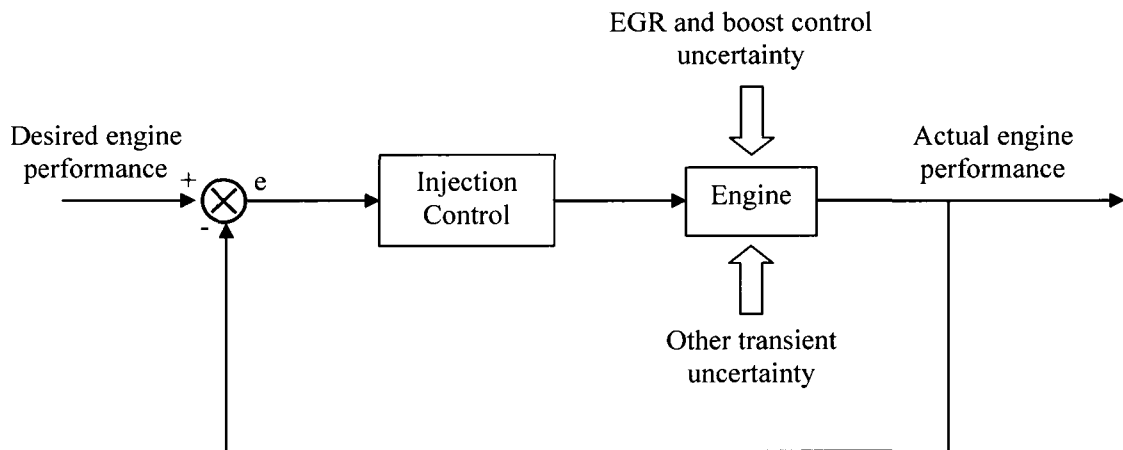
Figure 9-40: LTC adaptive control strategy (Zheng *et al.* 2007e).

CHAPTER X

GENERAL DISCUSSIONS

Conventional diesel engines have relatively precise control on the timing of the apparent fuel energy release process. When the fuel is injected towards the completion of the compression stroke, the ignition delay normally approximates 1ms or shorter in the HTC mode. However, when the ignition delay exceeds a threshold of approximately 1.5ms by EGR and/or multi-pulse early-injection, simultaneous reduction of NO_x and soot is achieved, which signifies the transition into the LTC regime (Zheng *et al.* 2006b). Nonetheless, the consistency of such long ignition delays is affected by fuel properties and a variety of engine operation parameters that include the homogeneity, air/fuel ratio, oxygen and diluent concentrations, boost and engine speed.

In addition to the diesel HCCI type of the LTC, the LTC may occur when the temperatures are too low to initiate formation of thermal NO_x (i.e. <1800K). When this is achieved in combination with EGR, the ignition delay may also be prolonged thereby facilitating more mixing time resulting in decreased soot formation. The diesel LTC may also occur if the temperatures are too low to initiate soot precursors on the rich side of the reaction zone (i.e. <1500K), which may be applicable to the smokeless rich combustion (Akihama *et al.* 2001, Kitamura *et al.* 2003). The combustion phasing, or ignition timing control, is identified as a major challenge for early injection diesel LTC modes. In addition, the increased UHC and CO emissions have been reported by many researchers. However, as shall be demonstrated below, the fraction of the energy lost in exhaust UHC and CO is dependent on the engine load.

210

10.1 Exhaust THC vs. Load

As has been reported, during the LTC mode of operation there is an increase in the emissions of UHC and CO. This may affect the fuel efficiency of LTC cycles. Nonetheless, the fraction of the UHC with respect to the engine input fuel could be evaluated from Equation 10-1, which is similar to Equation 7-1, where χ_i is the concentration of the THC in ppm and MW_i the reduced molecular weight of the THC (C_1H_m). Using equations 2-18 and 10-1, Figure 10-1 was produced to show the variation of HC_{Frc} where the engine load is represented by the IMEP. The fuel fraction of exhaust UHC is highly dependent on the load level. At high loads for instance, 5000ppm of UHC in the exhaust would translate to 5% of fuel energy while the same would be more than 15% at low loads.

$$HC_{Frc} = \left(\frac{\dfrac{\chi_i}{1 \times 10^6} \times \dfrac{MW_i}{MW_{Exh}} \times \dot{m}_{Exh}}{\dot{m}_f} \right) \times 100 \qquad \text{Equation 10-1}$$

Similarly, Figure 10-2 shows the variation of the equivalent HC_{Frc} with the change in η_{Ind} for an engine initially operating at an indicated efficiency of 50%. For the conditions investigated, a $\Delta\eta_{Ind}$ drop of 10% (i.e. η_{Ind} from 50 to 45%) would be equivalent to having 5% of the cylinder fuel going to the exhaust as summarised in Table 10-1. Because diesel and biodiesel HCCI suffers from elevated CO and THC emissions, it is not advantageous to operate in this mode under low load conditions. The single-shot EGR-incurred LTC mode has provided relatively favourable results at low loads (Zheng *et al.* 2006b, 2007d).

211
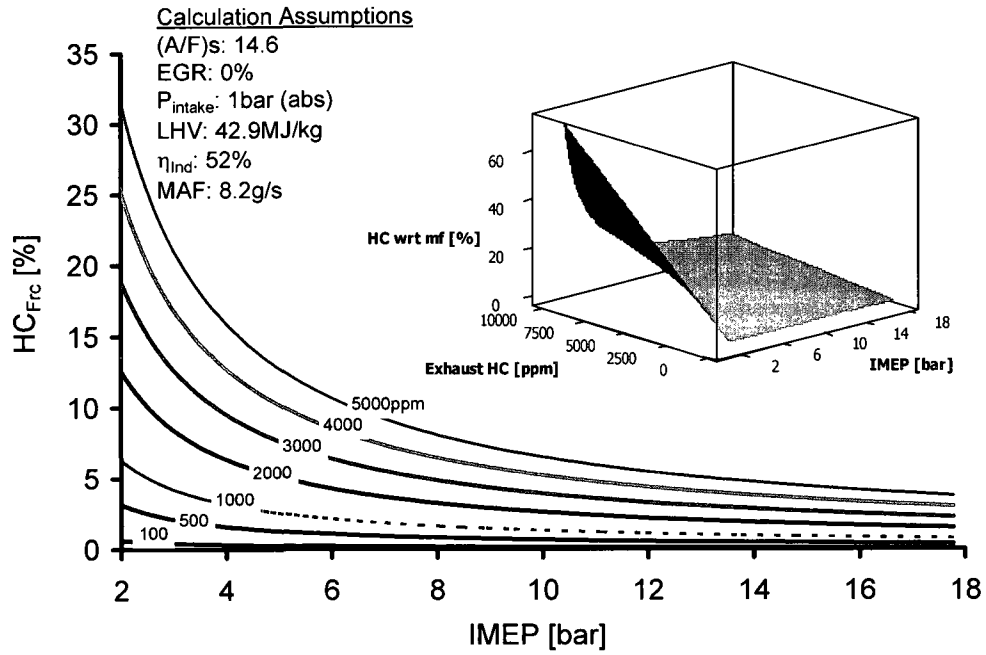
Figure 10-1: HC_{Frc} at different load conditions.
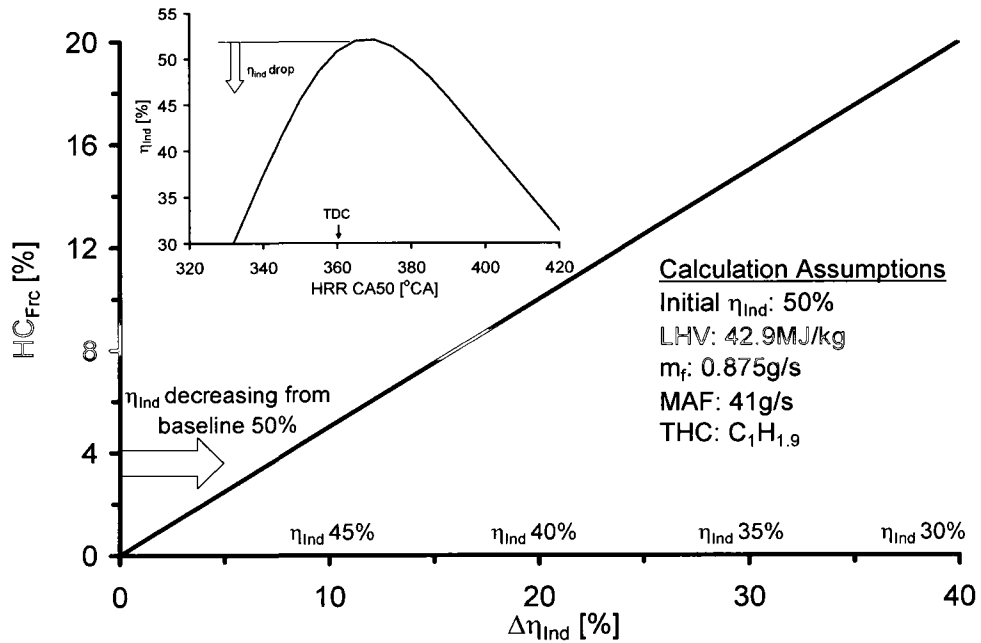
Figure 10-2: HC_{Frc} vs. $\Delta\eta_{Ind}$.

Table 10-2: Correlation between the HC_{Frc} and $\Delta\eta_{Ind}$ from η_{Ind} 50%.

$\Delta\eta_{Ind}$ [%]	η_{Ind} [%]	Equivalent HC_{Frc} [%]
Baseline	50	Baseline
10	45	5
20	40	10
30	35	15
40	30	20

10.2 Fuel Delivery Scheduling for Diesel LTC Cycles

As has been demonstrated in the distillation profiles of Figure 4-7, the volatility of diesel fuels, especially biodiesel fuels, is much lower than gasoline. This explains the implementation challenge to form a cylinder charge of high homogeneity with a diesel fuel. The timing of the combustion event in the LTC mode is critical for engine performance and emissions optimisation. For the implementation of early injection LTC such as HCCI mode, however, the fuel has to be sufficiently homogeneous before the onset of the main combustion event (Gustafson 2007). Below is the diesel/biodiesel fuel boiling characteristics analysis.

10.2 (a) Fuel Boiling Characteristics

The critical temperature is defined as the temperature above which a substance cannot be liquefied by pressure alone (Çengel & Boles 2002). Therefore, beyond the critical point, liquids behave as gases and the vapour pressure is the critical pressure. Equation 10-2 was employed by Zhu and Reitz (2001) for evaluating the critical properties and normal boiling temperatures of neat straight-chain hydrocarbons (normal alkanes) C_2 to C_{20}, i.e. Ethane to n-Eicosane, where χ could be the critical pressure, temperature or normal boiling temperature, χ_0, χ_1 and χ_2 are the respective empirical constants shown in

213

Table 10-3 and Mw is the respective molecular weight. Figure 10-3 shows the calculated

properties from Equation 10-2 (solid line) and the results from the National Institute of

Standards and Technology, NIST (red circles), which were in good agreement.

$$\chi = \chi_0 + \chi_1 Mw + \chi_2 Mw^2$$
<div align="right">Equation 10-2</div>

Table 10-3: Empirical constants for the determination of critical properties of normal-alkanes (Zhu & Reitz 2001).

Parameter	χ_0	χ_1	χ_2
Critical Pressure [bar]	5.559×10^1	-3.3177×10^{-1}	1.1166×10^2
Critical Temperature [bar]	2.2636×10^2	3.67431×10^0	2.9582×10^0
Normal Boiling Temperature [K]	1.1166×10^2	-6.3057×10^{-3}	-4.2393×10^{-3}
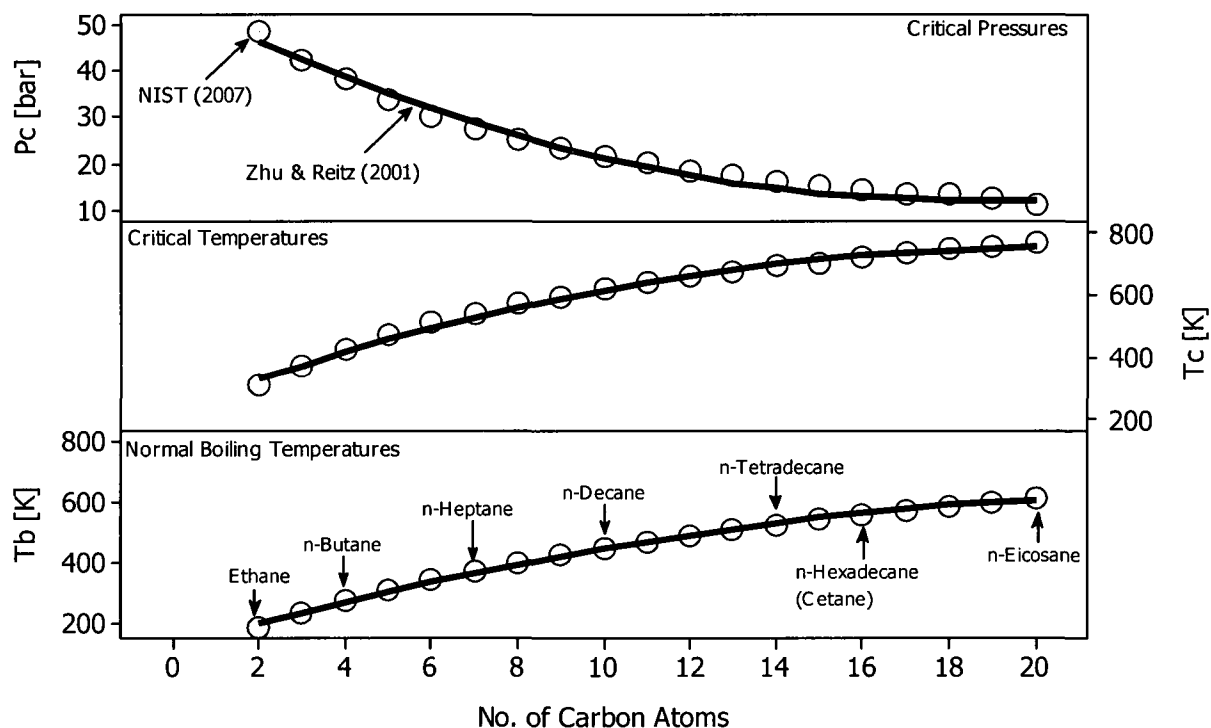
Figure 10-3: Critical properties of n-alkanes (Zhu & Reitz 2001, NIST 2007).

Because gasoline and diesel fuels are complex mixtures of hydrocarbons, their boiling

temperatures are not necessarily fixed as presented in Figure 10-3. Instead, they have a

wide range which is dependant on the constituents of the fuel. Gasoline fuel mainly contains C_5 to C_{12} hydrocarbons and the normal boiling temperature ranges from 25~180°C while diesel fuel mainly contains C_{10} to C_{22} hydrocarbons and normal boiling temperature ranging from 160~380°C (Chevron 2006). The diesel fuel UW1-1 employed in this research contained a mixture of paraffinic, naphthenic and aromatic hydrocarbons with carbon numbers in the range from C_{10} to C_{18} and boiling range, determined from the ASTM D86 procedure, from 175 to 350°C.

Zhu and Reitz (2001) also presented the critical mixing temperatures vs. critical mixing pressures for phase equilibria of both diesel and gasoline nitrogen systems from 20 to 500bar as shown in Figure 10-4. In comparison with diesel fuels, the critical mixing pressures of gasoline-nitrogen systems are considerably smaller. This is expected because of the high volatility of gasoline fuels. Considering the modern diesel engines, it is therefore possible for the diesel/biodiesel fuel to experience a critical mixing vaporisation process. Noted, compression pressures and temperatures in SI engines are in the range 20~30bar and 400 to 500K, while the same for diesel engines are 35~130bar and 650 to 900K, respectively (Zhu & Reitz 2001, Yan & Aggarwal 2006).

Figure 10-4 has been extended to show an approximation of the biodiesel fuel trends. Because biodiesel fuels have very low vapour pressures at room conditions (following ASTM D5191 test standard) thus high normal boiling temperatures (320~460°C), it is expected that the critical mixing temperature of biodiesel fuels would be higher than that of the diesel fuel.
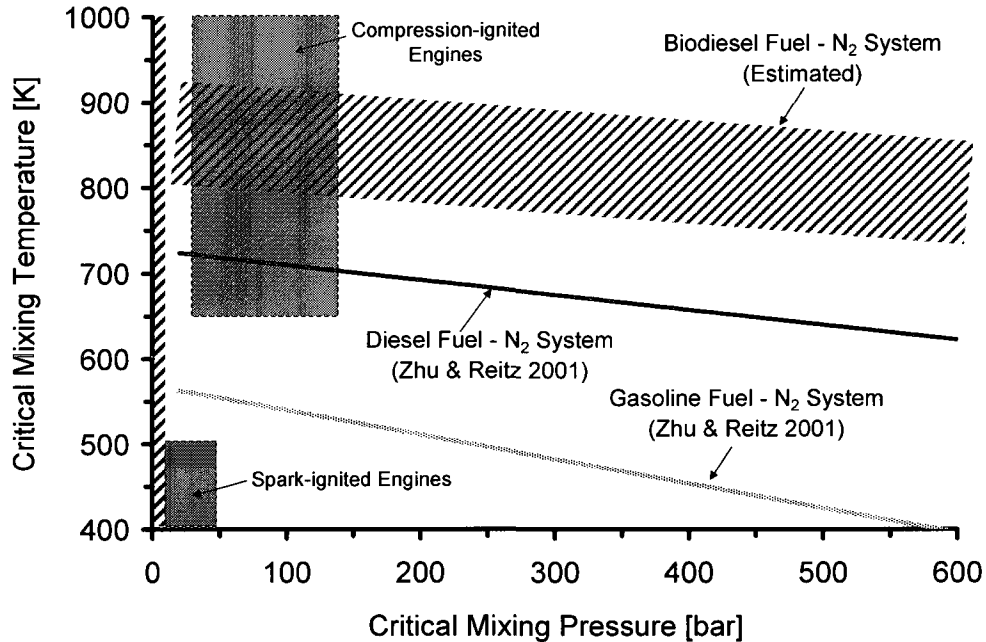
Figure 10-4: Variation of T_{cmix} with P_{cmix} for fuel-N_2 system.

From the above information, Figure 10-5 was generated to show the end of fuel condensation time (EFCT) for different fuels on a naturally aspirated diesel engine under motoring conditions. To minimise the fuel condensation in the cylinder during diesel/biodiesel LTC operation, the SOI should be after the EFCT for the compression stroke and before for the expansion stroke. Otherwise stated, the SOI should be after the critical mixing temperature of the fuel has been attained during the compression stroke. During the expansion, on the other hand, it should be before the temperature drops below the critical mixing temperature. Note, however, that the EFCT on the compression and expansion strokes is not axiomatically on the same mean temperature line. Unlike the compression stroke where temperatures would be increasing until TDC, the expansion stroke involves decreasing temperatures as the piston slides away from TDC. Consideration should thus be given for this fact. The EFCT may be extended during the expansion stroke if there was ignition before that location. In this case, the EFCT would

216

be determined by the energy released, fuel properties such as CN and expansion ratio of the engine.
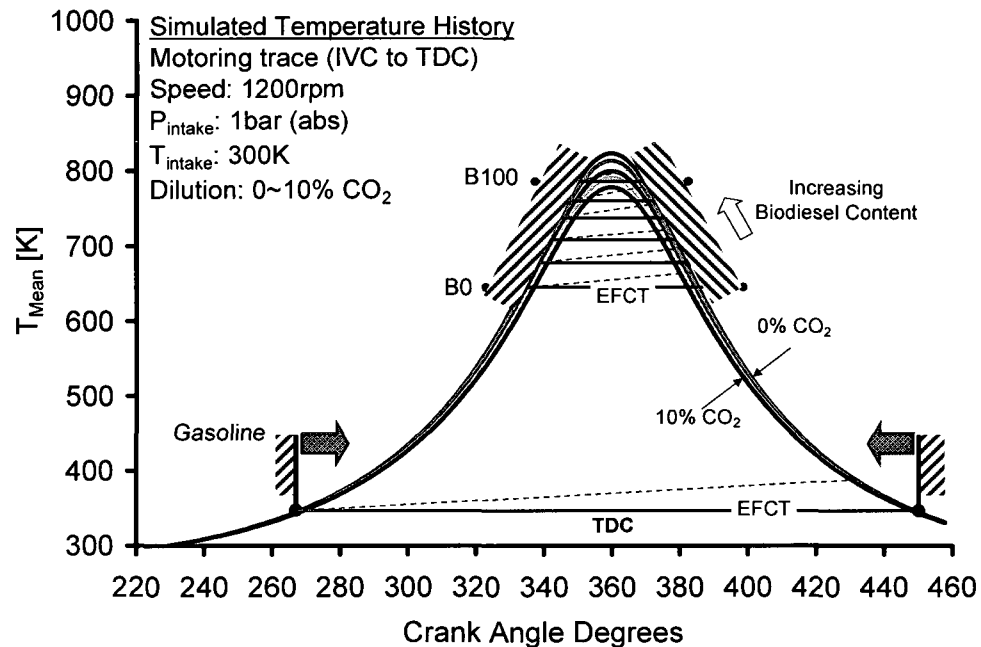
Figure 10-5: Motoring trace showing suggested EFCT for diesel/biodiesel LTC tests.

The cylinder wall temperatures do not normally exceed 150°C. Therefore, when fuels like methane, DME or gasoline are used in HCCI combustion mode, the fuel condensation effect on the cylinder wall is insignificant. When diesel or biodiesel fuels are employed, on the contrary, the cylinder wall condensation is a major concern because diesel and biodiesel fuels have comparatively low volatility. The condensation of the fuel can be a huge drawback on the engine efficiency. Compared with the conventional diesel HTC cycles the fuel efficiency of the diesel HCCI cycles enabled with intake port-injection is considerably lower, as shown in Figure 10-6 generated from the Yanmar NFD170 engine.
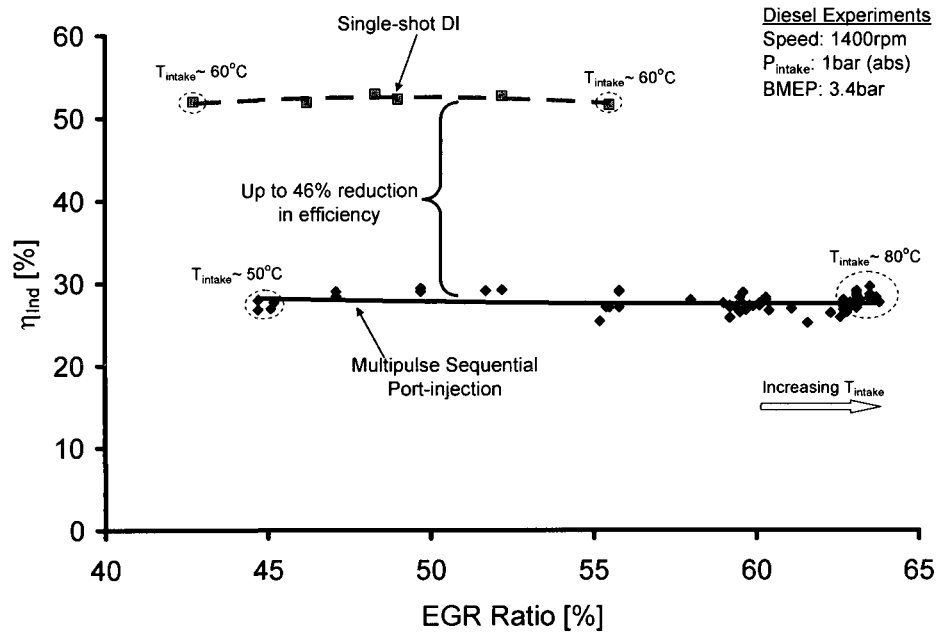
Figure 10-6: η_{Ind} for single-shot DI and sequential port injection tests.

In the intake port or early in-cylinder injection LTC mode, the use of diesel and biodiesel fuels presents a risk of the un-burnt fuel finding its way to the oil sump. Furthermore, in modern diesel engines equipped with DPFs, normally post injection is employed to facilitate DPF regeneration. If this is done inside the cylinder, the use of neat biodiesel fuels may result in substantial oil dilution and deterioration in the thermal efficiency. Figure 10-7 shows the engine oil dilution rates for diesel and biodiesel port injection tests which were previously reported (Zheng 2006c). Before the start of the port injection tests, the oil was drained from the engine and a known volume of fresh oil added. At the end of the tests, the oil was drained and measured under cold conditions. The oil dilution was simply determined by measuring the difference between the removed and freshly-added engine oil for a particular engine running time as shown in Equation 10-3. The composition of the removed oil was therefore not determined in this study.

218

$$\text{Oil Dilution Rate} = \frac{\text{Oil}_{\text{Out}} - \text{Oil}_{\text{in}}}{\text{Test Time}} \qquad\qquad \text{Equation 10-3}$$
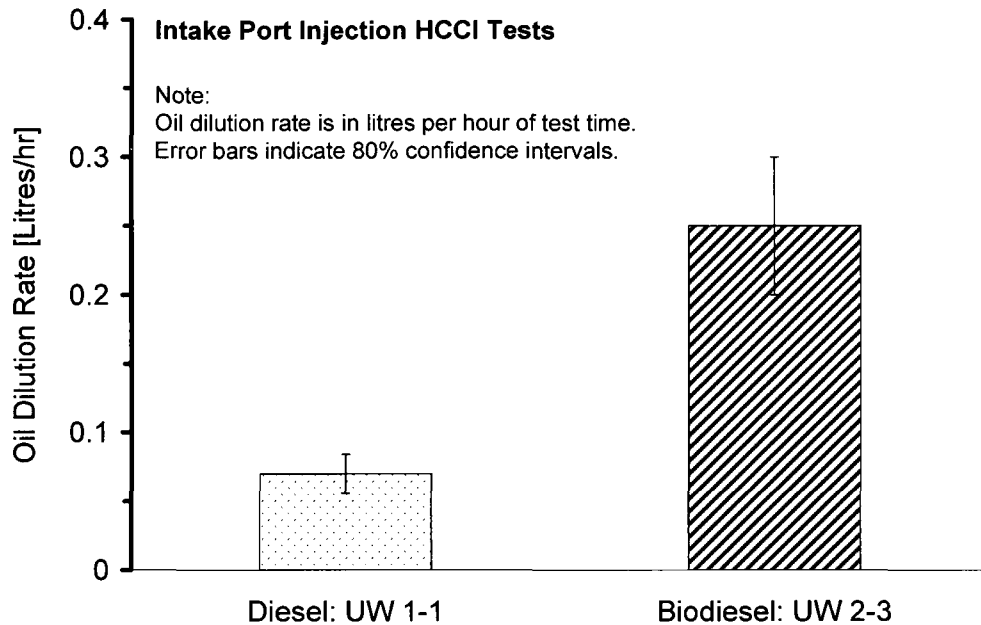
Figure 10-7: Engine oil dilution rates for diesel and biodiesel port injection tests.

10.2 (b) Fuel Spray Penetration

The fuel spray penetration length has an important influence on air utilisation, air/fuel mixture preparation and impingement (piston or cylinder) in the combustion chamber. Hiroyasu and Arai (1990) presented the correlation shown in Equation 10-4 for evaluating the spray penetration length where P_{inj} is the injection pressure and P_{amb} and ρ_{amb} are the ambient pressure and density during the injection, respectively, D is the nozzle diameter and t the time after SOI. Note that for in-cylinder injection, P_{amb} and ρ_{amb} would be the mean cylinder pressure and density during the injection duration, respectively. Hiroyasu and Arai's investigation was conducted on a mechanical pump injection system for the range $70 < P_{inj} < 150\text{bar}$ and P_{amb} of 30bar at 500rpm.

$$S = 2.95 \times \left(\frac{P_{inj} - P_{amb}}{\rho_{amb}} \right)^{0.25} \times \sqrt{D \times t}$$
                                                                    Equation 10-4

Neglecting the blow-by, the mass inside the cylinder may be considered as constant during compression and expansion strokes. As a result, during the compression stroke the ambient density will increase while it would decrease during the expansion stroke to satisfy the laws of physics as shown in Figure 10-8. For the conditions investigated, the density at TDC was 14 times the density at IVC. This would in turn affect the spray penetration length. *Ceteris paribus*, the in-cylinder decrease in penetration length with respect to the IVC condition is shown in Figure 10-9. The penetration length at TDC may be up to 50% lower than that at IVC, which presents a potential challenge regarding fuel impingement on the cylinder wall or piston during high-pressure in-cylinder early injection of diesel LTC mode. The spray-wall interaction would generate a fuel film on the lining leading to increased CO, UHC and soot emissions. Furthermore, the fuel film may wash away the lubricating oil thus increasing the engine wear.

Figure 10-10 shows the effect of injection pressure on spray penetration length where a reference injection pressure of 200bar was used which is similar to the NOP of the Yamnar NFD170 single-cylinder DI diesel engine. It is demonstrated that increasing the injection pressure increases the penetration length. With respect to a P_{inj} of 200bar, increasing the injection pressure to 1200bar for instance may result in a 60% increased penetration length.
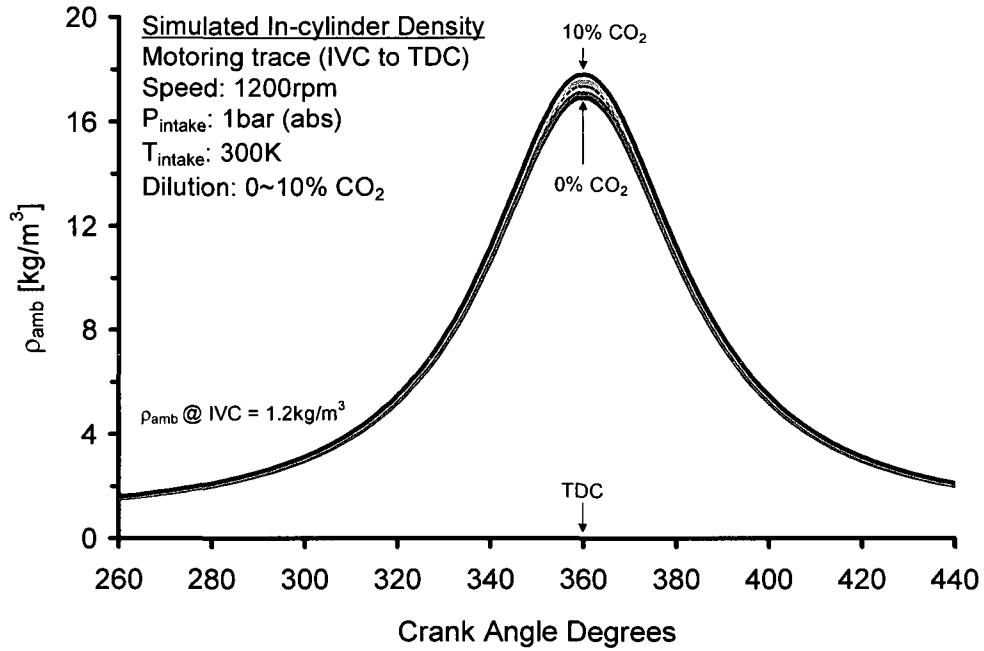
Figure 10-8: Variation of the in-cylinder ρ_{amb} for a motored trace.
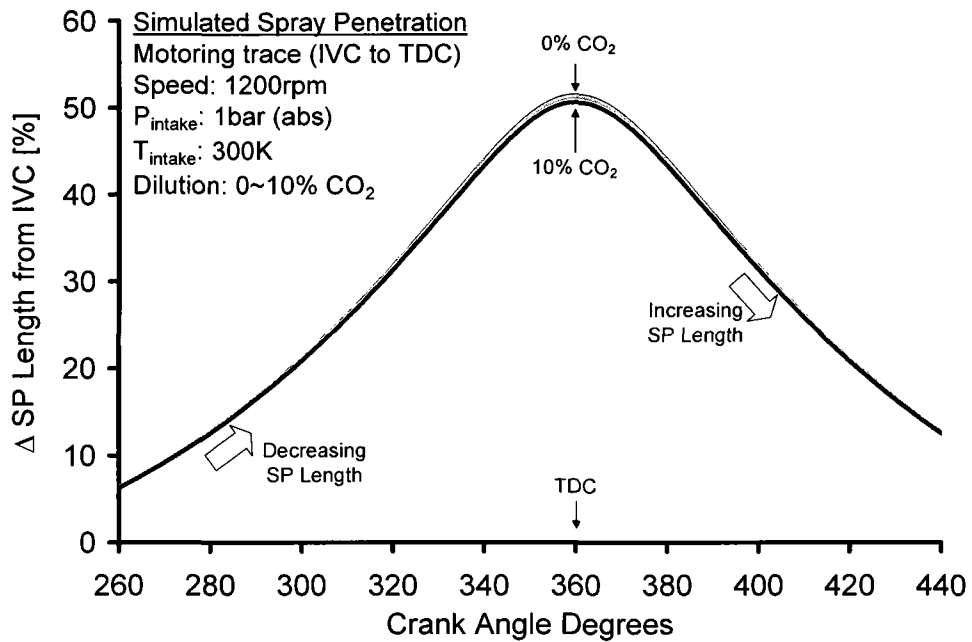
Figure 10-9: Decrease in the spray penetration length from IVC condition.
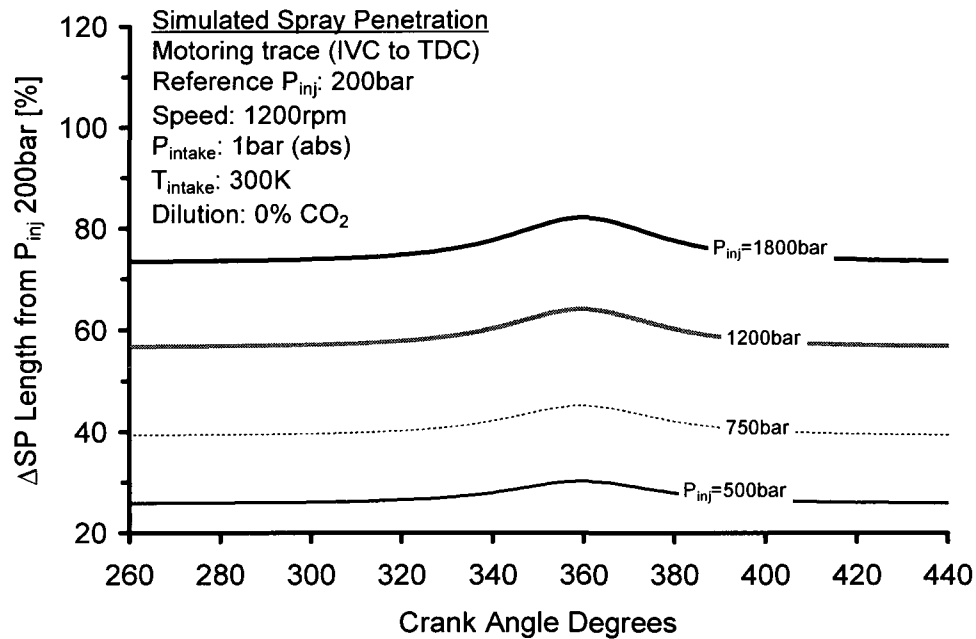
Figure 10-10: Effect of P_{inj} on spray penetration length.

Kennaird *et al.* (2002) investigated the influence of in-cylinder charge density and injection nozzle geometry on the behaviour of diesel sprays using high-speed imaging. Both vapour and liquid penetration profiles were investigated in operating conditions representative of modern turbocharged inter-cooled HSDI diesel engines. Using an injection pressure of 1600bar and ambient density of 42kg/m^3, Kennaird *et al.* employed Equation 10-5 to determine the best correlation with experimental data where K is an empirical constant, P_{inj} the injection pressure, P_{cyl} and ρ_{cyl} are the mean cylinder pressure and density during injection, respectively, D_o is the injector orifice diameter, t is the time after SOI and C a correction time constant. A constant value of K = 6.25 (instead of 2.95 employed by Hiroyasu and Arai) was found to give the best agreement with the experimental data for both mini-sac and valve covered orifice (VCO) nozzles.

$$S = K \times \left(\frac{P_{inj} - P_{cyl}}{\rho_{cyl}} \right)^{0.25} \times \sqrt{D_o \times (t - C)} \qquad \text{Equation 10-5}$$

Because the spray penetration is affected by the diameter of the nozzle orifice and the injection duration, it is not uncommon to employ multi-shot injection strategies with short injection durations, boost pressure (which increases P_{cyl} and ρ_{cyl}) and reduced orifice diameters (with increased number of holes) to minimise wall impingement in in-cylinder early injection diesel LTC mode (Helmantel 2004, Zheng 2006b). These strategies tend to reduce the spray penetration length at constant injection pressure.

Figures 10-11 and 10-12 show the KIVA simulation results for the effect of in-cylinder SOI on the evolution of the liquid fuel phase for an injector with a cone angle of 150° optimised for diesel HTC mode. For the conditions investigated, the early injection case had the highest amount of liquid fuel remaining at EVO. Because the mean cylinder temperature, T_{Mean}, at SOI was relatively low for the early injection case, the liquid fuel did not fully vaporise. Additionally, the early injection case showed increased fuel spray-to-cylinder wall interaction attributable to the large cone angle and increased penetration length at such conditions.
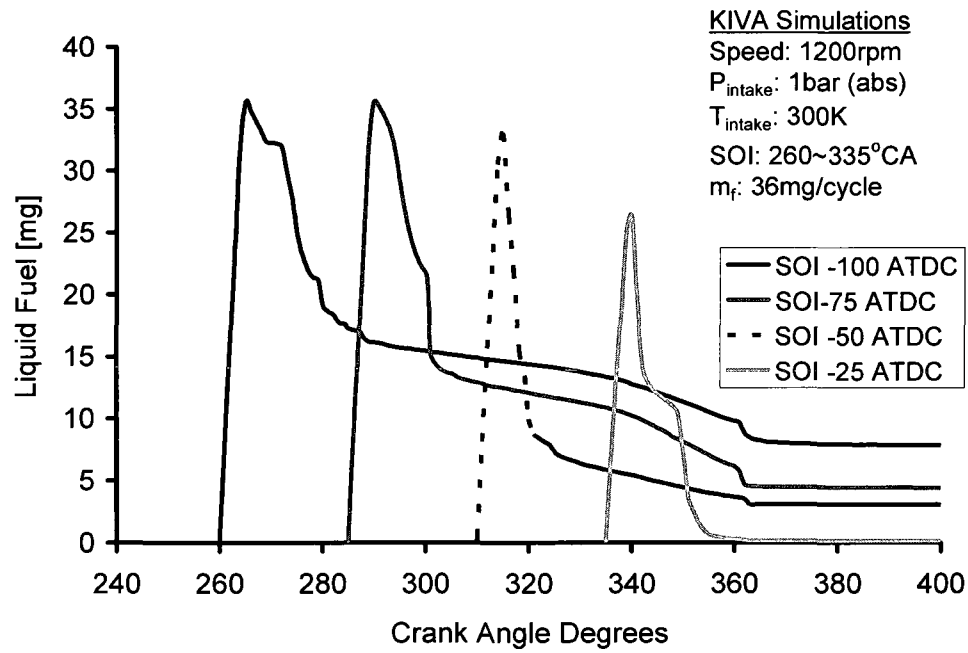
Figure 10-11: Evolution of in-cylinder fuel liquid phase - KIVA.
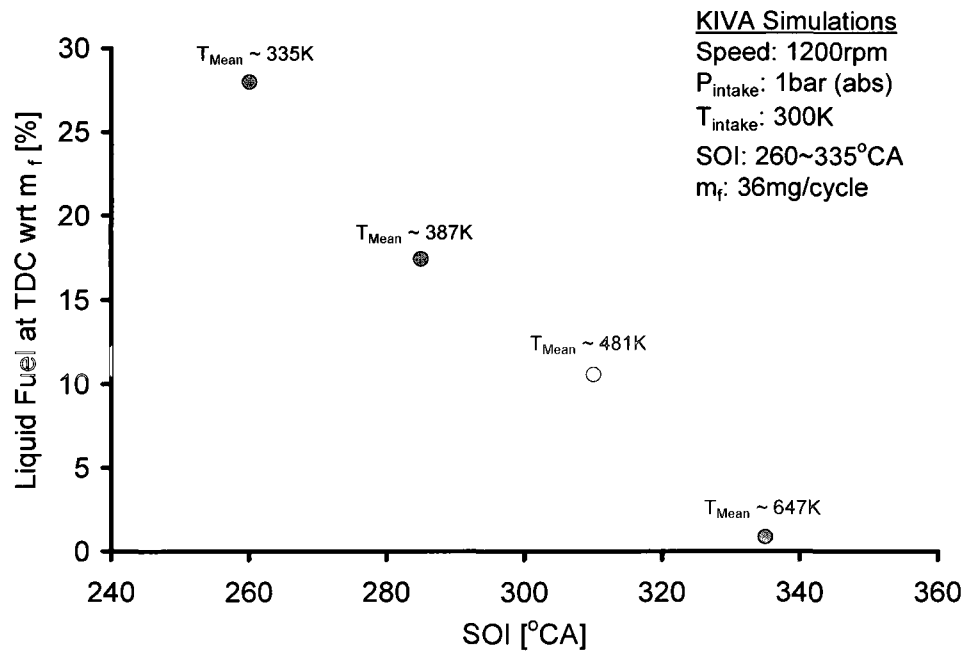
Figure 10-12: Effect of SOI on in-cylinder fuel liquid phase – KIVA.

From the above discussion, Figure 10-13 was generated to show some aspects of diesel LTC injection strategies that are summarised below.

The very early injection strategies which include early in-cylinder or port injection diesel/biodiesel LTC suffer from wall wetting (condensation, spray penetration) and pour vaporisation because the charge air may not be hot enough to maintain the fuel vapour phase. Furthermore, the strategy may have:

- certain early local homogeneous pockets which could experience chemical preparation and prematurely auto-ignite;

- some stoichiometric early pockets that survive effecting increased NO_x formation;

- increased UHC, CO and oil dilution and off-phasing of the combustion event leading to deterioration in thermal efficiency.

The late injection strategy may result in insufficient homogeneity, increased NO_x formation (becomes HTC combustion), increased soot at high load conditions, rough combustion if too close to TDC, low UHC and CO and high thermal efficiency.

The desirable injection is the one within the best window and best per shot injection duration. To reduce the dense fuel pockets, multi-pulse injections may be employed with minimal injector opening. This strategy, however, may result in reduced injector life and if piezo-electric injectors are employed the rise in temperature associated with dense and short injection pulses may result in increased piezo stack temperature, which may in turn affect the consistency and reliability of the injection strategy.

Early In-clyinder Injection
Diesel HTC Design

•Wall impingement
•↓ P_{inj} may be reqd.
•↑↑ HC and CO
•↑ smoke
•↓↓η

Early In-clyinder Injection
Diesel LTC Design

•Mid to high load
•Reduced impingement
•Chamber redesign
•↑ P_{inj} ok
•Piston impingement
 (If SOI is near-TDC)

Intake Port Injection
Diesel LTC Design

•Requires pre-heating
•↑↑ Condensation
•↑↑ Oil dilution
•↑↑ HC and CO
•↓↓η

Near-TDC Injection
Diesel HTC/LTC Design

•Low to mid load
•Chance of ↑ NOx
•High EGR
•↑ HC and CO
•↓η

EGR is necessary to: withhold the mixture from premature auto-ignition (more mixing)
moderate the rate-of-pressure rise
modulate combustion phasing

Figure 10-13: Summarised characteristics of diesel LTC injection strategies.

226

While homogeneous mixture formation through inlet port or very early in-cylinder injection is ideal for fuels with high volatility such as gasoline, it has proved to be quite problematic for heavier fuels such as diesel and biodiesel. Very advanced injection of heavy fuels may result in high UHC and CO emissions and increased fuel consumption and oil dilution. These problems could be attributed, in the main, to poor fuel vaporisation and fuel condensation on the cylinder wall lining as shown in Figure 10-14. The most common and preferred injection technique for diesel and biodiesel LTC is the direct in-cylinder method with the SOI after and before the EFCT for the compression and expansion strokes, respectively, which could be single-shot or multi-event.
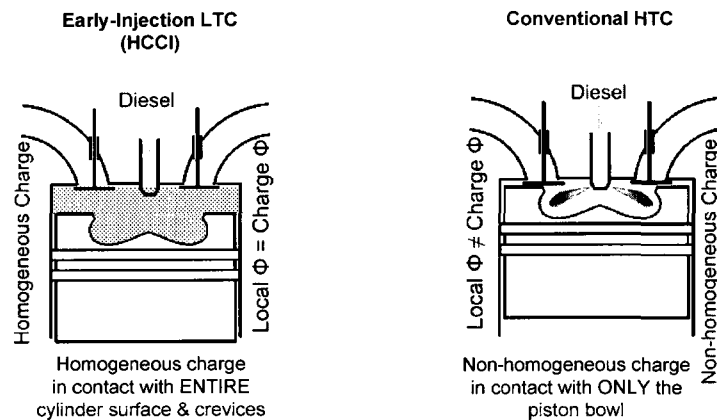
Figure 10-14: Diesel/biodiesel homogeneous LTC vs. non-homogeneous HTC modes (Zheng *et al.* 2007e).

10.3 Future Perspective of Biodiesel Fuel

In recent years, import dependency, along with economic and environmental security concerns have given rise to new government targets and incentives, aimed at reducing petroleum imports and increasing the consumption and production of renewable fuel (EMO 2006). Biodiesel is a partial replacement for the petroleum-derived diesel fuel. It is non-toxic, biodegradable, low in sulphur, aromatics free and renewable. Through a

process of transesterification, a fatty acid is reacted with alcohol and the resulting fatty acid methyl ester (FAME) or fatty acid ethyl ester (FAEE) is what is commonly referred to as biodiesel.

In the European Union (EU), rapeseed methyl ester (RME) is the most common source of the FAME and standard diesel may contain up to 5% (B5). However, the concern for food crop competition in some EU member states has necessitated the recent increased research and use of the biowaste-to-liquid (BTL) fuels, also referred to as the second generation biodiesel fuels. In the USA, soybean oil is the most common feedstock of the FAME and fleets commonly use diesel with up to 20% biodiesel by volume (B20). In Canada, genetically modified rapeseed oil (Canola) is the main feedstock in the Prairie provinces while yellow grease, waste animal fats and fish oil are mostly employed in the eastern provinces. In Asia Pacific, biodiesel research has increased in the last 10 years and the demand is expected to rapidly increase with palm oil being the main source for the FAME. Note also that biodiesel/bio-fuels research and use has accelerated in South America and Australasia while some African countries have initiated similar alternative fuels programmes.

Neat biodiesel fuel may be directly used in some diesel engines without prior engine modifications. However, the technology in diesel engines has continued to evolve and advanced injection systems consisting of high-pressure common-rail piezo-electric injection are already on the market. In these systems, the use of neat biodiesel fuel presents some concerns which include oxidative degradation, injector fouling, wear and

corrosion, among others. It is therefore concluded by this author that in the short term neat biodiesel application would be feasible in stationary power plants, especially the relatively low cost but robust diesel engines with mechanical injection configurations similar to the Yanmar NFD170. The use of neat biodiesel fuel in such engines would be met with relatively fewer short-term problems, if any. Conversely, for mobile applications, the introduction of cleaner diesel fuels and advanced common-rail injection systems on the market has presented an impetus for continued research in clean combustion with conventional diesel fuels. Furthermore, using B5 (from biodiesel meeting the ASTM D6751 or EN standards) and lower blends does not seem to have any harmful effects on the engines. Some engine original equipment manufacturers (OEMs) do recognise even higher blend levels. The long term effects of using neat biodiesel fuel on advanced common-rail diesel engines, therefore, still needs to be evaluated.

CHAPTER XI

CONCLUSIONS AND RECOMMENDATIONS

The main objective of the work underlying the dissertation was the in-cylinder simultaneous reduction of NO_x and soot in diesel-/biodiesel-fuelled engines. The work correlating the combustion process with the engine performance and emissions has contributed to the understanding of the diesel and especially biodiesel LTC modes. To achieve the dissertation objective, empirical investigations of conventional diesel and neat biodiesel fuels were conducted in the HTC and LTC modes. Moreover, modelling tools such as engine cycle simulation, chemical kinetics and multi-dimensional based were employed primarily to assist in the interpretation of the empirical results. The conclusions and recommendations from the research are discussed below.

11.1 Conclusions

The deductions from the modelling work are first discussed followed by the diesel fuel LTC empirical findings from the modern common-rail engine. Conclusions for the comparison of conventional diesel and neat biodiesel fuels on the naturally aspirated single-cylinder DI diesel engine with mechanical injection configuration are then discussed. Finally, conclusions from the biodiesel engine tests on a common-rail DI diesel engine with SOI, EGR and boost sweeps and multi-pulse injections are drawn.

CHAPTER XI – CONCLUSIONS AND RECOMMENDATIONS

11.1.1 Modelling Work

11.1.1 (a) Engine Cycle Simulations

The engine cycle simulations (0-D) have been enlightening to help identify the influencing parameters of diesel/biodiesel LTC fuel efficiency. The simulations indicated that compared to the combustion duration, the combustion phasing has significant effect on the engine thermal efficiency.

11.1.1 (b) Chemical Kinetics Simulations

Charge dilution of homogeneous LTC of the biodiesel and diesel fuels was simulated in CHEMKIN. Generally, the maximum gas temperatures were low, resulting in the prediction of low NO_x formation. Because the model employed was a perfectly stirred reactor, the engine-out soot, represented by the soot precursor C_2H_2, would be near-zero if ignition was attained. The C_2H_2 species were normalised with the fuelling rate and the in-cylinder evolution of the soot precursor examined. For the conditions investigated, the model diesel fuel produced more soot precursors than the model biodiesel fuel.

11.1.1 (c) Multidimensional Modelling

The KIVA ϕ-T planes for HTC showed rich regions at elevated temperatures where high soot formation is expected to occur at low injection pressures. As the injection pressure was increased, the combustion process developed into lean premixed burning at elevated temperatures resulting in increased engine-out NO_x emissions. The classical HTC NO_x/PM trade-off was captured by the KIVA simulations. For the LTC simulations however, the KIVA programme does not seem to capture the simultaneous reduction of

231

NO_x and soot. A more detailed reaction mechanism, especially for the soot formation, may have to be implemented in order to capture this interesting combustion regime.

11.1.2 Diesel Fuel LTC Tests

Empirical fuel efficiency analyses were conducted for the diesel LTC operation and enhanced with engine cycle simulations. This segment of the dissertation work is summarised with the conclusions below.

The empirical results indicate that the combustion phasing dominates the maximum attainable fuel efficiency of the engine that is further demonstrated with engine cycle simulations. However, the phasing domination cedes to high UHC production when the fuel combustion efficiency is severely deteriorated such as by excessive EGR. Note that the achieved fuel efficiency from this research was considered as higher than the efficiency achievable when strict in-cylinder control techniques are implemented in conventional modern diesel engines but lower than that without in-cylinder control.

In order to improve the fuel efficiency of diesel LTC operation the fuel injection can be controlled as such:

- single-shot with prolonged EGR at low load;

- 2~5 shots of late early-injection with EGR at medium load;

- 6~8 shots and EGR at high load.

11.1.3 Comparison of Diesel and Biodiesel Fuels

Motivated by the concern over depleting world reserves of fossil fuels and stringent emission regulations for harmful pollutants, neat biodiesel engine tests were conducted on a naturally aspirated four stroke single-cylinder DI diesel engine with mechanical injection configuration. Without prior engine modifications neat biodiesel fuels were utilised and the engine performance and emission comparisons made with a conventional diesel fuel. The results are summarised below.

11.1.3 (a) High Load Tests without EGR

At constant high load operating conditions, the engine-out NO_x emissions were dependent on the fuel CN, for the same SOI. The biodiesel fuel with a CN similar to (or lower than) the diesel fuel produced higher NO_x emissions than the diesel fuel. Conversely, the biodiesel fuels with a higher CN produced comparable NO_x emission levels with the diesel fuel. In conventional diesel HTC mode, a higher CN would result in a shortened ignition delay period thereby allowing less time for the air/fuel mixing before the premixed burning phase. Consequently, a stoichiometrically weak air/fuel mixture would be generated and burnt during the premixed phase resulting in relatively reduced NO_x formation. Generally the emissions of soot, CO and THC were lower for the engine fuelled with biodiesel.

11.1.3 (b) Medium and Low Load Tests with EGR

At steady-state, medium- and low-load conditions, the soot profile plotted against the ignition delay due to EGR had two distinct slopes. In *Slope 1*, the soot increased with

233

increasing EGR while in *Slope 2* the soot decreased with increasing EGR. The first slope was consistent with the HTC mode while the second with HCCI-enabling technologies and smokeless diesel combustion i.e. the LTC regime. The LTC slope had a narrow region of operation obtained between 60 and 70% EGR. A further increase in EGR resulted in increased cycle-to-cycle variation, CO and THC emissions and deterioration in the thermal efficiency.

To enter the EGR-incurred LTC regime, the ignition delay had to be prolonged by more than 50%. However, the ultra-low levels of NO_x and soot were achieved when the ignition delay was prolonged by 80 to 100%. In this region, the power loss was less than 25 and 20% under medium load and less than 20 and 10% under low load conditions for the diesel and biodiesel fuels, respectively; an indication of the comparatively low EGR tolerance for conventional diesel fuels. The results present a potential to further increase the EGR application limit for the biodiesel fuels. Despite the effective power loss during the LTC regime, the result indicated a profound improvement compared to the intake port-injection test results previously reported (Zheng *et al.* 2006c), which had several setbacks including substantial engine oil dilution.

An ignition delay correlation, for the single-cylinder engine employed, under the influence of EGR was developed. This considered the molecular and equivalent molecular oxygen concentrations in the intake and fuel, respectively. The correlation captured the ignition delay trends with good agreement. The pre-exponential coefficient,

a function of the oxygen concentrations in the intake air and fuel, was found to range from 4.3 to 4.6 for the diesel fuel and 3.9 to 4.2 for the biodiesel fuels.

11.1.4 Biodiesel Tests on a Common-rail DI Diesel Engine

- Compared to the conventional diesel fuel, the biodiesel fuel produced comparable engine-out NO_x emissions. The soot, CO and THC emissions were relatively lower for the biodiesel-fuelled engine. Due to the lower energy content of the biodiesel, the ISFC was higher resulting in a slight efficiency penalty.

- It was possible to retard the SOI for biodiesel further than that of the diesel fuel before the cyclic variability became intorelable. This was mainly attributed to the relatively higher CN of the biodiesel fuel.

- At fixed single-shot SOI, 8bar IMEP and rail pressure of 950bar, the biodiesel LTC mode was attained for the intake pressures higher than 1.2bar (abs). With the SOI sweep, on the contrary, the ultra-low simultaneous levels of the in-cylinder NO_x and soot for both diesel and biodiesel fuels were not attained. A combination of the SOI and EGR strategies, preferably under adaptive control schemes (Kumar *et al.* 2007), may facilitate an energy-efficient biodiesel LTC mode solution.

- For the single-shot tests, the biodiesel LTC mode was attained at elevated EGR levels with a penalty of high CO and THC emissions. At medium load conditions with increase of EGR, ultra-low NO_x emissions were achieved for multiple injections. However, for the very advanced SOI cases the poor biodiesel/air mixture preparation resulted in increased soot, CO and THC formation. Nonetheless, retarding the SOI and reducing the number of injections appeared to approach the LTC mode.

For the conditions investigated, the biodiesel was found to sustain a broader range of loads in the EGR-incurred LTC than the diesel fuel. This was mainly due to the biodiesel's higher CN and combustion-accessible fuel oxygen.

11.2 Recommendations

11.2.1 Diesel Low Temperature Combustion

The continuous research in enabling robust and high-efficient diesel LTC operation under high loads is recommended.

11.2.2 Biodiesel Tests

- The SOI for different fuels should be determined on the Yanmar NFD170 engine. This would be helpful in the determination of the ignition delay data.

- The Yanmar engine could be converted to a common-rail configuration with independent control of the SOI, rail pressure and boost for biodiesel optimisation tests. In the current mechanical configuration, however, the peak cylinder pressures should not exceed 120~130bar.

- The biodiesel engine tests on a common-rail diesel engine could be enlightening for the fuel characterisation in passenger car applications thus facilitating the identification of the future perspective of the fuels. Future tests on the common-rail engine should include increasing the injection and boost pressures and reducing the compression ratio and/or use of variable valve timing, among other strategies, for both single- and multi-event injection studies. Such approach may facilitate the

biodiesel LTC mode, thus the in-cylinder simultaneous reduction of NO_x and soot, at medium-to-high loads in common-rail diesel engines.

- It is likely to have a mixture of biodiesel fuels from different feedstocks in the fuel tank especially in Canada where the feedstock for commercial B100 varies from marine oil to yellow grease. The future work should also include continued engine tests with a biodiesel blends from different feedstocks.

- Further studies should also include the temporal analysis of NO_x and UHC formation, through use of the in-cylinder direct gas sampling system (i.e. the ultra-fast direct gas sampling system), to provide insights into the formation of NO_x and UHC in biodiesel-fuelled engines.

11.2.3 KIVA Simulations

An option of implementing a more detailed reaction mechanism in KIVA, especially for the soot prediction, should be considered (see Figure 11-1). This may help in capturing the simultaneous reduction of NO_x and soot in diesel LTC mode.
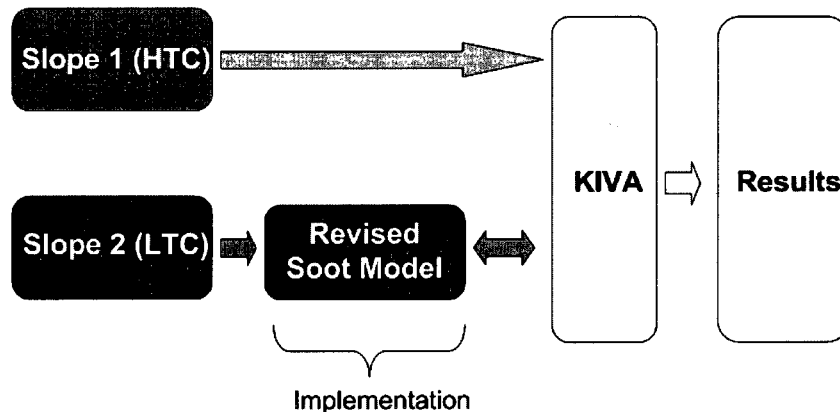
Figure 11-1: Recommended KIVA simulations approach for HTC and LTC.

13. Bosch R. GmbH, 2005. Retrieved 2005 from www.bosch-presse.de.

14. California Analytical Instruments Inc. (CAI), 2000, *Gas Analysers Manual*.

15. Çengel Y.A. and Boles M.A., 2002, *THERMODYNAMICS: An Engineering Approach*, 4th Edition, McGraw Hill.

16. Chen Z., Konno M., Oguma M and Yanai T., 2000, "Experimental Study of CI Natural Gas/DME Homogeneous Charge Engine", SAE Technical Paper No. 2000-01-0329.

17. Chevron Corporation, 2007. http://www.chevron.com/products/prodserv/fuels/diesel.

18. Choi C.Y. and Reitz R.D., 1999, "An Experimental Study on the Effects of Oxygenated Fuel Blends and Multiple Injection Strategies on DI Diesel Engine Emissions", Fuel 78, pp.1303-1317.

19. Choi C.Y., Bower R.D. and Reitz R.D., 1997, "Mechanisms of Emissions Reduction using Biodiesel Fuels", Final Report for the National Biodiesel Board.

20. Christensen M., Hultqvist A. and Johansson B., 1999, "Demonstrating the Multi-fuel Capability of a Homogeneous Charge Compression Ignition Engine with Variable Compression Ratio", SAE Technical Paper 1999-01-3679.

21. Chryssakis C.A., Assanis D.N., Kook S. and Bae C., 2005, "Effect of Multiple Injections on Fuel-Air Mixing and Soot Formation in Diesel Combustion using Direct Flame Visualisation and CFD Techniques", Proceedings of the ASME ICE Division 2005 Spring Technical Conference, Paper No. ICES2005-1016.

22. Curran H.J., Gaffuri P., Pitz W.J., Westbrook C.K., 1998, "A Comprehensive Modeling Study of n-Heptane Oxidation", Combustion and Flame, Vol. 114, pp 149-177.

23. Dorado M.P., Ballesteros E., Arnal J.M., Gomez J. and Lopez F.J., 2003, "Exhaust Emissions from a Diesel Engine Fuelled with Transesterified Waste Olive Oil", Fuel 82, pp. 1311-1315.

24. Easton V.J. and McColl J.H., 2007. Statistics Glossary. Retrieved from http://www.stats.gla.ac.uk/steps/glossary/index.html.

25. Ecopoint Inc., 2007. Retrieved from 2007 from http://www.dieselnet.com/standards.

26. Emerging Markets Online (EMO), 2006, "Biodiesel 2020: Global Market Survey, Case Studies and Forecasts". Retrieved 2006 from http://www.emerging-markets.com.

27. Fisher E.M., Pitz W.J., Curran H.J. and Westbrook C.K., 2000, "Detailed Chemical Kinetic Mechanisms for Combustion of Oxygenated Fuels", Proceedings of the Combustion Institute, Volume 28, pp 1579-1586.

28. Flynn P.F., Durrett R.P., Hunter G.L., zur Loye A.O., Akinyemi O.C., Dec J.E. and Westbrook W.C., 1999, "Diesel Combustion: An Integrated View Combining Laser Diagnostics, Chemical Kinetics and Empirical Validation", SAE Technical Paper No. 1999-01-0509.

29. Gamma Technologies, 2004, *GT-Power Version 6.1.*

30. Gurley Precision Instruments Inc., 2005. Retrieved from http://www.gurley.com.

31. Gustafson R., Lipinski M., Gopalakrishnan V., 2006, "Premix Charge Compression Ignition Combustion System Optimization", 12th Diesel Engine-Efficiency Emissions Research (DEER) Conference.

32. Han X., Asad U., Kumar R., **Mulenga M.C.**, Banerjee S., Wang M., Reader G.T. and Zheng M., 2007, "Empirical Studies of Diesel Low Temperature Combustion on a Modern Diesel Engine", Combustion Institute/Canadian Section (CI/CS).

33. Helmantel A., 2004, *Reducing Diesel Engine Emissions – An Experimental Investigation*, Thesis for the Degree of Licentiate in Engineering, Chalmers University of Technology.

34. Helmantel A. and Denbratt I., 2004, "HCCI Operation of a Passenger Car Common-Rail Di Diesel Engine with Early Injection of Conventional Diesel Fuel", SAE Technical Paper No. 2004-01-0935.

35. Helmantel A. and Denbratt I., 2006, "HCCI Operation of a Passenger Car DI Diesel Engine with an Adjustable Valve Train," SAE Technical Paper No. 2006-01-0029.

36. Hiroyasu H. and Arai M., 1990, "Structures of Fuel Sprays in Diesel Engines", SAE Technical Paper No. 900475.

37. Hiroyasu H., Yoshikawa S., Nishida K., Arai M, Oda H. and Suzuki M., 1990, "Total In-Cylinder Sampling Experiment on Emission Formation Processes in a DI Diesel Engine", SAE Technical Paper No. 902062.

38. Heywood J.B., 1988, *Internal Combustion Engine Fundamentals*, McGraw-Hill Inc.

39. İçingür Y. and Altiparmak D., 2003, "Effect of Fuel Cetane Number and Injection Pressure on a DI Diesel Engine Performance and Emissions", Energy Conversion and Management, Vol. 44, pp. 389-397.

40. Jacobs T.J., Bohac S.V., Assanis D.N. and Szymkowicz P.G., 2005, "Lean and Rich Premixed Compression ignition Combustion in a Light-Duty Diesel Engine", SAE Technical Paper No. 2005-01-0166.

41. Jhavar R. and Rutland C., 2005, "Effects of Mixing on Early Injection Diesel Combustion", SAE Technical Paper No. 2005-01-154.

42. Kee R.J. *et al.*, 2000, *CHEMKIN Collection*, Release 3.6, Reaction Design Inc., San Diego, CA, USA.

43. Kennaird D.A., Crua C., Lacoste J., Haikal M.R., Gold M.R. and Jackson N.S., 2002, "In-cylinder Penetration and Break-up of Diesel Spray using a Common-Rail Injection System", SAE Technical Paper No. 2002-01-1626.

44. Kidoguchi Y., Yang C., Kato R. and Miwa K, 2000, "Effects of Fuel Cetane Number and Aromatics on Combustion Process and Emissions of a Direct-injection Diesel Engine", JSAE Review 21, pp. 469-475.

45. Kitamura T., Ito T., Senda J. and Fujimoto H., 2002, "Mechanism of Smokeless Diesel Combustion with Oxygenated Fuels based on the Dependence of the Equivalence Ratio and Temperature on Soot Particle Formation", International Journal of Engine Research, Vol. 3, No 4, pp 223-248.

46. Knothe G., 2006, "Analyzing Biodiesel: Standards and Other Methods", Journal of American Oil Chemists' Society (JAOCS), Vol. 83, no. 10, pp 823-833.

47. Krisnangkura K., Yimsuwan T. and Pairintra R., 2006, "An Empirical Approach in Predicting Biodiesel Viscosity at Various Temperatures", Fuel 85, pp. 107-113.

48. Kodama Y., Nishizawa I., Sugihara T., Sato N., Iijima T. and Yoshida T., 2007, "Full-load HCCI Operation with Variable Valve Actuation System in a Heavy-Duty Diesel Engine", SAE Technical Paper No. 2007-01-0215.

49. Kumar R., Zheng M., Asad U. and Reader G.T., 2007, "Heat Release Based Adaptive Control to Improve Low Temperature Diesel Engine Combustion", SAE Technical Paper No. 2007-01-0771.

241

50. Ladommatos N., Parsi M. and Knowles A., 1996, "The Effect of Fuel Cetane Improver on Diesel Pollutant Emissions", Fuel 75, No. 1, pp. 8-14.

51. Ladommatos N, Abdelhalim S and Zhao H., 2000, "The effects of exhaust gas recirculation on diesel combustion and emissions. International Journal of Engine Research, Vol. 1, No. 1, p. 107-126.

52. Lawrence Livermore National Laboratory, Combustion Chemistry Group, 2002. Retrieved from http://www-cms.llnl.gov/combustion/combustion2.html, Chemical Kinetics Mechanisms.

53. Lin C-Y. and Lin H-A., 2006, "Diesel Engine Performance and Emission Characteristics of Biodiesel Produced by the Peroxidation Process", Fuel 85, pp. 298-305.

54. Liu Y., Tao F., Foster D.E. and Reitz R.D., 2005, "Application of a Multi-Step Phenomenological Soot Model to HSDI Diesel Multiple Injection Modelling", SAE Technical Paper No. 2005-01-0924.

55. McCrady J.P., Stringer V.L., Hansen A.C. and Lee C.F., 2007, "Computational Analysis of Biodiesel Combustion in a Low-Temperature Combustion Engine using Well-Defined Fuel Properties", SAE Technical Paper No. 2007-01-0617.

56. Miles P., 2006, "In-cylinder Flow and Mixing Processes in Light-Duty, Low-Temperature Diesel Combustion Systems", 3rd International Symposium on Homogeneous Charge Compression Ignition (HCCI), San Ramon, CA.

57. Miyamoto N., Ogawa H., Goto N. and Sasaki H., 1990, "Analysis of Diesel Soot Formation under Varied Ignition Lag with a Laser Light Extinction Method", SAE Technical Paper No. 90064.

58. Monyem A., Canakci M. and van Gerpen J.H., 1999, "Investigation of Biodiesel Thermal Stability under Simulated in-use Conditions", ASAE Paper No. 996112.

59. Monyem A., van Gerpen J.H., and Canakci M., 2001, "The Effect of Timing and Oxidation on Emissions from Biodiesel-fueled Engines", Transaction of the American Society of Agricultural Engineers (ASAE), Vol. 44(1), pp. 35~42.

60. Mueller C.J., Pitz W.J., Pickett L.M., Martin G.C., Siebers D.L. and Westbrook C.K., 2003, "Effects of Oxygenates on Soot Processes in DI Diesel Engines: Experiments and Numerical Simulations", SAE Technical Paper No. 2003-01-1791.

61. **Mulenga M.C.**, Reader G.T., Ting D.S-K. and Zheng M., 2003a, "Effect of Hydrogen Peroxide on Premixed Iso-octane/Air Combustion", ASME International Joint Power Generation Conference ASME Paper IJPGC2003-40108.

62. **Mulenga M.C**, Zheng M., Ting D.S-K., and Reader G.T., 2003b, "Prospect of Reduced CO and NO_x in Diesel Dual Fuel Engines", ASME Internal Combustion Engine Division and Rail Transportation Division Fall Technical Conference, ASME Paper ICEF2003-768.

63. **Mulenga M.C.**, Reader G.T., Ting D.S-K., and Zheng M., 2003c, "Potential for Reduced CO and NO_x Emissions from an HCCI Engine using H_2O_2 Addition", SAE Technical Paper 2003-01-3204.

64. Munson B.R., Young D.F. and Okiishi T.H., 2002, *Fundamentals of Fluid Mechanics*, 4th Edition, John Wiley & Sons Inc.

65. Murayama T., Zheng M., Chikahisa T., Oh Y., Fujiwara Y., Tosaka S. *et al.*, 1995, "Simultaneous Reductions of Smoke and NO_x from a DI Diesel Engine with EGR and Dimethyl Carbonate", SAE Transactions, Technical Paper No. 952518.

66. Najt P. M., 1983, "Compression-Ignited Homogeneous Charge Combustion", SAE Technical Paper No. 830264.

67. National Biodiesel Board, 2007. Retrieved 2007 from http://www.biodiesel.org.

68. National Institute of Standards and Technology (NIST), 2006. Retrieved 2006 from http://www.itl.nist.gov, Engineering Statistics Handbook.

69. National Institute of Standards and Technology (NIST), 2007. Retrieved 2007 from http://www.nist.gov/srd/, NIST Chemistry WebBook.

70. National Instruments Corporation, 2004, LabVIEW 7.1.

71. Natural Resources Canada (NRCan), 2007. Retrieved 2007 from http://oee.nrcan.gc.ca/transportation.

72. Natural Resources Canada, 2004, "Economic, Financial, Social Analysis and Public Policies for Biodiesel Phase 1".

73. Ogink R., 2004, *Computer Modeling of HCCI Combustion*, Ph.D. Thesis, Chalmers University of Technology.

74. Patterson J., Hassan M.G., Clarke A., Shama G., Hellgardt K. and Chen R., 2006, "Experimental Study of DI Engine Performance Using Three Different Biodiesel Fuels", SAE Technical Paper no. 2006-01-0234.

75. Rosca R., Rakosi E., Manolache G. and Niculaua M., 2005, "Fuel and Injection Characteristics for Biodiesel Type Fuel from Waste Cooking Oil", SAE Technical Paper No. 2005-01-3674.

76. Sazhin S.S., Sazhina E.M., Heikel M.R. and Marooney C., 1999, "The Shell Autoignition Model: A New Mathematical Formulation", Combustion and Flame 117, pp 529-540.

77. Sazhina E.M., Sazhin S.S., Heikal M.R. and Marroney C.J., 1999, "The Shell autoignition model: applications to gasoline and diesel fuels", Fuel 78, pp 389-401.

78. Siemens AG, 2003. Retrieved 2005 from www.siemens.com.

79. Stanglmaier R.H. and Roberts C.E., 1999, "Homogeneous Charge Compression Ignition, HCCI: Benefits, Compromises and Future Engine Applications", SAE Technical Paper No. 1999-01-3682.

80. Stone R, 1999, *Introduction to Internal Combustion Engines*, 3rd Edition, Macmillan.

81. Southwest Research Institute, 2007. Retrieved 2007 from http://www.swri.org.

82. Su W., Wang H and Liu B., 2005, "Injection Modulation for HCCI Diesel Combustion", SAE Technical Paper No. 2005-01-0117.

83. Syntroleum Corporation, 2007. Retrieved 2007 from http://www.syntroleum.com.

84. Tat M.E. and Van Gerpen J.H., 2002, "Physical Properties and Composition Detection of Biodiesel-diesel Fuel Blends", American Society of Agricultural Engineers (ASAE), Paper 026084.

85. Tat M.E. and van Gerpen J.H., 2003a, "Measurement of Biodiesel Speed of Sound and its Impact on Injection Timing", Final Report, National Renewable Energy Laboratory, NREL/SR-510-31462.

86. Tat M.E., 2003b, *Investigation of Oxides of Nitrogen Emissions from Biodiesel-fuelled Engines*, Ph.D. Thesis, Iowa State University.

87. Tate R.E., Watts K.C., Allen C.A.W. and Wilkie K.I., 2006a, "The Densities of Three Biodiesel Fuels at Temperatures up to 300°C", Fuel 85, pp. 1004-1009.

88. Tate R.E., Watts K.C., Allen C.A.W. and Wilkie K.I., 2006b, "The Viscosities of Three Biodiesel Fuels at Temperatures up to $300^{\circ}C$", Fuel 85, pp. 1010-1015.

89. Thring R.H., 1989, "Homogeneous-Charge Compression Ignition (HCCI) Engines", SAE Technical Paper No. 892069.

90. Turns S.R. 2000, *An Introduction to Combustion - Concepts and Applications*, 2nd Edition, Mc-Grawhill.

91. University of California - San Diego, Combustion Division of the Centre for Energy Research, 2003. Retrieved 2003 from http://maeweb.ucsd.edu/combustion/cermech, Chemical Kinetic Mechanisms for Combustion Application.

92. US Department of Energy (DOE), 2007. Retrieved 2007 from, http://www.eere.energy.gov/afdc, Energy Efficiency and Renewable Energy.

93. US Department of Energy, 2004, "Biodiesel Handling and Use Guidelines, November 2004", Energy Efficiency and Renewable Energy.

94. US Environmental protection Agency (EPA), 2002, "A Comprehensive Analysis of Biodiesel Impacts on Exhaust Emissions", EPA420-P-02-001.

95. US Environmental Protection Agency (EPA), 2004, "Highway Diesel Progress Review-Report 2", Office of Transportation and Air Quality, EPA420-R-04-004.

96. United States Environmental Protection Agency (EPA), 2007, "Environmental Technology Verification Report: Test Report of Mobile Source Emission Control Devices", EPA Cooperative Agreement No. CR831911-01-1.

97. Vedal S., 1995, "Health Effects of Inhalable Particles: Implications for British Columbia", Air Resources Branch, British Columbia Ministry of Environment, Lands and Parks.

98. Weall A. and Collings N., 2007, "High Homogeneous Compression Ignition in a Direct Injection Engine Fuelled with Diesel and Biodiesel", SAE Technical Paper No. 2007-01-2020 (JSAE20077123).

99. Yamane K., Ueta A. and Shimamoto Y., 2001, "Influence of Physical and Chemical Properties of Biodiesel Fuel on Injection, Combustion and Exhaust Emission Characteristics in a DI-CI Engine", Proceedings of the 5th International Symposium on Diagnostics and Modelling of Combustion in Internal Combustion Engines (COMODIA), pp. 402-409.

100. Yan C. and Aggarwal S.K., 2006, "A High-Pressure Droplet Model for Spray Simulations", American Society of Mechanical Engineers (ASME) Journal of Engineering for Gas Turbines and Power, Vol. 128, pp 482-492.

101. Yuan W., Hansen A.C. and Zhang Q., 2005, "Vapour Pressure and Normal Boiling Predictions for Pure Methyl Esters and Biodiesel Fuels", Fuel 84, pp. 943-950.

102. Zhao H., Lowry G. and Ladommatos N., 1996, "Time-resolved Measurements and Analysis of In-cylinder Gases and Particulates in Compression-Ignition Engines", SAE Transactions, Technical Paper No. 961168.

103. Zheng M. and Reader G.T., 1996, "Synthetic Atmosphere Engine Simulations (SAES) Programme, the University of Calgary.

104. Zheng M., 2002, *Fundamentals of Clean Diesel Engine Technology*, Lecture Notes, University of Windsor.

105. Zheng M., Reader G.T. and Hawley J.G., 2004, "Diesel Engine Exhaust Gas Recirculation – A Review on Advanced and Novel Concepts", International Journal of Energy Conversion and Management, Vol. 45, Issue 6, pp. 883-900.

106. Zheng M., Reader G.T., Wang D., Zuo J., Kumar R., **Mulenga M.C.**, Asad U., Ting D. S-K. and Wang M., 2005, "A Thermal Response Analysis on the Transient Performance of Active Diesel Aftertreatment", SAE Transactions Journal of Fuels and Lubricants, Technical Paper No. 2005-01-3885.

107. Zheng M. and Reader G.T., 2006a, *Internal Report*, Clean Diesel Engine Research Laboratory, University of Windsor.

108. Zheng M., Reader G.T., Kumar R., **Mulenga C.**, Asad U., Tan Y. and Wang M., 2006b, "Adaptive Control to Improve Low Temperature Diesel Engine Combustion", Advanced Combustion Technologies Session of the 12th Diesel Engine-Efficiency Emissions Research (DEER) Conference.

109. Zheng M., **Mulenga M.C.**, Reader G.T., Wang M. and Ting D.S-K., 2006c, "Influence of Biodiesel Fuel on Diesel Engine Performance and Emissions in Low Temperature Combustion", SAE Technical Paper No. 2006-01-3281.

110. Zheng M., Asad U., Kumar R., Reader G.T., **Mulenga M.C.**, Wang M. and Tjong J.S., 2007a, "An Investigation of EGR Treatment on the Emission and Operating Characteristics of Modern Diesel Engines", SAE Technical Paper No. 2007-01-1083.

111. Zheng M., **Mulenga M.C.**, Reader G.T., Tan Y., Wang M. and Tjong J, 2007b, "Neat Biodiesel Fuel Engine Tests and Preliminary Modelling", SAE Technical Paper No. 2007-01-0616.

112. Zheng M., **Mulenga M.C.**, Reader G.T., Wang M., Ting D.S-K. and Tjong J., 2007c, "Biodiesel Engine Performance and Emissions in Low Temperature Combustion", Fuel Journal (In Press, May 2007).

113. Zheng M., Tan Y., **Mulenga M.C.** and Wang M., 2007d, "Thermal Efficiency Analyses of Diesel Low Temperature Combustion Cycles", SAE Transactions Journal of Fuels and Lubricants, SAE Technical Paper No. 2007-01-4019.

114. Zheng M., Tan Y., Reader G.T. and Wang M., 2007e, "Adaptive Combustion Control to Improve Diesel HCCI Cycle Efficiency", ASME Paper No. ICEF 2007-1630.

115. Zhu G.-S. and Reitz R.D., 2001, "Engine Droplet High-Pressure Vaporization Modeling", American Society of Mechanical Engineers (ASME) Journal of Engineering for Gas Turbines and Power, Vol. 123, pp 412-492.

APPENDICES

APPENDIX A

A. Properties of Neat Alternative Fuels

Table A-1: Properties of neat alternative fuels (Bosch 1996, Chen *et al.* 2000, Turns 2000).

Fuel	MON	RON	CN	LHV [MJ/kg]	Boiling Point [°C]
Hydrogen		>130		120	-253
Methane	120	>127		50	-162
Propane	97	112		46.3	-43
n-Butane	89	94		45.8	1
Gasoline	82-89	90-100	13-17	42-44	25-215
Diesel			40-60	~42.5	180-360
Dimethyl Ether			55-60	28.8	-25
Fischer-Tropsch Diesel			74-81	~42.5	164-238
Natural Gas	120	>127	<6	45-49	-162
Liquefied Petroleum Gas	93-96	94-110	<3	~46	-30
Ethanol	89	107	<5	26.8	78
Methanol	92	106	<5	19.7	65
Biodiesel			49~65	37~38	320~420

Dimethyl Ether (DME)

Dimethyl ether (C_2H_6O or CH_3OCH_3) is attracting a lot of research both as an alternative fuel as well as dual fuel (Chen *et al.* 2000).

Table A-2 compares the properties of DME to conventional diesel fuel.

249

Table A-2: Some properties of DME and diesel fuels (Chen *et al.* 2000).

Fuel Property	DME	Diesel
Cetane Number	>55	40~55
Auto-ignition Temperature [°C]	235	250
Boiling Point [°C]	-25	180~370
Stoichiometric A/F	9	14.6
Liquid Viscosity [cP]	0.15	2~4
Calorific Value [MJ/kg]	28.8	42.5

With respect to conventional compression ignition engines, Table A-2 shows that DME has better ignition quality due to a higher CN and lower auto-ignition temperature. The lower boiling point of DME entails better atomisation and tests have shown that DME produces no soot compared to diesel fuel (Chen *et al.* 2000). The main challenges of using DME are its low viscosity, which affects the conventional film between needle and sleeve of the injector resulting in leakage and increased wear, and relatively high CN that would make the homogeneous LTC phasing over-advanced without the implementation of heavy EGR and/or reduced compression ratio.

APPENDIX B

B. Standard Specification for Neat Biodiesel Fuel B100

Table B-1: North American Biodiesel (B100) Standard ASTM D6751.

TESTS		ASTM TEST METHOD	LIMITS		UNITS
			Minimum	Maximum	
Acid Number		D664		0.5	mg KOH/g
Carbon Residue 100% Sample		D4530		0.050	% mass
Cetane Number		D613	47		-
Cloud Point		D2500		Report	°C
Copper Strip Corrosion, 3 hours at 50°C		D130		No. 3	-
Distillation of Petroleum Products at Reduced Pressure, Atmospheric Equivalent Temperature (AET), % Recovered		D1160		360 (90% recovered)	°C
Free Glycerine		D6584		0.02	% mass
Kinematic Viscosity at 40°C		D445	1.9	6.0	mm²/sec
Pensky-Martens Closed Cup Flash Point		D93	130		°C
Phosphorus Content		D4951		0.001	% mass
Sodium/Potassium (combined)		UOP391		0.0005 (5)	%mass (ppm)
Sulphated Ash		D874		0.020	% mass
Sulphur	S 5 Grade	D5453		0.0005 (5)	% mass (ppm)
	S 15 Grade	D5453		0.0015 (15)	
	S 500 Grade	D5453		0.05 (500)	
Total Glycerine		D6584		0.240	% mass
Water and Sediment		D2709		0.050	% volume

251

Table B-2: European Biodiesel (B100) Standards (Knothe 2006).

| PROPERTY | TEST METHOD | LIMITS | | UNITS |
		EN 14213 (Heating oil)	EN 14214 (Vehicle use)	
Easter Content	EN14103	96.5 min	96.5 min	% (mol/mol)
Density, 15°C	EN ISO 3675, EN ISO 1285	860-900	860-900	kg/m³
Viscosity, 40°C	EN ISO 3104, ISO 3105	3.5-5.0	3.5-5.0	mm²/s
Flash Point	EN ISO 3679	120 min	120 min	°C
Sulphur Content	EN ISO 20846, EN ISO 20884	10.0 max	10.0 max	mg/kg
Carbon Residue (10% distillation residue)	EN ISO 10370	0.30 max	0.30 max	% (mol/mol)
Cetane Number	EN ISO 5165	-	51 min	
Sulfated Ash	ISO 3987	0.02 max	0.02 max	% (mol/mol)
Water Content	EN ISO 12937	500 max	500 max	mg/kg
Total Contamination	EN 12662	24 max	24 max	mg/kg
Copper Strip Corrosion (3hr, 50°C)	EN ISO 2160	-	1	degree of corrosion
Oxidative Stability, 110°C	EN 14112	4.0 min	6.0 min	hour
Acid Number	EN 14104	0.50 max	0.50 max	mg KOH/g
Iodine Number	EN 14111	130 max	120 max	g I₂/100g
Linolenic Acid Content	EN 14103	-	12.0 max	% (mol/mol)
Content of FAME with ≥ 4 double bonds		1 max	1 max	% (mol/mol)
Methanol Content	EN 14110	-	0.20 max	% (mol/mol)
MAG, DAG, TAG Contents	EN 14105	0.8,0.2,0.2 max	0.8,0.2,0.2 max	% (mol/mol)
Free Glycerine	EN 14105, EN 14106	0.02 max	0.02 max	% (mol/mol)
Total Glycerine	EN 14105	-	5.0 max	% (mol/mol)
Group I Metals (Na + K)	EN 14108, EN 14109	-	5.0 max	mg/kg
Group II Metals (Ca + Mg)	prEN 14538	-	10.0 max	mg/kg
Phosphorus Content	EN 14107	-	-	mg/kg
Cold Filter Plugging Point	EN 116	-	-	°C
Pour Point	ISO 3016	0 max	-	°C
Heating Value	DIN 51900-1, DIN 51900-2	35 min	-	MJ/kg

252

APPENDIX C

C. CHEMKIN Simulation Fuel Properties

Table C-1: Some fuel characteristics used in the CHEMKIN simulations.

Oxygenates	Reduced Molecular Equation	Oxygen Content [mass %]	Stoichiometric Air/Fuel*	Specific Vapour Density (air=1)	LHV [MJ/kg]
Methyl Formate	CH_2O	53.3	4.56	2.1	16.2[b]
Methyl Butanoate	$CH_2O_{0.4}$	31.4	8.75	3.5	28.4[c]
Normal Heptane[a]	$CH_{2.3}$	0.0	15.11	3.5	44.9[d]

* Stoichiometric Air/Fuel ratio by mass; [a] Non-oxygenated fuel; [b] Methyl Formate reaction mechanism could be used to simulate smaller alkyl esters.

[b], [c] Chemical Hazards Response Information System (CHRIS), US Department of Transportation, US Coast Guard, www.chrismanual.com.

[d] Turns S.R., 2000, An Introduction to Combustion – Concepts and Applications, McGraw-Hill, Second Edition.

253

APPENDIX D

D. Exhaust Emissions Calculation

D.1 Converting NO$_x$, CO, THC ppm to g/kW-hr

Normally the emissions of CO, THC and NO$_x$ are acquired in parts per million (ppm). However, the EPA regulates reporting on a brake-specific basis in g/kW-hr (g/bhp-hr). Note, however, that for a single cylinder engine, the indicated-specific emissions are more realistic because unlike in a multi-cylinder engine, the one cylinder would bear all the frictional losses. Equation D-1 shows the formula employed, based on the metric system, to convert the emissions from ppm to g/kW-hr where χ_i is the exhaust gas concentration of species i [ppm], Mw$_i$ is the molecular weight of species i [kg/kmol], $\dot{m}_a$ is the mass air flow rate acquired from the MAF sensor [g/s] and $\dot{W}$ is the power output [kW].

$$\text{Emissions}\,[\text{g/kW - hr}] = \frac{[\chi_i]}{1000000} \times \frac{\text{Mw}_i}{29} \times \frac{\dot{m}_a \times 36000}{\dot{W}} \qquad \text{Equation D-1}$$

The emissions of CO are relatively simple to convert using Mw$_{CO}$ = 28kg/kmol. On the contrary, the NO$_x$ and THC emissions require a bit more intuition. With respect to the NO$_x$ readings, the sum of NO and NO$_2$ is used and the molecular weight of NO$_2$ (46kg/kmol) finally employed in Equation D-1. As discussed in Chapter I, in the environment the NO is oxidised to NO$_2$, a poisonous gas, which reacts in the presence of ultra-violet light with non-methane hydrocarbons to produce a photochemical smog. With respect to the total hydrocarbons, the molecular weight is conveniently represented by the reduced formula of the fuel as C$_1$ hydrocarbons. From Table 4-3, the Mw$_{C1}$ employed in

254

this dissertation were 13.9 kg/kmol for the diesel fuel and an average of 15.65 kg/kmol for the biodiesel fuels.

D.2 Converting Soot Readings to g/kW-hr

To convert the smoke readings from FSN to g/kW-hr, it is helpful to first obtain the soot concentration in mg/m^3. This could be achieved with the help of Equation 4-7. With the soot concentration known, Equation D-2 can be used to calculate the brake- or indicated-specific soot emissions in g/kW-hr where χ_{Soot} is the soot concentration [mg/m^3], $\dot{V}_a$ is the volumetric flow rate of the fresh air into the engine [m^3] and $\dot{W}$ the power output.

$$\text{Soot}\,[\text{g/kW - hr}] = \frac{[\chi_{Soot}]}{1000} \times \frac{\dot{V}_a \times 3600}{\dot{W}}$$

Equation D-2

If $\dot{m}_a$ is available instead of $\dot{V}_a$, Equation D-3 could be employed where ρ_{exh} is the density of the exhaust gas [kg/m^3] at the respective temperature and pressure.

$$\text{Soot}\,[\text{g/kW - hr}] = \frac{[\chi_{Soot}]}{1000} \times \frac{\dot{m}_a \times 3.6}{\rho_{exh} \times \dot{W}}$$

Equation D-3

D.3 Composite Emissions Calculation

Commonly, driving cycles are employed to determine the engine emissions. The total emissions are normally averaged using weighting factors for each driving mode. The

numerical emissions obtained using the weighted procedure are called composite

emissions and are evaluated from Equation D-4 (EPA, 2007).

$$\chi_{COMP} = \frac{\sum\limits_{i=1}^{i=n}(\psi_i \times \chi_i)}{\sum\limits_{i=1}^{i=n}(\psi_i \times P_i)}$$

Equation D-4

where χ_{COMP} is the weighted composite emission level for the respective species in g/kW-

hr (or g/hp-hr), ψ_i is the weighting factor for mode i, χ_i is the emissions for mode i, g/hr,

P_i is the power for mode i, kW (or hp) and n is the number of modes. Table D-1 is an

illustration of a typical 7-mode composite emissions evaluation.

Table D-1: Illustration of a typical 7-mode engine composite emissions evaluation.

Mode	Speed [rpm]	BMEP [bar]	P_i [kW]	ψ_i	$\psi_i P_i$ [kW]	χ_i [g/h]	$\psi_i \chi_i$ [g/h]
1		minimum					
2							
3							
4							
5							
6							
7							
Summation				**1.0**	**$\Sigma(\psi_i P_i)$**		**$\Sigma(\psi_i \chi_i)$**
Comments							

The summation of the weighting factors should equal unity. The emissions χ_i [g/h] are evaluated with the help of Equation D-1 for NO_x, CO and THC and Equation D-2 or D3 for the soot. The composite emissions, χ_{COMP}, are then determined from the weighted sums and reported in g/kW-hr (or g/hp-hr) for each species thus:

$$\Sigma(\psi_i \chi_i)/\Sigma(\psi_i P_i)$$

256

APPENDIX E

E. Estimation of the Start of Injection

The isentropic bulk modulus for biodiesel fuels ranges widely from 1490 to 1670MPa or more while that for petroleum diesels is around 1370 to 1477MPa (Tat & Van Gerpen 2003a, Rosca *et al.* 2005). The speed of sound can be evaluated using Equation E-1 (Munson *et al.* 2002) where B is the isentropic bulk modulus and ρ the density of the medium. The densities of diesel and biodiesel fuels reported in Table 4-3 were used in Equation 1 and the results for the variation of the speed of sound with the bulk modulus are shown in Figure E-1.

$$ c = \sqrt{\frac{B}{\rho}} $$
Equation E-1
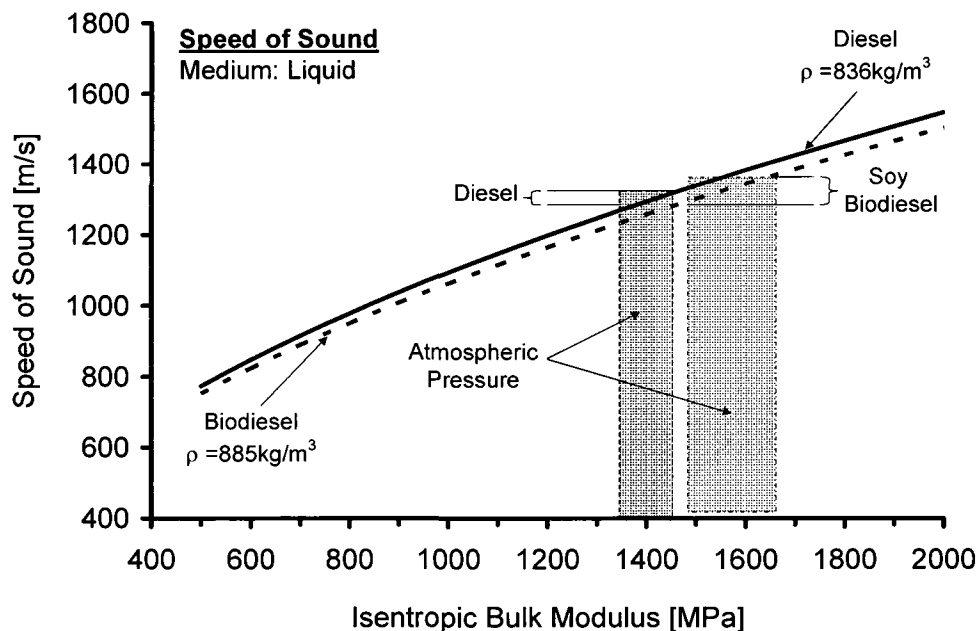
Figure E-1: Variation of the speed of sound with isentropic bulk modulus.

From the cases investigated, it was noted that the speed of sound in the biodiesel medium is expected to be only slightly higher than that in a diesel fuel medium. From Figure E-1, the maximum speeds would be 1382 and 1340m/s for biodiesel and diesel fuels, respectively. The estimated length between the fuel pump and injector nozzle for the Yanmar engine was 0.54m. Neglecting the effect of viscosity, the time taken for the pressure wave, propagating at the speed of sound, to traverse this length would be 0.39 and 0.40ms for biodiesel and diesel fuels, respectively. This corresponds to 3.3 and 3.4°CA for the respective fuels at the engine speed of 1400rpm. It was observed that the difference may not be captured by the cycle-averaged data at 1°CA resolution. However, it may be captured by the online adaptive control scheme employed in the laboratory at 0.1°CA resolution, which is beyond the scope of this dissertation.

A more detailed calculation was also conducted using the results of Tat and van Gerpen (2002) who investigated the physical properties of biodiesel-diesel fuel blends. They proposed Equation E-2 for the determination of the density and isentropic bulk modulus and E-3 for the speed of sound. In the equations, A is the density [g/cm^3] or isentropic bulk modulus [MPa], C_1 to C_8 are the respective empirical constants shown in Table E-1, T is the temperature [°C], P is the pressure [MPa], B_x is the volumetric fraction of biodiesel in the mixture [%] and c the speed of sound [m/s]. The correlations were obtained from 1 to 325bar pressure and 20°C.

$$A = C_1 T + C_2 P + C_3 B_x + C_4 \qquad \text{Equation E-2}$$

$$c = C_1 T + C_2 P + C_3 B_x + C_4 \times T \times P + C_5 \times P \times B_x + C_6 P^2 + C_7 B_x^2 + C_8 \qquad \text{Equation E-3}$$

Table E-1: Empirical constants for biodiesel-diesel blend properties from Tat (2002).

Samples	C_1	C_2	C_3	C_4	C_5	C_6	C_7	C_8
Density [g/cm^3]								
No. 2 Blends	2.6324×10^{-4}	5.8574×10^{-4}	-6.5302×10^{-4}	0.86671	-	-	-	-
No. 1 Blends	5.9030×10^{-4}	6.1040×10^{-4}	-6.5757×10^{-4}	0.83318	-	-	-	-
Isentropic Bulk Modulus [MPa]								
No. 2 Blends	1.1927	12.170	-9.7434	1838.4	-	-	-	-
No. 1 Blends	2.7763	12.206	-9.6579	1672.7	-	-	-	-
Speed of Sound [m/s]								
No. 2 Blends	-3.5972	4.6849	0.2362	1.4412×10^{-2}	-3.9667×10^{-3}	-1.6236×10^{-2}	8.8429×10^{-4}	1457
No. 1 Blends	-3.7043	5.0232	0.65479	1.4958×10^{-2}	-6.9146×10^{-3}	-1.7425×10^{-2}	11.812×10^{-4}	1415
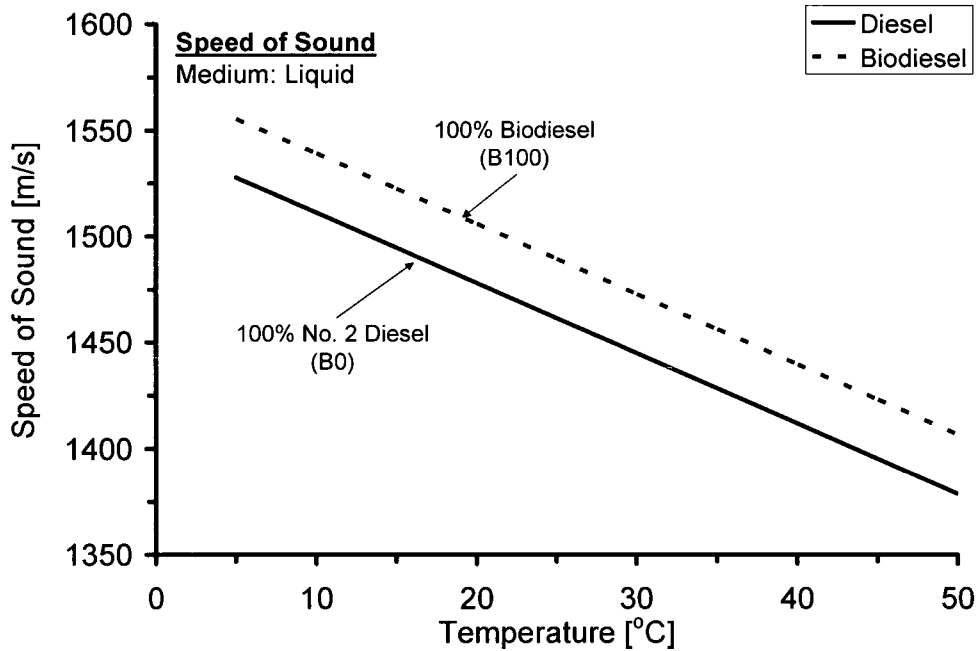
Figure E-2: Variation of the speed of sound with temperature.

Figure E-2 shows the variation of the speed of sound for 100% biodiesel and diesel fuels from Equation E-3. Assuming the fuel temperature in the high-pressure line to be 25°C, the speed of sound is 1489 and 1462m/s for biodiesel and diesel fuels, respectively. At these conditions, the pressure wave would take 0.36 and 0.37ms to traverse the high-pressure fuel line, corresponding to 3.0 and 3.1°CA at 1400rpm, respectively. The difference is similar to the estimation above.

SUMMARY

SUMMARY

The conventional diesel high temperature combustion (HTC) process has benefits of high engine power output and fuel efficiency. Unfortunately, the diesel HTC presents numerous challenges apropos of the in-cylinder reduction of nitrogen oxides (NO_x) and particulate matter (PM)/soot. Low temperature combustion (LTC) strategies, such as the homogeneous charge compression ignition (HCCI) and smokeless diesel combustion modes, together with the use of alternative fuels, offer a potential solution to simultaneously reduce the in-cylinder formation of NO_x and soot. The main objective of the work underlying the dissertation was the in-cylinder simultaneous reduction of NO_x and soot in diesel-/biodiesel-fuelled engines. The work has been systematic documentation, through refereed (peer reviewed) publications, and includes:

- Correlating the in-cylinder simultaneous reduction of NO_x and soot with the heat-release rates and ignition delay period;

- A novel approach to the fuel delivery scheduling commensurate with diesel/biodiesel low temperature (LTC) cycle efficiency proposing the end of fuel condensation time;

- An improved ignition delay correlation to include the effects of fuel oxygen, fuel Cetane number (CN) and intake O_2 concentration;

- An innovative approach to quantify the diesel/biodiesel LTC cycle efficiency in relation to combustion phasing, duration and shaping and the fraction of exhaust un-burnt hydrocarbons (UHC) with respect to the in-cylinder fuel.

- Demonstrating the use of neat biodiesel fuels without prior engine modifications for emissions and power output. The study contributes to the database of fuel properties

and would help biodiesel producers to investigate the engine performance and emissions of their B100 fuels/blends from various feedstocks.

To achieve the dissertation objective, empirical investigations of conventional diesel and neat (100%) commercial biodiesel (B100) fuels were conducted in the HTC and LTC modes. Furthermore, modelling tools such as engine cycle simulation, chemical kinetics and multi-dimensional based were employed primarily to assist in the interpretation of the empirical results. Below is a summary of the dissertation.

Thermal Efficiency Analyses of Diesel HTC and LTC Cycles

Thermal efficiency comparisons were made between the LTC and conventional diesel HTC cycles on a common-rail diesel engine with a conventional diesel fuel. To identify the major parameters that affect diesel LTC engine thermal efficiency, empirical studies were conducted under independently controlled exhaust gas recirculation (EGR), intake boost, and exhaust backpressure. Up to 8 fuel injection pulses per cylinder per cycle were applied to modulate the homogeneity history of the early injection diesel LTC operations in order to improve the phasing of the combustion process. It was concluded that in order to improve the fuel efficiency of diesel LTC operation the fuel injection could be controlled as such: using single-shot at low load with prolonged EGR (i.e. EGR-incurred LTC); at medium load with 2~5 shots of late early-injection with EGR; and at high load with 6~8 shots and EGR. Engine cycle (0-D), chemical kinetics (CHEMKIN) and multi-dimensional (KIVA) simulations were also performed primarily as a tool to assist in the interpretation of the empirical results.

Neat Biodiesel Fuel Tests on a Single Cylinder DI Diesel Engine

Using a single-cylinder direct injection (DI) diesel engine with mechanical injection configuration, comparisons were made between the use of neat commercial biodiesel (B100) fuels and a conventional diesel fuel in the HTC and LTC modes. Many researchers have reported relatively higher NO_x emissions when the engines were fuelled with biodiesel. In the present study, on the contrary, while maintaining the same high load condition, the engine-out NO_x emissions from the diesel fuel were comparable with those from a high-CN biodiesel fuel. For the investigated conditions, a higher CN-biodiesel fuel resulted in a shortened ignition delay period thereby allowing less time for the fuel/air mixing before the premixed burning phase. Consequently, a stoichiometically-weak fuel/air mixture was generated prior to (and burnt during) the premixed phase resulting in comparable engine-out NO_x levels. Generally the emissions of soot, carbon monoxide (CO) and total hydrocarbons (THC) were lower for the biodiesel-fuelled engine. Because of the relatively lower energy content of the biodiesel fuels, a slight penalty in the thermal efficiency was observed for the biodiesel-fuelled engine. Nonetheless, the results offered a promising perspective for the neat biodiesels.

The EGR was then extensively applied to initiate the LTC at low and medium load conditions. At steady-state conditions, the soot profile plotted against the ignition delay period had two distinct slopes; soot climbing and soot declining. The former was consistent with the HTC mode while the latter with the LTC mode such as HCCI-enabling technologies and smokeless diesel combustion. Simultaneous ultra-low engine-out levels of NO_x and soot were achieved in a narrow region of operation at elevated

EGR levels when the ignition delay was prolonged by 80 to 100%. A further increase in EGR resulted in increased cycle-to-cycle variation, CO and THC emissions and deterioration in the thermal efficiency especially for the diesel-fuelled engine. Furthermore, an ignition delay correlation for the fuels was developed for EGR levels from 0 to 65%. The correlation, which considered the fuel CN and oxygen concentrations in the intake air and fuel, captured the ignition delay trends with good agreement.

Neat Biodiesel Fuel Tests on a Common-Rail DI Diesel Engine

The combustion and emission characteristics of neat biodiesel fuels were investigated on a common-rail DI diesel engine under the independent control of the fuel injection, EGR, boost and backpressure to achieve the LTC mode. The fatty acid methyl esters derived from Canola oil, soybean oil, tallow and yellow grease were first blended according to the approximate volumetric proportions as may be readily procured in Ontario Province of Canada. In-cylinder combustion strategies such as single-shot with start of injection (SOI) sweeps, fixed SOI with EGR sweeps and multi-event injections were applied to modulate the homogeneity history of the biodiesel LTC operations. The conclusions from the research are summarised below:

- It was possible to retard the SOI for biodiesel further than that of the diesel fuel before the cyclic variability became intolerable. This was mainly attributed to the relatively higher CN of the biodiesel fuel.

- At fixed single-shot SOI, constant medium-to-high load conditions and a rail pressure of 950bar, the biodiesel LTC mode was attained for the intake pressures higher than

---

1.2bar (abs) at elevated EGR levels. With the SOI sweep strategy, on the contrary, the ultra-low simultaneous levels of engine-out NO_x and soot for both diesel and biodiesel fuels were not attained. A combination of the SOI and EGR strategies, preferably under adaptive control, may facilitate an energy-efficient biodiesel LTC mode solution.

- For the multi-event injections at medium load conditions, ultra-low engine-out NO_x emissions were achieved. However, at very advanced SOI cases the poor biodiesel/air mixture preparation resulted in increased soot, CO and THC formation. Nonetheless, retarding the SOI and reducing the number of injections appeared to approach the LTC mode, presenting a potential for the simultaneous reduction of in-cylinder NO_x and soot formation in biodiesel-fuelled common-rail DI diesel engines.

At the conditions investigated, the biodiesel was found to sustain a broader range of loads in the EGR-incurred LTC than the diesel fuel. This was mainly attributable to the biodiesel's higher CN and combustion-accessible fuel oxygen.

Keywords: Biodiesel fuel, common-rail diesel engines, conventional diesel fuel, EGR, HCCI, HTC, ignition delay, LTC, simultaneous reduction of NO_x and soot, 0-D modelling, CHEMKIN, KIVA.

VITA AUCTORIS

VITA AUCTORIS

NAME: Mwila Clarence Mulenga.

PLACE OF BIRTH: Lusaka Province, Zambia.

YEAR OF BIRTH: 1972.

EDUCATION: School Certificate & General Certificate of Education (1990)

Kitwe Boys' Secondary School

Kitwe, Copperbelt Province, Zambia.

B.Eng. Mechanical (Year of Completion 1996)

University of Zambia

Lusaka, Lusaka Province, Zambia.

MSc. Automotive Engineering (Year of Completion 2002)

Chalmers University of Technology

Göteborg, Västergötland, Sweden.

MSc. Thesis conducted at Robert Bosch GmbH

Schwieberdingen, Baden-Württemberg, Germany.

Ph.D. Candidate (2007)

University of Windsor

Mechanical, Automotive & Materials Engineering

Windsor, Ontario Province, Canada.